Charles University

Faculty of Science

Study program: Developmental and Cell Biology

Mgr. Jarmila Princová

New interconnections between lipid metabolism and chromatin regulation

Nové spojitosti mezi metabolismem lipidů a regulací chromatinu

Doctoral thesis

Supervisor: RNDr. Martin Převorovský, PhD.

Prague, 2023

Prohlašuji, že jsem závěrečnou práci zpracovala samostatně a že jsem uvedla všechny použité informační zdroje a literaturu. Tato práce ani její podstatná část nebyla předložena k získání jiného nebo stejného akademického titulu.

V Praze dne 27.2.2023 ……

Mgr. Jarmila Princová

Dále prohlašuji, že jsem pravdivě uvedla svůj podíl na publikovaných manuskriptech uvedených v kapitole “Results”.

V Praze dne 27.2.2023 ……

Mgr. Jarmila Princová

……

Školitel: RNDr. Martin Převorovský, PhD.

Acknowledgements

First of all, I would like to thank my supervisor RNDr. Martin Převorovský, PhD. without whom I would not return to academic research and who has, over the years, become a good friend. I'm extremely grateful to the current and past members of the Laboratory of Microbial Genomics, namely Anna Marešová, Viacheslav Zemlianski, Adéla Kmochová, Kateřina Svobodová, Patrik Hohoš and Róbert Zach, for fruitful scientific discussion, their help with experiments but mainly for the friendly and supportive atmosphere that made this thesis possible. Many thanks also to Anna Janovská, who enthusiastically helped me to develop a working acetyl-CoA quantification method that has eluded me for years.

I would like to express my deepest appreciation to my husband, Peťo, not only for the dinners when I was writing this thesis but also for his efforts at tempering my perfectionism. Always. Special thanks also goes to my family and friends for their endless support and encouragement.

Abstract

Lipid metabolism has been implicated in changes of chromatin modifications resulting in altered gene expression. Such regulation is important for cellular differentiation or cancer progression, however, the mechanism of how altered metabolic flux leads to targeted changes in chromatin modifications which then regulate gene transcription or heterochromatin maintenance is still poorly understood. We describe that fission yeast cells defective in fatty acid synthesis show increased expression of a subset of stress-response genes. This altered gene expression depends on the SAGA and NuA4 histone acetyltransferases and is associated with increased acetylation of histone H3 at lysine 9 in the corresponding gene promoters. Moreover, diminished fatty acid synthesis results in increased cellular resistance to oxidative stress. Additionally, the lipid metabolism mutants display chromatin alterations in centromeres and subtelomeres, regions of constitutive heterochromatin. We propose that changes in lipid metabolism can regulate histone acetylation and transcription of specific stress-response genes, but also lead to more global changes in heterochromatin. And while we clearly see the consequences of increased stress-response genes which result in promoting redox homeostasis, the implications of altered heterochromatin upon fatty acid synthesis perturbation are less evident. We also show that the nitrogen signaling affects mitotic fidelity and lipid metabolism in the fission yeast, but further experiments are required to determine whether increased fatty acid synthesis is actually the cause of mitotic defects rescue as observed in *cbf11Δ* cells and other cell-untimely-torn mutants in nitrogen-rich conditions. Overall, we have elucidated how fatty acid synthesis contributes to the regulation of chromatin modifications, maintenance of genome integrity, and oxidative stress resistance.

Key words: lipid metabolism, histone acetylation, stress resistance, subtelomeric heterochromatin

Abstrakt

Metabolismus lipidů je úzce spjat s modifikacemi chromatinu, které ovlivňují genovou expresi. Tato regulace je důležitá pro buněčnou diferenciaci nebo růst rakovinných buněk, nicméně mechanismus, jakým změny v buněčném metabolismu ovlivňují chromatinové modifikace, které následně regulují genovou transkripci nebo udržování heterochromatinu, nebyl dodnes objasněn. Popsali jsme, že buňky kvasinek *Schizosaccharomyces pombe* defektní v syntéze mastných kyselin vykazují zvýšenou expresi genů stresové odpovědi, která závisí na aktivitě histonacetyltransferáz SAGA a NuA4 a je spojena se zvýšenou acetylací histonu H3 na lysinu 9 v odpovídajících genových promotorech. Navíc snížená syntéza mastných kyselin vede ke zvýšené buněčné rezistenci vůči oxidativnímu stresu. Kromě toho mutanty metabolismu lipidů vykazují změny konstitutivního heterochromatinu na centromerách a subtelomerách. Navrhli jsme proto, že změny v metabolismu lipidů mohou regulovat acetylaci histonů a transkripci specifických genů stresové odpovědi, ale také vést ke globálním změnám v heterochromatinu. Zatímco zvýšená exprese stresových genů podporuje redoxní homeostázu, důsledky změn heterochromatinu vlivem snížené syntézy mastných kyselin zatím nedokážeme spolehlivě interpretovat. Ukázali jsme také, že signální dráhy reagující na dostupnost dusíku ovlivňují spolehlivost mitózy a metabolismus lipidů u kvasinek *S. pombe*. Na podkladě současných experimentů ale není jasné, zda je zvýšená syntéza mastných kyselin v podmínkách bohatých na dusík příčinou pozorovaného snížení výskytu mitotických defektů v buňkách *cbf11Δ* a dalších mutantech s tzv. “cut” fenotypem. Tato práce přispěla k objasnění, jakým způsobem syntéza mastných kyselin reguluje modifikace chromatinu, udržování integrity genomu a odolnost buněk vůči oxidativnímu stresu.

Klíčová slova: metabolismus lipidů, acetylace histonů, rezistence na stres, subtelomerický heterochromatin

List of abbreviations

3-MB-PP1	ATP-competitive analog, CAS 956025-83-5
α-KG	α-ketoglutarate
ACC	acetyl-coenzyme A carboxylase
ACL(Y)	ATP-citrate lyase
AcCoA	acetyl-coenzyme A
ACSS2	acyl-CoA synthetase short-chain family member 2
AMP	adenosine monophosphate
AMPK	AMP-activated protein kinase
CoA	coenzyme A
CDK	cyclin-dependent kinase
ChIP-seq	chromatin immunoprecipitation followed by deep sequencing
DAG	diacylglycerol
DAPI	4',6-diamidino-2-phenylindole
DMSO	dimethyl sulfoxide
EDTA	ethylenediaminetetraacetic acid
ER	endoplasmic reticulum
FA	fatty acid
FAD	flavin adenine dinucleotide
GAM-HRP	goat anti-mouse antibody linked with horseradish peroxidase
GAR-HRP	goat anti-rabbit antibody linked with horseradish peroxidase
GFP	green fluorescent protein
GO	gene ontology
H3K9	lysine 9 of histone H3
H3K9ac	acetyl-lysine 9 of histone H3
H3K9me2	dimethyl-lysine 9 of histone H3
HAT	histone acetyltransferase
HDAC	histone deacetylase
I/R	ischemia reperfusion
JMJD	Jumonji C family demethylase
KMT	histone lysine methyltransferase

LD	lipid droplet
LLPS	liquid-liquid phase separation
LSD1	lysine-specific histone demethylase 1A
MAPK	mitogen-activated protein kinase
MT	methyltransferase
NAFLD	non-alcoholic fatty liver disease
OD	optical density
PA	phosphatidic acid
PAGE	polyacrylamide gel electrophoresis
PBS	phosphate-buffered saline
PDC	pyruvate dehydrogenase complex
PL	phospholipid
RT-qPCR	reverse transcription followed by quantitative polymerase chain reaction
SAH	S-adenosylhomocysteine
SAM	S-adenosyl-methionine
SAPK	stress-activated protein kinase
SDS	sodium dodecyl sulfate
SE	steryl ester
TAG	triacylglycerol
TBS	Tris-buffered saline
TCA	trichloroacetic acid
TCA	tricarboxylic acid (when referring to TCA or the Krebs cycle)
TET	ten-eleven translocation protein family
THF	tetrahydrofolate
TOR	target of rapamycin
TORC1	target of rapamycin complex I
TTBS	Tris-buffered saline with Tween 20
UPR	unfolded-protein response
WT	wild-type
YES	yeast extract medium with supplements

Table of Contents

1. INTRODUCTION

Lipids are fundamental components of all living organisms. Thanks to their extensive chemical diversity they perform multiple biological functions including but not limited to energy storage, compartmentalization, cell division, trafficking and signal transduction [1]. Cellular growth and proliferation is associated with biosynthesis of lipids while aging or stress usually stall biosynthesis and promote catabolism of the lipid stores [2]. Like many other physiological processes that are kept in balance via negative feedback loops, altered lipid metabolism also brings about changes in cellular resistance to stress and viability [3–5]. Remarkably, the interplay between lipid metabolism and oxidative stress resistance is involved in the development of human diseases such as cancer or heart ischemia (Figure 1.1). Although a mere change in lipid composition of cells and especially of biological membranes has an effect on stress resistance [3,4], the regulation is often more complex can be achieved, for example, by gene expression changes based on altered lipid metabolism [6]. Multiple aspects of the observed interplay between lipid metabolism regulation and stress resistance remain elusive, especially the factors and mechanism ensuring specificity of the response.

1.1 Interconnections between lipid metabolism and oxidative stress response in disease

Lipid metabolism reprogramming is one of the hallmarks of cancer development and has been extensively studied. Briefly, rapid proliferation of tumor cells requires large amounts of lipids, which are supplied by increased *de novo* lipogenesis and fatty acid uptake, hence, inhibitors of these two processes are used as therapeutic targets and multiple drugs are in clinical trials (for recent reviews see [3,7–9]). Lipid metabolism also affects the stress resistance of cancer cells. First, *de novo* lipogenesis and fatty acid uptake increase saturation of cell membranes by providing saturated and monounsaturated fatty acids, which are less sensitive to lipid peroxidation compared to polyunsaturated fatty acids, thus increasing the resistance of cancer cells to oxidative stress and chemotherapy treatment [3,4]. On the other hand, fatty acid synthesis inhibition by the knockout of acetyl-CoA carboxylase (ACC), the first and rate-limiting enzyme of fatty acid synthesis catalyzing the carboxylation of acetyl-CoA to produce malonyl-CoA, in murine liver cells led to

increased tumor incidence, likely by increasing resistance of ACC-knockout mice to oxidative stress [5].

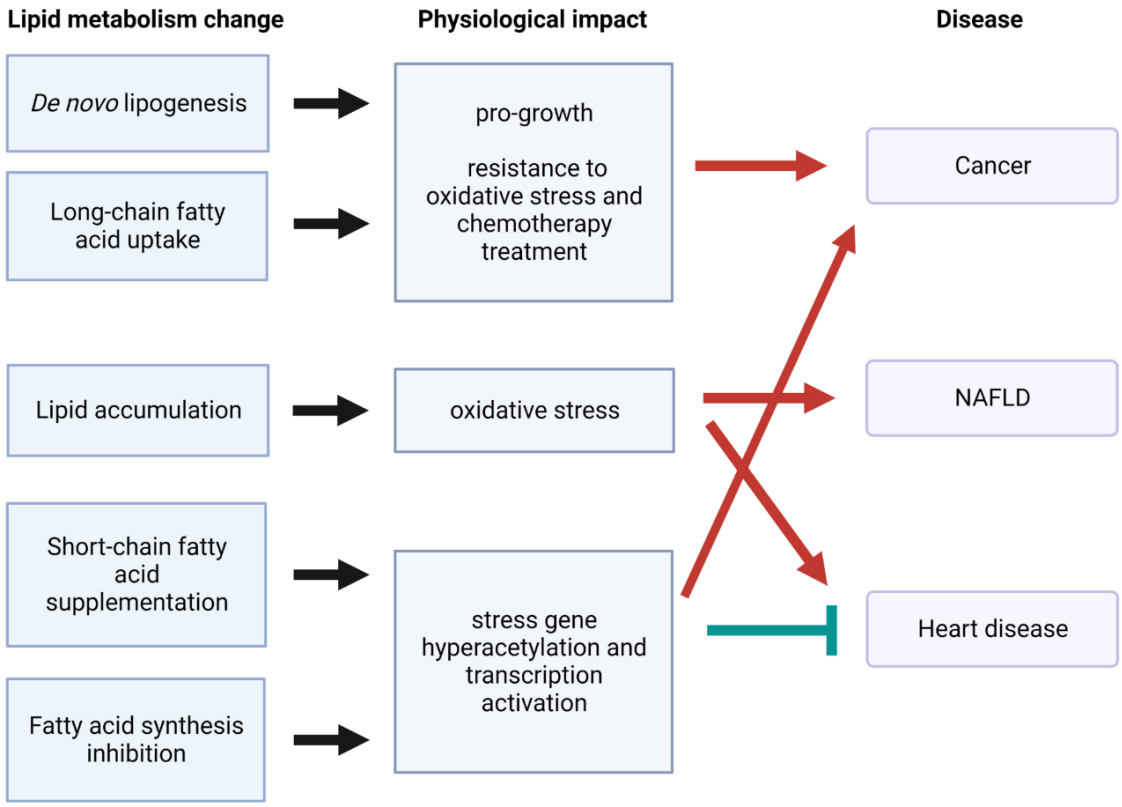

Figure 1.1 Diseases connecting oxidative stress response and lipid metabolism perturbation. Schematic overview representing the physiological impact and implications in the disease state upon lipid metabolism perturbation. Aggravating and alleviating effects on the disease progression are indicated by the red and green arrows, respectively. For more details see the main text. Figure was created in BioRender software.

Non-alcoholic fatty liver disease (NAFLD) is the most prevalent chronic liver disease and is characterized by fat accumulation in hepatocytes in the absence of alcohol consumption, viral infection or drugs causing steatosis. The perturbed lipid metabolism in NAFLD disturbs the antioxidant balance in the liver leading to oxidative stress [10,11]. Additionally, lipid metabolism and oxidative stress are interconnected in heart disease. Fatty acids metabolized by β-oxidation and feeding into oxidative phosphorylation in the mitochondria are the major energy source in heart cells [12]. However, during ischemia, when myocardium is not sufficiently supplied by blood

containing oxygen and nutrients, the electron transport chain is blocked and fatty acids accumulate thus leading to ROS production and oxidative stress [13,14]. On the other hand, elevation of acetyl-CoA concentration by sodium octanoate (8C), acetate or pyruvate supplementation significantly improved heart function after ischemia reperfusion (I/R) injury. Mechanistically, acetyl-CoA reduced I/R injury by promoting histone acetylation which in turn activated the expression of antioxidant genes and inhibited cardiomyocyte apoptosis [6].

1.2 The molecular mechanisms of oxidative stress response regulation by lipid metabolism

Oxidative stress is defined as an imbalance between oxidants and antioxidants in favor of the oxidants, leading to a disruption of redox signaling and control and/or molecular damage [15]. Therefore, oxidative stress response encompasses a set of biological processes that are affected in order to return the cell into homeostasis. Disturbances or changes to the lipid metabolism have been shown to affect the oxidative stress response using several molecular mechanisms including regulation of lipid droplets and stress-gene induction by regulating chromatin modifications, which will be covered in this chapter.

1.2.1 Lipid droplets

Oil and water do not mix, which is why the cellular neutral lipids are stored as lipid droplets (LD) composed of a hydrophobic lipid core surrounded by a monolayer of amphipathic glycerolipids. The acyl chains of the glycerolipids are integrated into the hydrophobic core while the polar head groups are in contact with the polar environment such as cytoplasm. Lipids are energetically rich and, as expected, lipid droplets serve as centers for energy homeostasis. However, the functions of lipid droplets are numerous including prevention of lipotoxicity and oxidative stress management, viral pathogenesis or protein quality control [16]. Importantly, lipid droplets are evolutionarily well conserved and occur in all branches of the tree of life. While the LDs occurring in different organisms and cellular compartments differ in size, shape and composition, all share the same fundamental molecular characteristics [17]. The following sections describe the eukaryotic cytoplasmic LDs unless specified otherwise.

1.2.1.1 Lipid droplet composition and biogenesis

Lipid droplets are generally spherical in shape ranging between 0.1 - 5 μm in diameter in nonadipocytes [18]. The main lipid components of the hydrophobic core are triglycerides and steryl esters at ratios which vary not only in different organisms but also inside individual cells [19]. Additionally, other nonpolar molecules including vitamins A and E, steroid hormones and signaling lipids are sequestered into LDs [20]. Proteins are also integral members of LDs with 100-150 protein species in a prototypical mammalian cell [21] and 35-40 in the budding yeast [22]. The predominant proteins in LDs are enzymes involved in lipid metabolism but also proteins functioning in membrane trafficking and protein degradation. Since no specific LD-targeting sequence exists, other mechanisms for protein targeting have been described. Class I LD proteins, usually containing hydrophobic hairpins, insert into the ER and laterally diffuse in the membrane into the growing LD (for more description of LD biogenesis see below). Class II LD proteins insert directly from the cytosol into the LD phospholipid monolayer through amphipathic α-helices that recognize packing defects in the membrane [16].

The precise mechanism of LD formation is not yet clearly understood, however, LDs originate from specific subdomains within the ER containing a defined set of proteins and lipids, and the prevailing model consists of the following steps: 1. Nucleation of the LD by neutral lipid production in the ER membrane; 2. Oil lens formation between the leaflets of the ER membrane; 3. LD budding toward cytosol; 4. LD maturation (Figure 1.2) [23].

Nucleation

Diacylglycerol (DAG) is produced from phosphatidic acid by the lipin phosphatase complex, which controls the balance between membrane growth and lipid storage [24]. DAG is the immediate precursor to triacylglycerol (TAG) formation and LD biogenesis. The produced neutral lipids are trapped within the ER membrane and accumulate at sites containing ER-residential acyltransferases [25].

Lens formation

Upon reaching a critical concentration, neutral lipids form lens-like structures, likely by phase separation as they decrease interaction with other membrane components [26]. In the beginning nascent LDs are relatively mobile within the ER membrane, however, with further growth the lens becomes fixed in the membrane by the seipin complex, which becomes the hub for LD-biogenesis

factors. At this stage, LDs are observable by BODIPY 493/503 or Nile Red staining as diffraction-limited puncta [27,28].

Budding

Drastic changes to the ER membrane are required in order to change the symmetrical neutral lipid lens into a cytoplasm-facing LD bud covered by a phospholipid monolayer. Although the mechanism of this vectorial budding is not fully elucidated, both lipids (DAG, PA) and proteins are known to be involved (FIT family and perilipins) [29].

Maturation

Majority of mature LDs appear to associate with the ER membrane throughout their lifetime, however, the extent of the interaction between ER and LD seems to vary from short lipidic bridges to junctions over a large fraction of the LD surface [23,29]. Although several models propose that LDs can detach from the ER membrane, no fission machinery has been described so far [30].

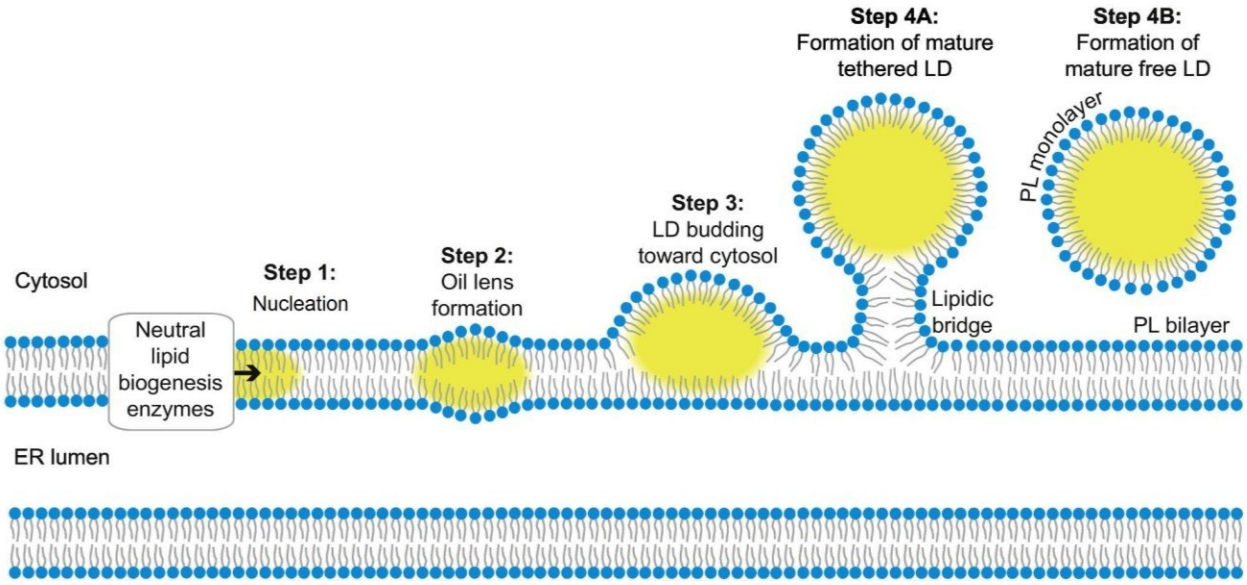

Figure 1.2 Lipid droplet biogenesis from the ER membrane. LD biogenesis starts with the synthesis of neutral lipids (yellow) that are released within the ER phospholipid (PL) bilayer by enzymes associated with the ER membrane. As the neutral lipids accumulate, an oil lens is formed and subsequently buds asymmetrically toward the cytosol to form a mature LD covered by a PL monolayer. LDs can either remain connected to the ER membrane via a lipidic bridge or a larger fraction of the membrane surface. Alternatively, LDs may also be fully released from the ER membrane. Adapted from [23].

1.2.1.2 Lipid droplets in stress control

Cellular adaptations to stress are often manifested by metabolic remodeling and one of the most universally observed adaptations is the increased production of lipid droplets. During stress LDs function as nutrient reservoirs, as safeguards against protein and lipid toxicity and as signaling platforms for immune response pathways [29,31]. It is curious that starvation, a nutritional stress, induces expansion of energy storage LDs. This strategy is crucial for cell survival during long-term starvation and is regulated by the TORC signaling [32,33]. However, where do the LDs come from when nutrient sources are scarce? One known source is the rewiring of lipid metabolism from phospholipids to TAG by the lipin activity [32] and the other is macro-autophagy [34]. In addition to functioning as a nutrient source during starvation, the LDs have the propensity to store otherwise toxic lipids and proteins that accumulate during normal metabolism or during stress. For example, it has been shown that localization of squalene, a hydrocarbon precursor of cholesterol, to LDs is important to prevent its toxicity [35]. During oxidative stress the LDs protect lipids from peroxidation and sequester already damaged lipids or proteins [20]. However, this detoxification property is also often exploited by cancer cells [36]. An imbalance between unfolded proteins and their chaperones is known as ER stress and triggers the unfolded protein response (UPR). Activation of UPR leads to reduced protein translation, increased transcription of genes involved in the ER stress response and ER-associated protein degradation (ERAD) [37]. UPR is also associated with LD accumulation [38] which is believed to protect against ER stress by removing misfolded proteins and maintaining ER lipid homeostasis [39].

1.2.1.3 Lipid droplets as biotechnological factories

Lipid droplets represent a promising target for synthetic biology and biotechnological applications. Knowledge of LD biogenesis and behavior under stress provides the means to engineer LDs at the required amount and containing desired lipophilic molecules. Moreover, the low density of LDs allows for feasible extraction and purification using density-gradient centrifugation. Taken together, there has been a considerable interest in tapping into the LD biotechnological potential in recent years. Terpenoids have a wide range of industrial uses such as specialty fuels, agrochemicals, fragrances, nutraceuticals, and pharmaceuticals. A study by Sadre *et al*. describes a high-yield synthesis of specific terpenoids in engineered LD-accumulating leaves of *Nicotiana benthamiana*, a close relative of tobacco, when precursor availability is enhanced [40]. Additionally, LD-resident proteins, such as oleosin, can be utilized for efficient targeting into LDs.

An antifungal peptide PAF102 used for multiple applications in crop protection and food preservation was produced in rice seeds [41] or in a well-established *Pichia pastoris* cell factory using the plant oleosin fusion technology at commercially relevant yields [42]. Strikingly, the storage capacity for high-value lipophilic compounds such as terpenes can be increased by designing yeast cells with more or larger LDs based on the lipid chain flexibility that determines their selective migration into LDs [43]. Nevertheless, the applications of LDs in biotechnology remain largely unexplored although several interesting uses such as improvement of food crops by enhancing their nutritional quality have been proposed [17].

1.2.1.4 Lipid droplets in the fission yeast

The fission yeast, *Schizosaccharomyces pombe*, is a rod-shaped unicellular eukaryote that is ~7–14 μm in length and ~4 μm wide. It grows by tip elongation and divides by medial fission. It has a rapid life cycle with a generation time in vegetative growth of 2–4 h at 36˚C–25˚C in complex and minimal media [44]. The fission yeast is predicted to have diverged from the budding yeast *Saccharomyces cerevisiae* hundreds of millions of years ago and, at the molecular level, is as closely related to humans as it is to the budding yeast [45]. Thanks to its low-cost cultivation, easy genetic manipulation and conservation of biological processes between *S. pombe* and higher eukaryotes, it is well established as a model organism [46].

The fission yeast LDs are primarily composed of triacylglycerols (TAG) and steryl esters (SE) with slightly prevailing SEs over TAGs (56:44) during logarithmic growth and with reverse ratio SE:TAG 36:64 during stationary phase in glucose-based medium. SEs were found to be primarily saturated, with palmitate (16:0) and stearate (18:0) being the dominant species. On the other hand, palmitate, stearate and oleate (18:1) are almost equally represented TAG species in logarithmic phase cells, while the fraction of the unsaturated oleate increased at the expense of palmitate in stationary phase cells. Additionally, LDs in stationary phase cells are larger and with higher lipid content compared to logarithmic phase cells [47]. Importantly, LD biogenesis is regulated by cell cycle progression [48], as it was later described also for mammalian cells [49], and occurs primarily during G2 phase of the cell cycle when new LDs are formed by both *de novo* formation from the ER and by LD fission [48]. Lipin, the phosphatidic acid phosphatase, converts phosphatidic acid to DAG and, as described above, its activity is required for LD biogenesis [50]. In *S. pombe* and *S. cerevisiae* lipin activity is negatively regulated by the CDK, which is necessary

to ensure nuclear envelope expansion during anaphase of the closed mitosis [51,52]. Interestingly, lipin in the related fission yeast *Schizosaccharomyces japonicus* is not inhibited during mitosis thus limiting membrane availability and inducing nuclear envelope rupture as a physiological process of the semi-open mitosis [52]. Moreover, the potential for biotechnological use of *S. pombe* in production of valuable oils has been explored recently [53].

1.3.1 Regulation of transcription by lipid metabolism

Dynamic regulation of gene expression is critical for adaptation to changing local conditions and multiple mechanisms have evolved to transduce the changes in intracellular metabolism to transcriptional responses. In prokaryotes, metabolism controls gene expression through allosteric interactions between metabolites and transcription factors [54]. This mechanism was introduced by Jacob and Monod when they discovered the *lac* operon [55]. The general principle behind specific gene regulation is based on DNA binding proteins that regulate transcription of genes containing their specific recognized sequence and recruit RNA polymerase in direct proportion to their binding ability [56]. However, eukaryotic metabolic regulation of transcription is more complex and often indirect including nutrient sensors such as AMP-activated protein kinase or target of rapamycin (TOR) complex and post-translational modifications of transcription factors [57]. Nevertheless, eukaryotic cells have retained also the ability to directly modulate gene expression by metabolites and metabolic enzymes. First, similarly to bacteria, metabolites may function as ligands of transcription factors. Fatty acids have been described to bind peroxisome proliferator-activated receptors (PPAR) which has been even utilized in drug design of several commercially available therapeutics [58]. Second, metabolic enzymes that typically localize to the cytoplasm or mitochondria can be also found in the nucleus where they modify histones or transcription regulators such as glyceraldehyde-3-phosphate dehydrogenase, the glycolytic enzyme that converts glyceraldehyde 3-phosphate into 1,3-bisphosphoglycerate, which is selectively recruited in S phase to the H2B promoter and is essential for the S phase-specific H2B gene transcription [59], or the pyruvate kinase, the final glycolytic enzyme producing pyruvate and ATP, which has the ability to phosphorylate histone H3 and also function as transcriptional coactivator [60]. Third, deposition and removal of DNA and chromatin modifications affecting gene expression requires metabolites that are intermediates of distinct metabolic pathways. It has led to the hypothesis that chromatin modifications directly respond to fluctuations in the concentrations of these metabolites to modulate gene expression [61]. Additionally, several enzymes producing metabolites required for chromatin modifications are enzymatically active also in the nucleus [60].

1.3.1.1 Metabolic regulation of chromatin modifications

Nucleosomes, the basic units of chromatin, consist of an octamer of the four core histones (H3, H4, H2A and H2B) wrapped by 145-147 base pairs of DNA [62]. Histones are subject to a wide variety of covalent modifications including acetylation, methylation, phosphorylation, ubiquitylation, sumoylation, succinylation, glutarylation, propionylation and butyrylation [63,64]. DNA can also be chemically modified, most often by methylation to form 5-methylcytosine [65]. Together, chemical modifications of histones and DNA comprise the epigenome. Chromatin modifications regulate chromatin structure and function directly, by affecting the dynamics of the nucleosome, or indirectly by nucleosome-binding proteins recognizing the various modifications that can stabilize or reposition the nucleosome, regulate higher-order assemblies of chromatin or recruit other proteins. An important aspect of nucleosome dynamics is the spontaneous unwrapping of DNA from the histone octamer that exposes protein binding sites in nucleosomal DNA that are otherwise buried, and upon protein binding the unwrapping equilibrium shifts, facilitating more unwrapping. This explains how sequence-specific DNA binding can occur in the presence of nucleosomes. Histone modifications located near the DNA entry/exit site of the nucleosome, such as H3K9ac or H3K14ac facilitate unwrapping [66].

Chromatin modifications are usually deposited and removed by specific enzymes called “writers" and “erasers”, respectively, and require specific metabolites for the reaction to occur [61]. Here, we will focus on the histone and DNA modifications that are most affected by the metabolic state of the cell and especially by lipid metabolism. Histone and DNA methylation requires *S*-adenosyl-methionine (SAM) as a methyl donor. This metabolite is generated by the combined activities of the serine-glycine-one carbon metabolism and the methionine cycle (Figure 1.3A) [67]. Notably, the fission or budding yeast genome does not appear to contain DNA methylation and there are no known DNA methyltransferases, although cytosine methylation is an abundant tRNA modification [68,69]. Histone lysine methyltransferases (KMT) use SAM to mono-, di- or trimethylate the amide nitrogen of lysine with the release of *S*-adenosyl-homocysteine, a competitive inhibitor of methyltransferases (Figure 1.3B). Thus, the intracellular SAM:SAH ratio drives methyltransferase activity [70]. Histone methylation can be removed by two mechanisms - by LSD1 family demethylase catalyzing an amine oxidation reaction dependent on the FAD coenzyme, or by Jumonji C family demethylase (JMJD) and ten-eleven translocation (TET) proteins catalyzing

dioxygenation reaction that requires Fe^{2+}, oxygen and α-ketoglutarate (α-KG) [71]. Remarkably, high levels of α-KG promote demethylation of H3K27me3, H3K9me3 or H4K20me3 [72].

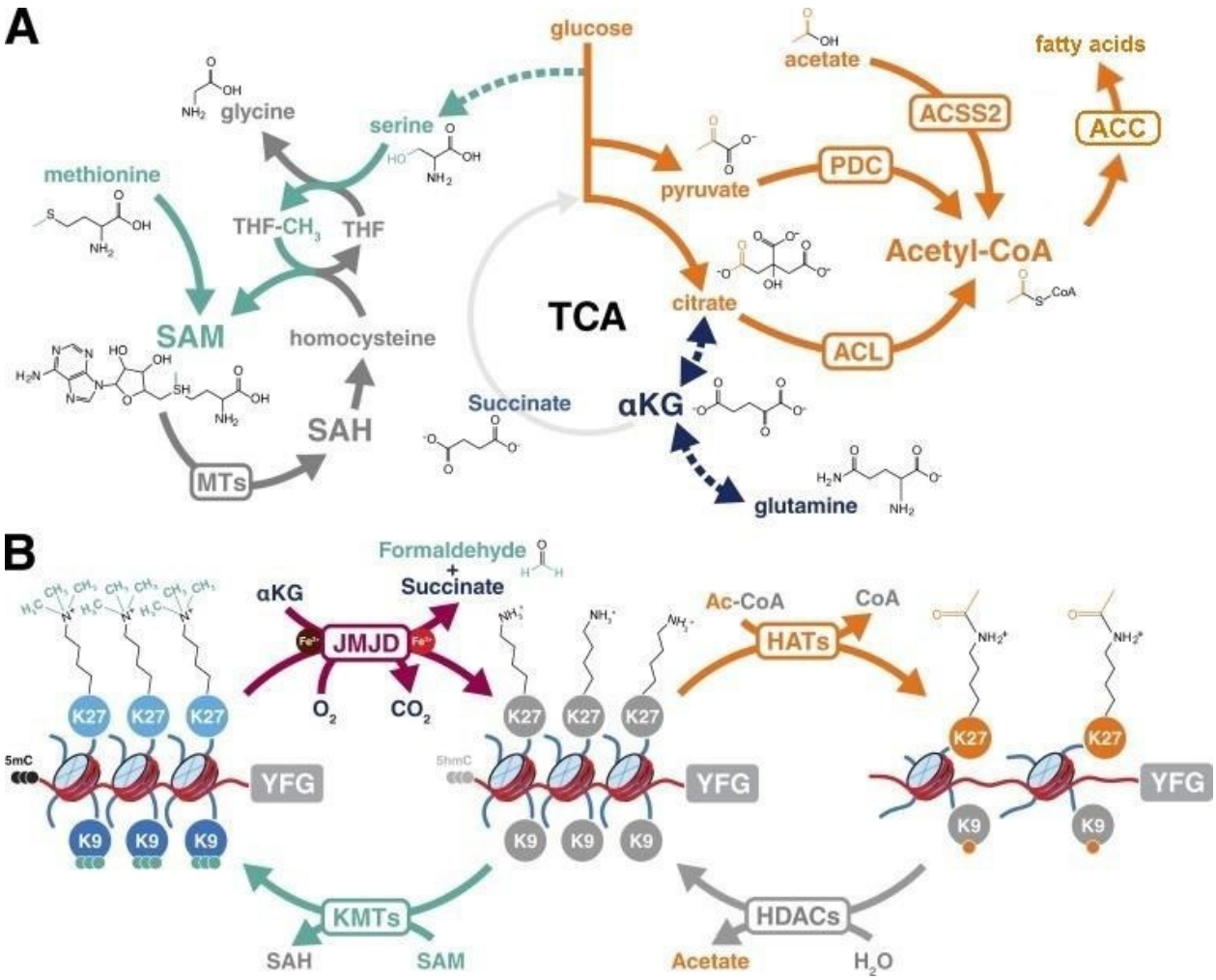

Figure 1.3 Metabolic pathways providing substrates for chromatin modifiers. (A) Metabolic pathways involved in the generation of chromatin-modifying metabolites. Generation of SAM is required for DNA and histone methylation (turquoise), acetyl-CoA is needed for histone acetylation (orange) and α-KG is used as a cofactor for histone demethylation (dark blue). Importantly, fatty acid synthesis is a major pathway consuming the nucleocytosolic pool of acetyl-CoA and, as such, competes with HATs for substrate. **(B)** Chromatin-modifying enzymes require intermediary metabolites as substrates or cofactors. Silenced chromatin is shown on the left, open chromatin is shown on the right, and an unmodified state is indicated in the center. Color coding is as in A, with methyl marks in turquoise and acetylation in orange. Adapted from [61].

While histone methylation is associated with both transcriptionally active and inactive chromatin depending on the local chromatin context and particular methylated amino acid residue [73], histone acetylation primarily occurs in accessible and transcriptionally active chromatin [74]. The acetylation of histones is performed by histone acetyltransferases (HAT) using acetyl-CoA as a substrate. Interestingly, HATs usually acetylate several distinct histone lysines and non-histone targets such as transcription factors [75]. On the other hand, the removal of histone lysine acetylation is catalyzed by histone deacetylases (HDAC) through amide hydrolysis (Figure 1.3B) [76]. Acetyl-CoA is a central cellular metabolite produced in multiple cellular compartments - peroxisomes, mitochondria, cytosol and nucleus, however, these acetyl-CoA pools are mostly separated, except for the common nucleocytoplasmic pool [77]. Peroxisomes are small ubiquitous membrane-enclosed organelles that are involved in fatty acid β-oxidation in many organisms and the produced acetyl-CoA can be exported to the cytosol via the carnitine shuttle [78]. In mitochondria, acetyl-CoA can be generated from the oxidation of pyruvate, β-oxidation of fatty acids or amino acid degradation (Figure 1.3A). Although mitochondrial acetyl-CoA cannot be directly transported from the mitochondrial matrix to the cytosol, citrate generated from acetyl-CoA during the TCA cycle can be exported by the citrate carrier [79] and acetyl-CoA is regenerated in the cytosol by the activity of the ATP-citrate lyase (ACL) [80]. To some extent, the carnitine shuttle is also able to export acetyl-CoA from the mitochondria [81]. In the cytoplasm, acetyl-CoA can be synthesized from acetate by the acyl-CoA synthetase short-chain family member 2 (ACSS2) or, as mentioned above, from citrate by ACL and, curiously, both enzymes also associate with chromatin in the nucleus [82,83]. Moreover, the mitochondrial pyruvate dehydrogenase complex (PDC) can translocate from the mitochondria to the nucleus where it locally produces acetyl-CoA [84] (Figure 1.3A). Importantly, the nucleocytoplasmic pool of acetyl-CoA is shared between histone (and other protein) acetylation and fatty acid (FA) biosynthesis which occurs in the cytosol, therefore, changes in the dynamics of the FA synthesis affect the availability of acetyl-CoA for histone acetyltransferases (Figure 1.3A) [85].

Over the past decade, additional acyl-histone modifications have spurred broad interest (Figure 1.4) [74,86–88]. Succinyl-CoA, most commonly known as a TCA cycle intermediate, can be generated in the nucleus by the oxoglutarate dehydrogenase, a traditionally mitochondrial TCA

enzyme, and be used as a substrate for histone succinylation [89,90]. Propionyl-CoA and crotonyl-CoA, derivatives of short-chain fatty acids, have also been detected to modify histone lysines [91,92]. Histone acetyltransferases and deacetylases are not specific to acetyl-CoA as a substrate and were shown to utilize also other acyl-CoAs [87]. Lysine acylations have been proposed to occur also by non-enzymatic addition due to their reactivity if present in sufficient concentration, which is thought to occur mostly in the mitochondria [93]. Additionally, no specific acyl-CoA modifier has been identified yet. However, are the acyl-CoA histone modifications physiologically relevant or only a side-effect of HAT promiscuity and high reactivity? The existence of specific readers of histone acylation supports their physiological importance. The YEATS domain protein family and DPF proteins of the double PHD finger domain family were shown to prefer crotonylated H3K9 over acetylated H3K9 [94–96] and YEATS domain protein GAS41 was identified as a reader of succinyl-lysine [97].

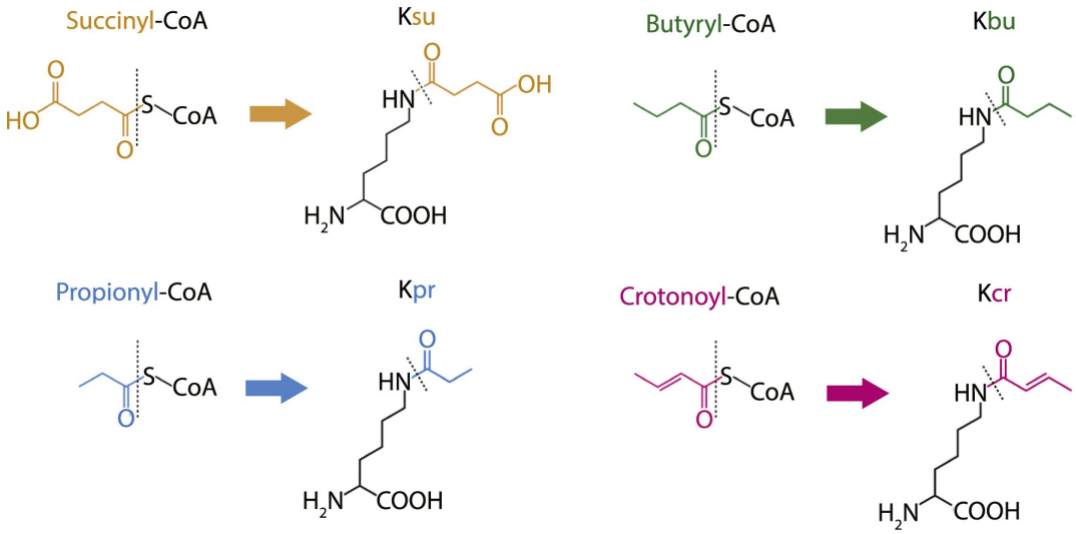

Figure 1.4 Acyl-CoAs as histone modifications. Adapted from [86].

Curiously, even after almost 60 years since the discovery of histone acetylation the function of this modification is still a matter of intensive debate. Although originally proposed by Allfrey et al. in 1964 to positively regulate transcription [98], it is not clear today whether acetylation merely correlates with or leads to gene expression activation [99,100]. Transcription and histone acetylation are so intertwined that identifying which process is upstream means answering the chicken or the egg problem. Histone acetylation is thought to promote transcription by two mechanisms. First, histones are highly basic proteins that tightly bind DNA and lysine acetylation

neutralizes the charge on histones, causing DNA unwrapping and higher accessibility for the transcription machinery [66]. Second, histone acetylation is recognized by reader proteins that can directly or indirectly recruit the RNA polymerase II or promote its progression [101,102]. Additionally, progressing RNA Pol II interacts with HAT-containing complexes such as SAGA or NuA4 via the carboxy-terminal domain (CTD), forming a positive feedback loop between active transcription and histone acetylation [103]. Intriguingly, a recent study showed that synthetic designer histone H4 tetraacetylation increased the rate of transcriptionally competent chromatin formation ~3-fold in comparison with the absence of acetylation [104]. Similarly, histone acylation is associated with open chromatin and transcribed genes [91,105,106]. However, it seems plausible that since histone acetyltransferases utilize a variety of acyl-CoA substrates the *in situ* ratio of available acyl-CoAs might determine the major histone modification. This is supported by a recent study by Gowans et al. where they showed that H3K9 acetylation is replaced by crotonylation when energy sources become limited and, in this case, crotonylation is associated with reduced expression of growth genes [107]. Notably, detection of specific histone acetylation genome-wide using ChIP-seq relies on highly specific antibodies, whose availability is often limited and, therefore, a considerable proportion of our knowledge about histone acylation functions comes from *in vitro* transcription assays on designer chromatin with site-specific histone acylations [88].

1.3.1.2 Biochemical considerations for gene expression regulation by metabolite dynamics

Metabolites are clearly the substrates required for histone modifications, however, can the physiological changes in metabolite levels cause a change in gene expression via altered levels of a histone modification? In order to affect the rate of the enzymatic reactions catalyzed by the histone writers and erasers, the Michaelis constant (K_M) of the enzyme must be equal to, or higher than, the range of physiological concentrations of the substrate. Therefore, if substrate concentration is well above the enzymatic K_M, such as in the case of ATP and kinases, small fluctuations in substrate concentration do not affect the reaction rate [108]. In contrast, cytosolic and nuclear concentrations of acetyl-CoA and SAM appear to be comparable to the K_M of histone acetyltransferases and methyltransferases (in μM range), respectively, supporting the hypothesis of metabolic control of histone modifications. Moreover, the reaction products, or other related endogenous metabolites such as acyl-CoAs in case of HATs or SAH in case of KMTs, are often

competitive inhibitors of substrate binding that affect reaction rates even when substrate concentrations are sufficient to saturate the enzyme [109].

Although direct regulation of gene expression by metabolism seems conceivable, the limitations of current technology need to be acknowledged. Today, it is still almost impossible to estimate subcellular concentrations of individual metabolites. While the mass spectrometry-based technology is both very sensitive and specific, metabolite extraction remains to be the bottleneck in providing better quality results. To date, most estimates of metabolite concentration are based on whole-cell analyses and thus scramble different subcellular pools with vastly different substrate concentrations [110]. The majority of studies on compartmentalized metabolism have used differential or gradient centrifugation, most often to study mitochondrial metabolome. A more recent approach employed immunoaffinity enrichment of subcellular compartments. Nevertheless, both fractionation methods require processing time that leads to measurement artifacts caused by metabolic changes that occurred during the fractionation process [111]. Although isotope labeling during fractionation can be used to assess metabolic activity during fractionation, the true metabolite concentrations will only be recovered by having detailed knowledge about metabolic pathways and expected flux [112]. Other direct methods for metabolite quantification are the emerging technologies of mass spectrometry and Raman imaging. In these cases sample preparation does not involve destructive processing steps, however, the analysis is limited by mass and spatial resolution or type of analyzed metabolite [113,114]. Alternatively, indirect methods such as biosensors can be employed for profiling subcellular metabolism in living cells. Recently, fluorescent sensors to measure metabolite levels such as coenzyme A or H_2O_2 in multiple cellular compartments have been developed [115,116].

Complementarily, determining *in vivo* enzymatic properties of chromatin modifiers, such as the Michaelis constant, is also challenging. While the classic enzymology approach developed by Michaelis and Menten was broadly used over the past century to describe a vast variety of enzymes, it is based on *in vitro* measurements of a homogeneous system with many molecules of the same type, i.e. enzyme, substrate and inhibitor, and thus does not describe well *in vivo* conditions [117]. In the case of chromatin modifying enzymes in live cells, new methods are needed to determine enzymatic activities of large multiprotein complexes of which histone HATs

and KMTs are a part. Importantly, the histone modifier kinetics needs to be based on single molecules, because on each chromatin locus only one molecule is present as part of complexes such as COMPASS or SAGA which are often associated with other complexes functioning in chromatin remodeling or transcription. Moreover, each chromatin locus is potentially unique due to variation in the complex composition, and it also changes over time based on the cell cycle phase or environmental conditions. In recent years, the methods for single-molecule measurement have remarkably advanced and have been used, for example, to describe DNA unwrapping or to identify novel transcription elongation factors [118–120]. Although the single-molecule *in vitro* methods are usually consistent with bulk *in vivo* analyses, further development of live cell imaging methods is required to capture the single-molecule behavior *in vivo*.

1.3.1.3 Novel insights into transcription factor binding and histone modifications

Gene expression is controlled by transcription factors (TFs), a class of proteins that recognize specific DNA sequence motifs within regulatory regions, giving rise to distinct transcription programs. Most eukaryotic TFs bind short DNA motifs whose occurrence in the genomes far exceeds the number of sites that are actually bound by the TF in a given cell [121]. How specificity is achieved and how this limited binding influences transcription across the genome is still a matter of debate. This restriction conceivably occurs through DNA modifications such as methylation and the nucleosome that can be post-translationally modified. *In vivo*, TFs operate within the context of chromatinized DNA, unlike in traditional *in vitro* analyses where naked DNA is used. Nucleosome core particles comprise 145 bp to 147 bp of DNA wrapped around the histone octamer protein core and this configuration leaves only a fraction of the nucleosomal DNA freely accessible to binding factors [62]. Additionally, most TF motifs are too long to be entirely solvent-facing on the nucleosome and only a small subset of TFs, called the pioneer transcription factors, seems to be able to overcome chromatin to establish a transcriptionally favorable environment by themselves. The pioneer factors subsequently enable other transcription factors, nucleosome remodeling complexes and histone modifiers to interact with nucleosome-bound DNA (Figure 1.5A) [122,123]. Alternatively, TFs can also interact with DNA by a passive mechanism when the nucleosome structure is temporarily disrupted by another cellular event such as DNA replication or repair [124]. A systematic characterization of nucleosome-TF interactions across mammalian TF families revealed several modes of nucleosome engagement (Figure 1.5B) and includes (1) binding spanning the two gyres of nucleosomal DNA; (2) orientational preference; (3) end

preference; (4) periodic preference; and (5) preferential binding to the dyad region. Binding of most TFs facilitated nucleosome displacement. The hypothesis suggested by Zhu et al. is based on the mechanism of DNA-TF-nucleosome ternary complex formation, which is relatively unstable because the TFs prefer free DNA over nucleosomal DNA [125]. The TFs using the end binding mode may be regulated by histone acetylation, in particular. In this mechanism TFs are associated with DNA close to the entry and exit positions of the nucleosome, whose extent of exposure is expanded upon histone acetylation in the process of nucleosomal DNA unwrapping (breathing) [66].

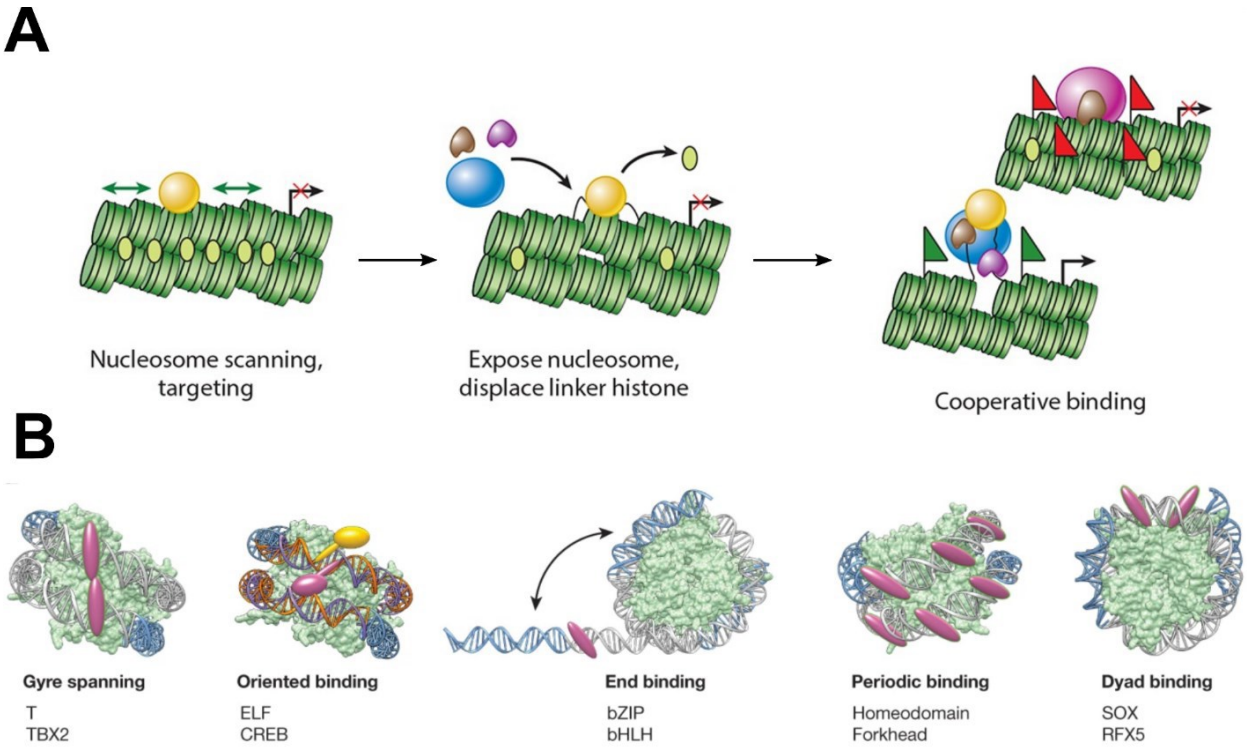

Figure 1.5 Binding modes of transcription factors to chromatinized DNA. (A) Process of chromatin engagement by pioneer transcription factors. (1) The pioneer transcription factor (gold sphere) scans laterally across chromatin and searches for a target nucleosome/DNA sequence. (2) The pioneer TF exposes the underlying DNA in chromatin and displaces linker histone (light green ellipse). (3) The pioneer TF enables binding of other transcription factors, coactivators or corepressors, and nucleosome remodelers. Green flags represent activating histone modifications; red flags represent repressive histone modifications. Adapted from [123]. **(B)** In the gyre spanning mode the DNA grooves align across the two nucleosomal DNA gyres and can specifically associate with TF dimers, or TFs having long recognition helices or multiple DNA binding domains. The dual-gyre binding is possible only on nucleosomal DNA, and it thus stabilizes the nucleosome from dissociation, and may therefore function to lock a nucleosome in place at a specific position. The oriented binding mode is induced by breaking the local rotational symmetry of DNA and promotes nucleosome dissociation. TFs with the end binding mode associate with nucleosomal DNA close to the entry and exit positions. This preference is in line with the probability of spontaneous nucleosomal DNA unwrapping, which decreases from the end to the center [66]. In the periodic mode TFs bind every ~10.2 bp on nucleosomal DNA because the nucleosome allows access to DNA from only one side of the DNA helix. TFs that bind to short motifs, or to discontinuous motifs, are still able to occupy the available periodic positions on nucleosomal DNA. TFs employing the dyad binding mode bind close to the nucleosomal dyad, a region that contains only a single DNA gyre and features the thinnest histone disk [62]. Adapted from [125].

Traditionally, histone modifications were viewed as instructive for transcriptional regulation based on the "epigenetic code", however, recent studies have challenged this hypothesis and suggest that histone marks serve as an interaction platform for histone reader proteins with a variety of catalytic and non-catalytic functions affecting transcription mostly indirectly [126]. From the global perspective, the nuclear structure is given by the sum of histone modifications. This is exemplified by nuclear blebbing, formation of abnormal protrusions of the nuclear envelope, upon increase in the global histone acetylation or decrease in the global histone methylation which leads to expansion of chromatin volume [127]. At the molecular level, histone modifications may alter histone tail charge, thus causing differential electrostatic interactions with neighboring molecules, and also create a docking platform for histone reader proteins that have the ability to physically interact with additional proteins or another chromatin region. Together, chromatin and other nuclear proteins form a dynamic 3-D structure of the nucleus. During the past decade the theory of liquid-liquid phase separation (LLPS) as the driving force of nuclear organization was developed [128,129]. LLPS represents the condensation of macromolecules into a concentrated liquid-like droplet that segregates from a less dense surrounding environment (Figure 1.6). These liquid-like droplets could be induced by weak interactions between multivalent macromolecules that have multiple interaction domains, repeated structural domains, or intrinsically disordered regions (IDR). Phase separation could then support the dynamic creation of nuclear subdomains, in which specific proteins or molecules are concentrated [130]. It is being increasingly appreciated that the liquid-like condensed state is likely a fundamental state of cellular proteins along with the native (soluble) state and the amyloid (a solid-like condensate) state, with distinct biological functions associated with each state [131]. A classic example of LLPS within nucleus are the nucleolar subcompartments - the fibrillar center where rRNA is transcribed, the dense fibrillar component where rRNA is processed and the granular component where rRNA is assembled into pre-ribosomal particles [132]. Each nucleolar subcompartment displays liquid-like character with rapid and almost complete fluorescence recovery after photobleaching (FRAP) and liquid-like coalescence events [133]. It has been shown that Pol II and the Mediator complex at high concentrations form transcriptional condensates at highly regulated genes via IDRs [134]. Moreover, specificity of TFs can be affected by condensate formation such as in the case of budding yeast stress-response TFs Msn2 and Yap1 that have DNA-binding domains with affinity for the same DNA sequences but occupy different genomic locations and regulate a separate set

of genes. This genomic specificity is encoded by the IDRs that likely form nuclear condensates [135]. Additionally, gene silencing in heterochromatin is at least in part driven by H3K9me-HP1-dependent LLPS. Condensate formation in heterochromatin promotes exclusion of phase-incompatible transcription factors and Pol II and thus ensures silencing of the DNA (Figure 1.6) [136–138]. Interestingly, even though acetylation generally diminishes the chromatin LLPS and droplet formation, highly acetylated chromatin forms a new phase separated state in the presence of bromodomain-containing proteins. These acetylation-rich droplets have distinct physical properties and can be immiscible with unmodified chromatin droplets, mimicking nuclear chromatin subdomains [139].

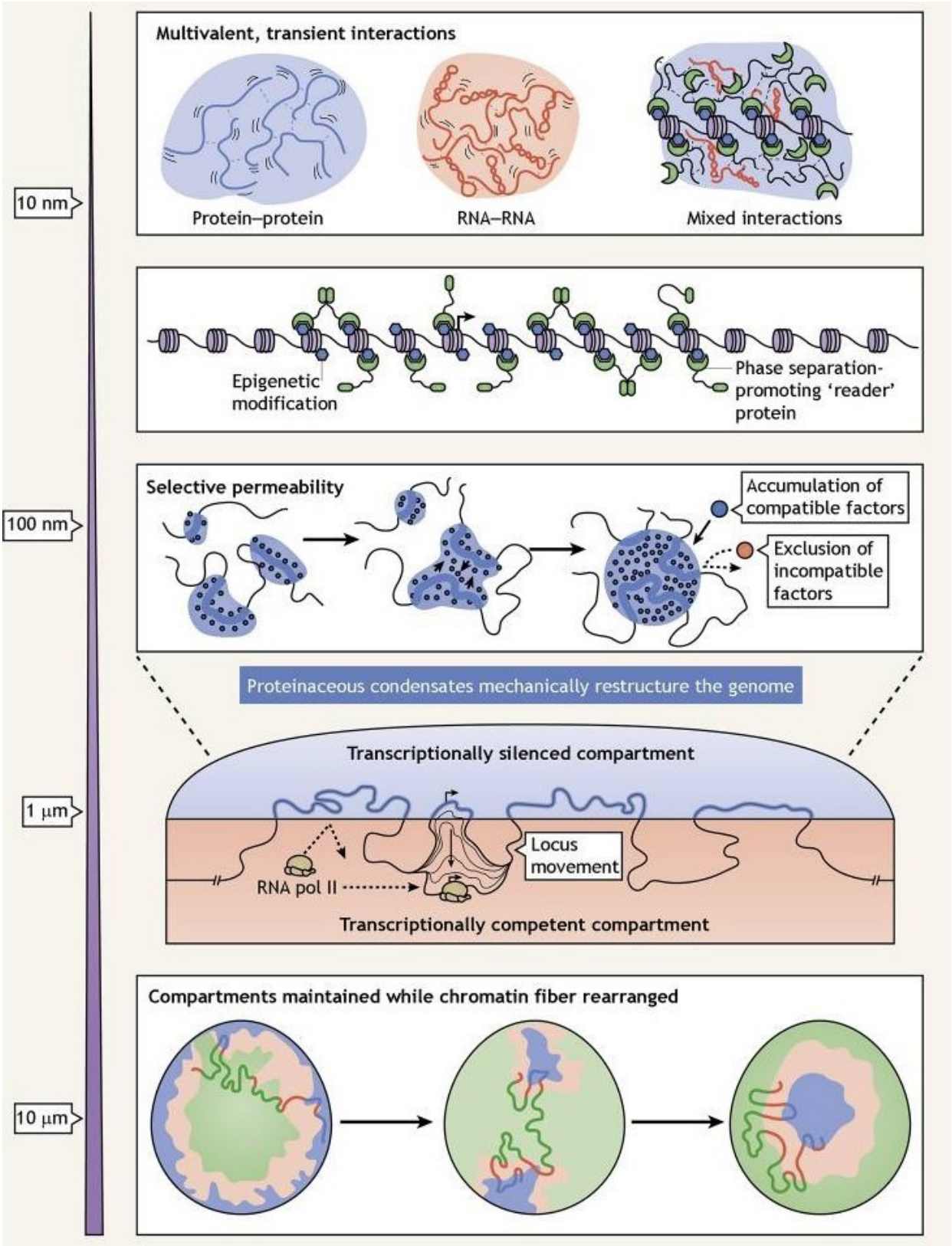
Multivalent, transient interactions
Protein–protein
RNA–RNA
Mixed interactions
10 nm
Epigenetic modification
Phase separation-promoting 'reader' protein
Selective permeability
Accumulation of compatible factors
Exclusion of incompatible factors
100 nm
Proteinaceous condensates mechanically restructure the genome
Transcriptionally silenced compartment
1 μm
Locus movement
RNA pol II
Transcriptionally competent compartment
Compartments maintained while chromatin fiber rearranged
10 μm

Figure 1.6 Nuclear liquid condensates and their function. Liquid-liquid phase separation occurs by multivalent and transient interactions between macromolecules that have multiple interaction domains, repeated structural domains, or intrinsically disordered regions (IDR) such as proteins and RNA which are both abundant in the nucleus. At the chromatin level epigenetic modifications associate with histone reader proteins that often include IDRs and promote condensate formation. LLPS causes selective permeability within the nucleus as it leads to accumulation of phase-compatible factors and exclusion of incompatible factors, and can create interaction hubs of functionally-related chromatin regions. At a larger scale, condensate formation induces nuclear compartmentalization such as the boundary between heterochromatin and euchromatin. For example, Pol II and TF access is limited to transcriptionally active chromatin by condensate formation. Importantly, locus movement between transcriptionally silenced and competent chromatin is enabled by altering the histone modifications and the associated reader proteins. Moreover, the liquid-like state of the condensates allows to maintain mobility and reversible association of those components so that disassembly and reassembly of the condensates may occur based on the cell cycle or various stress signals. Adapted from [140].

1.3.1.4 Subnuclear metabolic niches

The effect of metabolite levels on global histone acetylation and methylation is well documented and mechanistically understood [61]. Intriguingly, a growing number of studies have also described specific changes in histone acetylation upon manipulating acetyl-CoA metabolism. First, lipid-derived acetyl-CoA can provide up to 90% of acetyl-carbon for histone acetylation in mammalian cells, and supplementation with the octanoate FA results in histone hyperacetylation and induction of specific genes, distinct from those induced by glucose-derived acetyl-CoA [141]. Second, nuclear acetyl-CoA synthesized by chromatin-associated ACSS2 in mouse neurons resulted in increased histone acetylation and expression of specific memory-related genes [142]. Third, elevation of acetyl-CoA by sodium octanoate supplementation in live mice led to an increase in histone acetylation and gene expression activation of antioxidant genes, thus resulting in inhibited cardiomyocyte apoptosis [6]. Although specific changes in histone acetylation and gene expression were observed, no study so far elucidated the mechanism how the specificity is achieved because acetyl-CoA is a small and seemingly freely-diffusible molecule. Contrarily, even small molecule diffusion is not that free in the cell due to molecular crowding since the cellular proteins encompass a large fraction of the total cellular volume [143].

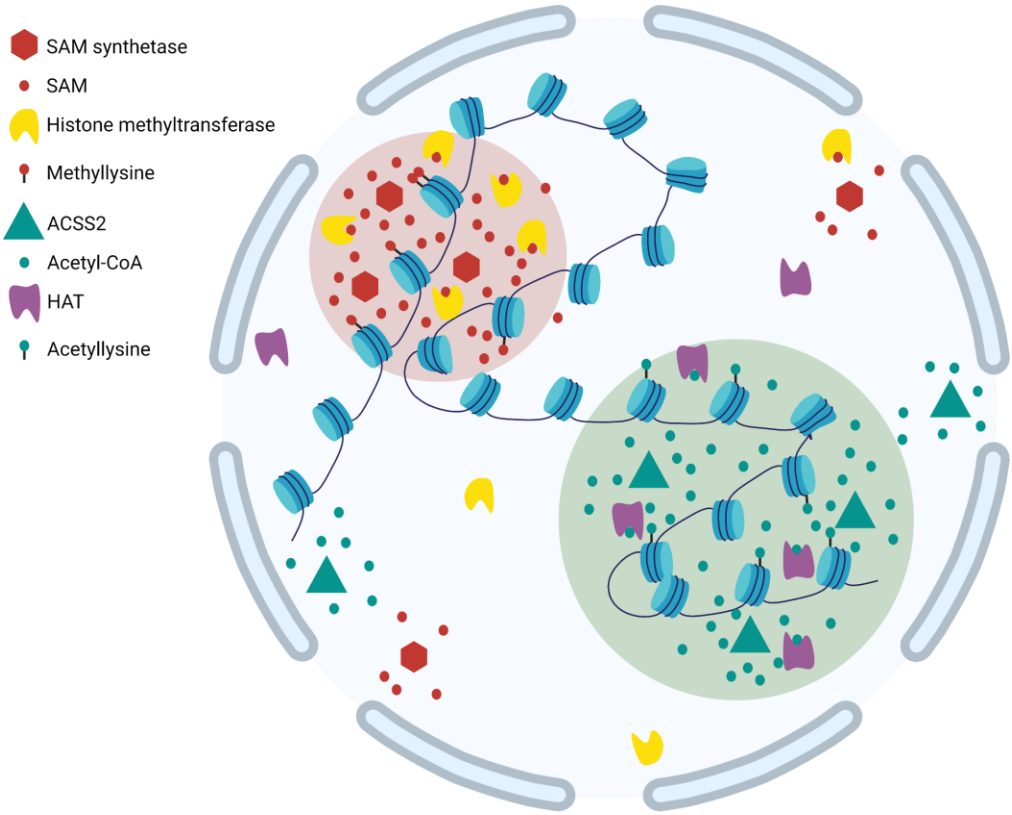

Figure 1.7 Nuclear metabolic niches. Condensate formation within the nucleus could locally increase concentrations of metabolic enzymes, their products used as substrates for histone modifications, and histone-modifying enzymes, thus promoting local histone modifications. The locus- or domain-specific microenvironment might further help to recruit (or retain) specific readers, transcription factors as well as the transcriptional machinery. Shown here are putative metabolic niches (with symbols for nucleosomes, metabolic enzymes, and chromatin modifiers) in which acetyl-CoA and ACSS2 or SAM and SAM synthetase are enriched. HATs or KMTs could then modify the histones within the niche with higher probability than outside the niche due to locally increased concentration of substrate. Figure was created in BioRender software.

An interesting concept within the field of metaboloepigenetics are the subnuclear metabolic niches. In this model, site-specific recruitment of metabolic enzymes to genomic regions could facilitate the creation of nuclear microdomains with, for example, elevated acetyl-CoA or SAM levels which are then utilized as cofactors by chromatin modifiers, thus contributing to the accurate control of gene expression (Figure 1.7) [88,144]. As described above, metabolic enzymes catalyzing the synthesis of acetyl-CoA and other acyl-CoAs or SAM have been detected in the nucleus and they could produce locally available metabolites. How such local enrichment of metabolites could be maintained or how the metabolic enzymes are recruited to these subdomains is so far unknown.

Formation of liquid-liquid phase separation (LLPS) within the nucleus was proposed as a mechanism which could lead to local accumulation of specific enzymes or metabolic factors [145]. The existence of membrane-less compartments is further supported by over 400-fold difference in diffusion coefficients of 40-nm genetically-encoded nanoparticles observed within the fission yeast cytoplasm. This result demonstrates the vast heterogeneity in cytoplasmic viscosity within single cells [146]. Overall, nuclear architecture, in particular localization of chromatin-modifying enzymes and availability of metabolites required for histone modifications, appears to be the driving force behind targeted cellular response to changes in intracellular metabolism although the mechanisms how it can be achieved are not yet fully understood.

2. MATERIALS AND METHODS

2.1 Yeast culture and transformation

Fission yeast cells were grown according to standard procedures [147] in complex yeast extract medium with supplements (YES). Routine optical density (OD) measurements of liquid cell cultures were taken using the WPA CO 8000 Cell Density Meter (Biochrom). A list of strains used in this study is provided in Table 2.1.

Strains with deletions of *Δcbf11, Δpyp1* and *Δptc1* were constructed using the pClone system [148]. The plasmids used in strain construction are listed in Table 2.2. The *Δpyp2* prototrophic strain was created by a standard genetic cross of its auxotrophic parent [149] and JB32.

Table 2.1 List of strains

Strain	**Genotype**	**Source**
JB32	*h+s*	Lab stock
JB149	*h- sty1Δ::ura4 ura4-D18*	Lab stock
MP44	*h+ cbf11Δ::kanR*	[150]
MP584	*h- sty1-GFP:kanMX6*	[149]
MP589	*h+ pyp2Δ::natMX6*	This study
MP591	*h- sty1-GFP:kanMX6 cbf11Δ::natR*	This study
MP597	*h+ pyp2Δ::natMX6 cbf11Δ::kanR*	This study
MP606	*h- ppc1-537*	[151]
MP636	*h- Pcut6MUT*	[152]
MP713	*h+ pyp1Δ::NatMX4*	This study
MP714	*h+ ptc1Δ::HphMX4*	This study
MP718	*h+ pyp1Δ::NatMX4 cbf11Δ::KanR*	This study

MP723	*h+ ptc1Δ::HphMX4 cbf11Δ:KanR*	This study
MP809	*h+ sty1.T97A ura4-D18*	[153]
MP810	*h+ sty1.T97A ura4-D18 cbf11Δ::natR*	[152]

Table 2.2 List of plasmids

ID	Vector	Experiment/use	Source
pMP90	pCloneKAN1	KO vector for *cbf11* (*kanR* cassette)	[152]
pMP91	pCloneNAT1	KO vector for *cbf11* (*natR* cassette)	[150]
pMP158	pCloneHYG1	KO vector for *ptc1* (*hygR* cassette)	This study
pMP159	pCloneNAT1	KO vector for *pyp1* (*natR* cassette)	This study

2.2 Fluorescence microscopy

For observation of nuclear morphology, exponentially growing cells were fixed in 70% ethanol, rehydrated in water, stained with ~1 μg/mL DAPI and photographed using the Olympus CellR system or the Leica DM750 microscope.

Cells expressing Sty1-GFP from its endogenous chromosomal locus [149] were grown in YES to exponential phase and treated with 0.5 mM H_2O_2. Aliquots were taken at indicated times and fixed by 10% formaldehyde for 15 min. Then, cells were washed three times with PBS. To observe Sty1-GFP localization, cell suspension was loaded onto lectin-coated slides [154] **(publication #2)** and imaged using the Olympus CellR microscope system.

2.3 Cell length measurement

Exponentially growing cells were fixed by 10% formaldehyde for 15 min, washed three times with PBS, stained with calcofluor (50 μg/ml) and imaged using the Leica DM750 microscope. Cell length at division was determined using the ImageJ 1.52p software [155].

2.4 Immunodetection of phosphorylated Sty1

Cells were cultivated in 50 mL YES to exponential phase and treated or not with 0.5 mM H_2O_2 for 30 min. 20 mL culture was collected for lysate preparation of both unstressed and stressed cells (1000g, 3 min, RT). Cells were washed with 3 mL STOP buffer (150mM NaCl; 50mM NaF; 25mM HEPES; 1.5mM NaN_3; pH = 8), resuspended in 1 mL STOP buffer and collected again. The cell pellet was stored at -80°C before preparing lysate. Native lysates were prepared by breaking cells using FastPrep-24 (MPI) 3x20s at 6.5 m/s in NP-40 buffer (6mM Na_2HPO_4, 4mM $NaH_2PO_4 \bullet H_2O$, 1% NONIDET P-40, 150mM NaCl, 2mM EDTA, 50mM NaF) with FY protease inhibitors (Serva) and phosphatase inhibitor cocktail 2 and 3 (Sigma). Lysate concentration was determined using Pierce™ Detergent Compatible Bradford Assay Kit (Thermo Scientific, 23246) and equal protein amounts in standard Laemmli buffer were loaded onto denaturing 12% Tris-glycine SDS gel. The proteins were transferred onto nitrocellulose membrane using standard wet blotting procedure. The membrane was blocked in 5% milk (Biorad) in TTBS at 37°C for 30 min and incubated overnight at 4-8°C with primary antibodies anti-phospho-p38 and anti-PSTAIR in 4 ml blocking solution. After vigorous wash in TTBS the membrane was incubated with secondary antibodies α-rabbit HRP diluted 1:2000 and α-mouse HRP diluted 1:5000 diluted in 5% milk in TTBS for 60 min at room temperature on rocker. Membrane was washed in TTBS and TBS. The list of all primary and secondary antibodies used is listed in Table 2.3 and 2.4, respectively. Chemiluminescence was detected using the Amersham ECL Prime Western Blotting Detection Reagent and the LAS 4000 imaging system.

2.5 Immunodetection of histones

Cells were grown to exponential phase in 25 mL YES at 32°C, an equivalent of 20 ml at OD 0.5 was collected (1000g, 3 min, RT) and the pellets were flash frozen. Denatured TCA cell extracts were prepared as follows: cell pellets were resuspended in 200 µl ice-cold 20% TCA and transferred to 2 ml screw cap tube with glass beads. Cells were broken in FastPrep-24 4x 20s at 6.5 m/s with 4-5 min cooling on ice between cycles. Then 400 µl 5% TCA was added and spun out of beads (400g, 1 min, 4°C). The lysate was centrifuged (16000g, 6 min, 4°C) and the pellet was washed twice with 1 mL ice-cold acetone. The pellet was resuspended in 200 µl extraction buffer (8M urea, 4% SDS, 1/100 FY inhibitors; room temperature) with inhibitors added just before processing. Upon protein solubilization samples were loaded onto 15% SDS-PAGE gel

with Laemmli buffer and separated using electrophoresis. After protein transfer onto 0.2 µm nitrocellulose membrane, the membrane was blocked for 1 hour at RT in 5% BSA in TTBS on rocker. Membrane was incubated with primary antibodies anti-H3 and anti-H3K9ac overnight at 4-8°C in 2 mL 2.5% BSA in TTBS and washed vigorously in TTBS. Then, the membrane was incubated 1 hour at RT with 2 ml 5% BSA in TTBS + 1:4000 GAR-HRP. Wash after secondary antibody and chemiluminescence detection was performed as described above for Sty1-P. For detection of H4, the membrane was stripped in stripping buffer (40 mL 10% SDS, 7.8 mL 4x Tris-HCl pH 6.8, 9.4 ul BME) at 50°C with shaking (ThermoMixer) covered with aluminum foil. The membrane was washed 4x 5 min in TTBS and blocked again with 5% BSA in TTBS for 1 hour at RT. The membrane was incubated with primary antibodies anti-H4, anti-H4ac and anti-PSTAIR, and with 1:4000 GAR-HRP (for H4 and H4ac) or GAM-HRP secondary antibodies as described above. The list of all primary and secondary antibodies used is listed in Table 2.3 and 2.4, respectively.

Table 2.3 List of primary antibodies

Antibody	**Source**	**Dilution**
anti-H3	Abcam, ab1791	1:5000
anti-H3K9ac	Abcam, ab4441	1:1000
anti-H4	Abcam, ab10158	1:1000
anti-H4ac	Upstate, 06-866	1:1000
anti-PSTAIR	Sigma, P7962	1:10000
anti-phospho-p38	Cell Signal. Tech., 9211S	1:1000

Table 2.4 List of secondary antibodies

Antibody	**Source**	**Dilution**
GAM-HRP	Cell Signal. Tech., 7076S	Indicated in text
GAR-HRP	Cell Signal. Tech., 7074S	Indicated in text

2.6 RT-qPCR

2 ml of exponentially growing cell culture was collected and flash frozen. Total RNA was extracted from cell pellet using the MasterPure Yeast RNA Purification Kit including a DNase treatment step (Epicentre), and converted to cDNA using random primers and the RevertAid Reverse Transcriptase kit (ThermoFisher Scientific). Quantitative PCR was performed using the 5x HOT FIREPol EvaGreen qPCR Supermix (Solis Biodyne) and the LightCycler 480 II instrument (Roche). For normalization, *act1* (actin) and *rho1* (Rho1 GTPase) were used as reference genes. Three biological experiments were performed. The primers used are listed in Table 2.5.

Table 2.5 List of primers

ID	Sequence	Experiment
MP137	TCCTCATGCTATCATGCGTCTT	RT-qPCR *act1* (fwd)
MP138	CCACGCTCCATGAGAATCTTC	RT-qPCR *act1* (rev)
MP169	GGTCTATGTTCCCACTGTTT	RT-qPCR *rho1* (fwd)
MP170	CTTCTTGTCCAGCCGTA	RT-qPCR *rho1* (rev)
PD07	GCGTCACTCGTCACATTA	ChIP-qPCR *pyp2* (fwd)
PD08	TGCTAAGCGACCGTTTATT	ChIP-qPCR *pyp2* (rev)
MP33	GCGCACGTCAAGACTGTC	universal KO checking primer (*kanMX6/natMX6* cassette), downstream, fwd
MP144	GTCGTTAGAACGCGGCTACA	universal KO checking primer, upstream, rev
MP150	AGGGATCGAAAGACATCCGC	*cbf11* KO checking primer, upstream, fwd, product size 953 bp (with MP144)
MP151	GCTTGTACACACGGCCTTCAA	*cbf11* KO checking primer, downstream, rev, product size 823 (with MP33)
JT40	GAAAGTCTCGGGCAAGTATC	RT-qPCR *pyp1* (fwd)
JT41	AGTTTGAGCAGCAGAGTAAG	RT-qPCR *pyp1* (rev)
JT42	GCGTAGGTCTATGGAGGATAC	RT-qPCR *ptc1* (fwd)
JT43	GTAGTCAGATGCTTGAATGCC	RT-qPCR *ptc1* (rev)
JT44	CTGAGTTGCGAGGACCTAAC	RT-qPCR *ptc2* (fwd)
JT45	ATCGTATGTATCACCGCTTCC	RT-qPCR *ptc2* (rev)
JT46	GAAGATGATTCCACCAACGG	RT-qPCR *ptc3* (fwd)
JT47	TTCCTCCTCGGCTTTATGAG	RT-qPCR *ptc3* (rev)
JT50	AAAATCTAGAATCAACGTGCTTTTG GTTCCC	*pyp1* KO upstream flanking region, XbaI, fwd, 805 bp

JT51	AAAACTCGAGTGTTTTGTATTAAGA ATATTTGGCCTT	*pyp1* KO upstream flanking region, XhoI, rev, 805 bp
JT52	AAAATCTAGAATCTTTGTTCCTGCA AGTTTGTCTT	*pyp1* KO downstream flanking region, XbaI, rev, 473 bp
JT53	AAAAAGATCTTTTTGACTGGATTTT TCTTGGCA	*pyp1* KO downstream flanking region, BglII, rev, 473 bp
JT54	TTTGTGGGGTTCTGCATTCTG	*pyp1* KO upstream checking primer
JT55	GGCCGTTTTAGACGAGGACC	*pyp1* KO downstream checking primer
JT56	AAAAGCTAGCTTGGCGGCATAGCC AAGAGC	*ptc1* KO upstream flanking region, NheI, fwd, 674 bp
JT57	AAAAAAGCTTCTCGGGCATTTACGT CACGC	*ptc1* KO upstream flanking region, HindIII, rev, 674 bp
JT58	AAAAGCTAGCCAGTGGCACGCAGA TTGGAGG	*ptc1* KO downstream flanking region, NheI, rev, 201 bp
JT59	AAAAGGATCCGGACATGGTTTTCCT TTGGGTCG	*ptc1* KO downstream flanking region, BamHI, rev, 201 bp
JT60	TGTCCCCTCAAATCCGTCCT	*ptc1* KO upstream checking primer
JT61	TTGATTCGAACAGTGGCACG	*ptc1* KO downstream checking primer
JT62	TTTAACTCTTCTTTCGGACGG	RT-qPCR *ptc4* (fwd)
JT63	ATTATTCGCAGCATCTTGAGG	RT-qPCR *ptc4* (rev)

2.7 Histone ChIP-seq data analysis

Sample isolation, sequencing and general data analysis was described previously [152] **(publication #3)**. Genes with altered H3K9ac in lipid metabolism mutants were assigned as follows: H3K9ac read coverage in *cbf11Δ* and *Pcut6MUT* samples was normalized to WT using the deepTools 3.5.1 [156] bigwigCompare (log2 scale, binsize 100) and regions with > 0.6 and < 0.6 fold change were selected as regions with increased and decreased H3K9ac occupancy, respectively. Based on the selected regions, corresponding genes were assigned if they overlapped the region or occurred downstream of the region hence the region represents the gene promoter. Genes conserved in both biological experiments were further analyzed for gene ontology enrichment which was performed using the GO term finder (https://go.princeton.edu/cgi-bin/GOTermFinder) [157].

2.8 *Pcut6MUT* RNA-seq

MP636 (*Pcut6MUT*) and JB32 (WT) cells were cultured in 12 mL YES to exponential phase (OD 0.5) and 10 mL was harvested (600g, 2 min) and the cell pellet was flash-frozen. RNA was extracted using acidic phenol - chloroform mixture followed by DNase treatment and cleanup using RNeasy columns (QIAgen 74104). RNA was eluted by TE buffer and quality was assessed on Bioanalyzer 2100 (Agilent) before sequencing. Samples were prepared from 3 biological replicates of MP636 and 1 biological experiment of JB32. Sequencing libraries were synthesized using KAPA mRNA HyperPrep Kit (Illumina platform) (Roche, KK8581) and analyzed on Illumina Nextseq 500 using NextSeq 500/550 High Output Kit v2.5 (75 Cycles) (Genetica, 20024906) with single-end, 75 bp, dual index 2x8 bp setup. The sequencing and library preparation was performed at the Institute of Molecular Genetics of the Czech Academy of Sciences (RVO–68378050). The *S. pombe* reference genome sequence and annotation were obtained from PomBase [158,159]. Read quality was checked using FastQC version 0.11.9 (https://www.bioinformatics.babraham.ac.uk/projects/fastqc/), and after trimming Illumina adapters and parts of reads with low base calling quality using Trimmomatic version 0.39 [160] the resulting reads were aligned to the *S. pombe* genome using HISAT2 2.1.0 [161] and SAMtools 1.10 [162,163]. Read coverage tracks were then computed and normalized to the respective mapped library sizes using deepTools 3.5.1 [156]. Mean read coverage from 3 *Pcut6MUT* samples was normalized to mean read coverage of 3 WT samples sequenced previously (V. Zemlianski, unpublished) using the deepTools 3.5.1 [156] bigwigCompare (log2 scale, binsize 10). For analysis of differentially expressed genes using DEseq2 package in R/Bioconductor [164–166], 3 *Pcut6MUT* samples were compared with 4 WT (JB32) samples out of which 1 sample was sequenced along with *Pcut6MUT* and 3 WT samples were sequenced previously (V. Zemlianski, unpublished).

3. RESULTS

My unpublished findings regarding lipid metabolism and its impact on chromatin biology and stress response will be presented in this chapter together with my published research papers obtained during my PhD studies.

3.1 Mitotic defects in fission yeast lipid metabolism “cut” mutants are suppressed by ammonium chloride

As a co-author of this publication I have performed the analysis of lipid droplet content and contributed strongly to the development of the lipid droplet image analysis tool. (IF 2.458[1]).

Zach R, Tvarůžková J, Schätz M, Tupa O, Grallert B, Převorovský M. Mitotic defects in fission yeast lipid metabolism 'cut' mutants are suppressed by ammonium chloride. FEMS Yeast Res. 2018 Sep 1;18(6):foy064. doi: 10.1093/femsyr/foy064.

This publication is marked as publication #1 in the text of this thesis.

[1] Impact factor according to the Journal Citation Reports, Clarivate Analytics, in the year of publication.

FEMS Yeast Research, 18, 2018, foy064

doi: 10.1093/femsyr/foy064
Advance Access Publication Date: 19 June 2018
Research Article

RESEARCH ARTICLE

Mitotic defects in fission yeast lipid metabolism 'cut' mutants are suppressed by ammonium chloride

Ró bert Zach[1,†], Jarmila Tvarůžková[1], Martin Schätz[1,2,‡], Ondřej Ťupa[1,2], Beáta Grallert[3] and Martin Převorovský[1,*,§]

[1]Department of Cell Biology, Faculty of Science, Charles University, Prague, Czech Republic, [2]Department of Computing and Control Engineering, University of Chemistry and Technology, Prague, Czech Republic and [3]Department of Radiation Biology, Institute for Cancer Research, Oslo University Hospital, Oslo, Norway

*Corresponding author: Department of Cell Biology, Faculty of Science, Charles University, Vinic˘na´ 7, Prague 2, 128 43, Czech Republic. Tel: +420 221951769; Fax: +420 221951758; E-mail: prevorov@natur.cuni.cz

One sentence summary: Ammonium chloride, a nitrogen source used in fission yeast growth media, was found to rescue cell division defects in mutants with perturbed lipid metabolism.

Editor: Terrance Cooper

†Ro´ bert Zach, http://orcid.org/0000-0002-7604-1648
‡Martin Scha¨ tz, http://orcid.org/0000-0003-0931-4017
§Martin Pr˘evorovsky´, http://orcid.org/0000-0003-0277-8361

ABSTRACT

Fission yeast 'cut' mutants show defects in temporal coordination of nuclear division with cytokinesis, resulting in aberrant mitosis and lethality. Among other causes, the 'cut' phenotype can be triggered by genetic or chemical perturbation of lipid metabolism, supposedly resulting in shortage of membrane phospholipids and insufficient nuclear envelope expansion during anaphase. Interestingly, penetrance of the 'cut' phenotype in mutants of the transcription factor *cbf11* and acetyl-coenzyme A carboxylase *cut6*, both related to lipid metabolism, is highly dependent on growth media, although the specific nutrient(s) affecting 'cut' occurrence is not known. In this study, we set out to identify the growth media component(s) responsible for 'cut' phenotype suppression in *L'cbf11* and *cut6–621* cells. We show that mitotic defects occur rapidly in *L'cbf11* cells upon shift from the minimal EMM medium ('cut' suppressing) to the complex YES medium ('cut' promoting). By growing cells in YES medium supplemented with individual EMM components, we identified ammonium chloride, an efficiently utilized nitrogen source, as a specific and potent suppressor of the 'cut' phenotype in both *L'cbf11* and *cut6–621*. Furthermore, we found that ammonium chloride boosts lipid droplet formation in wild-type cells. Our findings suggest a possible involvement of nutrient-responsive signaling in 'cut' suppression.

Keywords: *Schizosaccharomyces pombe*; *cut6*; *cbf11*; mitosis; ammonium chloride; cell cycle progression

INTRODUCTION

Faithful progression through cell cycle phases is essential for successful cell reproduction and transmission of genetic information to daughter cells. The whole process is tightly regulated and culminates with mitosis followed by cytokinesis. In standard growth media, the fission yeast *Schizosaccharomyces pombe* features very short G1 and S phases, a long G2 phase (~70% of the cycle) and a rapid mitosis, during which the nuclear envelope does not break down. Thus, when grown in standard complex medium (YES; yeast extract with supplements), the daughter nuclei have already completed S phase by the time cytokinesis has finished (Sabatinos and Forsburg 2010).

Received: 19 January 2018; **Accepted:** 15 June 2018

Interestingly, this timing can be influenced by manipulating G1 duration by providing the cells with different sources of nitrogen (Carlson *et al.* 1999).

Numerous *S. pombe* mutants have been identified in which septation and/or cytokinesis erroneously take place in the absence of normal sister chromatid separation. This often results in the so-called 'cut' terminal phenotype of undivided nucleus being intersected by the septum (Uemura and Yanagida 1984; Hirano *et al.* 1986; Samejima *et al.* 1993; Saitoh *et al.* 1996; Pr˘evorovsky´ *et al.* 2009). Most known 'cut' genes are directly involved in chromosome condensation, sister chromatid separation or anaphase progression (Yanagida 1998). Intriguingly, the 'cut' phenotype has also been described in mutants of several lipid metabolism genes (Saitoh *et al.* 1996; Pr˘evorovsky´ *et al.* 2009) and chemical inhibition of lipid synthesis leads to the 'cut' phenotype (Saitoh *et al.* 1996; Takemoto *et al.* 2016). During anaphase in *S. pombe*, the nuclear envelope undergoes rapid expansion, and it has recently been shown that fatty acid synthesis and phospholipid production are critical for successful separation of daughter nuclei and proper chromosome segregation (Makarova *et al.* 2016; Takemoto *et al.* 2016).

Cbf11 is a transcription factor belonging to the CSL (CBF1/RBP-Jκ/Suppressor of Hairless/LAG-1) family (Pr˘evorovsky´, Pu˘ ta and Folk 2007). Cbf11 regulates cell cycle progression and cell adhesion, and cells lacking *cbf11* show high incidence of the 'cut' phenotype when grown in YES (Pr˘evorovsky´ et al. 2009, 2016; Kwon *et al.* 2012). We have recently shown that Cbf11 regulates several lipid metabolism genes, including the essential *cut6* acetyl-coenzyme A carboxylase gene (Pr˘evorovsky´ et al. 2015, 2016). Cut6 is the rate-limiting enzyme of fatty acid synthesis and the *cut6–621* mutant exerts the 'cut' phenotype at restrictive temperature. The precise nature of the *cut6–621* mutation is not known (Saitoh *et al.* 1996). We have shown that decreased Cut6 activity likely contributes to the 'cut' phenotype of *L′cbf11* cells (Pr˘evorovsky´ *et al.* 2016). Curiously, several *L′cbf11*-associated defects can be suppressed by deletion of *pka1* or *sty1*, encoding the nutrient-sensing protein kinase A (PKA) catalytic subunit and general stress-response MAP kinase, respectively. Furthermore, the 'cut' phenotype of *L′cbf11* and *cut6–621* cells is largely diminished when cells are grown in the minimal defined EMM medium (Pr˘evorovsky´ et al. 2015, 2016).

Temperature-sensitive mutations in *cut4* and *cut9*, encoding essential anaphase promoting complex (APC/C) subunits, cause loss of viability at increased temperature when cells are grown in complex, yeast extract-based YPD medium. Notably, the lethality can be suppressed by inactivating the PKA pathway in the *cut4–533* and *cut9–665* mutants, or by growing the cells in EMM medium in the case of *cut4–533* (Yamashita *et al.* 1996; Yamada, Kumada and Yanagida 1997).

These observations collectively suggest that the availability of specific nutrients and/or signaling through nutrient-responsive pathways play an important role in the proper coordination of nuclear and cellular division. However, the nature of the nutrient(s) affecting this coordination is currently unknown. In this study, we set out to identify the EMM medium component(s) responsible for 'cut' phenotype suppression in the *L′cbf11* and *cut6–621* lipid metabolism mutants.

MATERIALS AND METHODS

Strains, media and cultivations

Schizosaccharomyces pombe strains used in this study were JB32 (*h*$^+$), MP44 (*h*$^+$ *L′cbf11::kanR*) (Pr˘evorovsky´ *et al.* 2015), MP218 (*h*$^+$ *cut6–621*) (Saitoh *et al.* 1996) and MP594 (*h*$^+$ *ptl2:GFP-kanR L′cbf11::natR*) (Yang *et al.* 2016). Unless indicated otherwise in the text, *S. pombe* cells were grown at 32°C according to standard procedures (Moreno, Klar and Nurse 1991). Temperature-sensitive strains were grown at 25°C, or at the semi-permissive temperature of 30°C. Cultivation media used in this study included the minimal defined EMM (Formedium, UK), complex YES (0.5% yeast extract, 3% glucose, 50 mg L^{-1} each of adenine, uracil, L-histidine, L-leucine and L-lysine) and YES variants supplemented with EMM-contained chemical compounds at concentrations listed in Table S1 (Supporting Information) (EMM composition as declared by the manufacturer). For medium shift experiments, exponentially growing *S. pombe* cells cultured in EMM were collected by centrifugation (1000 × g, 3 min, 25°C), resuspended in the same volume of fresh YES and incubated at 32°C. In all other experiments, cultures were grown in the indicated media for the whole duration of the experiment.

For growth rate measurements, *S. pombe* cells were first grown exponentially in YES. Culture volumes corresponding to ~1.2 × 10^6 cells were collected and centrifuged (1000 × g, 3 min, 25°C). Supernatants were removed and cell pellets were washed with the appropriate media. The resulting cell suspensions were then centrifuged again (1000 × g, 3 min, 25°C), supernatants were discarded, and cell pellets were resuspended in 1.5 mL of appropriate media. Aliquots of 1.4 mL of resulting cell suspensions were loaded into 12-well plates and introduced into the VarioSkan Flash plate reader (Thermo Scientific). Plates were incubated at 32°C with background shaking (180 spm, rotation diameter 20 mm). Optical densities were measured at 10 min intervals at λ = 595 nm. Doubling times (DT) were calculated according to the formula DT = 1/k, where k represents the slope of logarithmic phase of growth. Microsoft Excel 2007 was used for data processing and determination of k-value.

Microscopy

For nuclear staining, exponentially growing *S. pombe* cells were collected by centrifugation (1000 × g, 3 min, 25°C) and fixed by resuspending in 70% ethanol. Ethanol-fixed cells were centrifuged again (1000 × g, 3 min, 25°C) and resuspended in deionized H_2O. Cells were stained in suspension with 1 μg mL^{-1} 4′,6-diamidine-2′-phenylindole dihydrochloride (DAPI). Cell images were taken using the Olympus Cell R and Leica AF 6000LX microscopic systems. Frequency of 'cut' phenotype occurrence was determined by manual counting of 'cut' cells using the ImageJ software, version 1.51j8 (Schneider, Rasband and Eliceiri 2012). At least 200 cells per sample were analyzed.

For lipid droplet visualisation in live cells, exponentially growing *S. pombe* cells were stained in suspension with 0.1 μg mL^{-1} BODIPY™ 493/503 (Thermo Fisher Scientific) and briefly mixed by vortexing. No washes or sample dilution/concentration steps were performed to avoid stressing the cells or affecting their metabolism. Cells were centrifuged (1000 × g, 3 min, 25°C) and promptly imaged on soybean lectin-coated slides using the Olympus Cell R microscope. For imaging Ptl2-GFP, cells were fixed with 10% formaldehyde for 15 min, and washed three times with PBS, followed by microscopy. Fluorescent images were acquired as 16-bit Z-stacks (0.3 μm step size, 10 steps) in the green channel and were processed using the ImageJ software, version 1.51n (Schneider, Rasband and Eliceiri 2012) as maximum intensity projections. Care was taken to image all samples with the same exposure

settings and to adjust brightness and contrast of all images identically in order to ensure adequate comparison of lipid droplet staining.

Computational analysis of lipid droplet content

For every image, a mask corresponding to regions of dead or incompletely imaged cells was manually created. Each z-stack image was processed separately with a recursive thresholding method. The initial step was to separate cells from background using quantization to five levels. Further processing was done on the layer with the highest intensity by segmentation (Dougherty 2009). Dots with the lowest intensity were detected by this step. All segmented objects with area larger than 800 pixels or with non-circular shape were recursively taken to the next step of the segmentation process with a higher threshold value. The result of each level of the recursive thresholding method was a binary mask with segmented dots. The second step was to merge all segmented areas from the analyzed z-stacks. The last step was to remove detected objects that belonged to cells classified as dead or not present completely in the image, and objects having area smaller than 4 pixels. The final output of this process was a list of detected objects (i.e. lipid droplets) with extracted features. All processing was done in MATLAB Version: 9.2.0.556344 (R2017a) using Image Processing Toolbox Version 10.0 and Parallel Computing Toolbox Version 6.10.

RESULTS

The 'cut' phenotype of *L'cbf11* mutant manifests rapidly upon shift from EMM to YES medium

We previously showed that *L'cbf11* cells grown as batch cultures in the minimal EMM medium showed improved growth rate and greatly diminished incidence of the 'cut' phenotype compared to *L'cbf11* cells grown in the complex YES medium (Pr˘evorovsky´ et al. 2015, 2016). By performing a timecourse experiment, we now examined the dynamics of 'cut' occurrence upon shift from EMM to YES. Wild-type (WT) and *L'cbf11* cells were grown to exponential phase in EMM and culture aliquots were taken every hour. After 2 h of sampling, cells were collected by centrifugation, resuspended in YES and grown further. Cultures were sampled for four more hours and the frequency of 'cut' cells was determined by microscopy (Fig. 1). The medium shift did not show any immediate marked negative impact on culture growth rate, as determined by optical density measurements. However, at later timepoints the growth of *L'cbf11* cells slowed down significantly (timepoint 2 h vs 6 h; $P = 0.0026$; one-sided paired *t*-test). By contrast, the growth rate of WT cells did not decrease after the shift to YES (Fig. 1A). Strikingly, the occurrence of 'cut' phenotype in *L'cbf11* cells started to increase rapidly following the shift, reaching ~30% at 6 h, whereas WT cells showed little change in 'cut' frequency (Fig. 1B, C). Given the slow growth rate of *L'cbf11* cultures in YES (Pr˘evorovsky´ *et al.* 2009), these results imply that already the very first mitosis after medium shift was affected in *L'cbf11* cells. Our previous results indicated that some nutrient(s) present in EMM but absent or limiting in YES are responsible for the observed mitotic defects, as opposed to a situation in which YES would contain a 'poison' component (Pr˘evorovsky´ *et al.* 2015). Such rapid response thus indicates that the beneficial nutrient(s) is depleted very fast upon medium shift and/or a rapid change in nutrient-dependent signaling is involved in triggering the 'cut' phenotype in the *L'cbf11* mutant.

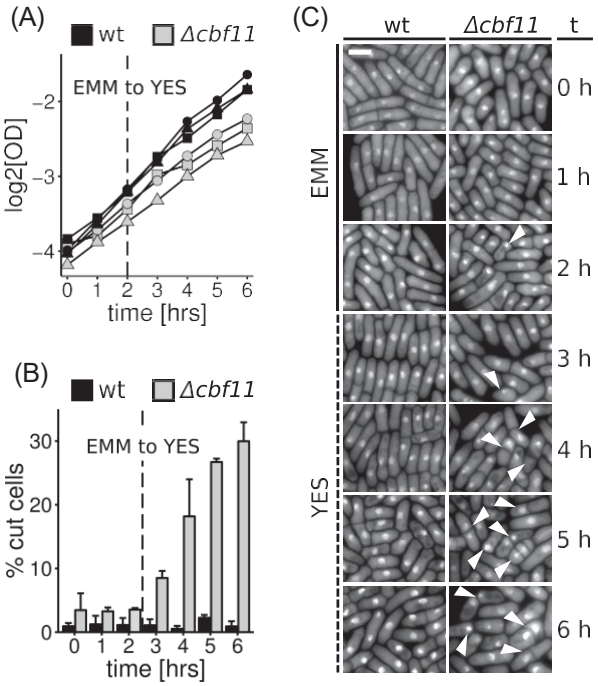

Figure 1. Dynamics of 'cut' phenotype occurrence in WT and *L'cbf11* upon shift from EMM to YES medium. (**A**) Growth curves of cells pre-cultured in EMM and then shifted to YES. No lag was apparent immediately after the shift. Data from three independent experiments are shown. (**B**) 'cut' *L'cbf11* cells start to accumulate within 1 hour after shift to YES. Mean values + SD of three independent experiments are shown. (**C**) Representative images of DAPI-stained cells from (B). 'Cut' cells are marked with arrowheads; scale bar = 5 μm.

'Minerals' component of EMM is responsible for growth rate suppression of *L'cbf11* cells

We next wanted to identify the particular EMM component(s) responsible for suppressing defects in the *L'cbf11* mutant. We first focused on suppression of growth rate defects. We supplemented YES with various EMM components and compared growth with standard YES and EMM. According to the medium manufacturer, apart from glucose EMM is comprised of three categories of chemicals: 'minerals', 'vitamins' and 'trace elements' (see Table S1, Supporting Information). WT cells grow faster in YES than in EMM (Petersen and Russell 2016), and YES supplementation had little effect on their growth rate. Of the three groups of supplements, only 'minerals' could improve growth (i.e. reduce the doubling time) of *L'cbf11* cells when added to YES (Fig. 2), even though the growth improvement was not statistically significant. Nevertheless, any specific impact of 'minerals' on the mitotic defects of *L'cbf11* cells remained to be established.

Addition of ammonium chloride to YES suppresses mitotic defects of *L'cbf11* and *cut-621* cells

To directly test the impact of EMM components on 'cut' phenotype occurrence, we performed experiments with supplemented YES variants and analyzed the percentage of 'cut' cells by microscopy. We found that the 'minerals' component of EMM was able to suppress 'cut' incidence in *L'cbf11* cultures (Fig. 3A). To identify the specific component(s) responsible for this suppressive effect, we analyzed 'cut' phenotype frequencies in YES supplemented with individual components of the

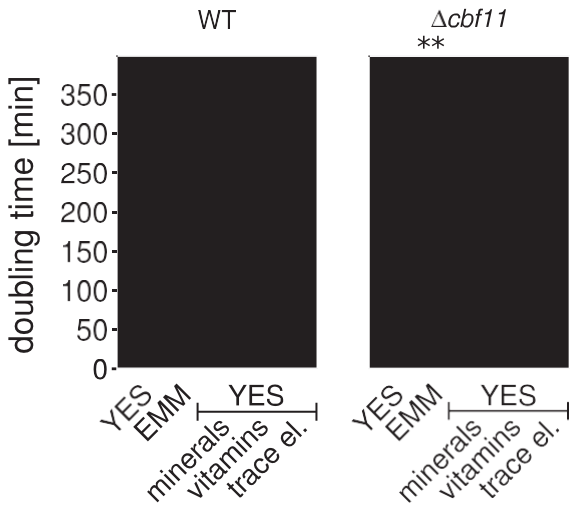

Figure 2. Effects of EMM medium components on doubling times of *L'cbf11* cultures. Addition of the 'minerals' group of EMM components can reduce the time required for biomass doubling of *L'cbf11* cells in YES. Data from ≥4 independent experiments are shown; horizontal lines represent mean values; significance of differences in *L'cbf11* doubling time in various media compared with *L'cbf11* grown in YES was tested by one-sided unpaired t-test: ** $P \leq 0.01$.

EMM 'minerals' mix (phthalic Acid K^+, Na_2HPO_4, NH_4Cl, $MgCl_2$, $CaCl_2$, KCl, Na_2SO_4). We observed strong 'cut' suppression in *L'cbf11* cells when ammonium chloride (NH_4Cl), which serves as the nitrogen source in EMM, was added to YES (Fig. 3A). Both WT and *L'cbf11* cells failed to grow in YES supplemented with the 'minerals' component Na_2HPO_4 (data not shown).

Cbf11 is a regulator of gene expression with a pleiotropic mutant phenotype (Pr˜evorovsky´ et al. 2009, 2015). To determine whether other, less pleiotropic, 'cut' mutants related to lipid metabolism can also be rescued by NH_4Cl, we analyzed the *cut6–621* temperature-sensitive mutant at the semi-permissive temperature of 30°C. Expression of the *cut6* acetyl-coenzyme A carboxylase gene is regulated directly by Cbf11, and the *cut6–621* mutant also shows high frequency of the 'cut' phenotype when grown in YES at semi-permissive temperature (Pr˜evorovsky´ *et al.* 2016). Indeed, the *cut6–621* mitotic defects were diminished when NH_4Cl was added to the growth medium (Fig. 3B), demonstrating that multiple lipid metabolism 'cut' mutants can be rescued by the addition of NH_4Cl.

The Cut6 enzyme requires biotin for its function and biotin uptake is mediated by the Vht1 proton-biotin symporter, that functions optimally under acidic pH (Stolz 2003). Differences in the pH of the growth media might thus affect Cut6 function and 'cut' phenotype occurrence. Therefore, we measured the pH of the growth media used in this study (Fig. 3C). We found that while EMM was indeed more acidic than YES, there was little change in YES pH upon addition of NH_4Cl. Furthermore, the only 'minerals' component able to lower pH when added to YES was potassium phthalate, which had no significant suppressive effect on 'cut' phenotype frequency (Fig. 3A). Since cellular metabolic processes might affect the cell's environment, we next measured pH of conditioned media in which cells had been grown overnight. As shown in Fig. 3D, the EMM medium is rather well buffered and its pH did not change much during cell cultivation. By contrast, both YES and YES supplemented with NH_4Cl showed poor buffering capacity and became acidified during cell culture, but still remained more basic than both fresh and conditioned EMM. As shown in Fig. 1B, 'cut' *L'cbf11* cells

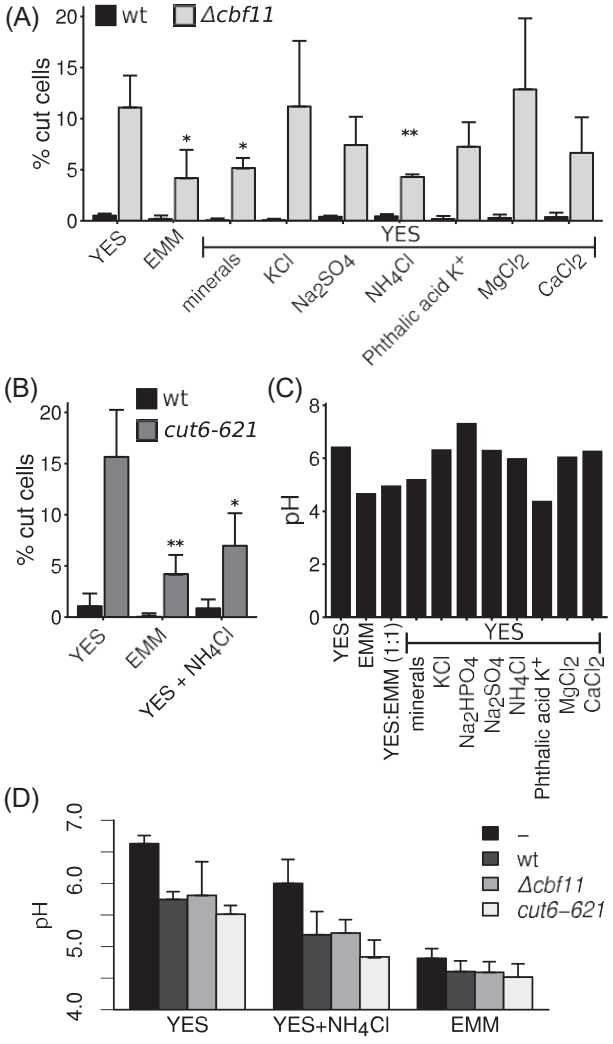

Figure 3. Effects of EMM medium components on 'cut' phenotype frequency in *L'cbf11* and *cut6–621* cultures. (**A**) Addition of the 'minerals' group of EMM components, and specifically addition of NH_4Cl, suppress mitotic defects of *L'cbf11* cells in YES. (**B**) Addition of NH_4Cl suppresses mitotic defects of *cut6–621* cells in YES at semi-permissive temperature. Mean values + SD of three independent experiments are shown in (A) and (B); significance of differences in 'cut' phenotype frequencies in *L'cbf11* or *cut6–621* in various media compared with corresponding mutant cultures grown in YES was tested by one-sided unpaired *t*-test: * $P \leq 0.05$, ** $P \leq 0.01$. (**C**) pH values for all media used in this study, before addition of cells. (**D**) pH values of selected conditioned media after overnight culture of the indicated strains. pH values of fresh media are indicated by ,,-'; means + SD of three independent experiments are shown.

appear rapidly after medium shift, so the factor affecting mitotic fidelity is likely present even in fresh, unconditioned media. Furthermore, we have previously shown that supplementing biotin in concentrations high enough to bypass the need for the Vht1 transporter had no suppressive effect on 'cut' frequency in *L'cbf11* cells (Stolz 2003; Pr˜evorovsky´ *et al.* 2016). It is therefore unlikely in this case that the pH of the medium plays a role in 'cut' phenotype suppression.

Ammonium chloride boosts lipid droplet formation

Fatty acid synthesis and production of membrane phospholipids are required for mitotic nuclear envelope expansion

and prevention of the 'cut' phenotype (Makarova *et al.* 2016; Takemoto *et al.* 2016). Since the addition of NH_4Cl suppressed mitotic defects of lipid metabolism 'cut' mutants grown in YES (Fig. 3), we tested whether this suppression was associated with changes in lipid metabolism. To this end, we determined the distribution of lipid droplets in exponentially growing WT, *L'cbf11* and *cut6–621* cells cultured in YES (with or without NH_4Cl) and EMM at 30°C. Lipid droplets are storage bodies composed of neutral triacylglycerols and sterol esters. Their formation shows cell-cycle and growth-phase dynamics (Long *et al.* 2012; Meyers *et al.* 2017) and they serve as a useful proxy for monitoring lipid biosynthesis (Rostron, Rolph and Lawrence 2015). Storage neutral lipids can be used to produce the membrane phospholipids required during mitosis (Makarova *et al.* 2016). Interestingly, higher lipid droplet formation was found in *S. pombe* cells grown in EMM than in YES (He *et al.* 2014).

First, we stained live, exponentially growing cells with BODIPY 493/503 to visualize neutral lipids. BODIPY dyes are insensitive to pH (Karolin *et al.* 1994) and, thus, should not be affected in this regard by the different growth media used. Stained cells were then imaged using fluorescence microscopy, and lipid droplets were identified by computational image analysis. As shown in Fig. 4A-C, lipid droplets in WT cells grown in EMM or YES supplemented with NH_4Cl were more abundant and typically had higher staining intensity than in cells grown in plain YES. This suggests that NH_4Cl can indeed boost fatty acid and/or neutral lipid production in *S. pombe*. The *cut6–621* mutant grown at semi-permissive temperature in YES showed aberrant lipid droplet distribution with many cells having abnormally large, intensely stained lipid bodies, while some showing only very faint lipid droplet staining. According to our image analysis, this aberrant distribution was not significantly rescued in EMM or in YES with NH_4Cl (data not shown). *L'cbf11* cells have decreased lipid droplet abundance when grown in YES and many cells do not contain any detectable lipid droplets at all. Both these phenotypes, low lipid droplet abundance and cell-to-cell heterogeneity, were largely rescued by growing *L'cbf11* cells in EMM (Fig. 4A and (Pr˘evorovsky´ *et al.* 2015)). By contrast, in YES with NH_4Cl the population heterogeneity persisted, with some cells showing wild type-like lipid droplet patterns and others having very few or no detectable lipid droplets (Fig. 4A). No significant rescue in lipid droplet distribution by NH_4Cl was detected by automated image analysis either (data not shown).

Next, we asked whether 'cut' cells specifically exerted any differences in lipid droplet content compared to 'non-cut' cells. We employed *L'cbf11* cells expressing GFP-tagged triacylglycerol lipase Ptl2, a marker of lipid droplets (Yang *et al.* 2016). Cells growing exponentially in YES were fixed, stained with DAPI, and their lipid droplet content and nuclear phenotype were determined by microscopy and manual image analysis. We found a significant overlap between 'cut' cells and the subpopulation devoid of any detectable lipid droplets (Fig. 4D). Moreover, 'cut' *L'cbf11* cells had significantly lower numbers of lipid droplets compared to 'non-cut' *L'cbf11* cells (Fig. 4E), demonstrating association between the 'cut' phenotype and lipid droplet content in the *L'cbf11* mutant. The biological significance of this link and any causal relationships remain to be determined.

In summary, while ammonium chloride can boost lipid production in WT cells, it remains unclear whether it also boosts specifically the production of membrane phospholipids required for successful nuclear division. To clarify the issue, a more direct readout of membrane phospholipid synthesis in 'cut' mutants will be needed.

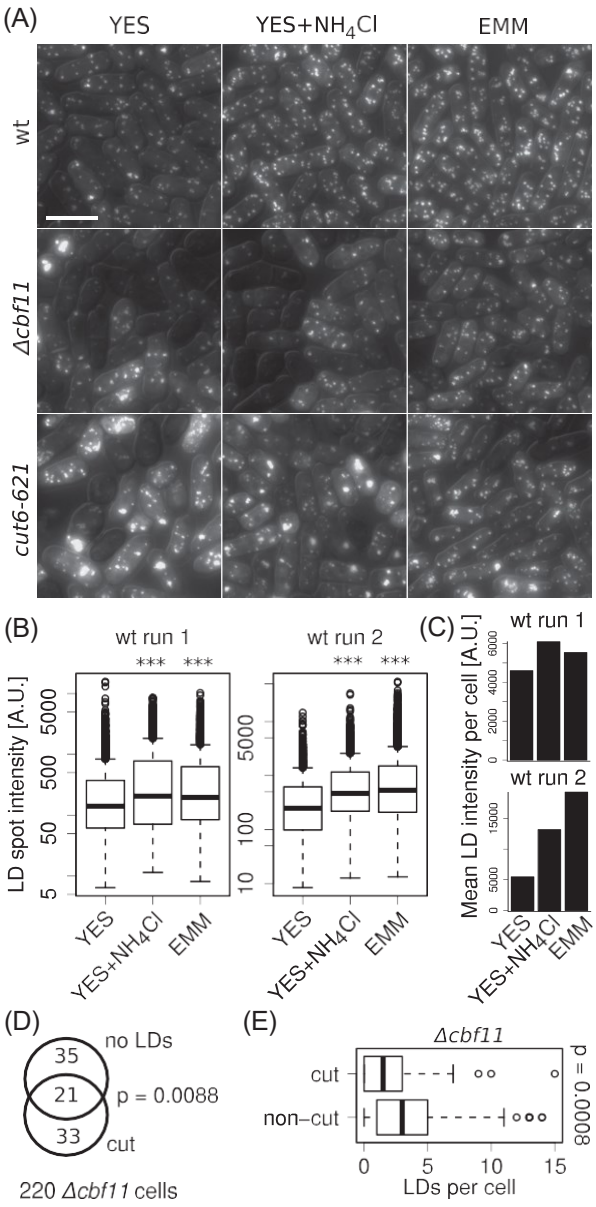

Figure 4. Lipid droplet formation in cells grown in YES, YES + NH_4Cl, and EMM. (**A**) Representative images of WT, *L'cbf11* and *cut6–621* cells stained with BODIPY™ 493/503 to visualize neutral lipids. DIC overlay is shown to mark cell boundaries. Scale bar = 10 μm. (**B**) Area-integrated staining intensities of individual lipid droplets in WT cells grown in the indicated media. Data from two independent experiments are shown; >180 cells were analyzed per sample. Significance of differences from distribution in YES was tested by one-sided unpaired Wilcoxon test: *** $P \leq 0.001$. (**C**) Means of total lipid droplet signal intensities per WT cell. (**D**) *L'cbf11* cells with the 'cut' phenotype are enriched for cells lacking detectable lipid droplets (one-sided Fisher's exact test). (**E**) In the *L'cbf11* mutant, 'cut' cells contain fewer lipid droplets compared to 'non-cut' cells (one-sided unpaired Wilcoxon test).

DISCUSSION

Fission yeast mutants in the genes *cbf11* and *cut6* show the mitotic 'cut' phenotype when grown in complex medium (Saitoh *et al.* 1996; Pr˘evorovsky´ *et al.* 2009). Cut6 is an essential acetyl-coenzyme A carboxylase involved in fatty acid synthesis, while Cbf11 is a transcription factor that regulates multiple genes involved in lipid metabolism, including *cut6*. We have

previously shown that the mitotic defects in *L'cbf11* and *cut6–621* can be rescued by growing the cells in the minimal EMM medium (Prˇevorovskyˊ et al. 2015, 2016). We have now identified ammonium chloride (NH_4Cl), a major component of EMM and an efficiently utilized nitrogen source, as the compound specifically responsible for the rescue. Furthermore, we have shown that addition of NH_4Cl increases lipid droplet content in WT cells, suggesting that NH_4Cl affects fatty acid and/or neutral lipid metabolism.

The YES medium is often referred to as 'rich', which is rather confusing in terms of nitrogen content. Based on information from various media manufacturers, YES typically contains ~0.06% nitrogen, embedded in a range of substances such as amino acids, nucleobases and vitamins. These substances differ in the ease with which their nitrogen is utilized by fission yeast cells, many of them representing 'poor' nitrogen sources (Petersen and Russell 2016). Moreover, a complex enzymatic apparatus is required to utilize such varied mixture of nitrogen sources. On the other hand, EMM contains ~0.13% nitrogen, more than twice as much as YES does. Importantly, the vast majority of this nitrogen is present as just one substance—ammonium chloride, a 'good' nitrogen source. Thus, with regard to nitrogen, EMM is the 'rich' medium, not YES. Since *S. pombe* shows exquisite sensitivity to both nitrogen source quantity and quality (Davie, Forte and Petersen 2015), the difference between YES and EMM is significant and concordant with the observed differential effects of these media on cell physiology and mitotic fidelity.

We found that NH_4Cl boosted lipid droplet content in exponentially growing WT cells (Fig. 4A). Curiously, accumulation of lipids and/or lipid droplets in yeasts has previously been linked rather with nutrient-poor conditions, such as stationary phase in *S. pombe* (Meyers *et al.* 2017), nitrogen limitation in *Yarrowia lipolytica* (Kerkhoven *et al.* 2016), or TORC1 inhibition by rapamycin in *S. cerevisiae* (Madeira *et al.* 2015). However, increased lipid droplet content in EMM vs YES has already been reported by others for *S. pombe* (He *et al.* 2014). Importantly, the lipid droplet increase triggered by NH_4Cl or EMM is modest (i.e. increased 'baseline exponential content') compared to the pronounced lipid droplet accumulation in stationary *S. pombe* cells. Therefore, these might be two independent phenomena with distinct regulation, each taking place at a different stage of culture growth.

The 'cut' phenotype occurrence upon perturbation of lipid metabolism has been previously ascribed to insufficient fatty acid production and membrane phospholipid supply during anaphase, when rapid expansion of the nuclear envelope takes place. Hampered nuclear elongation during the anaphase of a closed mitosis then results in the collapse of the division spindle (Makarova *et al.* 2016; Takemoto *et al.* 2016). So what could be the mechanism whereby NH_4Cl rescues the 'cut' mitotic defects? One possibility is that NH_4Cl increases membrane phospholipid production, thereby providing mutants with compromised lipid metabolism with the required nuclear envelope components. While we found association between the 'cut' phenotype and decreased lipid droplet content in the *L'cbf11* strain, we did not see any significant corrective effect of NH_4Cl on lipid droplet amount and distribution in either *L'cbf11* or *cut6–621* mutant cells (Fig. 4). Since lipid droplet content represents a complex and only indirect readout of phospholipid production capacity and/or might not be reliable in mutants with deregulated lipid metabolism, the nature of the NH_4Cl-mediated suppression of mitotic defects with regard to lipid metabolism needs to be studied further, using more direct readouts. Interestingly, lipid metabolism is extensively regulated during the cell cycle in both yeast and human cells (the latter featuring an open mitosis) and this dynamics is important for successful cell division (Stumpf *et al.* 2013; Atilla-Gokcumen *et al.* 2014; Blank *et al.* 2017).

NH_4Cl is not directly utilized in fatty acid synthesis, so any NH_4Cl-dependent changes in lipid metabolism are likely brought about indirectly, possibly via nitrogen-sensitive signaling pathways. Indeed, the mitotic defects of *L'cbf11* cells are also rescued by mutations in major nutrient-responsive kinases, *pka1* and *sty1* (Prˇevorovskyˊ *et al.* 2015), both of which are sensitive to nitrogen availability (Maeda *et al.* 1994; Shiozaki and Russell 1996). Moreover, the lethality of the temperature-sensitive 'cut' mutants in *cut4* and *cut9*, encoding subunits of APC/C likely unrelated to lipid metabolism, can be rescued by PKA inactivation and/or by growing the cells in EMM. Nevertheless, the specific impact on 'cut' occurrence or the particular nutrient(s) responsible for the suppression were not analyzed (Yamashita *et al.* 1996; Yamada, Kumada and Yanagida 1997). Therefore, a common theme emerges where 'cut' phenotype caused by a broad range of defects can be rescued by altered nutrient availability and/or sensing. However, it remains to be established whether there is one common molecular mechanism of nutrient-related 'cut' suppression, or whether multiple (complementary) mechanisms exist. One possible speculative mechanism involves NH_4Cl acting via Pka1/Sty1-dependent signaling to modulate lipid metabolism in a manner promoting production of membrane phospholipids, thus supporting timely nuclear envelope expansion and faithful mitotic progression.

In future, it will be interesting to determine how fission yeast cells (and particularly 'cut' mutants related to lipid metabolism) respond to different doses of NH_4Cl. It will also be important to examine the effects of other ammonium sources (e.g. ammonium sulfate, which is used in some fission yeast media) and other nitrogen sources, in general, including suboptimal ones. The potential involvement of TOR signaling, another major nitrogen-responsive regulator, in the suppression of the 'cut' phenotype should also be addressed.

SUPPLEMENTARY DATA

Supplementary data are available at *FEMSYR* online.

ACKNOWLEDGEMENT

We thank Dr. Jakub Hranıˊcˇek for pilot AAS analyses of YES and EMM media composition, Ondrˇej Sˇebesta for help with microscopy, Eva Krellerovaˊ and Adeˊla Kmochovaˊ for technical assistance, members of the GenoMik and ReGenEx labs for their help and discussions, Erik Boye for critical comments on this manuscript and Yasushi Hiraoka for strains. The *cut6–621* strain was provided by The Yeast Genetic Resource Center Japan. Microscopy was performed in the Laboratory of Confocal and Fluorescence Microscopy co-financed by the European Regional Development Fund and the state budget of the Czech Republic (Project no. CZ.1.05/4.1.00/16.0347 and CZ.2.16/3.1.00/21515).

FUNDING

This work was supported by the Charles University [PRIMUS/MED/26, UNCE 204013, GAUK 1308217, SVV 260310], the European Union [Erasmus+ to R.Z.], the Norwegian Cancer Society and the Norwegian South-Eastern Health Authority.

Conflict of interest. None declared.

REFERENCES

Atilla-Gokcumen GE, Muro E, Relat-Goberna J *et al.* Dividing cells regulate their lipid composition and localization. *Cell* 2014;**156**:428–39.

Blank HM, Perez R, He C *et al.* Translational control of lipogenic enzymes in the cell cycle of synchronous, growing yeast cells. *EMBO J* 2017;**36**:487–502.

Carlson CR, Grallert B, Stokke T *et al.* Regulation of the start of DNA replication in *Schizosaccharomyces pombe*. *J Cell Sci* 1999;**112**:939–46.

Davie E, Forte GMA, Petersen J. Nitrogen regulates AMPK to control TORC1 signaling. *Curr Biol* 2015;**25**:445–54.

Dougherty G. *Digital Image Processing for Medical Applications*. Cambridge: Cambridge University Press, 2009.

He Y, Yam C, Pomraning K *et al.* Increase in cellular triacylglycerol content and emergence of large ER-associated lipid droplets in the absence of CDP-DG synthase function. *MBoC* 2014;**25**:4083–95.

Hirano T, Funahashi SI, Uemura T *et al.* Isolation and characterization of *Schizosaccharomyces pombe cut* mutants that block nuclear division but not cytokinesis. *EMBO J* 1986;**5**:2973–9.

Karolin J, Johansson LBA, Strandberg L *et al.* Fluorescence and absorption spectroscopic properties of dipyrromethene boron difluoride (BODIPY) derivatives in liquids, lipid membranes, and proteins. *J Am Chem Soc* 1994;**116**:7801–6.

Kerkhoven EJ, Pomraning KR, Baker SE *et al.* Regulation of amino-acid metabolism controls flux to lipid accumulation in *Yarrowia lipolytica*. *npj Syst Biol Appl* 2016;**2**:16005.

Kwon EG, Laderoute A, Chatfield-Reed K *et al.* Deciphering the Transcriptional-Regulatory network of flocculation in *Schizosaccharomyces pombe*. Kumar A (ed.). *PLoS Genet* 2012;**8**:e1003104.

Long AP, Manneschmidt AK, VerBrugge B *et al.* Lipid droplet de novo formation and fission are linked to the cell cycle in fission yeast. *Traffic* 2012;**13**:705–14.

Madeira JB, Masuda CA, Maya-Monteiro CM *et al.* TORC1 inhibition induces lipid droplet replenishment in yeast. *Mol Cell Biol* 2015;**35**:737–46.

Maeda T, Watanabe Y, Kunitomo H *et al.* Cloning of the *pka1* gene encoding the catalytic subunit of the cAMP-dependent protein kinase in *Schizosaccharomyces pombe*. *J Biol Chem* 1994;**269**:9632–7.

Makarova M, Gu Y, Chen J-S *et al.* Temporal regulation of lipin activity diverged to account for differences in mitotic programs. *Curr Biol* 2016;**26**:237–43.

Meyers A, Chourey K, Weiskittel TM *et al.* The protein and neutral lipid composition of lipid droplets isolated from the fission yeast, *Schizosaccharomyces pombe J Microbiol* 2017;**55**:112–22.

Moreno S, Klar A, Nurse P. Molecular genetic analysis of fission yeast *Schizosaccharomyces pombe*. *Methods Enzymol* 1991;**194**:795–823.

Petersen J, Russell P. Growth and the environment of *Schizosaccharomyces pombe*. *Cold Spring Harb Protoc* 2016;**2016**: doi: 10.1101/pdb.top079764.

Pr˘evorovsky´ M, Grous˘l T, Stan˘urova´ J *et al.* Cbf11 and Cbf12, the fission yeast CSL proteins, play opposing roles in cell adhesion and coordination of cell and nuclear division. *Exp Cell Res* 2009;**315**:1533–47.

Pr˘evorovsky´ M, Oravcova´ M, Tvaru˚z˘kova´ J *et al.* Fission yeast CSL transcription factors: Mapping their target genes and biological roles. *PLoS One* 2015;**10**:e0137820.

Pr˘evorovsky´ M, Oravcova´ M, Zach R *et al.* CSL protein regulates transcription of genes required to prevent catastrophic mitosis in fission yeast. *Cell Cycle* 2016;**15**:3082–93.

Pr˘evorovsky´ M, Pu˚ta F, Folk P. Fungal CSL transcription factors. *BMC Genomics* 2007;**8**:233.

Rostron KA, Rolph CE, Lawrence CL. Nile red fluorescence screening facilitating neutral lipid phenotype determination in budding yeast, *Saccharomyces cerevisiae*, and the fission yeast *Schizosaccharomyces pombe*. *Antonie Van Leeuwenhoek* 2015;**108**:97–106.

Sabatinos SA, Forsburg SL. Molecular genetics of *Schizosaccharomyces pombe*. *Methods Enzymol* 2010;**470**:759–95.

Saitoh S, Takahashi K, Nabeshima K *et al.* Aberrant mitosis in fission yeast mutants defective in fatty acid synthetase and acetyl CoA carboxylase. *J Cell Biol* 1996;**134**:949–61.

Samejima I, Matsumoto T, Nakaseko Y *et al.* Identification of seven new *cut* genes involved in *Schizosaccharomyces pombe* mitosis. *J Cell Sci* 1993;**105**:135–43.

Shiozaki K, Russell P. Conjugation, meiosis, and the osmotic stress response are regulated by Spc1 kinase through Atf1 transcription factor in fission yeast. *Genes Dev* 1996;**10**:2276–88.

Schneider CA, Rasband WS, Eliceiri KW. NIH Image to ImageJ: 25 years of image analysis. *Nat Methods* 2012;**9**:671–5.

Stolz J. Isolation and characterization of the plasma membrane biotin transporter from *Schizosaccharomyces pombe*. *Yeast* 2003;**20**:221–31.

Stumpf CR, Moreno MV, Olshen AB *et al.* The translational landscape of the mammalian cell cycle. *Mol Cell* 2013;**52**:574–82.

Takemoto A, Kawashima SA, Li J-J *et al.* Nuclear envelope expansion is crucial for proper chromosomal segregation during a closed mitosis. *J Cell Sci* 2016;**129**:1250–9.

Uemura T, Yanagida M. Isolation of type I and II DNA topoisomerase mutants from fission yeast: single and double mutants show different phenotypes in cell growth and chromatin organization. *EMBO J* 1984;**3**:1737–44.

Yamada H, Kumada K, Yanagida M. Distinct subunit functions and cell cycle regulated phosphorylation of 20S APC/cyclosome required for anaphase in fission yeast. *J Cell Sci* 1997;**110**:1793–804.

Yamashita YM, Nakaseko Y, Samejima I *et al.* 20S cyclosome complex formation and proteolytic activity inhibited by the cAMP/PKA pathway. *Nature* 1996;**384**:276–9.

Yanagida M. Fission yeast cut mutations revisited: control of anaphase. *Trends Cell Biol* 1998;**8**:144–9.

Yang H-J, Osakada H, Kojidani T *et al.* Lipid droplet dynamics during *Schizosaccharomyces pombe* sporulation and their role in spore survival. *Biol Open* 2016:8–10.

3.2 Analysis of lipid droplet content in fission and budding yeasts using automated image processing

As the first author of this method publication I have performed all microscopic experiments included in the figures and required for troubleshooting of cell/media staining. I was the co-architect and tester of the image analysis software, although the actual Matlab script was developed by Ing. Ondřej Ťupa and Dr. Martin Schätz. (IF 1.163).

Princová J, Schätz M, Ťupa O, Převorovský M. Analysis of Lipid Droplet Content in Fission and Budding Yeasts using Automated Image Processing. J Vis Exp. 2019 Jul 17;(149). doi: 10.3791/59889.

This publication is marked as publication #2 in the text of this thesis.

Video Article

Analysis of Lipid Droplet Content in Fission and Budding Yeasts using Automated Image Processing

Jarmila Princová[1], Martin Schätz[1], Ondřej Ťupa[1], Martin Převorovský[1]

[1]Faculty of Science, Charles University

Correspondence to: Martin Převorovský at prevorov@natur.cuni.cz

URL: https://www.jove.com/video/59889
DOI: doi:10.3791/59889

Keywords: Immunology and Infection, Issue 149, neutral lipid storage, fluorescence microscopy, quantitative microscopy, BODIPY 493/503, *Schizosaccharomyces pombe*, *Schizosaccharomyces japonicus*, *Saccharomyces cerevisiae*

Date Published: 7/17/2019

Citation: Princová, J., Schätz, M., Ťupa, O., Převorovský, M. Analysis of Lipid Droplet Content in Fission and Budding Yeasts using Automated Image Processing. *J. Vis. Exp.* (149), e59889, doi:10.3791/59889 (2019).

Abstract

Lipid metabolism and its regulation are of interest to both basic and applied life sciences and biotechnology. In this regard, various yeast species are used as models in lipid metabolic research or for industrial lipid production. Lipid droplets are highly dynamic storage bodies and their cellular content represents a convenient readout of the lipid metabolic state. Fluorescence microscopy is a method of choice for quantitative analysis of cellular lipid droplets, as it relies on widely available equipment and allows analysis of individual lipid droplets. Furthermore, microscopic image analysis can be automated, greatly increasing overall analysis throughput. Here, we describe an experimental and analytical workflow for automated detection and quantitative description of individual lipid droplets in three different model yeast species: the fission yeasts *Schizosaccharomyces pombe* and *Schizosaccharomyces japonicus*, and the budding yeast *Saccharomyces cerevisiae*. Lipid droplets are visualized with BODIPY 493/503, and cell-impermeable fluorescent dextran is added to the culture media to help identify cell boundaries. Cells are subjected to 3D epifluorescence microscopy in green and blue channels and the resulting z-stack images are processed automatically by a MATLAB pipeline. The procedure outputs rich quantitative data on cellular lipid droplet content and individual lipid droplet characteristics in a tabular format suitable for downstream analyses in major spreadsheet or statistical packages. We provide example analyses of lipid droplet content under various conditions that affect cellular lipid metabolism.

Video Link

The video component of this article can be found at https://www.jove.com/video/59889/

Introduction

Lipids play crucial roles in cellular energy and carbon metabolism, synthesis of membrane components, and production of bioactive substances. Lipid metabolism is fine-tuned according to environmental conditions, nutrient availability and cell-cycle phase[1]. In humans, lipid metabolism has been connected to diseases, such as obesity, type II diabetes and cancer[2]. In industry, lipids produced by microorganisms, such as yeasts, represent a promising source of renewable diesel fuels[3]. Cells store neutral lipids in so-called lipid droplets (LDs). These evolutionarily conserved bodies are composed of triacylglycerols, steryl esters, an outer phospholipid monolayer and associated proteins[1]. LDs originate in the endoplasmic reticulum, exert cell-cycle or growth-phase dynamics, and are important for cellular lipid homeostasis[1]. LD number and morphology can be used as a convenient proxy when assaying lipid metabolism under various growth conditions or when screening a panel of mutants. Given their dynamic nature, techniques capable of analyzing the properties of individual LDs are of particular interest in studies of lipid metabolism.

Various yeast species have been used to describe lipid-related metabolic pathways and their regulation, or used in biotechnology to produce interesting compounds or fuels[1]. Furthermore, for model yeasts, such as the budding yeast *Saccharomyces cerevisiae* or the distantly related fission yeast *Schizosaccharomyces pombe*, genome-wide deletion strain libraries are available that can be used for high-throughput screens[4,5]. Recently LD composition and dynamics have been described in *S. pombe*[6,7,8,9], and mutants related to lipid metabolism have been isolated in the emerging model yeast *Schizosaccharomyces japonicus*[10].

Numerous techniques are available to study LD content and dynamics. Most employ some kind of staining of LDs with lipophilic dyes such as Nile Red or BODIPY 493/503. The latter shows more narrow excitation and emission spectra, and increased specificity towards neutral lipids (LDs) as opposed to phospholipids (membranes)[11]. Fluorimetric and flow-cytometry methods have been used successfully in various fungal species to uncover genes and growth conditions that affect storage lipid content[12,13,14,15]. While these methods are suitable for high-throughput applications, they cannot measure the numbers and morphology of individual LDs in cells, which can differ dramatically between growth conditions and genotypes. Coherent Raman scattering or digital holographic microscopy are label-free methods that yield LD-level data, but require specialized expensive equipment[16,17,18]. Fluorescence microscopy, on the other hand, can provide detailed data on LD content, while utilizing commonly available instruments and image analysis software tools. Several analysis workflows exist that feature various degrees of sophistication and automation in cell/LD detection from image data, and are optimized for different cell types, such as metazoan cells with large LDs[19,20,21], or budding yeasts[17,22,23]. Some of these approaches only work in 2D (e.g., on maximum projection images), which may fail to reliably

describe the cellular LD content. To our knowledge, no tools exist for determination of LD content and morphology from fission yeast microscopic data. Development of automated and robust LD-level analyses would bring increased sensitivity and enhanced statistical power, and provide rich information on neutral lipid content, ideally in multiple yeast species.

We have developed a workflow for LD content analysis from 3D fluorescence microscopy images of yeast cells. Live cells are stained with BODIPY 493/503 and Cascade Blue dextran to visualize LDs and determine cell boundaries, respectively. Cells are immobilized on glass slides and subjected to z-stack imaging using a standard epifluorescence microscope. Images are then processed by an automated pipeline implemented in MATLAB, a widely used (commercial) package for statistical analyses. The pipeline performs image preprocessing, segmentation (cells vs. background, removal of dead cells), and LD identification. Rich LD-level data, such as LD size and fluorescence intensity, are then provided in a tabular format compatible with major spreadsheet software tools. The workflow was used successfully to determine the impact of nitrogen source availability on lipid metabolism in *S. pombe*[24]. We now demonstrate the functionality of the workflow in *S. pombe*, *S. japonicus* and *S. cerevisiae*, using growth conditions or mutants that affect cellular LD content.

Protocol

1. Preparation of Solutions and Media

1. **Prepare lipid staining solution.**
   1. To prepare stock lipid staining solution dissolve 10 mg of BODIPY 493/503 in 10 mL of anhydrous DMSO (final concentration 1 mg/mL). Dissolve the whole content of a 10 mg BODIPY 493/503 vial to prevent loss of material during weighing.
      CAUTION: DMSO may pass through the skin. Wear appropriate personal protective equipment.
   2. Prepare working lipid staining solution by mixing 100 µL of the 1 mg/mL BODIPY 493/503 stock solution and 900 µL of anhydrous DMSO (final concentration 0.1 mg/mL).
   3. Aliquot the stock and working solutions, and store at -20 °C.
      NOTE: Dissolved BODIPY 493/503 is stable for several years at -20 °C. However, the solution has to be protected from moisture and light.
2. To prepare stock solution for cell boundary visualization, dissolve 25 mg of Cascade Blue dextran (whole vial) in 2.5 mL of deionized water (final concentration 10 mg/mL). Aliquot the stock solution and store at -20 °C protected from light.
3. To prepare microscope slide coating solution, dissolve 5 mg of soybean lectin in 5 mL of deionized water (final concentration 1 mg/mL). Aliquot the lectin solution and store at -80 °C.
   NOTE: The lectin solution is stable for several years at -80 °C. Aliquots currently at use may be stored at -20 °C.
4. **Prepare cultivation media.**
   1. To prepare 400 mL of complex YES cultivation medium for *S. pombe* and *S. japonicus,* dissolve 2 g of yeast extract and 0.1 g of SP supplements (if required for auxotrophic mutants) in 340 mL of deionized water in a 500 mL bottle and autoclave. Add 60 mL of 20% (w/v) of separately autoclaved or filter-sterilized glucose in aseptic conditions.
   2. To prepare 400 mL of defined EMM cultivation medium for *S. pombe* and *S. japonicus,* dissolve 4.9 g of EMM broth without dextrose in 360 mL of deionized water in a 500 mL bottle and autoclave. Add 40 mL of 20% (w/v) of separately autoclaved or filter-sterilized glucose in aseptic conditions.
      NOTE: For general guidelines on *S. pombe* and *S. japonicus* cultivation see[25] and[26], respectively.
   3. To prepare 300 mL of complex YPAD cultivation medium for *Saccharomyces cerevisiae*, dissolve 3 g of yeast extract, 6 g of peptone and 30 mg of adenine sulphate in 270 mL of deionized water in a 500 mL bottle and autoclave. Add 30 mL of 20% (w/v) of separately autoclaved or filter-sterilized glucose in aseptic conditions.
   4. To prepare 300 mL of defined minimal medium for *S. cerevisiae,* dissolve 2 g of yeast nitrogen base (without amino acids) in 270 mL of deionized water in a 500 mL bottle and autoclave. Add 30 mL of 20% (w/v) of separately autoclaved or filter-sterilized glucose in aseptic conditions.
      NOTE: For general guidelines on *S. cerevisiae* cultivation see[27].

2. Cell Cultivation

1. **Growing *S. pombe* or *S. japonicus* to exponential or early stationary phase.**
   1. In the morning, inoculate 5 mL of YES medium with fresh fission yeast biomass. Incubate at 32 °C with shaking (180 rpm) for several hours.
      NOTE: For all cultivations, use Erlenmeyer flasks having 10 times the volume of culture to ensure proper aeration. Some laboratories prefer to grow fission yeasts at 30 °C, but cultivation temperature of 32 °C results in shorter doubling times without detrimental effects to the cells, thus reducing the total time required to perform an experiment[25,28].
   2. In late afternoon of the same day (after at least 6 hours of cultivation), dilute the culture with fresh YES medium to a 10 mL final culture volume so that it reaches the desired optical density (OD) (or number of cells/mL) the following morning, and incubate at 32 °C with shaking (180 rpm). It is of advantage to know the doubling time of each used strain to accurately determine the dilution factor (use Equation 1).

Equation 1 $$V_{culture} = \frac{V_{final} \cdot OD_{final}}{OD_{current} \cdot 2^{\frac{t - t_{lag}}{t_{DT}}}}$$

Where $V_{culture}$ is the preculture volume needed for dilution, V_{final} is the total volume of the new culture (10 mL for standard cultivations), OD_{final} is the desired OD to be reached the following morning, $OD_{current}$ is the currently measured OD of the preculture, t is the time of

cell growth until harvesting, t_{lag} is duration of the lag phase (depends on laboratory conditions, needs to be empirically defined) and t_{DT} is the doubling time of the strain.
NOTE: When exponential-phase cells are to be analyzed, do not let precultures reach the stationary phase as this dramatically alters cell physiology (including LD content) for several subsequent generations.

3. In the morning of imaging day, if the culture reached slightly higher OD than required (in case of exponential-phase cells), dilute it with fresh YES and continue incubation for at least two more doubling times before staining of LDs. Otherwise proceed directly to staining (Section 3).

2. **Growing *S. cerevisiae* to exponential and stationary phase.**
    1. In the afternoon, inoculate 10 mL of YPAD medium with a small amount of fresh budding yeast biomass and incubate overnight at 30 °C with shaking (180 rpm).
    2. The morning of imaging day, dilute the culture to OD 0.1 in 10 mL of YPAD medium and grow to the required OD (e.g., OD 1 for exponential phase). Perform any culture dilutions as described in step 2.1.2. Proceed to staining (Section 3).

3. Lipid Droplet Staining

1. Prepare a microscope cover slip for each sample to be imaged. Spread 1 µL of slide coating solution onto a clean cover slip using the long side of a horizontally positioned pipette tip. Allow the coating solution to dry completely and store the cover slips in a dust-free environment.
NOTE: Glass slides and coverslips can be cleaned prior to use if required. The cleaning procedure consists of washing with dishwashing detergent, rinsing with water, overnight soaking in 3% hydrochloric acid, and washing with distilled water. Cleaned slides and coverslips are stored in pure ethanol until use.
2. Measure the OD of cell culture or number of cells/mL, as required. Try to reach similar values among all tested strains to ensure comparable experimental conditions.
3. Pipette 1 mL of each cell culture to a 1.5 mL microcentrifuge tube. For *S. cerevisiae* only, add 5 µL of the slide coating solution, vortex briefly, and incubate at 30 °C with shaking for 5 min.
4. Add 1 µL of the lipid staining solution to each culture aliquot and vortex briefly. Then add 10 µL of the cell boundary visualization solution and vortex briefly.
NOTE: Do not prepare pre-mixed solutions of both stains as this leads to fluorescence quenching of BODIPY 493/503.
5. Collect the cells by centrifugation (1,000 x *g*, 3 min, RT) and remove almost all supernatant (~950 µL). Resuspend the cells in the remaining supernatant.
6. Pipette 2 µL of the dense cell suspension on a lectin-coated cover slip and place onto a clean microscope slide. The cells should form a monolayer. Proceed to microscopy (Section 4) as quickly as possible to minimize artefacts in imaging; process maximum of two samples at a time.

4. Setting up the Microscope and Imaging

1. **Optimize imaging conditions.**
NOTE: Setting up the microscope requires long exposures to strong light sources that could cause damage to the sample and skew results. Therefore, set up the imaging conditions using a dedicated sample slide that will not be further used for LD quantification.
    1. Focus on the cells using phase contrast or differential interference contrast (DIC).
    NOTE: Phase contrast or DIC images may be taken for reference, but they are not used during the automated image analysis step.
    2. Set z-stack settings to span the whole cell volume. The total vertical distance depends on the cell size; the number of optical slices depends on the numerical aperture of the objective (point spread function in z-axis). Set the focus to move relative to the central focal plane.
    NOTE: The optimal number of slices is often set by the microscope control software and does not need to be calculated manually. The typical cell widths are 3-5 µm for *S. pombe*, 4-7 µm for *S. japonicus*, and 3-7 µm for *S. cerevisiae*.
    3. To image LDs, set light intensity and exposure time in the green channel (excitation and emission maxima of BODIPY are 493 and 503 nm, respectively).
    NOTE: BODIPY 493/503 is a very bright fluorochrome; however, it may get bleached rapidly with overly strong light intensity. Moreover, LDs are mobile in live cells, thus minimize exposure time and capture the full green-channel z-stack first (before switching to the blue channel) to prevent blurring artifacts. Also, take into account the linear range of the camera for signal intensity to avoid saturated pixels.
    4. To image cell boundaries, set light intensity and exposure time in the blue channel (excitation and emission maxima of Cascade Blue dextran are 400 and 420 nm, respectively).
    NOTE: Signal intensity in the blue channel is required for image segmentation, but it is not used for LD quantification itself. Therefore, optimal settings in this channel are not crucial for analysis.
    5. If possible, create an automated experimental workflow in the microscope control software to facilitate imaging of multiple samples under standardized conditions.

2. Once imaging conditions have been optimized, image samples to be used for quantification. Focus on the cells and image them in green and blue channels as described in Step 4.1.
NOTE: All images must be acquired using the same settings to allow comparison between samples. Image multiple fields of view per sample to obtain robust, representative data.
3. Save the blue and green channel z-stack images as 16-bit multi-layer TIFF files (i.e., two files per field of view). Include words “green” or “blue” in the corresponding file names. Proceed with image analysis (Section 5).

5. Image Analysis

1. **Visually check the quality of acquired images.**
    1. Open microscopic images in ImageJ[29,30] or other suitable image analysis software.
    2. Remove any image stacks containing a considerable number of cells that moved during acquisition (and thus created blurring artifacts).
    3. Remove any image stacks containing highly fluorescent non-cell particles in the blue channel (e.g., dirt on microscope slide or cover slip, impurities in cultivation medium).
    NOTE: Very bright non-cell objects in the blue channel may create cell detection artifacts or may interfere with detection of cells in their vicinity.
    4. Remove any image stacks containing a large proportion of dead cells (i.e., cells with increased blue fluorescence compared to live cells).
    NOTE: While the presence of a small proportion of dead cells in the sample is typically not a problem and these cells are automatically discarded during analysis, some dead or dying cells may occasionally be recognized as live cells by the segmentation algorithm and thus skew the reported results.

2. **Analyze images in the MATLAB software.**
    1. Create a main folder and copy all MATLAB scripts to this location.
    2. Create a sub-folder ("pombe", "cerevisiae" or "japonicus") and copy input TIFF image files to this location.
    3. Start MATLAB, open script MAIN.m and run it. In the menu select the yeast species to be analyzed and start image processing.
    NOTE: Some of the parameters required for cell and LD detection are pre-set for the particular species, others are determined automatically during image processing. The pre-set values were determined empirically and depend on several factors such as objective magnification, camera type and sensitivity, and imaging settings. If required, users may edit the script files to change the organism-specific presets to better reflect their experimental setup. Namely, during cell recognition acceptable object sizes are given by the "minArea" and "maxArea" parameters, and the minimum fraction of filled volume within the object boundaries is given by the "Solidity" parameter. For LD recognition, the brightness threshold is given by the "th" parameter (its value is affected mostly by image bit depth and fluorescence signal intensity), and maximum acceptable LD size is given by the "MaxArea" parameter.
    4. Inspect and process the output files as required using a spreadsheet editor or statistical package; the workflow produces semicolon-separated CSV files, and segmented TIFF files with detected cell objects and LDs.
    NOTE: The workflow segments images into background and cell objects, where each cell object may be composed of multiple adjacent cells. Therefore, the output in "xxxx_cells.csv" files does not represent single-cell data and should only be used to calculate per-unit-of-cell-volume metrics.

Representative Results

The whole procedure is summarized in **Figure 1** for the fission yeasts (the budding yeast workflow is analogous), and below we provide examples of how the workflow can be used to study LD content in three different yeast species under various conditions known to affect cellular LD content. Each example represents a single biological experiment.

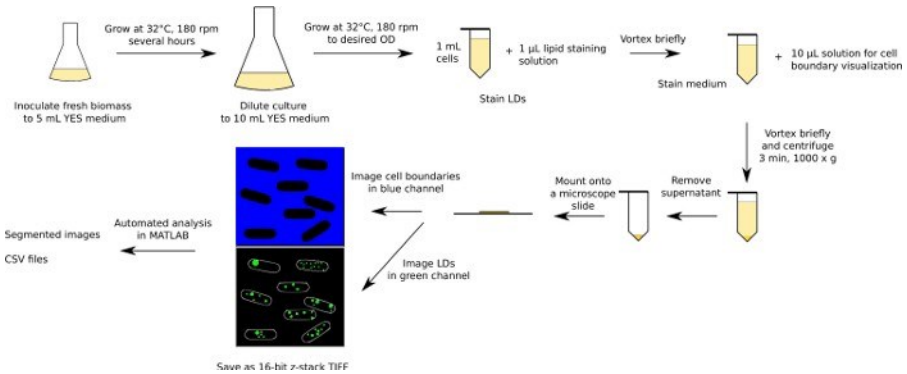

Figure 1: Schematic diagram of the experimental and analytical workflow. The workflow for fission yeasts is shown as an example. Please click here to view a larger version of this figure.

First, we analyzed *S. pombe* cells (**Figure 2**). Wild-type (WT; h^{+s}) cells were grown to exponential phase in either the complex YES medium or defined EMM medium. Compared to YES, fewer LDs and higher LD staining intensity per unit of cell volume were detected in EMM (**Figure 2A-C**). Moreover, individual LDs formed in EMM medium were larger and displayed increased total staining intensity (**Figure 2D, E**). This is in agreement with previous findings of increased storage lipid content in cells grown in EMM[24]. The *ppc1* gene encodes a phosphopantothenate-cysteine ligase required for coenzyme A synthesis. The temperature-sensitive *ppc1-88* mutant shows a marked decrease in LD content when grown at the restrictive temperature[31], providing an example of cells with low BODIPY 493/503 signal (**Figure 2A**). Accordingly, compared to wild type (grown at 32°C), smaller LDs with lower total staining intensity were detected in *ppc1-88* cells grown in YES following a shift to 36°C (**Figure 2D, E**), without any apparent change in LD number per unit of cell volume (**Figure 2B**).

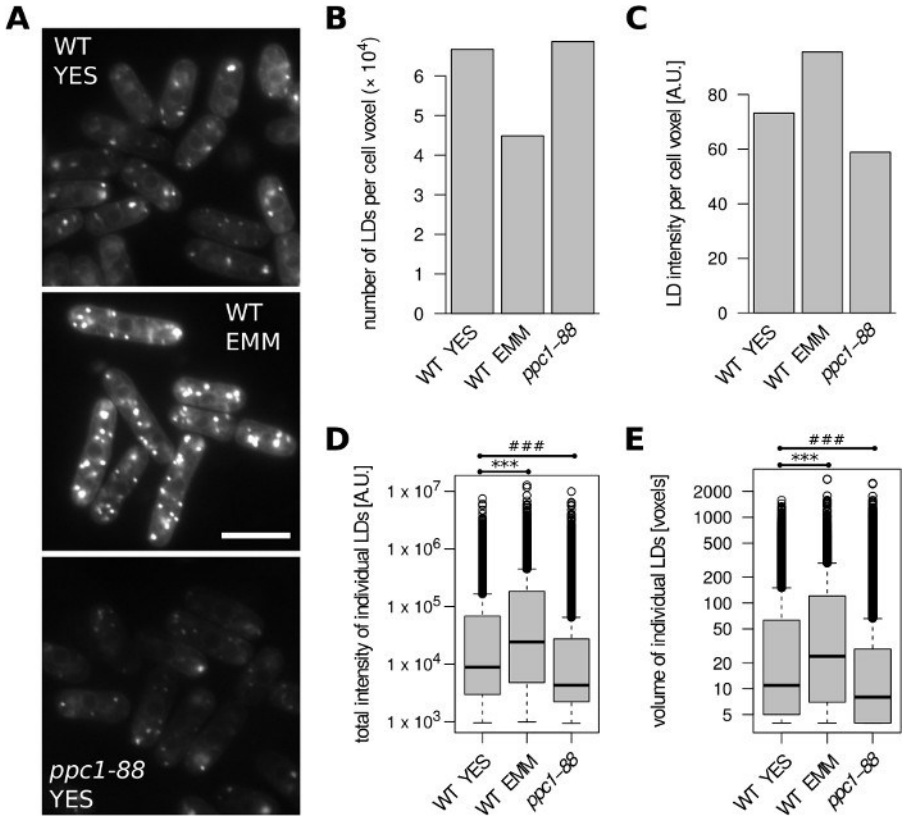

Figure 2: Impact of growth media and lipid metabolism mutation on LD content in *S. pombe*. Wild type (WT) and *ppc1-88* cells were grown to exponential phase in the complex YES or defined EMM medium, as indicated. WT cells were grown at 32 °C. The temperature-sensitive *ppc1-88* cells were grown at 25°C and shifted to 36°C for 2 hours prior to analysis. (**A**) Representative unprocessed microscopic images of LDs stained with BODIPY 493/503. A single optical slice is shown for each condition; 10% overlay with inverted blue channel was added to better visualize cell boundaries. Scale bar = 10 µm. (**B**) Number of identified LDs per unit of cell volume. (**C**) Fluorescence intensity of identified LDs per unit of cell volume. (**D**) Distributions of total fluorescence intensities of all identified LDs. ***, ### unpaired Wilcoxon test $p = 1.7 \times 10^{-107}$, $p = 3.7 \times 10^{-132}$, respectively. (**E**) Distributions of volumes of all identified LDs. ***, ### unpaired Wilcoxon test $p = 6.8 \times 10^{-71}$, $p = 1 \times 10^{-64}$, respectively. Data in panels B-E were derived from 242, 124 and 191 cell objects for the WT YES, WT EMM and *ppc1-88* samples, respectively. Please click here to view a larger version of this figure.

Next, we quantified LD content in *S. japonicus* cells (*h*$^+$ *matsj-2017*)[32] from exponential and early-stationary cultures grown in YES (**Figure 3A**). Cells entering stationary phase showed markedly decreased number of LDs per unit of cell volume compared to exponentially growing cells (**Figure 3B**), while volume-normalized LD fluorescence intensity decreased slightly between the two conditions (**Figure 3C**). The early stationary-phase LDs were typically moderately larger in size and had moderately higher total fluorescence intensity compared to LDs from exponentially growing cells (**Figure 3D, E**).

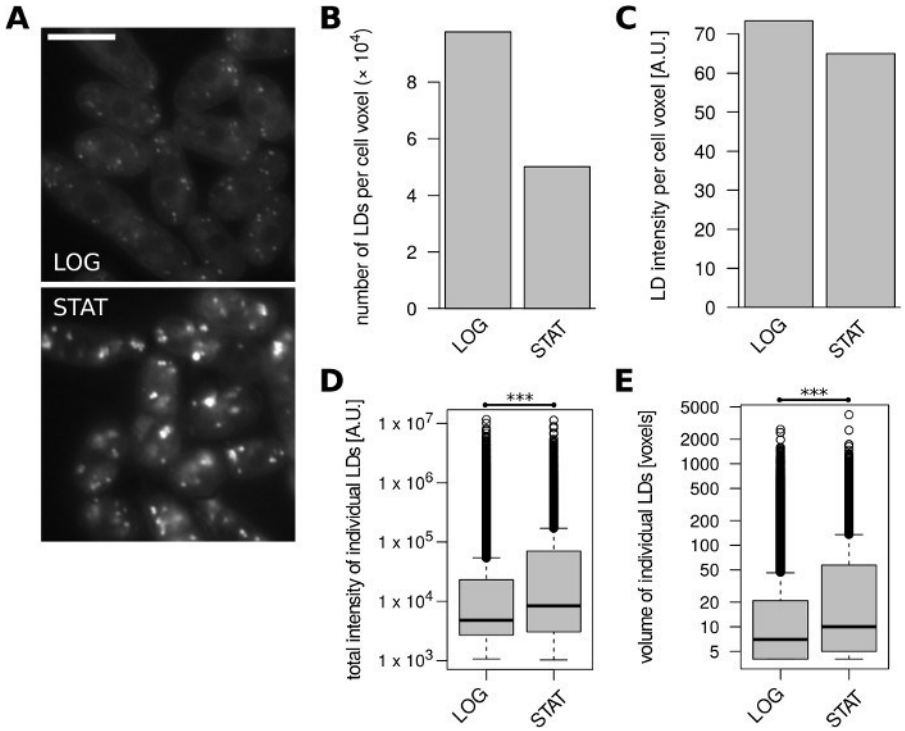

Figure 3: LD content in *S. japonicus* cells changes with growth phase. Exponentially growing (LOG) and early stationary phase (STAT) cells were analyzed. (**A**) Representative unprocessed microscopic images of LDs stained with BODIPY 493/503. A single optical slice is shown for each condition; 10% overlay with inverted blue channel was added to better visualize cell boundaries. Scale bar represents 10 µm. (**B**) Number of identified LDs per unit of cell volume. (**C**) Fluorescence intensity of identified LDs per unit of cell volume. (**D**) Distributions of total fluorescence intensities of all identified LDs. *** unpaired Wilcoxon test $p = 1.3 \times 10^{-114}$. (**E**) Distributions of volumes of all identified LDs. *** unpaired Wilcoxon test $p = 2.4 \times 10^{-85}$. Data in panels B-E were derived from 274 and 187 cell objects for the LOG and STAT samples, respectively. Please click here to view a larger version of this figure.

Finally, we analyzed *S. cerevisiae* cells of the widely used BY4741 laboratory strain (*MATa his3Δ1 leu2Δ0 met15Δ0 ura3Δ0*) grown to exponential and stationary phase, respectively, in the complex YPAD medium. Budding yeast cells typically accumulate storage lipids upon entry into stationary phase[1], and we were able to recapitulate these findings (**Figure 4**). Stationary cells contained somewhat fewer LDs per unit of volume compared to exponentially growing cells (**Figure 4B**), but their volume-normalized LD fluorescence intensity almost doubled (**Figure 4C**). This sharp increase in overall LD content was due to the much higher fluorescence intensity and volume of individual LDs in stationary phase (**Figure 4D, E**).

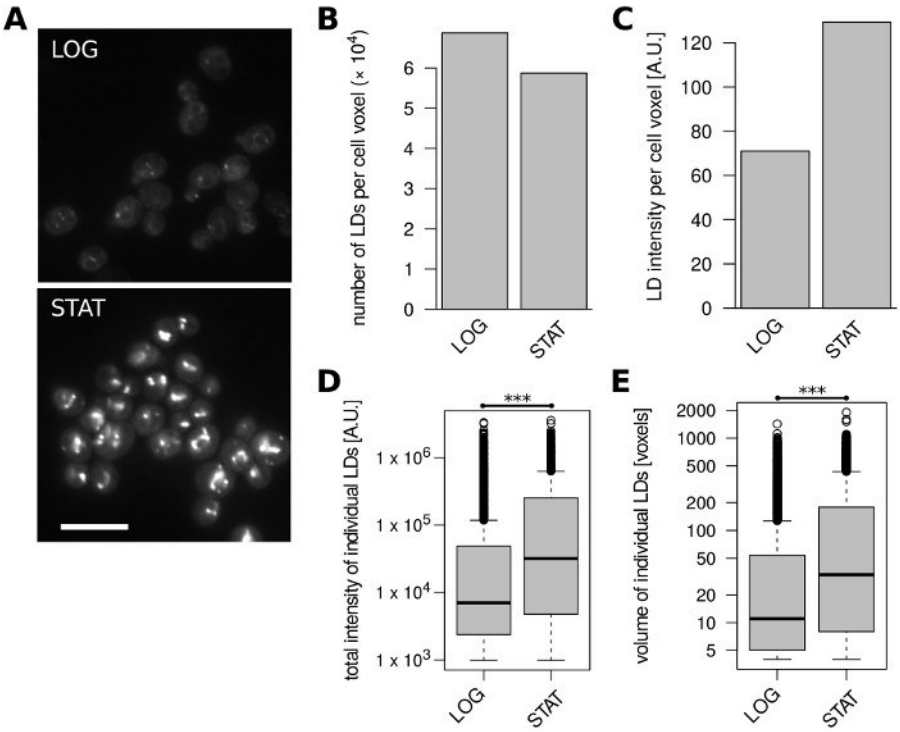

Figure 4: LD content in *S. cerevisiae* cells changes with growth phase. Exponentially growing (LOG) and stationary phase (STAT) cells were analyzed. (**A**) Representative unprocessed microscopic images of LDs stained with BODIPY 493/503. A single optical slice is shown for each condition; 10% overlay with inverted blue channel was added to better visualize cell boundaries. Scale bar represents 10 µm. (**B**) Number of identified LDs per unit of cell volume. (**C**) Fluorescence intensity of identified LDs per unit of cell volume. (**D**) Distributions of total fluorescence intensities of all identified LDs. *** unpaired Wilcoxon test $p = 4.6 \times 10^{-78}$. (**E**) Distributions of volumes of all identified LDs. *** unpaired Wilcoxon test $p = 3.7 \times 10^{-63}$. Data in panels B-E were derived from 430 and 441 cell objects for the LOG and STAT samples, respectively. Please click here to view a larger version of this figure.

Thus, our analysis workflow can detect changes in LD number, size and lipid content in three different and morphologically distinct yeast species under various conditions that positively or negatively affect cellular LD content.

Discussion

The understanding of lipid metabolism and its regulation is important for both basic biology, and clinical and biotechnological applications. LD content represents a convenient readout of lipid metabolism state of the cell, with fluorescence microscopy being one of the major methods used for LD content determination. The presented protocol allows automated detection and quantitative description of individual LDs in three different and morphologically distinct yeast species. To our knowledge, no similar tools exist for the fission yeasts. The MATLAB scripts required for image processing are included as Supplementary files, and are also available from the Figshare repository (DOI 10.6084/m9.figshare.7745738) together with all raw and processed image and tabular data from this manuscript, detailed descriptions of the CSV output files, and R scripts for downstream data analysis and visualization. Also, the latest version of the MATLAB scripts is available from GitHub (https://github.com/MartinSchatzCZ/LipidDots-analysis).

Successful LD analysis is largely dependent on the quality of the raw fluorescence images obtained. For optimal performance of the segmentation algorithms, clean glass slides devoid of dust particles should be used for microscopy, the cells should form a monolayer (the actual number of cells per field of view is not a critical parameter), and should not contain a large proportion of dead cells. Also, the z-stack imaging should start slightly below and end slightly above the cells. Depending on the particular microscopic setup, users may need to adjust some of the parameters in the image processing scripts (such as "th" for image background intensity threshold). While the current method is able to detect and describe individual LDs in the segmented cell objects, the workflow does not produce truly single-cell data due to difficulties with automated separation of all individual cells. Instead, LD content per unit of cell volume generalized for the whole sample is reported. This limitation may hamper data interpretation in analyses of heterogeneous cell populations. Also, care should be taken when working with cells with altered transport of small molecules (e.g., efflux pump mutants), as this might affect the intracellular BODIPY 493/503 concentration and LD staining, as observed for the Nile Red lipophilic dye[33,34].

Staining the medium with the cell-impermeable Cascade Blue fluorescent dextran is a convenient way of distinguishing cells from the background[35], which can be applied to many (if not all) yeast species. It also helps with automated removal of dead cells from the analysis as these will turn blue upon staining. Any dying or sick (and thus partially permeable for dextran) cells detected as alive can be removed during data analysis steps based on the "IntensityMedianBlue" value of the detected cell objects. In principle, the whole workflow can be used to detect various other cellular structures, such as DNA repair foci, provided the structures can be labelled with suitable fluorophores. The workflow should also be applicable to cells of other (yeast) species, further broadening its utility.

Disclosures

The authors have nothing to disclose.

Acknowledgments

This work was supported by Charles University grants PRIMUS/MED/26, GAUK 1308217 and SVV 260310. We thank Ondřej Šebesta for help with microscopy and development of the image analysis pipeline. We thank the ReGenEx lab for *S. cerevisiae* strains, and JapoNet and Hironori Niki's lab for *S. japonicus* strains. The *ppc1-88* strain was provided by The Yeast Genetic Resource Center Japan. Microscopy was performed in the Laboratory of Confocal and Fluorescence Microscopy co-financed by the European Regional Development Fund and the state budget of the Czech Republic (Project no. CZ.1.05/4.1.00/16.0347 and CZ.2.16/3.1.00/21515).

References

1. Koch, B., Schmidt, C., Daum, G. Storage lipids of yeasts: a survey of nonpolar lipid metabolism in *Saccharomyces cerevisiae*, *Pichia pastoris*, and *Yarrowia lipolytica*. *FEMS Microbiology Reviews.* **38** (5), 892–915 (2014).
2. Krahmer, N., Farese, R. V., Walther, T.C. Balancing the fat: lipid droplets and human disease. *EMBO Molecular Medicine.* **5** (7), 973–83 (2013).
3. Lazar, Z., Liu, N., Stephanopoulos, G. Holistic Approaches in Lipid Production by *Yarrowia lipolytica*. *Trends in Biotechnology.* **36** (11), 1157–1170 (2018).
4. Kim, D.-U. et al. Analysis of a genome-wide set of gene deletions in the fission yeast *Schizosaccharomyces pombe*. *Nature Biotechnology.* **28** (6), nbt.1628-9 (2010).
5. Giaever, G., Nislow, C. The yeast deletion collection: a decade of functional genomics. *Genetics.* **197** (2), 451–65 (2014).
6. Meyers, A. et al. The protein and neutral lipid composition of lipid droplets isolated from the fission yeast, *Schizosaccharomyces pombe*. *Journal of Microbiology (Seoul, Korea).* **55** (2), 112–122 (2017).
7. Meyers, A. et al. Lipid Droplets Form from Distinct Regions of the Cell in the Fission Yeast *Schizosaccharomyces pombe*. *Traffic (Copenhagen, Denmark).* **17** (6), 657–69 (2016).
8. Long, A.P. et al. Lipid droplet de novo formation and fission are linked to the cell cycle in fission yeast. *Traffic (Copenhagen, Denmark).* **13** (5), 705–14 (2012).
9. Yang, H.-J., Osakada, H., Kojidani, T., Haraguchi, T., Hiraoka, Y. Lipid droplet dynamics during *Schizosaccharomyces pombe* sporulation and their role in spore survival. *Biology Open.* 8–10 (2016).
10. Aoki, K., Shiwa, Y., Takada, H., Yoshikawa, H., Niki, H. Regulation of nuclear envelope dynamics via APC/C is necessary for the progression of semi-open mitosis in *Schizosaccharomyces japonicus*. *Genes To Cells: Devoted To Molecular & Cellular Mechanisms.* **18** (9), 733–52 (2013).
11. Karolin, J., Johansson, L.B.A., Strandberg, L., Ny, T. Fluorescence and Absorption Spectroscopic Properties of Dipyrrometheneboron Difluoride (BODIPY) Derivatives in Liquids, Lipid Membranes, and Proteins. *Journal of the American Chemical Society.* **116** (17), 7801–7806 (1994).
12. Bozaquel-Morais, B.L., Madeira, J.B., Maya-Monteiro, C.M., Masuda, C.A., Montero-Lomeli, M. A new fluorescence-based method identifies protein phosphatases regulating lipid droplet metabolism. *PloS One.* **5** (10), e13692 (2010).
13. Sitepu, I.R. et al. An improved high-throughput Nile red fluorescence assay for estimating intracellular lipids in a variety of yeast species. *Journal of Microbiological Methods.* **91** (2), 321–8 (2012).
14. Rostron, K.A., Lawrence, C.L. Nile Red Staining of Neutral Lipids in Yeast. *Methods in Molecular Biology (Clifton, N.J.).* **1560**, 219–229 (2017).
15. Romero-Aguilar, L., Montero-Lomeli, M., Pardo, J.P., Guerra-Sánchez, G. Lipid Index Determination by Liquid Fluorescence Recovery in the Fungal Pathogen *Ustilago Maydis*. *Journal of Visualized Experiments.* (134), 1–6 (2018).
16. Gupta, A., Dorlhiac, G.F., Streets, A.M. Quantitative imaging of lipid droplets in single cells. *The Analyst.* (2018).
17. Wolinski, H., Bredies, K., Kohlwein, S.D. Quantitative imaging of lipid metabolism in yeast: from 4D analysis to high content screens of mutant libraries. *Methods in Cell Biology.* **108**, 345–65 (2012).
18. Campos, V., Rappaz, B., Kuttler, F., Turcatti, G., Naveiras, O. High-throughput, nonperturbing quantification of lipid droplets with digital holographic microscopy. *Journal of Lipid Research.* **59** (7), 1301–1310 (2018).
19. Ranall, M. V., Gabrielli, B.G., Gonda, T.J. High-content imaging of neutral lipid droplets with 1,6-diphenylhexatriene. *BioTechniques.* **51** (1), 35–6, 38–42 (2011).
20. Schnitzler, J.G. et al. Nile Red Quantifier: a novel and quantitative tool to study lipid accumulation in patient-derived circulating monocytes using confocal microscopy. *Journal of Lipid Research.* **58** (11), 2210–2219 (2017).
21. Bombrun, M., Gao, H., Ranefall, P., Mejhert, N., Arner, P., Wählby, C. Quantitative high-content/high-throughput microscopy analysis of lipid droplets in subject-specific adipogenesis models. *Cytometry. Part A : the journal of the International Society for Analytical Cytology.* **91** (11), 1068–1077 (2017).
22. Capus, A., Monnerat, M., Ribeiro, L.C., de Souza, W., Martins, J.L., Sant'Anna, C. Application of high-content image analysis for quantitatively estimating lipid accumulation in oleaginous yeasts with potential for use in biodiesel production. *Bioresource Technology.* **203**, 309–17 (2016).
23. Lv, X. et al. Identification of gene products that control lipid droplet size in yeast using a high-throughput quantitative image analysis. *Biochimica et biophysica acta. Molecular and Cell Biology Of Lipids.* **1864** (2), 113–127 (2018).
24. Zach, R., Tvarůžková, J., Schätz, M., Ťupa, O., Grallert, B., Převorovský, M. Mitotic defects in fission yeast lipid metabolism "cut" mutants are suppressed by ammonium chloride. *FEMS Yeast Research.* **18** (6), 1–7 (2018).
25. Petersen, J., Russell, P. Growth and the Environment of *Schizosaccharomyces pombe*. *Cold Spring Harbor Protocols.* **2016** (3), pdb.top079764 (2016).

26. Aoki, K., Furuya, K., Niki, H. *Schizosaccharomyces japonicus*: A Distinct Dimorphic Yeast among the Fission Yeasts. *Cold Spring Harbor Protocols.* **2017** (12), (2017).
27. Curran, B.P.G., Bugeja, V. Basic investigations in Saccharomyces cerevisiae. *Methods in Molecular Biology (Clifton, N.J.).* **1163**, 1–14 (2014).
28. Sabatinos, S.A., Forsburg, S.L. Molecular genetics of *Schizosaccharomyces pombe. Methods in Enzymology.* **470** (10), 759–95 (2010).
29. Schindelin, J., Rueden, C.T., Hiner, M.C., Eliceiri, K.W. The ImageJ ecosystem: An open platform for biomedical image analysis. *Molecular Reproduction and Development.* **82** (7–8), 518–29 (2015).
30. Schindelin, J. et al. Fiji: an open-source platform for biological-image analysis. *Nature Methods.* **9** (7), 676–82 (2012).
31. Nakamura, T., Pluskal, T., Nakaseko, Y., Yanagida, M. Impaired coenzyme A synthesis in fission yeast causes defective mitosis, quiescence-exit failure, histone hypoacetylation and fragile DNA. *Open Biology.* **2** (9), 120117 (2012).
32. Furuya, K., Niki, H. Isolation of heterothallic haploid and auxotrophic mutants of *Schizosaccharomyces japonicus. Yeast.* **26** (4), 221–233 (2009).
33. Ivnitski-Steele, I. et al. Identification of Nile red as a fluorescent substrate of the *Candida albicans* ATP-binding cassette transporters Cdr1p and Cdr2p and the major facilitator superfamily transporter Mdr1p. *Analytical Biochemistry.* **394** (1), 87–91 (2009).
34. Wolinski, H., Kohlwein, S.D. Microscopic analysis of lipid droplet metabolism and dynamics in yeast. *Methods in Molecular Biology (Clifton, N.J.).* **457** (1), 151–63 (2008).
35. Graml, V. et al. A genomic Multiprocess survey of machineries that control and link cell shape, microtubule organization, and cell-cycle progression. *Developmental Cell.* **31** (2), 227–239 (2014).

3.3 Stress-activated protein kinase regulation in the lipid mutant *cbf11Δ*

Cellular viability is largely dependent on the ability of the cell to cope with stress. Therefore, key players of stress signaling need to be faithfully regulated. The stress-activated protein kinase Sty1, orthologous to *S. cerevisiae* Hog1 and human p38, is the master regulator of stress response in the fission yeast [167,168]. Upon various stress stimuli Sty1 is hyperactivated by the MAPK cascade of phosphorylation [168]. However, prolonged Sty1 activation blocks cell cycle progression [169,170], cytokinesis [171] and growth [172] and, therefore, the Sty1 kinase needs to be timely inactivated. There are six phosphatases acting on Sty1 and inhibiting it - the tyrosine phosphatases Pyp1 and Pyp2 and serine/threonine phosphatases Ptc1, Ptc2, Ptc3 and Ptc4 [149,173–176]. We have previously observed that Sty1 activatory phosphorylation during exogenous oxidative stress caused by hydrogen peroxide is diminished in the lipid metabolism mutant *cbf11Δ* compared to WT cells (Figure 3.1B) [177] although many Sty1-dependent genes are upregulated in this mutant [150]. Based on these contradicting results we hypothesized that the activity of Sty1 phosphatases might be higher in *cbf11Δ* cells. Indeed, using RT-qPCR we found out that the expression of Sty1 phosphatases *ptc1*, *pyp1* and *pyp2* was increased in *cbf11Δ* cells compared to WT (Figure 3.1A). Therefore, we created double mutants of *cbf11Δ* and the respective Sty1-targeting phosphatase deletion strains and examined Sty1 phosphorylation. We have detected a partial rescue of diminished Sty1 phosphorylation upon deletion of either *pyp1* or *pyp2* in *cbf11Δ* cells (Figure 3.1BC), suggesting, that increased activity of Pyp1 and Pyp2 phosphatases might be the cause of the apparently low phosphorylation of Sty1 in *cbf11Δ* (i.e. a more rapid phosphorylation turnover). Curiously, deletion of *cbf11Δ* in *ptc1Δ* mutant strain causes a synthetic growth defect, the double mutant grows very poorly in complex YES medium and the majority of cells display defects in DNA integrity (Figure 3.1D). Another approach to assess Sty1 activity is to observe Sty1 localization using fluorescence microscopy, since the Sty1 kinase is translocated to the nucleus upon activation [178]. Curiously, some cells lacking *cbf11* displayed very bright Sty1-GFP signal in both nucleus and the cytoplasm even without exogenous stress (Figure 3.1E, time 0 min) which suggested that a subpopulation of exponentially growing *cbf11Δ* cells contains increased total Sty1 levels and hyperactivated Sty1. Upon hydrogen peroxide treatment Sty1 was localized predominantly in the nucleus in majority of observed WT and *cbf11Δ* cells, however, the heterogeneity in Sty1-GFP brightness of *cbf11Δ* culture persisted (Figure 3.1E). Overall, these

observations suggest that Sty1 activity is deregulated in *cbf11Δ* cells and that there is considerable cell to cell variation.

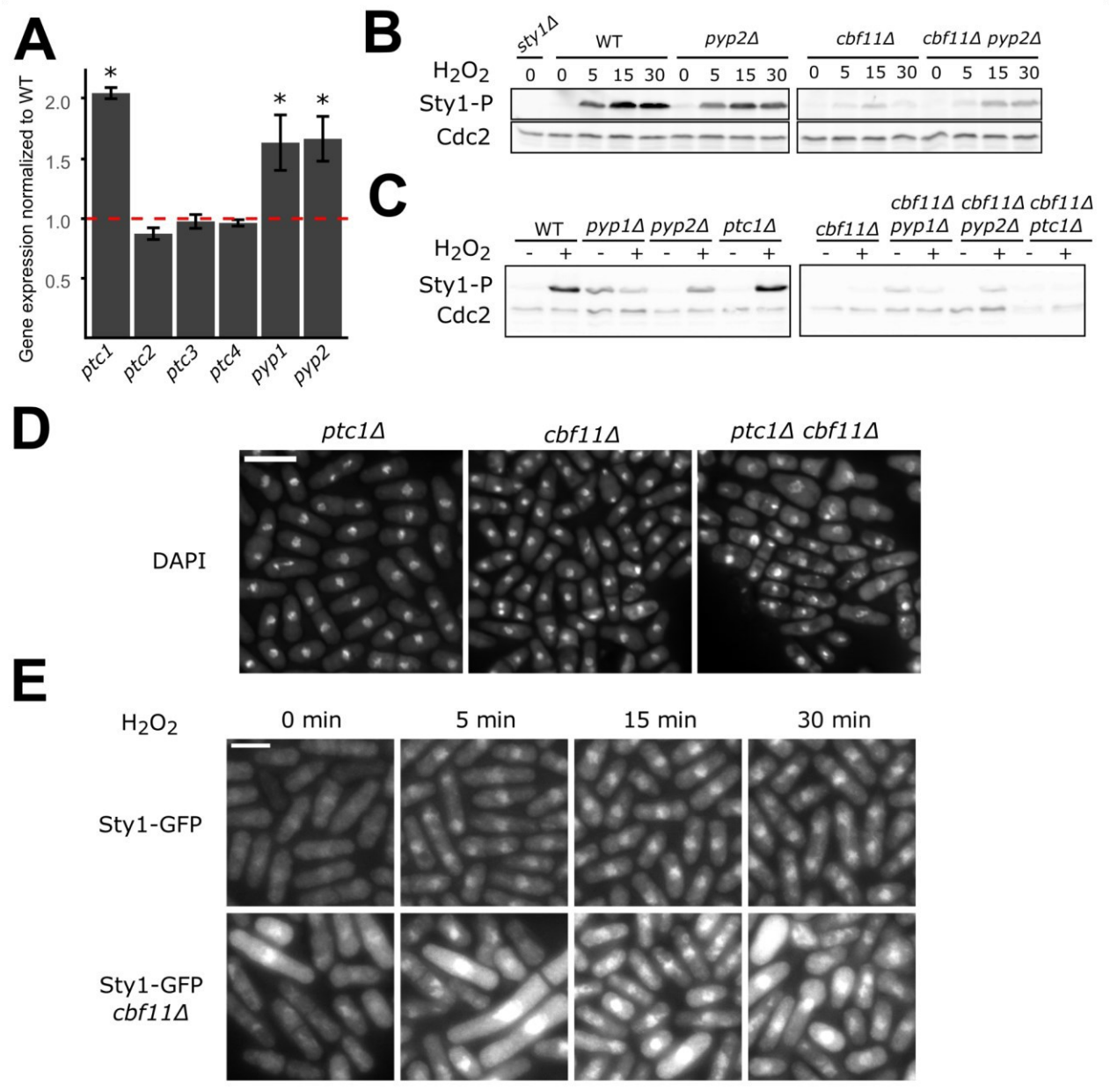

Fig 3.1 Sty1 activity dynamics is altered in *cbf11Δ* cells.

(A) Expression of Sty1-inactivating phosphatases in *cbf11Δ* cells was measured using RT-qPCR. Values shown are normalized to gene expression in WT cells (equal expression of WT and *cbf11Δ* is indicated by the red dashed line). Mean and SD values of three independent replicates are shown. One-sided Mann-Whitney U test was used to determine statistical significance. Significantly increased gene expression in *cbf11Δ* cells ($p = 0.05$) is indicated with an asterisk.

(B) Timecourse western blot analysis of Sty1 phosphorylation in WT, *cbf11Δ*, *pyp2Δ* and *cbf11Δ pyp2Δ* cells treated or not with 0.5 mM H_2O_2 in YES medium. Aliquots of cell cultures were collected at indicated times (in minutes). Cells lacking *sty1* are used as a negative control for the anti-Sty1-P antibody.
(C) Western blot analysis if Sty1 phosphorylation in Sty1 phosphatase mutant cells *pyp1Δ*, *pyp2Δ* and *ptc1Δ,* and double mutants with *cbf11Δ* treated or not with 0.5 mM H_2O_2 for 30 minutes in YES medium.
(D) Cells with the indicated genotypes were grown in YES and stained by DAPI to visualize nuclei. The scale bar represents 10 μm.
(E) Timecourse analysis of Sty1 localization during oxidative stress was performed using fluorescence microscopy of Sty1-GFP expressing WT or *cbf11Δ* cells. Aliquots of cell cultures treated with 0.5 mM H_2O_2 were fixed with 10% formaldehyde at the indicated times. The scale bar represents 10 μm.

Notably, Sty1 MAPK also functions as a positive regulator of mitosis. Although *sty1* is not essential for logarithmic growth, cells upon Sty1 inactivation enter mitosis later compared to WT cells as exhibited by the elongated cell phenotype (Figure 3.2A, B) [174,175,179]. Based on the intriguing findings described above that Sty1 is deregulated in *cbf11Δ* cells we aimed to construct the *sty1Δ cbf11Δ* double mutant, however, we have repeatedly failed to do so and observed a strong selective pressure for retaining a translocated copy of the *cbf11* gene, suggesting that the double mutant is very sick or lethal [150]. In order to overcome this issue we have utilized the analog-sensitive Sty1 allele [153] whose kinase activity is inhibited by the analog addition. As expected, the *sty1-as cbf11Δ* double mutant displayed defects in multiple growth aspects upon Sty1 inhibition. First, the rate of colony growth is slower upon Sty1 inhibition in *cbf11Δ* cells [152] (**publication #3**). Second, although *cbf11Δ* cells are shorter compared to WT [150] the introduction of the analog-sensitive Sty1 allele even without adding the analog causes elongation of the cells (Figure 3.2A and B), overriding the phenotype of *cbf11* deletion. Third, majority of the observed *sty1-as cbf11Δ* cells elongate upon Sty1 inhibition (addition of 3-MB-PP1) even more than the *sty1-as* cells do (Figure 3.2A and B), leading to extremely long cells with often fragmented nuclei (Figure 3.2C). It needs to be noted, however, that a fraction of *sty1-as cbf11Δ* cells was viable after the addition of 3-MB-PP1 suggesting that either, Sty1 activity is not sufficiently inhibited by the analog or Sty1 is not essential for growth of *cbf11Δ* cells. Nevertheless, the results above strongly indicate that Sty1 is required for cell cycle progression of *cbf11Δ* cells.

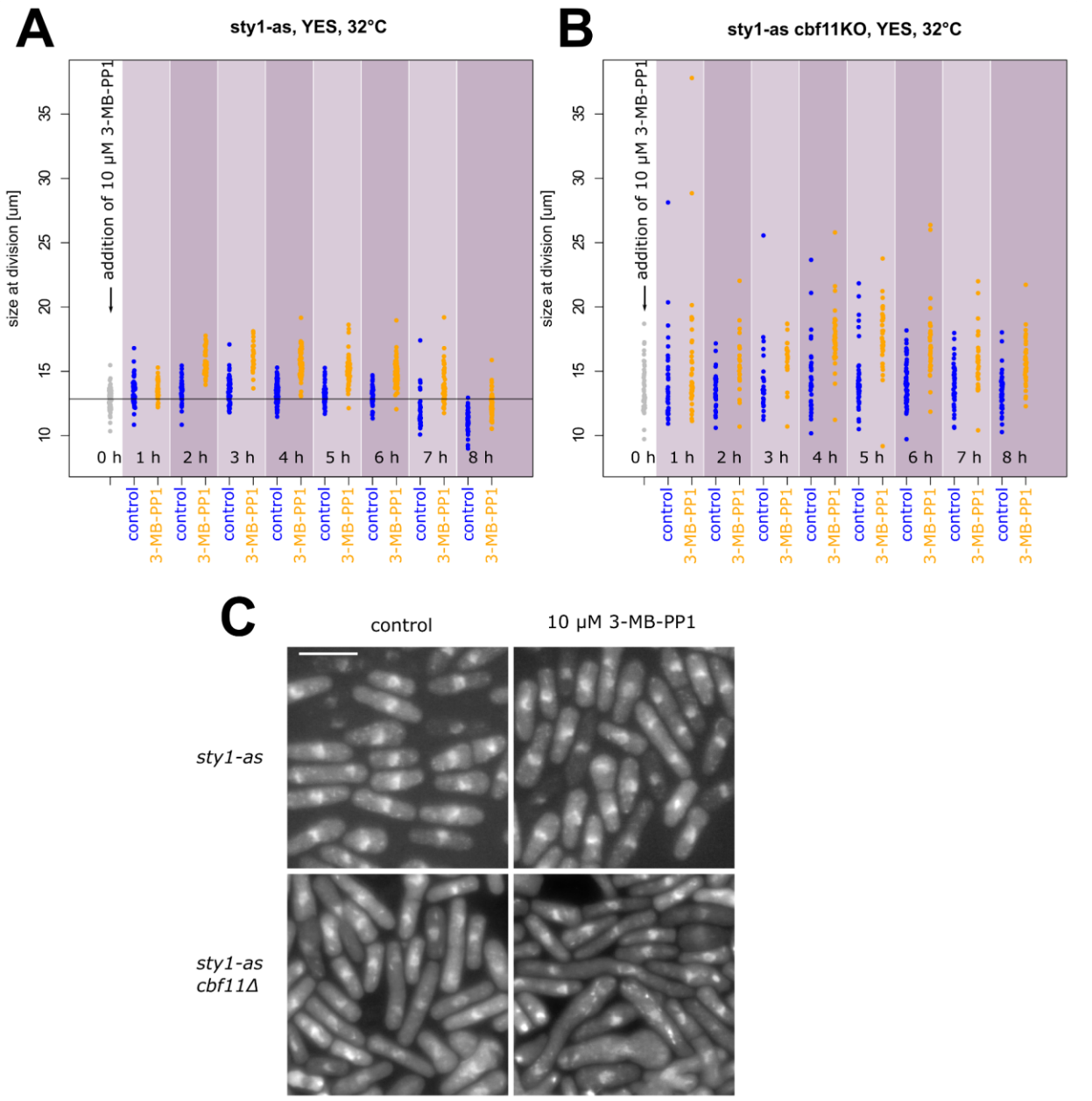

Fig 3.2 *cbf11Δ* cells require active Sty1 for cell cycle progression.

(A, B) The length of fully septated cells expressing the analog-sensitive *sty1* allele upon addition of 3-MB-PP1 or DMSO (control) in WT (A) or *cbf11Δ* background (B) was measured. Each dot represents a single cell. **(C)** *sty1-as* and *sty1-as cbf11Δ* cells were treated with DMSO (control) or 10 µM 3-MB-PP1 for 4 hours and stained by DAPI to visualize nuclei. The scale bar represents 10 µm.

3.4 Perturbed fatty-acid metabolism is linked to localized chromatin hyperacetylation, increased stress-response gene expression and resistance to oxidative stress

As the first author of this publication I have performed all experiments shown in Figs 1C, 2ACE, 3C, 4DEF, 5, S1E, S2, S4, S5. I have written the manuscript text, prepared figures and designed experiments together with my supervisor Dr. Martin Převorovský. Shortly before this manuscript was first submitted for publication, we found out that the group of Prof. Elena Hidalgo (UPF, Barcelona, Spain) was also working on the relationship between Cbf11 and Sty1, and they had reproduced many of our findings. We agreed to publish the results from both laboratories jointly, resulting in a shared first authorship. (IF 6.020)

Princová J, Salat-Canela C, Daněk P, Marešová A, de Cubas L, Bähler J, Ayté J, Hidalgo E, Převorovský M. Perturbed fatty-acid metabolism is linked to localized chromatin hyperacetylation, increased stress-response gene expression and resistance to oxidative stress. PLoS Genet. 2023 Jan 10;19(1):e1010582. doi: 10.1371/journal.pgen.1010582.

This publication is marked as publication #3 in the text of this thesis.

PLOS GENETICS

RESEARCH ARTICLE

Perturbed fatty-acid metabolism is linked to localized chromatin hyperacetylation, increased stress-response gene expression and resistance to oxidative stress

Jarmila Princova´[1☯], Clàudia Salat-Canela[2☯], Petr Daněk[1], Anna Mares˘ova´, Laura de Cubas[2], Ju¨rg Ba¨hler[3], Jose´ Ayte´[2], Elena Hidalgo[2], Martin Převorovský´ [1]*

1 Laboratory of Microbial Genomics, Department of Cell Biology, Faculty of Science, Charles University, Prague, Czech Republic, **2** Oxidative Stress and Cell Cycle Group, Universitat Pompeu Fabra, C/Dr. Aiguader, Barcelona, Spain, **3** Institute of Healthy Ageing and Department of Genetics, Evolution & Environment, University College London, London, United Kingdom

☯ These authors contributed equally to this work.
* prevorov@natur.cuni.cz

OPEN ACCESS

Citation: Princova´ J, Salat-Canela C, Daněk P, Mares˘ova´ A, de Cubas L, Ba¨hler J, et al. (2023) Perturbed fatty-acid metabolism is linked to localized chromatin hyperacetylation, increased stress-response gene expression and resistance to oxidative stress. PLoS Genet 19(1): e1010582. https://doi.org/10.1371/journal.pgen.1010582

Editor: Geraldine Butler, University College Dublin, IRELAND

Received: October 18, 2022

Accepted: December 19, 2022

Published: January 10, 2023

Peer Review History: PLOS recognizes the benefits of transparency in the peer review process; therefore, we enable the publication of all of the content of peer review and author responses alongside final, published articles. The editorial history of this article is available here: https://doi.org/10.1371/journal.pgen.1010582

Data Availability Statement: The microarray data are available from the ArrayExpress database (https://www.ebi.ac.uk/arrayexpress/) under

Abstract

Oxidative stress is associated with cardiovascular and neurodegenerative diseases, diabetes, cancer, psychiatric disorders and aging. In order to counteract, eliminate and/or adapt to the sources of stress, cells possess elaborate stress-response mechanisms, which also operate at the level of regulating transcription. Interestingly, it is becoming apparent that the metabolic state of the cell and certain metabolites can directly control the epigenetic information and gene expression. In the fission yeast *Schizosaccharomyces pombe*, the conserved Sty1 stress-activated protein kinase cascade is the main pathway responding to most types of stresses, and regulates the transcription of hundreds of genes via the Atf1 transcription factor. Here we report that fission yeast cells defective in fatty acid synthesis (*cbf11*, *mga2* and ACC/*cut6* mutants; FAS inhibition) show increased expression of a subset of stress-response genes. This altered gene expression depends on Sty1-Atf1, the Pap1 transcription factor, and the Gcn5 and Mst1 histone acetyltransferases, is associated with increased acetylation of histone H3 at lysine 9 in the corresponding gene promoters, and results in increased cellular resistance to oxidative stress. We propose that changes in lipid metabolism can regulate the chromatin and transcription of specific stress-response genes, which in turn might help cells to maintain redox homeostasis.

Author summary

The production of fatty acids and lipids in general creates energy reserves and provides essential building blocks for cellular membranes. Oxidative stress, on the other hand, is a condition caused by increased concentration of oxidants, such as reactive oxygen species, which becomes harmful to the cells and triggers an oxidative stress response to mitigate damage. While these two processes are seemingly unrelated, we now provide evidence

accession number E-MTAB-6761. The raw ChIP-seq data are available from the ArrayExpress database under the accession number E-MTAB-11081. The scripts used for ChIP-seq data processing and analysis are available from https://github.com/mprevorovsky/ox-stress_histones.

Funding: This work was supported by the Univerzita Karlova v Praze [grant number PRIMUS/MED/26 to M.P.], Grantova´ Agentura, Univerzita Karlova[grant number GA UK 1170217 to J.P.], Ministerio de Ciencia, Innovacio´n y Universidades (Spain) [grant numbers PGC2018-093920-B-I00 to E.H. and PGC2018-097248-B-I00 to J.A.] and Unidad de Excelencia Mar´ıa de Maeztu (Spain) [grant number CEX2018-000792-M to E.H. and J. A.], and a Wellcome Trust Senior Investigator Award [grant number 095598/Z/11/Z] to J.B. The funders had no role in study design, data collection and analysis, decision to publish, or preparation of the manuscript.

Competing interests: The authors declare that they have no conflict of interest.

that there is actually a specific regulatory connection between fatty acid metabolism and cellular resistance to oxidative stress. Using the fission *Schizosaccharomyces pombe* as a model, we show that multiple conditions that lower fatty acid production, including mutations of lipogenic enzymes and their regulators, or chemical inhibition of fatty acid synthesis, specifically boost the expression of a subset of stress-responsive genes, and increase cellular resistance to hydrogen peroxide. This regulatory link relies on histone acetyltransferases and is connected with promoter hyperacetylation at the affected genes. Our findings highlight the intricate interconnections between the metabolic state of the cell and the regulation of gene expression.

Introduction

Oxidative stress occurs when the equilibrium between the production and the detoxification of oxidants is disturbed, leading to damage of cellular molecules [1]. Importantly, oxidative stress is associated with multiple cardiovascular and neurodegenerative diseases, diabetes, cancer, psychiatric disorders and aging [2–5]. However, under physiological conditions that create increased oxidant levels, such as mitochondrial respiration or fatty acid (FA) oxidation, the cellular antioxidant mechanisms are typically able to maintain cellular redox homeostasis and prevent oxidative stress [1,6].

In the fission yeast *Schizosaccharomyces pombe*, the Sty1 stress-activated protein kinase (SAPK) cascade, homologous to the mammalian p38 mitogen-activated protein kinase, is the main pathway responding to most types of stress conditions, including oxidative stress. Once activated, Sty1 translocates to the nucleus, where it phosphorylates and activates its main target, the basic zipper-containing transcription factor Atf1, leading to an extensive transcriptional response [7,8]. Analyses of genes showing differential expression in response to various stresses identified the core environmental stress response (CESR) as a group of genes that are jointly regulated under all or most environmental stresses. Remarkably, the regulation of most CESR genes depends on Sty1 and, to a lesser extent, on Atf1 [9,10]. During oxidative stress, the Pap1 (pombe AP-1-like) transcription factor is also involved in triggering stress gene expression, especially under less severe insults (e.g., treatment with 0.2 mM hydrogen peroxide) which are insufficient to fully activate the Sty1-Atf1 pathway. Additionally, there is crosstalk between the two pathways and some genes, such as the catalase ctt1, are regulated by both Atf1 and Pap1 [11,12]. Importantly, even under favourable conditions some level of Sty1 activity is needed for proper cell-cycle progression, especially for timing the entry into mitosis [13,14].

The CSL (CBF1, Su(H), Lag-1) family protein Cbf11 and the IPT/TIG ankyrin repeat-containing protein Mga2 are transcription factors regulating lipid-metabolism genes. Their target genes include the acetyl-CoA carboxylase *cut6*, the acyl-CoA desaturase *ole1*, the long chain fatty acid-CoA ligases *lcf1* and *lcf2*, or the triacylglycerol lipases *ptl1* and *ptl2* [15,16]. The loss of Mga2 causes a general disruption of the lipidome [16], while cells lacking Cbf11 have a decreased amount of lipid droplets and show mitotic defects [17]. Curiously, we have previously shown that many CESR genes are upregulated in the *cbf11Δ* deletion mutant cells, but the reason for these changes is not clear [15].

It has become apparent in recent years that the cellular metabolic state can directly affect the regulation of gene expression through the availability of selected metabolites that serve as substrates for various chromatin modifying enzymes. For example, the metabolite acetyl-CoA is central to multiple biosynthetic pathways as well as to histone acetylation by histone acetyltransferases (HATs). Perturbations in acetyl-CoA levels lead to altered histone acetylation and

gene transcription [18–20]. Acetyl-CoA is also utilized during FA synthesis, including its first and rate-limiting step catalyzed by the acetyl-CoA carboxylase (ACC). Intriguingly, ACC inhibition increases the acetylation of bulk histones and affects gene expression in yeast [21]. However, the significance and the physiological consequences of such interconnections between the metabolic state and gene expression patterns are only beginning to be understood. In this study, we show that a decrease in FA synthesis leads to increased expression of specific stress-response genes accompanied by promoter histone hyperacetylation, and to increased resistance to hydrogen peroxide (H_2O_2)-induced oxidative stress in fission yeast.

Materials and methods

Plasmid construction

The Cas9/sgRNA_TEFp (pMP134) and Cas9/sgRNA_*cbf11* (pMP153) plasmids were constructed as previously described [22]. sgRNAs targeted to the TEF promoter region of the *natMX6* cassette and to *cbf11* ORF, respectively, were inserted into the pMZ374 plasmid carrying an empty sgRNA site and a sequence encoding the Cas9 endonuclease [23]. Briefly, the whole pMZ374 was amplified by NEB Q5 polymerase (using AJ11 and AJ12, and AJ29 and AJ30 oligonucleotides, respectively), 5' ends of purified PCR products were phosphorylated, and plasmid ends were ligated together. The final plasmids were verified by restriction cleavage and sequencing. pMZ374 was a gift from Mikel Zaratiegui (Addgene plasmid # 59896; http://n2t.net/addgene:59896; RRID:Addgene_59896). Lists of oligonucleotides and plasmids used in this study are provided in Tables A and B in S1 Text, respectively.

Strains, media and cultivations

Fission yeast cells were grown according to standard procedures [24] in either complex yeast extract medium with supplements (YES) or Edinburgh minimal medium (EMM). A list of strains used in this study is provided in Table C in S1 Text.

For construction of Cbf11-TAP scarless knock-in strain, the CRISPR/Cas9-based strategy was adapted from [22]. MP15 cells (*h- cbf11-ctap4*::*natR ura4-D18 leu1-32 ade6-M216*) [15] were synchronized in G1 and transformed with a fragment of the *cbf11-TAP* sequence (plasmid pMaP27 digested by SalI and EcoO109I) as template for homologous recombination together with the Cas9/sgRNA_*TEFp* plasmid (pMP134). After selection on EMM+ade+leu plates, the smallest colonies were re-streaked onto non-selective YES plates to allow for elimination of the deleterious Cas9 plasmid. The integration of *cbf11-TAP* was verified by PCR (primers MaP169 and MP28) and sequencing. Expression of Cbf11-TAP protein was verified by western blot with an anti-TAP antibody (Thermo Scientific, CAB1001). Prototrophic *cbf11-TAP* strain was then prepared by standard crossing and revalidated.

The Cbf11DBM-TAP scarless knock-in strain was constructed and validated analogously in two steps. First, to insert the DNA-binding mutation (R318H; DBM) [25] into the *cbf11* endogenous locus MaP70 cells (*h- cbf11-3HA*::*natMX6 ura4-D18 leu1-32 ade6-M216*) were synchronized in G1 phase and transformed with a Cas9/sgRNA plasmid targeting Cas9 next to the desired DBM mutation site in *cbf11* ORF (Cas9/sgRNA_*cbf11;* pMP153), and a *cbf11DBM-TAP* DNA fragment as template for homologous recombination (plasmid pMaP11 digested by SalI and EcoO109I). Introduction of the DBM mutation was verified by PCR (primers MP53 and MP54) coupled with restriction digestion with HpaII, and by sequencing. The resulting strain (MP670) contained the DBM mutation, but retained the HA tag and *natMX6* cassette at the *cbf11* locus. In the second step the MP670 cells were transformed with the pMP134 plasmid targeting the *natMX6* cassette, and the pMaP11 fragment described above as template for homologous recombination. The final prototrophic strain

cbf11DBM-TAP (MP712) was then prepared by standard crossing and validated by PCR, restriction cleavage, sequencing and western blot as described above.

All other strains constructed in this study were created using standard genetic methods [26], or the pClone system [27] for deletion of *cbf11*, *ssp2* or *mga2* genes.

Spot tests

Exponentially growing cells were 10-fold serially diluted and spotted onto YES plates containing various concentrations of H_2O_2 (Sigma-Aldrich, H1009) or 125 μM menadione sodium bisulfite (Sigma-Aldrich, M5750) for oxidative stress-resistance assays, or 3-MB-PP1 (Sigma-Aldrich, 529582) for Sty1 inhibition. The spots were allowed to dry and plates were incubated at 30˚C or 32˚C until cell growth was evident. Due to the unstable nature of H_2O_2, the plates were poured on the day of spotting and YES agar was cooled to 45˚C prior to adding the stressor.

RT-qPCR

The RT-qPCR results shown in all relevant figures except for Fig 1B (top panel) and 1F were obtained as follows: Total RNA was extracted from cells using the MasterPure Yeast RNA Purification Kit including a DNase treatment step (Epicentre), and converted to cDNA using random primers and the RevertAid Reverse Transcriptase kit (ThermoFisher Scientific). Quantitative PCR was performed using the 5x HOT FIREPol EvaGreen qPCR Supermix (Solis Biodyne) and the LightCycler 480 II instrument (Roche). For RT-qPCR, *act1* (actin) and *rho1* (Rho1 GTPase) were used as reference genes. The primers used are listed in Table A in S1 Text.

The RT-qPCR results shown in Fig 1B (top panel) and 1F were obtained as follows: Total RNA was extracted from 40 ml of cells at logarithmic phase by standard phenol/chloroform method, as described earlier [28]. 100 μg of total RNA was incubated with recombinant DNase I (Roche, 04716728001) for 30 min at 37˚C and the reaction was stopped by incubation at 75˚C for 10 min. Reverse transcription was performed on 2 μg of DNase-treated RNA using High-Capacity cDNA Reverse Transcription Kit (Applied Biosystems, 00777852) following manufacturer's instructions. The cDNA was diluted 1:2 prior to PCR amplification. cDNA was quantified by Real-Time PCR on Light Cycler II using Light Cycler 480 SYBR Green I Master (Roche, 04887352001).

One-sided Mann-Whitney U test was used to determine statistical significance. All statistical tests were performed on data normalized only to reference genes, however, gene expression values normalized to WT or other suitable control sample were used for plotting to allow for more intelligible visualization.

In vivo measurement of roGFP2-Tpx1.C169S oxidation

Wild-type (WT) and *cbf11Δ* cells were transformed with plasmid p407.C169S, constitutively expressing the H_2O_2 reporter protein roGFP2-Tpx1.C169S. To measure basal and induced H_2O_2 levels, fluorescence of the probe was determined as described before [29]. Briefly, roGFP2 exhibits two excitation maxima at 400 nm and 475–490 nm when fluorescence emission is monitored at 510 nm, and the ratio between the two maxima varies upon oxidation by peroxides. Strains were grown in EMM to an OD_{600} of 1, and fluorescence of the cultures was analyzed in 96-well plates before and after the addition of extracellular H_2O_2. For calculation of the degree of oxidation of the sensor (OxD), we first subtracted the equivalent fluorescence values of cells lacking the plasmid, and then used the formula displayed in [29].

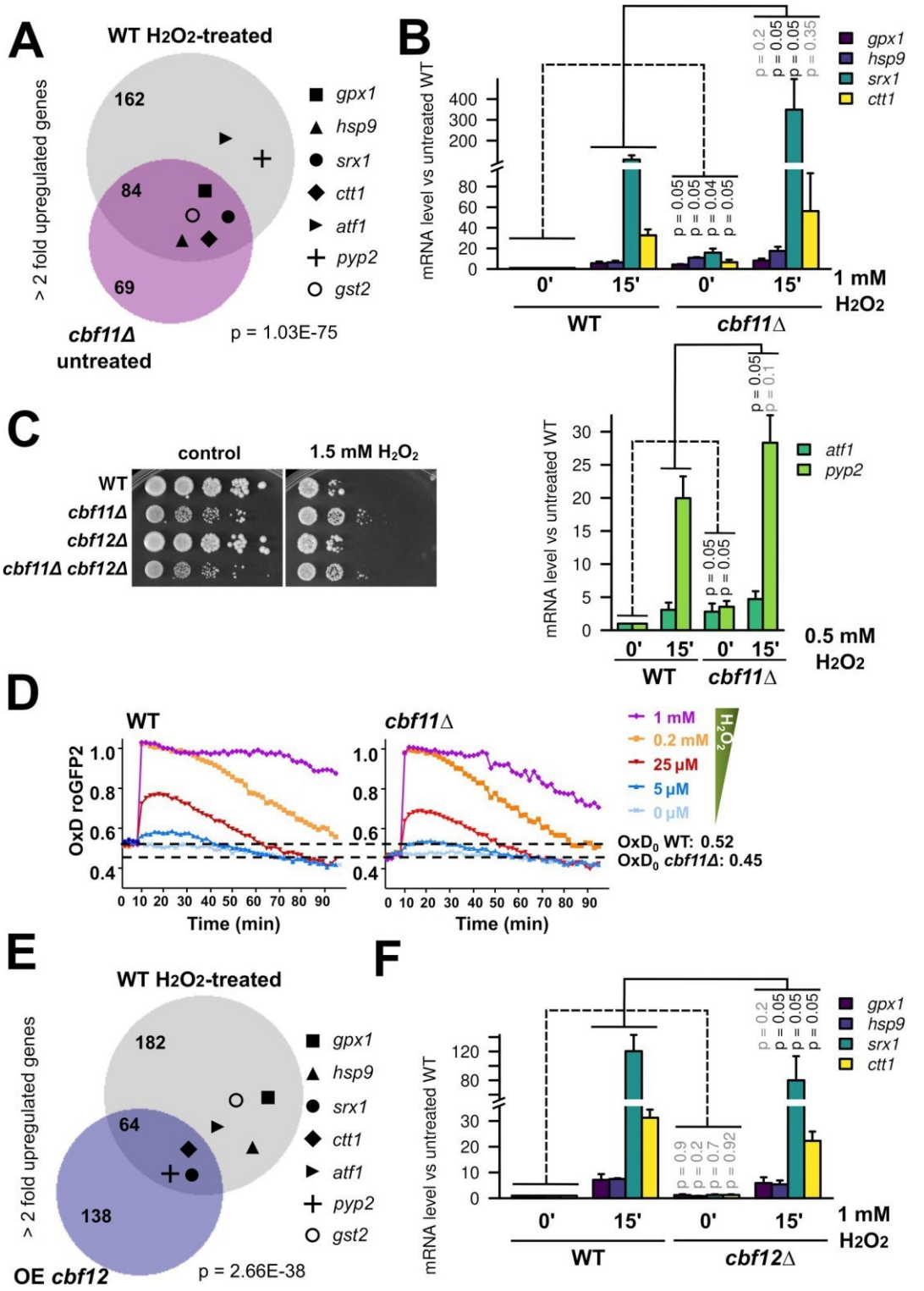

Fig 1. Absence of Cbf11 leads to activation of stress-response genes. (A) Venn diagram of genes upregulated more than 2-fold in WT cells after 15 min treatment with 1 mM H_2O_2 in EMM medium (data from [34]), and genes upregulated more than 2-fold in *cbf11Δ* cells growing exponentially in YES medium (data from [15]). The group membership of stress genes from panel B is indicated with symbols. Overlap significance was determined by two-sided Fisher's exact test. **(B)** Expression of the indicated stress genes in WT and *cbf11Δ* cells treated or not with the indicated concentrations of H_2O_2 for 15 min in YES was analyzed by

RT-qPCR. Mean and SD values of three independent replicates are shown. One-sided Mann-Whitney U test was used to determine statistical significance. **(C)** Survival and growth under oxidative stress of WT, *cbf11Δ*, *cbf12Δ* and *cbf11Δ cbf12Δ* cultures spotted on YES plates containing 1.5 mM H_2O_2. **(D)** *cbf11Δ* displays lower steady-state intracellular H_2O_2 levels, and detoxifies extracellular peroxides faster than WT cells. The indicated concentrations of H_2O_2 were directly added to EMM cultures of WT and *cbf11Δ* cells transformed with plasmid p407.C169S. The degree of probe oxidation on scale from 0 (fully reduced) to 1 (fully oxidized) is indicated on the Y axis (OxD roGFP2). The starting levels of probe oxidation in each strain background (OxD_0) are indicated by dashed horizontal lines. Mean values from three biological replicates are shown. **(E)** Venn diagram of genes upregulated more than 2-fold in WT cells after 15 min treatment with 1 mM H_2O_2 in EMM medium (data from [34]), and genes upregulated more than 2-fold in cells overexpressing Cbf12 grown in EMM (data from [15]). The group membership of stress genes from panel B is indicated with symbols. Overlap significance was determined by two-sided Fisher's exact test. **(F)** Expression of the indicated stress genes in WT and *cbf12Δ* cells treated or not with 1 mM H_2O_2 for 15 min in YES was analyzed by RT-qPCR. Mean and SD values of three independent replicates are shown. One-sided Mann-Whitney U test was used to determine statistical significance.

https://doi.org/10.1371/journal.pgen.1010582.g001

TCA extracts and immunoblotting

TCA extracts were prepared as described [30]. Atf1 was detected with a polyclonal anti-Atf1 antibody [31], phosphorylated Sty1 was detected with an anti-phospho-p38 antibody (Cell Signaling, 9215), and total Sty1 protein was detected with a polyclonal antibody [32].

Pap1 microscopy

Cells expressing Pap1-GFP from its endogenous chromosomal locus [33] were grown in YES to exponential phase, treated as required and fixed by 10% formaldehyde for 15 min. Then, cells were washed three times with PBS. To observe Pap1-GFP localization, cell suspension was loaded onto lectin-coated slides and imaged using the Olympus CellR microscope system.

Microarray analysis

Cells were grown to exponential phase (OD_{600} 0.5) in the YES medium at 32˚C. At time 0, H_2O_2 was added to all cultures to the final concentration of 0.74 mM. Culture aliquots were harvested immediately before, and 15 and 60 minutes after H_2O_2 addition by centrifugation for 2 minutes at 1000 g, room temperature, and then snap frozen in liquid nitrogen. RNA extraction and labelling, sample hybridization to custom in-house dual-colour cDNA microarrays, and microarray data processing were performed as described previously [15]. Individual Cy3-labelled samples were hybridized together with a Cy5-labelled reference pool (an equimolar pool from all 9 samples in this study). The microarray data are available from the ArrayExpress database (https://www.ebi.ac.uk/arrayexpress/) under accession number E-MTAB-6761.

ChIP-qPCR

ChIP-qPCR analysis of Cbf11-TAP shown in the main text was performed as described previously [15].

For ChIP-qPCR of Atf1-HA shown in the main text and ChIP-qPCR of Cbf11-TAP and Cbf11-HA shown in the supplementary files cells were grown in EMM medium and chromatin isolation was performed as described elsewhere [34]. Commercial IgG Sepharose Beads (GE Healthcare, 17-0969-01) were used in order to immunoprecipitate TAP-tagged proteins.

H3 and H3K9ac ChIP-seq

Two independent replicates were performed. Cells were cultivated to exponential growth phase (OD_{600} 0.5) in the complex YES medium and fixed by adding formaldehyde to the final concentration of 1%. After 30 min incubation, the remaining formaldehyde was quenched by 125 mM glycine. Cells were washed with PBS and broken with glass beads. Extracted

chromatin was sheared with the Bioruptor sonicator (Diagenode) using 15 or 30 cycles (for biological replicate 1 and 2, respectively) of 30 s on, 30 s off at high power settings. For all immunoprecipitations (IP) within a biological replicate the same amount of chromatin extract was used (2.5 or 3.7 mg of total protein); 1/10 of the total chromatin extract amount was kept for input DNA control. For each IP 5 μg of antibody (H3: Ab1791, H3K9ac: Ab4441, all Abcam) were incubated with the chromatin extract for 1 hour at 4˚C with rotation. Then, 50 μl of BSA-blocked Protein A-coated magnetic beads (ThermoFisherScientific, 10002D) were added to the chromatin extract-antibody suspension and incubated for further 4 hours at 4˚C with rotation. The precipitated material and input chromatin extract were decrosslinked, treated with RNase A and proteinase K. DNA was purified using phenol-chloroform extraction and sodium acetate/ethanol precipitation. In biological replicate 2, DNA purification on AMPure XP beads (Beckman Coulter, AC63880) was performed following the phenol-chloroform extraction to remove low-molecular fragments and RNA. Concentration of DNA was measured using the Quantus fluorometer (Promega) and fragment size distribution was checked on Agilent Bioanalyzer using the High Sensitivity DNA Assay. Library construction and sequencing were performed by BGI Tech Solutions (Hong Kong) using the BGISEQ-500 sequencing system.

ChIP-seq data analysis

The *S*. *pombe* reference genome sequence and annotation were obtained from PomBase (release date 2018-09-04) [35,36]. Read quality was checked using FastQC version 0.11.8 (https://www.bioinformatics.babraham.ac.uk/projects/fastqc/), and reads were aligned to the *S*. *pombe* genome using HISAT2 2.1.0 [37] and SAMtools 1.9 [38,39]. Read coverage tracks (i.e., target protein occupancy) were then computed and normalized to the respective mapped library sizes using deepTools 3.3.1 [40]. The list of genes upregulated as part of the core environmental stress response ("CESR-UP" genes) was obtained from [9]. The CESR-UP genes were further divided into two groups based on whether or not the genes were also upregulated in untreated *cbf11Δ* cells [15]. The deepTools 3.5.1 were then used to create average-gene H3 and H3K9ac occupancy profiles for the respective CESR-UP gene subgroups and for all fission yeast genes as a control. The raw ChIP-seq data are available from the ArrayExpress database under the accession number E-MTAB-11081. The scripts used for ChIP-seq data processing and analysis are available from https://github.com/mprevorovsky/ox-stress_histones.

Acetyl-CoA measurement

Cells grown to exponential phase (OD_{600} 0.5) in the YES medium were collected by centrifugation (1000 g, 5 min) or vacuum filtration (25 ODs). The filter with cell pellet was immediately transferred to 25 ml methanol (-20˚C). Samples were centrifuged (3000 g, 5 min, -4˚C, brake 5) and supernatant was decanted. Then 410 μl of 50% freezer-cooled methanol with 10 μM PIPES was added. Cells were broken using glass beads on FastPrep 6.5 m/s, 20 s, 6 cycles. Crude extracts were ultrafiltered using 10kDa filter Amicon Ultra 0.5 ml Ultracel-10K (UFC501096). Samples were evaporated at room temperature on SpeedVac and dissolved in 40 μl 50% acetonitrile. The samples were analyzed on a Dionex Ultimate 3000RS liquid chromatography system coupled to a TSQ Quantiva mass spectrometer (ThermoScientific). A ZIC- HILIC column (150 mm × 2.1 mm, 5 μm, Merck) was used for separation of analytes. The column was maintained at room temperature and an injection of 1–2 μl of the sample was applied. The gradient elution took 20.5 min and was set from 5% A to 70% A and then 70% A was held for 2 min. A column equilibration step followed and lasted 9 min (A: 10 mM ammonium bicarbonate pH 9.3, B: 97% acetonitrile, flow rate 200 μl/min). Electrospray ionization

with switching polarity mode ran under following conditions: ion transfer tube temperature 350˚C, vaporizer temperature 275˚C, spray voltage 3500/3000 V (depends on the polarity mode), sheath gas 35 and aux gas 15. For targeted determination of analytes, SRM assay was developed previously by infusing pure compounds.

Growth curves

OD_{600} was recorded during 24–30 h for cells growing in YE at 30˚C from an initial OD_{600} of 0.1 using an automated measurement as previously described [41]. When indicated, H_2O_2 was added to the cultures.

Results

Absence of Cbf11 leads to upregulation of stress-response genes and increased resistance to H_2O_2

In our previous studies, we identified fission yeast genes that change their expression upon genetic manipulation of the *cbf11* and/or *cbf12* CSL transcription factor genes (deletion, overexpression). We also noted that these deregulated genes were enriched for stress-response genes [15]. More recently, we described the transcriptional signatures of wild-type (WT) cells under oxidative stress [34]. Interestingly, when comparing these datasets, we found that 55% of the genes upregulated more than two-fold in cells lacking Cbf11 were also upregulated under oxidative stress in a WT strain ($p = 1.03 \times 10^{-75}$; Fig 1A). This finding raises the possibility that a genuine oxidative-stress response is triggered in cells lacking Cbf11, and/or that Cbf11 acts as a direct or indirect repressor of oxidative stress-response genes.

To examine these possibilities further, we first validated our genome-wide data using RT-qPCR. To this end, we selected representative stress-response genes: *srx1*, *ctt1*, *gpx1*, *hsp9* and *gst2*, which code for sulfiredoxin, catalase, glutathione peroxidase, heat shock protein 9, and glutathione S-transferase, respectively [35]. We also included *atf1* and *pyp2*, which encode a transcription factor and a protein phosphatase that regulate the cellular response to oxidative stress [8,42], and were previously reported to be upregulated ~1.8-fold in *cbf11Δ* [15]. We found that all selected genes indeed showed moderately increased basal expression in untreated *cbf11Δ* compared to WT, and became further upregulated upon H_2O_2 treatment, reaching even higher transcript levels than in WT (Figs 1B and 2D).

Next, we tested whether the upregulation of oxidative stress-response genes in *cbf11Δ* cells has any physiological consequences. We found that compared to WT, *cbf11Δ* cells were more resistant to H_2O_2, both when grown on solid media (Fig 1C) and in liquid cultures (S1A–S1D Fig). Furthermore, when we introduced the roGFP2-Tpx1.C169S peroxide-sensitive redox probe [29], *cbf11Δ* cells showed lower basal levels of probe oxidation (OxD_0 of 0.45), which indicates lower steady-state levels of intracellular H_2O_2 compared to WT (OxD_0 of 0.52) (Fig 1D). Of note, a decrease of the OxD_0 for roGFP2-Tpx1.C169S has previously been reported for cells expressing constitutively active Sty1 [29]. Furthermore, cells lacking Cbf11 were also able to detoxify extracellular peroxides faster than WT (compare the reduction slopes of WT and *cbf11Δ* cells in Fig 1D), suggesting a higher peroxide scavenging capacity of these cells. Notably, *cbf11Δ* cells are not resistant to the superoxide generator menadione (S1E Fig), which triggers a different type of stress response than H_2O_2 does [10,43]. Moreover, *cbf11Δ* cells are sensitive to cold stress [44], hypoxia [16] and the microtubule poison thiabendazole [45], suggesting their resistance to H_2O_2 is a highly specific phenomenon. Taken together, we have confirmed that oxidative stress-response genes are moderately upregulated in untreated *cbf11Δ* cells, and these cells are resistant to oxidative stress triggered by H_2O_2.

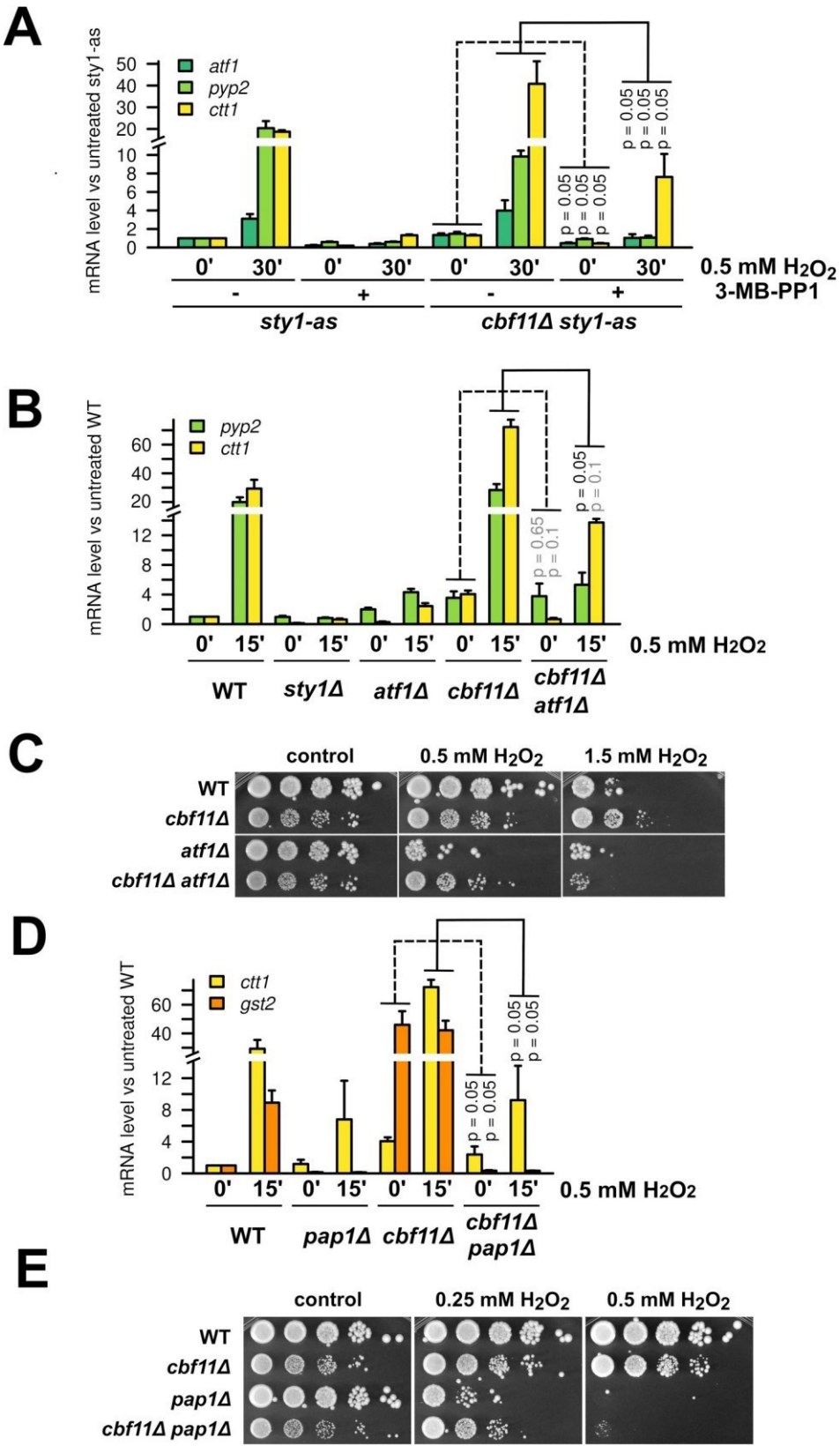
A
mRNA level vs untreated sty1-as
atf1
pyp2
ctt1
p = 0.05
0' 30' 0' 30' 0' 30' 0' 30'
0.5 mM H2O2
3-MB-PP1
sty1-as
cbf11Δ sty1-as
B
mRNA level vs untreated WT
pyp2
ctt1
p = 0.65
p = 0.1
p = 0.05
p = 0.1
0' 15' 0' 15' 0' 15' 0' 15' 0' 15'
0.5 mM H2O2
WT
sty1Δ
atf1Δ
cbf11Δ
cbf11Δ atf1Δ
C
control
0.5 mM H2O2
1.5 mM H2O2
WT
cbf11Δ
atf1Δ
cbf11Δ atf1Δ
D
mRNA level vs untreated WT
ctt1
gst2
p = 0.05
0' 15' 0' 15' 0' 15' 0' 15'
0.5 mM H2O2
WT
pap1Δ
cbf11Δ
cbf11Δ pap1Δ
E
control
0.25 mM H2O2
0.5 mM H2O2
WT
cbf11Δ
pap1Δ
cbf11Δ pap1Δ

Fig 2. -Stress-gene activation in *cbf11Δ* cells is dependent on Sty1 and Atf1. (A) Expression of the indicated stress genes in *sty1-as* and *cbf11Δ sty1-as* cells treated or not with the Sty1-as inhibitor 3-MB-PP1 and 0.5 mM H_2O_2 for 30 min in YES medium was analyzed by RT-qPCR. Mean and SD values of three independent replicates are shown. One-sided Mann-Whitney U test was used to determine statistical significance. **(B)** Expression of the indicated stress genes in WT, *sty1Δ*, *atf1Δ*, *cbf11Δ*, and *cbf11Δ atf1Δ* cells treated or not with 0.5 mM H_2O_2 for 15 min in YES was analyzed by RT-qPCR. Mean and SD values of three independent replicates for *pyp2* and two independent replicates for *ctt1* transcript are shown. One-sided Mann-Whitney U test was used to determine statistical significance. **(C)** Survival and growth under oxidative stress of WT, *cbf11Δ*, *atf1Δ* and *cbf11Δ atf1Δ* cultures spotted on YES plates containing the indicated concentrations of H_2O_2. **(D)** Expression of the indicated stress genes in WT, *pap1Δ*, *cbf11Δ*, and *cbf11Δ pap1Δ* cells treated or not with 0.5 mM H_2O_2 for 15 min in YES was analyzed by RT-qPCR. Mean and SD values of three independent replicates are shown. One-sided Mann-Whitney U test was used to determine statistical significance. **(E)** Survival and growth under oxidative stress of WT, *cbf11Δ*, *pap1Δ* and *cbf11Δ pap1Δ* cultures spotted on YES plates containing the indicated concentrations of H_2O_2.

https://doi.org/10.1371/journal.pgen.1010582.g002

We have previously shown that Cbf12, the other fission yeast CSL paralog, acts as a Cbf11 antagonist [15,44]. Therefore, we investigated whether Cbf12 could positively regulate the transcriptional response to oxidative stress. We found that ~32% of the genes upregulated in cells overexpressing Cbf12 were also induced after oxidative stress treatment in WT cells ($p = 2.66 \times 10^{-38}$), even though only 3 of our selected reference genes (*ctt1*, *srx1* and *pyp2*), were upregulated more than two-fold under both conditions (Fig 1E). However, when we analyzed *cbf12Δ* cells using RT-qPCR, we did not observe any decrease in basal transcript levels of the selected stress-response genes, and we only detected a slightly weaker stress gene induction after stress imposition compared to WT (Fig 1F). Furthermore, we did not detect any notable impact of loss of Cbf12 on the transcriptome-wide response to oxidative stress (see below). Finally, the *cbf12Δ* strain did not show altered resistance to H_2O_2 (Fig 1C) or menadione (S1E Fig), indicating that Cbf12 only plays a minor role, if any, in the cellular response to oxidative stress. For that reason, we decided to focus on the role of Cbf11 in modulating stress-gene expression.

Increased stress-gene expression in *cbf11Δ* cells depends on the Sty1-Atf1 and Pap1 pathways

Expression of oxidative stress-response genes and resistance to H_2O_2 in WT fission yeast cells are critically dependent on the Sty1 kinase and its downstream target, the Atf1 transcription factor [10,12]. Therefore, we tested the requirement for Sty1 and Atf1 in the oxidative stress-related phenotypes of *cbf11Δ* cells.

We previously failed to construct the *cbf11Δ sty1Δ* strain and noted a strong selective pressure for retaining a translocated copy of the *cbf11* gene, suggesting that the double mutant is very sick or lethal [15]. Cbf11 and Sty1 exert antagonistic effects on cell-cycle progression, where the G2/M transition is accelerated in *cbf11Δ* cells and delayed in *sty1Δ* cells. Therefore, the poor viability of *cbf11Δ sty1Δ* cells might be due to a conflict in cell-cycle regulation [15,13,14]. To circumvent these issues, we used an analog-sensitive Sty1 allele in the current study [46]. As expected, the *cbf11Δ sty1-as* double mutant showed impaired growth upon Sty1 inhibition (S2 Fig).

Next, we determined whether Sty1 kinase activity is needed for triggering the transcriptional response to H_2O_2 in *cbf11Δ* cells. Inhibition of Sty1-as indeed led to severely reduced induction of stress-gene transcripts in H_2O_2 in both WT and *cbf11Δ* (Fig 2A, timepoints 30'). Importantly, even the basal transcript levels of oxidative stress-response genes in untreated *cbf11Δ* cells were partially dependent on the Sty1 kinase activity (Fig 2A, timepoints 0'). Similarly, expression of stress-response genes in *cbf11Δ* cells was also partially dependent on Atf1 (Fig 2B), even though the impact of *atf1* deletion was not as severe as Sty1 inhibition. Furthermore, we found that Atf1 was also partially required for the increased resistance of *cbf11Δ* cells to H_2O_2 both on solid media and in liquid culture (Figs 2C and S1B).

Under low H_2O_2 concentrations, a detoxification system regulated by the Pap1 transcription factor becomes crucial to fight oxidative stress. Importantly, there is crosstalk between the Sty1 and Pap1 pathways and, furthermore, some stress-response genes are regulated by both Pap1 and Atf1 [11,12]. We therefore assessed the role of Pap1 in the increased stress-gene expression and H_2O_2 resistance of the *cbf11Δ* mutant. Strikingly, we found that deletion of *pap1* partially suppressed the increased expression of catalase (*ctt1*; gene coregulated by Atf1) and largely abrogated the increased expression of glutathione S-transferase 2 (*gst2*) in untreated *cbf11Δ* cells (Fig 2D). Moreover, we found that Pap1 is required for survival of *cbf11Δ* cells in the presence of low to medium doses of H_2O_2 (Fig 2E), which is consistent with the known critical role of Pap1 in the induction of catalase expression under oxidative stress [11,12].

In summary, these data suggest that the Sty1-Atf1 and Pap1 pathways are required for the moderate upregulation of stress-response genes observed in untreated *cbf11Δ* cells, and for the increased tolerance to H_2O_2 of the *cbf11Δ* strain.

The impact of Cbf11 on stress-gene expression is likely indirect

Since the canonical stress-response pathways are required for stress-gene upregulation in *cbf11Δ* cells (Fig 2), we explored the following possibilities: 1) *cbf11Δ* cells might experience intrinsic oxidative stress that would result in the activation of the Sty1-Atf1 and/or Pap1 pathways, or 2) Cbf11 might counteract the activation of the stress-response pathways in WT cells. To test these hypotheses, we first analyzed the phosphorylation (i.e., activation) status of both Sty1 and Atf1 in cells lacking Cbf11. As shown in Fig 3A, no increase in phosphorylation of either Sty1 or Atf1 was observed in *cbf11Δ* cells, suggesting that the canonical Sty1-mediated stress response is not triggered in unstressed *cbf11Δ* cells, and neither does Cbf11 seem to block Sty1 activation.

Next, we tested whether Cbf11 could block the binding of Atf1 to stress-responsive promoters. We have previously reported two different subsets of stress genes: (i) in unstressed conditions, Atf1 is pre-bound to the first subset of genes, including *gpd1* and *hsp9*, and it is not recruited further after stress imposition; (ii) without stress, Atf1 shows relatively low occupancy at the second subset of genes, which includes *ctt1* and *srx1*, but is further recruited after stress imposition due to the activation of other transcription factors, such as Pap1 [34]. We found that Atf1 promoter occupancy in unstressed cells was not altered in *cbf11Δ* compared to WT (Fig 3B). Therefore, it is unlikely that Cbf11 could block or compete with Atf1 for binding to stress gene promoters.

Next, we tested the activation status of Pap1 in cells treated with cerulenin, an inhibitor of the fatty acid synthase (FAS) that triggers a phenotype similar to deletion of *cbf11* (see below). Pap1 undergoes activatory oxidation upon mild oxidative stress, which leads to the obstruction of its nuclear export signal. Pap1 then accumulates in the nucleus, where it facilitates stress-gene transcription [30,47,48]. Therefore, we treated WT cells expressing Pap1-GFP with cerulenin to induce *cbf11Δ*-like conditions, or with 0.2 mM H_2O_2, and observed Pap1 localization. While Pap1 clearly accumulated in the nucleus after the mild H_2O_2 treatment, Pap1 localization was indistinguishable from untreated cells after treatment with cerulenin, showing no signs of increased Pap1 activation under *cbf11Δ*-like conditions (Fig 3C).

Since Cbf11 was previously shown to co-precipitate with Atf1 [49], we also examined the possibility of Cbf11 recruitment to the promoters of stress genes, where it could directly repress their expression under non-stressed conditions, although our previous Cbf11 ChIP-seq analysis did not indicate a clear presence of Cbf11 at stress genes [15]. Nevertheless, we tried to detect Cbf11 by ChIP-qPCR at several stress-gene promoters (both in untreated and

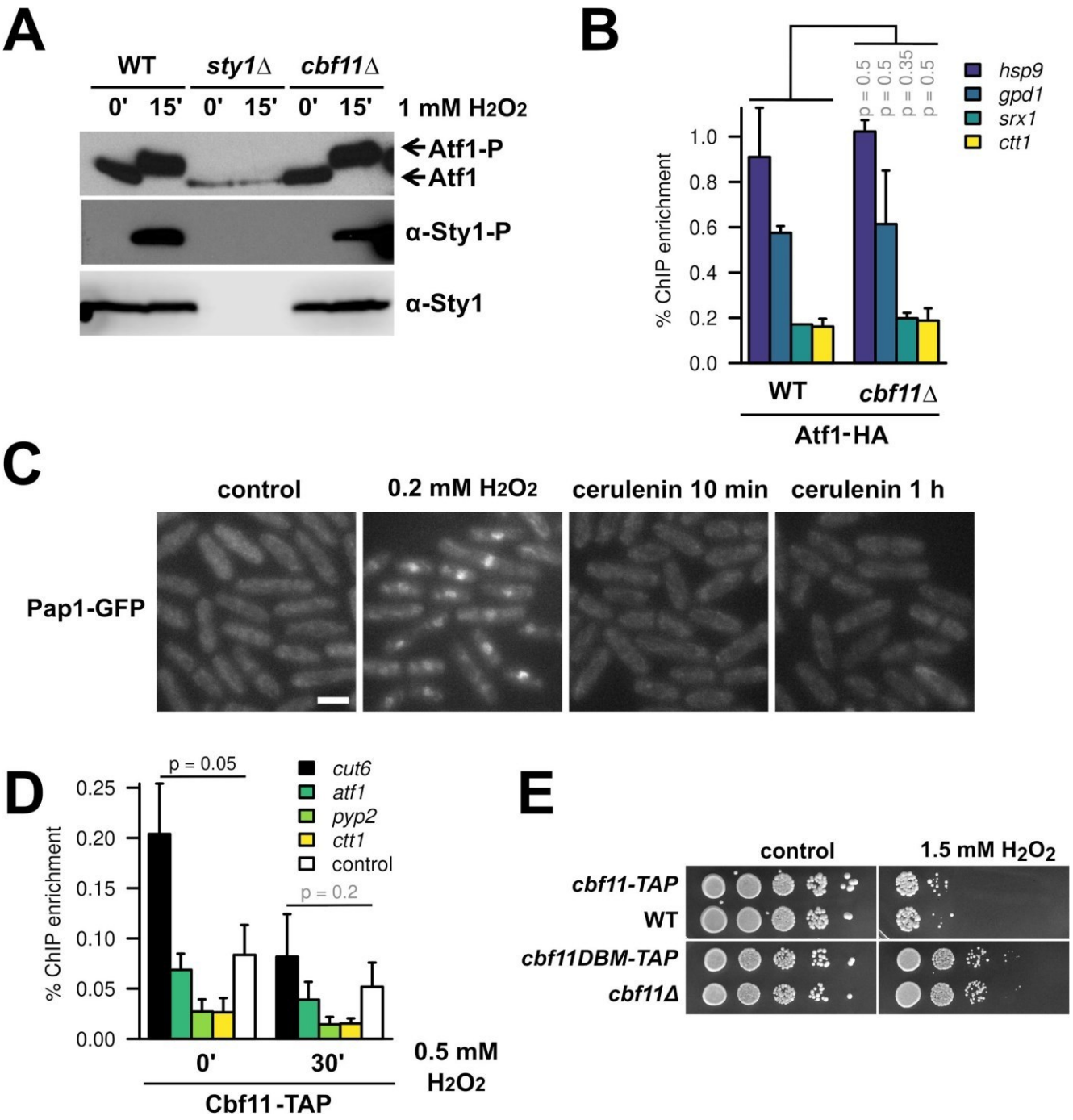

Fig 3. Cbf11 likely affects stress-gene expression indirectly. (A) Western blot analysis of Atf1 and Sty1 phosphorylation in WT, *sty1Δ*, and *cbf11Δ* cells treated or not with 1 mM H_2O_2 for 15 min in YES medium. Atf1 phosphorylation manifests as retarded migration through the gel. **(B)** Recruitment of Atf1 to the indicated stress-gene promoters was analyzed by ChIP-qPCR in untreated cells grown in EMM medium. Mean and SD values of two independent replicates are shown. Two-sided Mann-Whitney U test was used to determine statistical significance. **(C)** Pap1-GFP localization was observed in formaldehyde-fixed cells grown to exponential phase in YES using epifluorescence microscopy. Cells were either untreated (control), treated with 0.2 mM H_2O_2 for 25 min as a stressed control or treated with 20 μM cerulenin for 10 min and 1 hour to inhibit FA synthesis. Scale bar 5 μm. **(D)** Recruitment of Cbf11 to the indicated stress-gene promoters was analyzed by ChIP-qPCR in cells treated or not with 0.5 mM H_2O_2 for 30 min in YES. The *cut6* promoter is a positive control for Cbf11 binding [17];"control" is an intergenic locus with no Cbf11 binding (Chr I: 1,928,359–1,928,274). Mean and SD values of three independent replicates are shown. One-sided Mann-Whitney U test was used to determine statistical significance; since no stress promoter loci showed signal higher than the negative control locus, these loci were not tested statistically. **(E)** Survival and growth under oxidative stress of WT, *cbf11Δ*, *cbf11-TAP*, and *cbf11DBM-TAP* cultures spotted on YES plates containing 1.5 mM H_2O_2.

https://doi.org/10.1371/journal.pgen.1010582.g003

H_2O_2-treated cells), focusing on potential (weak) Cbf11 ChIP-seq peaks (Fig 3D) and known Atf1 binding sites (S3 Fig). The promoter of *cut6*, a well-characterized Cbf11 target gene involved in fatty-acid synthesis, served as a positive control. We assayed Cbf11 binding to DNA in both YES and EMM media, using HA- and TAP-tagged Cbf11, but we did not detect clear Cbf11 presence at the tested stress genes. Collectively, these results strongly argue that the repressive effect of Cbf11 on Sty1/Atf1-dependent stress-gene expression is brought about indirectly.

The R318H substitution in the beta-trefoil domain of Cbf11 (Cbf11DBM) abolishes its binding to the canonical CSL response element [25]. To test whether its DNA-binding activity is at all required for Cbf11 to repress Sty1-Atf1 target genes, we introduced the DBM mutation into the endogenous *cbf11* locus. Notably, the *cbf11DBM* mutant resembled the full *cbf11* deletion in that it showed increased expression of stress-response genes (Fig 4D), and it was resistant to H_2O_2 (Fig 3E). Thus, the DNA-binding activity is critical for the Cbf11-mediated repression of stress genes. Overall, these data suggest that Cbf11 transcriptionally regulates some other, stress-unrelated, genes that in turn affect stress-gene expression.

Multiple lipid-metabolism mutants show derepression of stress genes and resistance to H_2O_2

Up to now, we analyzed the *cbf11Δ* response to oxidative stress using several representative genes. To also capture the global picture, we next performed a microarray analysis of gene expression in a timecourse experiment following H_2O_2 treatment. This transcriptome analysis confirmed the trends observed so far: many stress-responsive genes were moderately upregulated already in untreated *cbf11Δ* cells and were induced even further upon stress imposition (Fig 4A). Interestingly, the changes in the transcriptome of untreated *cbf11Δ* cells were mostly inductions: 134 genes were ≥2x upregulated, while only 10 genes were ≥2x downregulated compared to untreated WT cells (Fig 4B). This contrasts with the physiological reaction to H_2O_2 in WT cells, where stress-gene induction is accompanied by repression of numerous, mostly growth-related genes ([9] and Fig 4B, top panel). Importantly, only 2 out of the 10 genes downregulated in untreated *cbf11Δ* cells are known to be downregulated as part of the core environmental stress response in WT (*car2* and SPBPB7E8.01) [9]. These results are in agreement with our earlier notion that the increased stress-gene expression in untreated *cbf11Δ* cells is not merely a consequence of some hypothetical internal oxidative stress activating a genuine stress response.

We previously showed that several genes downregulated in *cbf11Δ* cells are related to lipid metabolism (e.g., FA synthesis) and that Cbf11 directly activates their transcription [15]. Indeed, three such direct Cbf11 target genes (*cut6*, *lcf2*, *ole1*) were also ≥2x downregulated in untreated *cbf11Δ* cells in the current microarray experiment (Fig 4C). Intriguingly, in *Saccharomyces cerevisiae* decreased FA synthesis caused by inhibition of the acetyl-CoA carboxylase (Cut6 in *S*. *pombe*) leads to chromatin hyperacetylation and changes in gene expression. Presumably, this is caused by increased availability of acetyl-CoA, which is used as substrate by both ACC and HATs [21]. Lipid-metabolism genes thus represent a potential link between Cbf11 transcription factor activity and changes in stress-gene expression. To examine such potential indirect regulation of stress genes by Cbf11, we assessed stress-gene expression and H_2O_2 resistance in other lipid-metabolism mutants. These included the Mga2 transcription factor that also regulates the ACC/*cut6* gene (*mga2Δ*; [16]) and the ACC/Cut6 enzyme itself (*Pcut6MUT* promoter mutant with ~50% reduction in expression [17] and *cut6-621* ts mutant [50]). Strikingly, all mutants showed increased expression of stress genes (Fig 4D), and all but the sick *cut6-621* ts mutant were also resistant to H_2O_2 (Fig 4E). To further probe the link

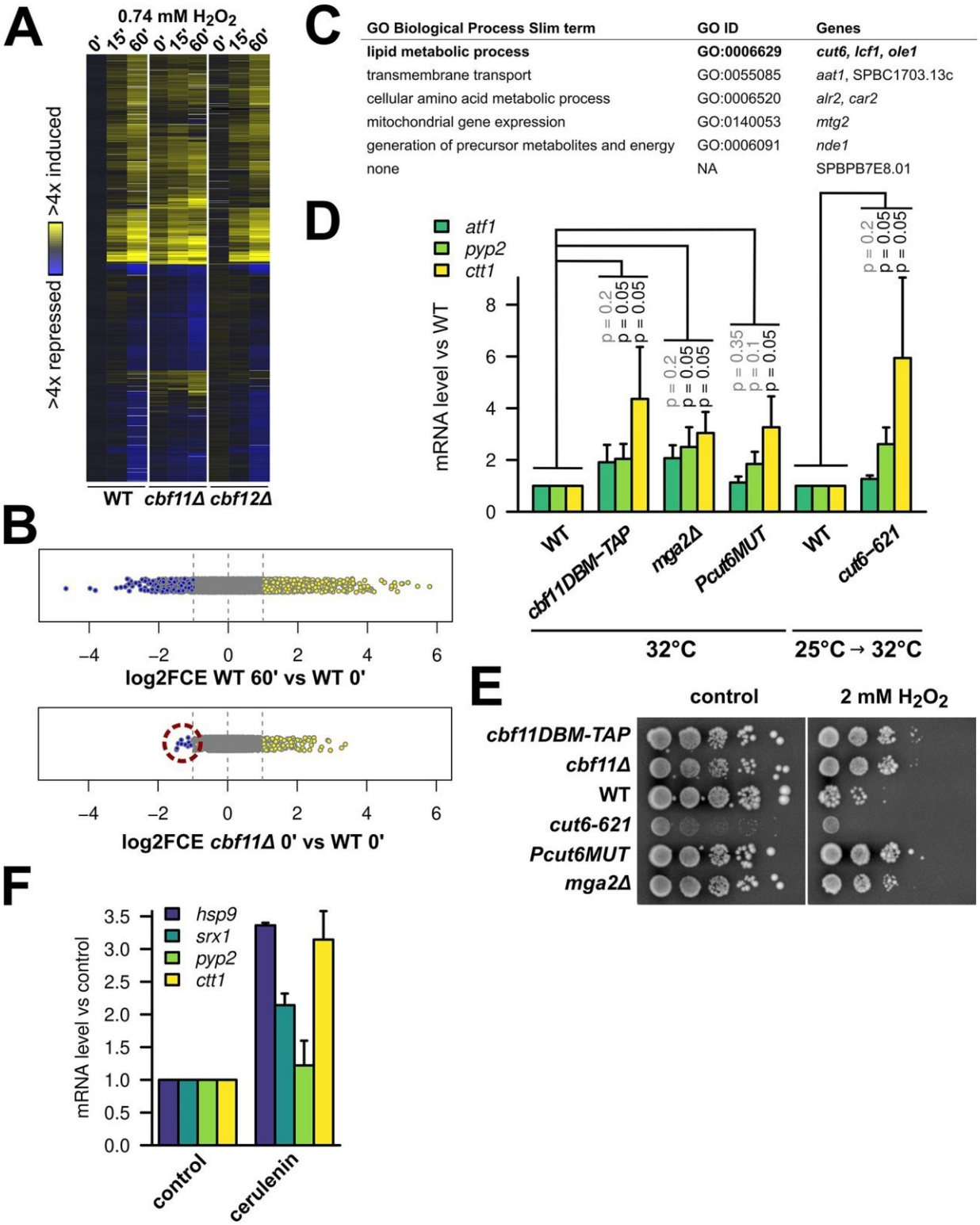

Fig 4. Perturbation of lipid metabolism leads to derepression of stress genes. (A) Heatmap of gene expression in WT, *cbf11Δ*, and *cbf12Δ* cells upon treatment with 0.74 mM H_2O_2 in YES medium. Transcript levels were determined by a timecourse microarray analysis and normalized to untreated WT values. Only genes showing ≥2-fold change in expression in at least one condition are shown. This experiment was performed once. **(B)** Distribution of all relative transcript levels in WT cells treated for 60 min with H_2O_2 and untreated *cbf11Δ* cells from the experiment in panel A. Values represent log2 of fold-changes in expression compared to untreated WT. Individual genes are shown as dots; blue and yellow dots

represent ≥2-fold down- and upregulated genes, respectively. The 10 genes downregulated in untreated *cbf11Δ* cells are highlighted with a red circle. **(C)** Biological functions of the 10 genes downregulated in untreated *cbf11Δ* cells from panel B were determined using slimmed Gene Ontology Biological Process annotations [35]. Known direct Cbf11 targets are in bold. **(D)** Expression of the indicated stress genes in untreated WT, *cbf11DBM-TAP*, *mga2Δ*, *Pcut6MUT*, and *cut6-621* cells growing in YES was analyzed by RT-qPCR. The temperature sensitive *cut6-621* mutant was shifted to a semi-restrictive temperature to inhibit Cut6 function prior to analysis. Mean and SD values of three independent replicates are shown. One-sided Mann-Whitney U test was used to determine statistical significance. **(E)** Survival and growth under oxidative stress of WT, *cbf11Δ*, *cbf11DBM-TAP*, *mga2Δ*, *Pcut6MUT*, and *cut6-621* cultures spotted on YES plates containing 2 mM H_2O_2. The plates were incubated at 32˚C, which is a semi-restrictive temperature for the *cut6-621* mutant. **(F)** Expression of the indicated stress genes in WT cells treated with DMSO (control) or 20 μM cerulenin for 1 hour in YES was analyzed by RT-qPCR. Mean and SD values of two independent replicates are shown.

https://doi.org/10.1371/journal.pgen.1010582.g004

between FA synthesis and stress-gene expression we treated exponentially growing WT cells with the FAS inhibitor cerulenin, which represents an acute intervention, as opposed to the chronic perturbations in mutants assayed so far. Also, the *fas1* and *fas2* genes, encoding the FAS subunits, are not regulated by Cbf11 [15]. Remarkably, we found that the chemical inhibition of FAS, which limits acetyl-CoA consumption by FA synthesis, also resulted in increased stress-gene expression (Fig 4F). Previously, FAS downregulation was found to increase resistance to H_2O_2 in the budding yeast, where the authors proposed that altered lipid composition might have lowered plasma membrane permeability for H_2O_2 [51]. While not being mutually exclusive, our data rather point to a novel regulatory link between FA synthesis on the one hand, and stress-gene expression and cellular resistance to oxidative stress on the other hand.

Stress genes derepressed in *cbf11Δ* cells show H3K9 hyperacetylation at their promoters

While it was previously shown that decreased FA synthesis leads to chromatin hyperacetylation in *Saccharomyces cerevisiae*, no effect on stress-response genes was reported [21]. Intriguingly, we previously showed that the Gcn5/SAGA histone acetyltransferase regulates the expression of stress genes in fission yeast via histone H3 acetylation at lysines 9 and 14 [52,53]. We decided to explore these links further.

First, to determine whether the increased expression of stress genes in the *cbf11Δ* lipid-metabolism mutant was associated with changes in their histone acetylation profiles, we performed ChIP-seq experiments. As previously described [53], the promoters of most stress genes are largely depleted of nucleosomes (compare the H3 levels at promoters and gene bodies in Fig 5A), but we could immunoprecipitate histones both upstream and downstream of the transcription start sites (TSS in Fig 5A). Thus, we determined the occupancy of total histone H3 and H3 acetylated at lysine 9 (H3K9ac), and analyzed their distribution at stress gene bodies and promoter regions. We focused on genes upregulated as part of the core environmental stress response in WT cells (CESR-UP; [9]), and further divided these genes based on their responsiveness to the absence of Cbf11. Strikingly, the CESR-UP genes upregulated in untreated *cbf11Δ* cells (n = 94) showed a marked increase in H3K9 acetylation at their promoters and beginning of gene bodies in *cbf11Δ* cells compared to WT, while no differences in total histone H3 occupancy between the two genotypes were observed (Figs 5A and S4A). Moreover, the H3K9ac profile of the remaining CESR-UP genes (n = 441) resembled the profile of all fission yeast genes, suggesting specificity of the observed hyperacetylation (Figs 5A and S4A).

Second, we have discovered that even a modest ACC/Cut6 overexpression (~2 fold, Fig 5B) is sufficient to substantially suppress the increased stress-gene expression and oxidative-stress resistance in the *cbf11Δ* lipid-metabolism mutant (Fig 5B and 5C). Additionally, although Cut6 overexpression does not affect stress-gene expression in unstressed WT cells (Fig 5B), *cut6OE* renders WT cells sensitive to H_2O_2 (Fig 5C), suggesting that increased FA synthesis

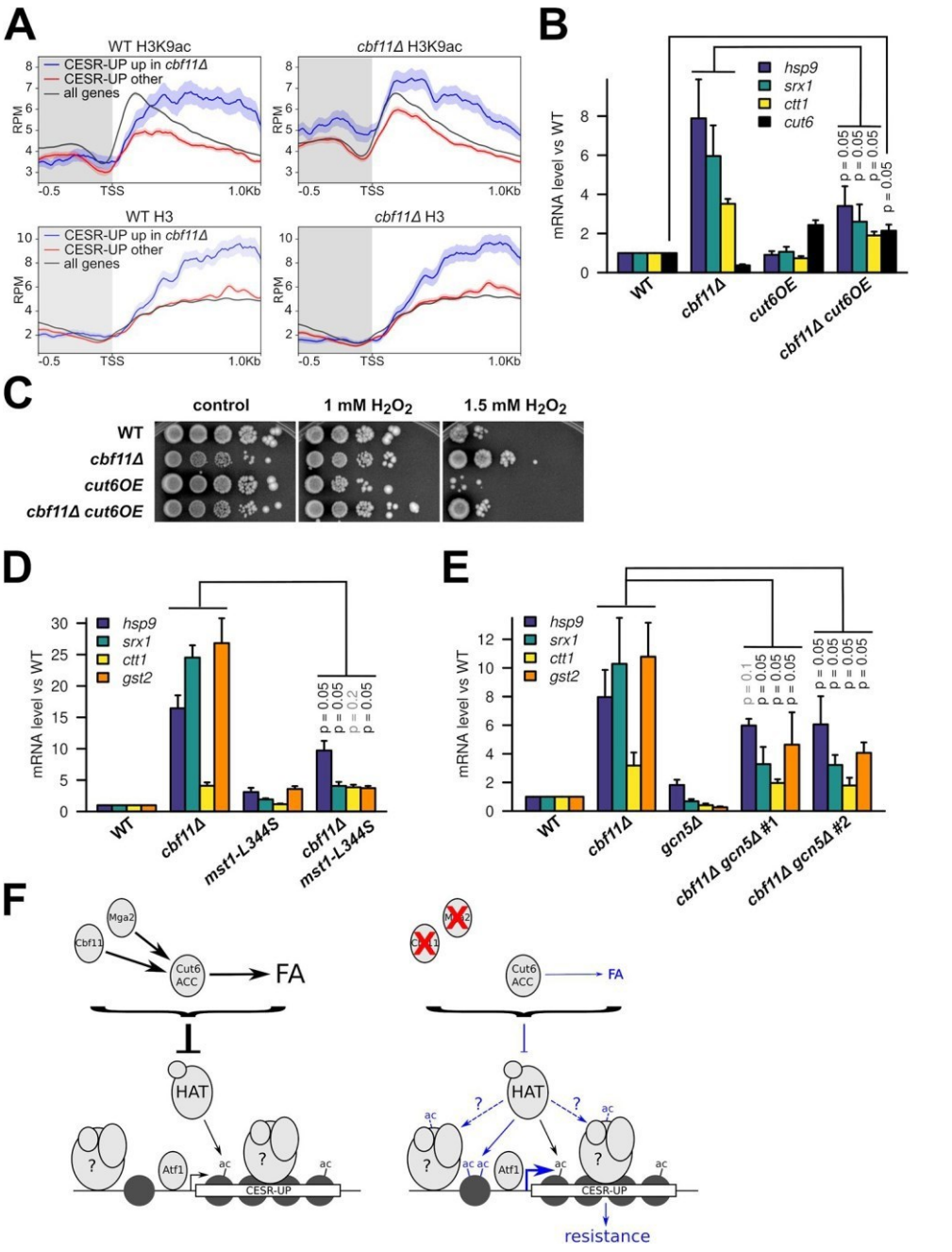

Fig 5. Derepression of stress genes in *cbf11Δ* cells is associated with H3K9 hyperacetylation in their promoters. **(A)** Average gene profiles of total H3 (bottom panels) and acetylated H3K9 (top panels) occupancy at stress gene regions in WT and *cbf11Δ* cells. Genes upregulated as part of the core environmental stress response (CESR-UP, [9]) have been divided into those showing upregulation in untreated *cbf11Δ* cells (blue; n = 94, [15]) and the rest (red; n = 441). Average profile of all fission yeast genes is also shown for comparison (black; n = 6952). The curves represent mean RPM (reads per million mapped reads) values ± SEM; results from one representative biological replicate are shown. The promoter region is shaded. TSS—transcription start site. **(B)** Expression of the indicated stress genes in untreated WT, *cbf11Δ*, *cut6OE* and *cbf11Δ cut6OE* cells growing in YES medium was analyzed by RT-qPCR. Mean and SD values of three independent replicates are shown. One-sided Mann-Whitney U test was used to determine statistical significance. **(C)** Survival and growth under oxidative stress of WT, *cbf11Δ*, *cut6OE* and *cbf11Δ cut6OE* cultures spotted on YES plates containing the indicated concentrations of H_2O_2. **(D)** Expression of the indicated stress genes in untreated WT, *cbf11Δ*, *mst1-L344S* and *cbf11Δ mst1-L344S* cells growing in YES medium was analyzed by RT-qPCR. All cultures were shifted to 32˚C (temperature restrictive for the *mst1-L344S* strain) prior to analysis. Mean and SD values of three independent replicates are shown. One-sided Mann-Whitney U test was used to determine

statistical significance. **(E)** Expression of the indicated stress genes in untreated WT, *cbf11Δ*, *gcn5Δ*, and two independent isolates of *cbf11Δ gcn5Δ* cells growing in YES medium was analyzed by RT-qPCR. Mean and SD values of three independent replicates are shown. One-sided Mann-Whitney U test was used to determine statistical significance. **(F)** A model of the crosstalk between lipid metabolism and stress resistance. The left panel shows the WT situation; the right panel shows the situation in mutants with decreased synthesis of FA, with differences highlighted in blue. Hypothetical chromatin remodelers and/or histone modifiers are denoted with a question mark. Dashed lines represent speculative interactions. See Discussion for more details.

https://doi.org/10.1371/journal.pgen.1010582.g005

can hamper the launch of an effective stress response. This observation further confirms the tight relationship between FA metabolism and stress-gene expression. Since ACC activity is hypothesized to affect the general availability of acetyl-CoA [21] we also tested the global levels of acetyl-CoA in lipid metabolism mutants by liquid chromatography-mass spectrometry (LC-MS). While we detected lower acetyl-CoA levels in the *ppc1-537* phosphopantothenate-cysteine ligase mutant strain, which is severely deficient in CoA synthesis [54], we did not find any significant changes in global acetyl-CoA levels in cell extracts of *cbf11Δ* or *Pcut6MUT* (S4B Fig). These findings, however, do not completely rule out the following possibilities: 1) local, compartmentalized changes in acetyl-CoA availability occur in these two mutants [55], as the nucleocytosolic acetyl-CoA pool, which is directly affected by ACC/Cut6, is not uniform and acetyl-CoA levels at chromatin need not correlate with the global acetyl-CoA levels [56]. Nevertheless, we currently cannot explain how such precise micro-compartmentalization could be achieved; 2) Any increase in the nucleocytosolic acetyl-CoA pool is rapidly consumed by active HATs, thus leading to increased chromatin acetylation without detectable changes in the steady-state concentration of acetyl-CoA. Moreover, the *S*. *cerevisiae* AMPK/Snf1 (AMP-activated protein kinase) is a known inhibitor of ACC, and *snf1Δ* budding yeast cells display decreased acetyl-CoA and histone acetylation levels [57]. Curiously, the loss of the *S*. *pombe* AMPK ortholog *ssp2* partially suppressed the stress-gene expression in *cbf11Δ* (S5A Fig), further stressing the importance for ACC activity in regulating the stress-gene expression.

Third, we tested the importance of individual characterized *S*. *pombe* histone acetyltransferases for the derepression of stress genes in *cbf11Δ* cells. We also included Elp3, the elongator complex acetyltransferase, which was proposed to act only in tRNA modification [58–60], but altered histone acetylation was observed in the *elp3Δ* mutant [61]. To this end, we constructed double mutants of *cbf11Δ* and the respective HAT mutations and assayed stress-gene expression in untreated cells using RT-qPCR. We have identified the essential MYST family Mst1 (Fig 5D) and the Gcn5/SAGA acetyltransferases (Fig 5E) as dominant regulators of the stress-gene expression in lipid metabolism mutant cells, while the other tested Gcn5-related N-acetyltransferase family members Hat1 and Elp3 (S5B Fig), the MYST family protein Mst2 or H3K59-specific HAT Rtt109 (S5C Fig) were largely dispensable for stress-gene upregulation in untreated *cbf11Δ* cells.

In summary, we have demonstrated a novel regulatory link between FA metabolism and cellular resistance to oxidative stress. When FA synthesis is decreased, a subset of stress-responsive genes becomes derepressed, making cells more resistant to H_2O_2. Furthermore, this process is associated with increased histone acetylation at the derepressed stress genes and depends on the activity of specific HATs.

Discussion

It is well established that metabolism and gene expression are reciprocally regulated to help cells respond efficiently to changes in both intrinsic and extrinsic factors [62]. However, the mechanisms underlying this complex regulatory crosstalk, and its diverse implications for cellular physiology are only incompletely understood. In this study, we show that perturbation of

lipid metabolism (or more specifically, the biosynthesis of FA) is associated with increased promoter histone H3K9 acetylation and HAT-dependent expression of stress-response genes, which leads to increased resistance of cells to exogenous oxidative stress. Furthermore, both the altered expression of stress genes and increased stress resistance depend on the canonical SAPK (Sty1-Atf1) and Pap1 pathways.

Both the lipid-metabolism regulators we analyzed (Cbf11, Mga2) and the Sty1 SAPK pathway affect multiple cellular processes, and their mutants show pleiotropic phenotypes. So, how can we distinguish whether our findings represent a genuine functional crosstalk between lipid metabolism and stress resistance or just some indirect effects of cellular stress? First, diverse types of stress activate a common set of stress-response genes and can lead to cross-protection against other, unrelated stresses [9,63]. Conversely, a mild dose of a particular stress can precondition cells to cope with a much higher dose of the same type of stress [64,65]. Several lines of evidence indicate that none of this can explain our observations, and that the increased resistance to oxidative stress of lipid-metabolism mutants is not merely due to the cells being intrinsically stressed. While proteins of the major stress-response pathways are indeed required for the increased oxidative-stress resistance of lipid-metabolism mutants, we have not detected increased levels of reactive oxygen species in untreated *cbf11Δ* cells (Fig 1D), and neither Sty1-Atf1 nor Pap1 were hyperactivated in untreated *cbf11Δ* cells (Fig 3A and 3C). Note that Sty1 also regulates entry into mitosis, so it is active to some extent even in unstressed cells, and only becomes hyperactivated under stressful conditions [13,14]. Moreover, our analysis of the transcriptome of untreated *cbf11Δ* cells identified mainly gene upregulation, which is unlike a typical stress response where a large group of genes is downregulated (Fig 4A and 4B). Second, the specificity of lipid-metabolism impingement on stress resistance is underlined by the phenotypes of the *cut6* acetyl-CoA carboxylase mutants (Figs 4D, 4E and 5B). In particular, the well-defined *Pcut6MUT* promoter mutation, which results in ~50% reduction of *cut6* mRNA levels and decreased amount of functional ACC/Cut6 protein without any notable pleiotropic defects [17], does also lead to increased stress-gene expression and resistance to oxidative stress, similar to *cbf11Δ* and *mga2Δ*. On the other hand, *cut6* overexpression in WT cells makes them more sensitive to oxidative stress (Fig 5C). Furthermore, the H_2O_2-resistant *cbf11Δ* mutant is not resistant to superoxide stress (S1E Fig), and is actually sensitive to a number of other stresses [16,44,45], highlighting the specificity of Cbf11 impact on stress gene expression. Taken together, the crosstalk between lipid metabolism and stress resistance appears to be a genuine phenomenon, and not just a side effect of a pleiotropic mutant phenotype.

How is the crosstalk between lipid metabolism and stress resistance mediated? Our results show that the DNA-binding activity of Cbf11 plays a critical role (Fig 3D), but Cbf11 does not seem to regulate stress-gene expression directly (Figs 3C and S3). Therefore, some Cbf11 (and/or Mga2) target gene(s) likely provide the connection between lipid metabolism and stress-gene expression. The Cut6 ACC is a strong candidate: 1) the *cut6* gene is regulated both by Cbf11 and Mga2 [16,17]; 2) ACC is a major consumer of acetyl-CoA, capable of affecting histone acetylation levels via limiting acetyl-CoA availability for HATs [21]; 3) hyperactive ACC results in hypoacetylated chromatin and stress-sensitive cells in budding yeast [57]; 4) decreased or increased expression of *cut6* alone results in inverse changes in the expression of stress genes (Figs 4D and 5B) and resistance to H_2O_2 (Figs 4E and 5C); and 5) promoters of stress genes upregulated in the *cbf11Δ* mutant showed increased H3K9 acetylation (Figs 5A and S4A). Importantly, H3K9 acetylation levels correlate with transcription [66], enhance binding of transcription factors [67] and promote transcriptional elongation by RNA polymerase II [52,68]. Gcn5/SAGA is a major H3K9-targeting HAT in the fission yeast [61], and it is important for proper stress-gene activation during oxidative stress [52]. Our data show that

Gcn5 is indeed important for the increased stress-gene expression in the *cbf11Δ* lipid mutant (Fig 5E). Strikingly, the evolutionarily conserved MYST family histone acetyltransferase Mst1 (ortholog of human Tip60, *S*. *cerevisiae* Esa1) with broad enzymatic specificity for both histone and non-histone targets [69,70] is also strongly required for the increased stress-gene expression in *cbf11Δ* cells (Fig 5D). Since Mst1 is not known to acetylate H3K9, some non-histone proteins, such as chromatin remodelers [71,72] or other transcription regulators [73], may be regulated by Mst1-dependent acetylation and help project the metabolic state into changes in gene expression (Fig 5F). Interestingly, *S*. *cerevisiae* Esa1 physically interacts with the stress-responsive transcription factors Msn2, Msn4 and Yap1 [69,74]. Thus, HAT activity and stress-gene promoter acetylation represent plausible candidates for the mechanistic link between lipid metabolism and stress-gene expression. We speculate that such changes in acetylation of histones or non-histone targets may create a more transcription-competent environment at stress-gene promoters, increasing moderately their basal (Sty1-Atf1 and/or Pap1-dependent) transcription rates in unstressed cells, and also boosting their ability to be induced during stress (Figs 1B and 2B).

While it is also formally possible that Cbf11 might directly repress the activity of Gcn5 and/or Mst1, we consider such scenario unlikely. First, Cbf11 does not bind to stress gene promoters, where it could have potentially restricted access to HATs or repressed HAT activity (Figs 3C and S3). Second, Cbf11 does not bind to the promoters of *gcn5* and *mst1*, and *gcn5* and *mst1* transcript levels do not change in *cbf11Δ* cells [15]. Third, stress gene expression is upregulated even in the *Pcut6MUT* mutant or upon cerulenin treatment (Fig 4D and 4F), where Cbf11 is intact, so the physical presence/absence of Cbf11 seems not to be critical.

The next question then is how specificity is achieved—why and how only a subset of stress-response genes become specifically upregulated upon perturbation of FA synthesis. Notably, the subset of CESR-UP genes upregulated in untreated *cbf11Δ*, whose promoters show H3K9 hyperacetylation in *cbf11Δ* cells, tend to have above-average nucleosome occupancy in their transcribed regions, unlike the other CESR-UP genes (see the total H3 levels in Figs 5A and S4A). This suggests that a particular chromatin structure and/or presence of a specific ensemble of chromatin remodelers and histone modifying enzymes make those genes more responsive to changes in the metabolic state. Notably, Gcn5 and Mst1, the HATs required for increased stress-gene expression in *cbf11Δ* cells, are the catalytic subunits of the histone acetyltransferase modules of transcription co-activator complexes SAGA and NuA4, respectively [75]. It is conceivable that other subunits or modules of the SAGA and NuA4 complexes might be responsible for the observed specificity in lipid metabolism-regulated transcription, e.g. by directing HAT complex recruitment to particular genes or by affecting HAT complex interactions with other proteins. For instance, the SAGA subunit Tra1 mediates the interaction between specific transcription factors at some loci but is dispensable at others [76]. Overall, however, the specificity of HATs towards gene promoters is not sufficiently characterized. Intriguingly, in mammalian cells, lipid-derived acetyl-CoA can provide up to 90% of acetyl-carbon for histone acetylation, and supplementation with the octanoate FA (which is turned into acetyl-CoA by beta-oxidation) results in histone hyperacetylation and induction of specific genes, distinct from those induced by glucose-derived acetyl-CoA. However, the mechanism whereby specificity is achieved is not clear [77]. Curiously, the ACSS2 acetyl-CoA synthetase was found to be physically associated with chromatin in mouse neurons, where it affects histone acetylation and expression of specific memory-related genes by targeted, on-site production of the acetyl-CoA substrate for HATs [78]. Importantly, in *S*. *pombe* the Acs1 acetyl-CoA synthetase is the key contributor to the nucleocytosolic acetyl-CoA pool [79], and it localizes predominantly to the nucleus [54]. Recruitment of Acs1 to specific genes could

thus potentially provide another means for the required specificity in transforming metabolic changes into changes in gene expression.

Finally, what is the purpose of such a crosstalk between lipid metabolism and stress-gene expression? In other words, what is the selective advantage of upregulating specific stress-response genes during decreased FA synthesis? Specific metabolic states are often associated with increased levels of distinct stressors, which can perturb cellular homeostasis. A metabolic control of the stress response would allow cells to better adapt to changes in cellular chemistry and ensure that any potential damage to cellular components is minimized. For example, FA synthesis is downregulated upon carbon-source limitation [80]. This is often followed by lipolysis and increased FA oxidation to compensate for the lack of energy resources. Notably, these FA catabolic processes generate increased levels of reactive oxygen species [81]. Therefore, a timely mild upregulation of oxidative stress-response genes in response to decreased FA synthesis could represent a useful safety precaution for the cell. Conversely, oxidative stress may, intriguingly, feed back to the regulation of lipid metabolism, as ACC/*cut6* transcript levels decrease upon treatment with H_2O_2 [9]. Curiously, perturbations of FA metabolism have been linked to altered stress resistance in *Caenorhabditis elegans*, even though the mechanism underlying this connection was not determined [82]. Another *C. elegans* study found that the NHR-49 nuclear hormone receptor, a known transcriptional regulator of lipid-metabolism genes, can also (perhaps indirectly) regulate the transcriptional response to fasting and peroxide stress, and is required for resistance to organic peroxides [83].

Moreover, several intriguing studies have described crosstalk between FA metabolism and stress resistance in mice. First, β-hydroxybutyrate, a ketone body produced from oxidized FA during fasting, prolonged exercise or in patients with diabetes, has been reported to protect against oxidative stress in the mouse kidney. β-hydroxybutyrate inhibits class I histone deacetylases, thereby enhancing H3K9 and H3K14 promoter acetylation and transcription of several stress genes [84]. Second, elevation of acetyl-CoA levels by octanoate supplementation reduced ischemia/reperfusion injury in the heart through promoting histone acetylation and antioxidant gene expression, thus inhibiting cardiomyocyte apoptosis [85]. Moreover, inhibition of FA synthesis by knocking out ACC in the mouse liver led to increased hepatic tumor burden, likely by increasing the resistance of tumor cells to oxidative stress [86]. These studies underscore that increased cellular resistance to oxidative stress can have both beneficial and detrimental consequences, and the use of ACC inhibitors for treating cancer in humans might bring about undesired development of resistance to standard ROS-generating chemotherapy. On the other hand, even a change of lipid metabolism in the opposite direction, namely increased synthesis of (saturated) FA, can protect cancer cells from oxidative stress by making their membrane lipids less susceptible to ROS and by affecting membrane permeability for chemotherapeutics [87]. Thus, the complex situation in metazoa highlights the importance of the particular cellular and organismal context for the final outcome of the crosstalk between FA metabolism and stress resistance.

Supporting information

S1 Fig. Resistance of *cbf11Δ* cells to oxidative stress partially depends on Atf1 and is specific for hydrogen peroxide. (A-D) Growth curves of stress-related mutants in the presence or absence of the indicated concentrations of H_2O_2 in YES medium. The *pyp1Δ* and *sty1Δ* strains represent strongly resistant and strongly sensitive controls, respectively. **(E)** Survival and growth under superoxide stress of WT, *cbf11Δ*, *cbf12Δ* and *cbf11Δ cbf12Δ* cultures spotted on YES plates containing 125 μM menadione.
(TIF)

S2 Fig. Lack of Sty1 activity further impairs growth of *cbf11Δ* cells. Exponentially growing WT, *cbf11Δ*, *sty1-as*, *cbf11Δ sty1-as*, and *sty1Δ* cultures were spotted on YES plates containing 10 μM Sty1-as inhibitor 3-MB-PP1 and incubated for the indicated number of days.
(TIF)

S3 Fig. Cbf11 does not bind to Atf1 binding sites at stress-gene promoters. (A,B) Recruitment of Cbf11-HA and Cbf11-TAP, respectively, to known Atf1 binding sites in the indicated stress gene promoters was analyzed by ChIP-qPCR in cells treated or not with 1 mM H_2O_2 for 5 min in EMM medium. The *cut6* promoter is a positive control for Cbf11 binding [15]; "control" is a locus with no expected Cbf11 binding. Mean and SD values of two (A) and three (B) independent replicates are shown. One-sided Mann-Whitney U test was used to determine statistical significance.
(TIF)

S4 Fig. Derepression of stress genes in *cbf11Δ* cells is associated with H3K9 hyperacetylation in their promoters (the second replicate) but not with altered total cellular acetyl-CoA levels. (A) Average gene profiles of total H3 (bottom panels) and acetylated H3K9 (top panels) occupancy at stress-gene regions in WT and *cbf11Δ* cells, respectively. Genes upregulated as part of the core environmental stress response (CESR-UP, [9]) have been divided into those showing upregulation in untreated *cbf11Δ* cells (blue; n = 94, [15]) and the rest (red; n = 441). Average profile of all fission yeast genes is also shown for comparison (black; n = 6952). The curves represent mean RPM (reads per million mapped reads) values ± SEM. The promoter region is shaded. TSS—transcription start site. **(B)** Total cellular acetyl-CoA levels in WT, *ppc1-537*, *cbf11Δ* and *Pcut6MUT* cell extracts were determined by LC-MS. Mean and SD values of four independent replicates for *ppc1-537* and five independent replicates for all other strains tested are shown. Two-sided Mann-Whitney U test was used to determine statistical significance.
(TIF)

S5 Fig. AMPK and histone acetyltransferases Elp3, Hat1, Rtt109 and Mst2 have limited effect on stress gene derepression in *cbf11Δ* cells. (A,B,C) Expression of the indicated stress genes in cells growing in YES medium was analyzed by RT-qPCR. Mean and SD values of three independent replicates are shown. One-sided Mann-Whitney U test was used to determine statistical significance.
(TIF)

S1 Text. Table A–List of oligonucleotides; Table B–List of plasmids; Table C–List of strains.
(DOCX)

S1 Data. Source numerical data.
(XLSX)

Acknowledgments

The authors would like to thank Eishi and Chiaki Noguchi for providing the *mst1ts* strain, Anna Janovska´ and the Laboratory of Mass Spectrometry at Biocev Research Center, Faculty of Science, Charles University for performing the LC-MS analyses, NBRP Japan for providing the *ppc1-537* strain, Simona Vesela´, Patrik Hoho˘s and Viacheslav Zemlianski for help with the *ssp2Δ* and *cbf11Δ ssp2Δ* strain construction, all members of the GenoMik and ReGenEx groups for their support and insightful discussions, and Eva Krellerova´, Ade´la Krac´ıkova´ and Kateřina Svobodova´ for their technical assistance.

Author Contributions

Conceptualization: Jarmila Princova´, Ju¨rg Ba¨hler, Jose´ Ayte´, Elena Hidalgo, Martin Převorovsky´.

Data curation: Jarmila Princova´, Clàudia Salat-Canela, Martin Převorovsky´.

Formal analysis: Jarmila Princova´, Clàudia Salat-Canela, Petr Daneˇk, Anna Mareˇsova´, Laura de Cubas, Jose´ Ayte´, Elena Hidalgo, Martin Převorovsky´.

Investigation: Jarmila Princova´, Clàudia Salat-Canela, Petr Daneˇk, Anna Mareˇsova´, Laura de Cubas, Martin Převorovsky´.

Resources: Anna Mareˇsova´, Laura de Cubas, Ju¨rg Ba¨hler.

Supervision: Jose´ Ayte´, Elena Hidalgo, Martin Převorovsky´.

Visualization: Jarmila Princova´, Clàudia Salat-Canela, Laura de Cubas, Martin Převorovsky´.

Writing – original draft: Jarmila Princova´, Clàudia Salat-Canela, Jose´ Ayte´, Elena Hidalgo, Martin Převorovsky´.

Writing – review & editing: Jarmila Princova´, Anna Mareˇsova´, Jürg Ba¨hler, Jose´ Ayte´, Elena Hidalgo, Martin Převorovsky´.

References

1. Sies H, Berndt C, Jones DP. Oxidative Stress. Annu Rev Biochem. 2017 Jun 20; 86:715–748. https://doi.org/10.1146/annurev-biochem-061516-045037 PMID: 28441057
2. Forman HJ, Zhang H. Targeting oxidative stress in disease: promise and limitations of antioxidant therapy. Nat Rev Drug Discov. 2021 Sep; 20(9):689–709. https://doi.org/10.1038/s41573-021-00233-1 PMID: 34194012
3. Tan BL, Norhaizan ME, Liew WP, Sulaiman Rahman H. Antioxidant and Oxidative Stress: A Mutual Interplay in Age-Related Diseases. Front Pharmacol. 2018 Oct 16; 9:1162. https://doi.org/10.3389/fphar.2018.01162 PMID: 30405405
4. O'Donnell P, Do KQ, Arango C. Oxidative/Nitrosative stress in psychiatric disorders: are we there yet? Schizophr Bull. 2014 Sep; 40(5):960–2. https://doi.org/10.1093/schbul/sbu048 PMID: 24714380
5. Aroor AR, DeMarco VG. Oxidative stress and obesity: the chicken or the egg? Diabetes. 2014 Jul; 63 (7):2216–8. https://doi.org/10.2337/db14-0424 PMID: 24962921
6. Nathan C, Cunningham-Bussel A. Beyond oxidative stress: an immunologist's guide to reactive oxygen species. Nat Rev Immunol. 2013 May; 13(5):349–61. https://doi.org/10.1038/nri3423 PMID: 23618831
7. Shiozaki K, Russell P. Conjugation, meiosis, and the osmotic stress response are regulated by Spc1 kinase through Atf1 transcription factor in fission yeast. Genes Dev. 1996 Sep 15; 10(18):2276–88. https://doi.org/10.1101/gad.10.18.2276 PMID: 8824587
8. Wilkinson MG, Samuels M, Takeda T, Toone WM, Shieh JC, Toda T, et al. The Atf1 transcription factor is a target for the Sty1 stress-activated MAP kinase pathway in fission yeast. Genes Dev. 1996 Sep 15; 10(18):2289–301. https://doi.org/10.1101/gad.10.18.2289 PMID: 8824588
9. Chen D, Toone WM, Mata J, Lyne R, Burns G, Kivinen K, et al, Ba¨hler J. Global transcriptional responses of fission yeast to environmental stress. Mol Biol Cell. 2003 Jan; 14(1):214–29. https://doi.org/10.1091/mbc.e02-08-0499 PMID: 12529438
10. Chen D, Wilkinson CR, Watt S, Penkett CJ, Toone WM, Jones N, et al. Multiple pathways differentially regulate global oxidative stress responses in fission yeast. Mol Biol Cell. 2008 Jan; 19(1):308–17. https://doi.org/10.1091/mbc.e07-08-0735 PMID: 18003976
11. Vivancos AP, Jara M, Zuin A, Sanso´ M, Hidalgo E. Oxidative stress in Schizosaccharomyces pombe: different H2O2 levels, different response pathways. Mol Genet Genomics. 2006 Dec; 276(6):495–502. https://doi.org/10.1007/s00438-006-0175-z PMID: 17043891
12. Quinn J, Findlay VJ, Dawson K, Millar JB, Jones N, Morgan BA, et al. Distinct regulatory proteins control the graded transcriptional response to increasing H(2)O(2) levels in fission yeast Schizosaccharomyces pombe. Mol Biol Cell. 2002 Mar; 13(3):805–16. https://doi.org/10.1091/mbc.01-06-0288 PMID: 11907263

13. Shiozaki K, Russell P. Cell-cycle control linked to extracellular environment by MAP kinase pathway in fission yeast. Nature. 1995 Dec 14; 378(6558):739–43. https://doi.org/10.1038/378739a0 PMID: 7501024

14. Lo´pez-Avile´s S, Lambea E, Moldo´n A, Grande M, Fajardo A, Rodr´ıguez-Gabriel MA, et al. Activation of Srk1 by the mitogen-activated protein kinase Sty1/Spc1 precedes its dissociation from the kinase and signals its degradation. Mol Biol Cell. 2008 Apr; 19(4):1670–9. https://doi.org/10.1091/mbc.e07-07-0639 PMID: 18272791

15. Převorovsky´ M, Oravcova´ M, Tvarůž˘kova´ J, Zach R, Folk P, Půta F, et al. Fission Yeast CSL Transcription Factors: Mapping Their Target Genes and Biological Roles. PLoS One. 2015 Sep 14; 10(9): e0137820. https://doi.org/10.1371/journal.pone.0137820 PMID: 26366556

16. Burr R, Stewart EV, Shao W, Zhao S, Hannibal-Bach HK, Ejsing CS, et al. Mga2 Transcription Factor Regulates an Oxygen-responsive Lipid Homeostasis Pathway in Fission Yeast. J Biol Chem. 2016 Jun 3; 291(23):12171–83. https://doi.org/10.1074/jbc.M116.723650 PMID: 27053105

17. Převorovsky´ M, Oravcova´ M, Zach R, Jorda´kova´ A, Ba¨ hler J, Půta F, et al. CSL protein regulates transcription of genes required to prevent catastrophic mitosis in fission yeast. Cell Cycle. 2016 Nov 16; 15 (22):3082–3093. https://doi.org/10.1080/15384101.2016.1235100 PMID: 27687771

18. Takahashi H, McCaffery JM, Irizarry RA, Boeke JD. Nucleocytosolic acetyl-coenzyme a synthetase is required for histone acetylation and global transcription. Mol Cell. 2006 Jul 21; 23(2):207–17. https://doi.org/10.1016/j.molcel.2006.05.040 PMID: 16857587

19. Choudhary C, Weinert BT, Nishida Y, Verdin E, Mann M. The growing landscape of lysine acetylation links metabolism and cell signalling. Nat Rev Mol Cell Biol. 2014 Aug; 15(8):536–50. https://doi.org/10.1038/nrm3841 PMID: 25053359

20. Wellen KE, Hatzivassiliou G, Sachdeva UM, Bui TV, Cross JR, Thompson CB. ATP-citrate lyase links cellular metabolism to histone acetylation. Science. 2009 May 22; 324(5930):1076–80. https://doi.org/10.1126/science.1164097 PMID: 19461003

21. Galdieri L, Vancura A. Acetyl-CoA carboxylase regulates global histone acetylation. J Biol Chem. 2012 Jul 6; 287(28):23865–76. https://doi.org/10.1074/jbc.M112.380519 PMID: 22580297

22. Rodr´ıguez-Lo´pez M, Cotobal C, Ferna´ndez-Sa´nchez O, Borbara´n Bravo N, Oktriani R, Abendroth H, et al. A CRISPR/Cas9-based method and primer design tool for seamless genome editing in fission yeast. Wellcome Open Res. 2017 May 5; 1:19. https://doi.org/10.12688/wellcomeopenres.10038.3 PMID: 28612052

23. Jacobs JZ, Ciccaglione KM, Tournier V, Zaratiegui M. Implementation of the CRISPR-Cas9 system in fission yeast. Nat Commun. 2014 Oct 29; 5:5344. https://doi.org/10.1038/ncomms6344 PMID: 25352017

24. Petersen J, Russell P. Growth and the Environment of Schizosaccharomyces pombe. Cold Spring Harb Protoc. 2016 Mar 1;2016(3):pdb.top079764. https://doi.org/10.1101/pdb.top079764 PMID: 26933253

25. Oravcova´ M, Teska M, Půta F, Folk P, Převorovsky´ M. Fission yeast CSL proteins function as transcription factors. PLoS One. 2013; 8(3):e59435. https://doi.org/10.1371/journal.pone.0059435 PMID: 23555033

26. Sabatinos SA, Forsburg SL. Molecular genetics of Schizosaccharomyces pombe. Methods Enzymol. 2010; 470:759–95. https://doi.org/10.1016/S0076-6879(10)70032-X PMID: 20946835

27. Gregan J, Rabitsch PK, Rumpf C, Novatchkova M, Schleiffer A, Nasmyth K. High-throughput knockout screen in fission yeast. Nat Protoc. 2006; 1(5):2457–64. https://doi.org/10.1038/nprot.2006.385 PMID: 17406492

28. Castillo EA, Vivancos AP, Jones N, Ayte J, Hidalgo E. Schizosaccharomyces pombe cells lacking the Ran-binding protein Hba1 show a multidrug resistance phenotype due to constitutive nuclear accumulation of Pap1. J Biol Chem. 2003 Oct 17; 278(42):40565–72. https://doi.org/10.1074/jbc.M305859200 PMID: 12896976

29. Carmona M, de Cubas L, Bautista E, Moral-Blanch M, Medraño-Ferna´ndez I, Sitia R, et al. Monitoring cytosolic H2O2 fluctuations arising from altered plasma membrane gradients or from mitochondrial activity. Nat Commun. 2019 Oct 4; 10(1):4526. https://doi.org/10.1038/s41467-019-12475-0 PMID: 31586057

30. Vivancos AP, Castillo EA, Jones N, Ayte´ J, Hidalgo E. Activation of the redox sensor Pap1 by hydrogen peroxide requires modulation of the intracellular oxidant concentration. Mol Microbiol. 2004 Jun; 52 (5):1427–35. https://doi.org/10.1111/j.1365-2958.2004.04065.x PMID: 15165244

31. Sanso´ M, Gogol M, Ayte´ J, Seidel C, Hidalgo E. Transcription factors Pcr1 and Atf1 have distinct roles in stress- and Sty1-dependent gene regulation. Eukaryot Cell. 2008 May; 7(5):826–35. https://doi.org/10.1128/EC.00465-07 PMID: 18375616

32. Jara M, Vivancos AP, Calvo IA, Moldo´n A, Sanso´ M, Hidalgo E. The peroxiredoxin Tpx1 is essential as a H2O2 scavenger during aerobic growth in fission yeast. Mol Biol Cell. 2007 Jun; 18(6):2288–95. https://doi.org/10.1091/mbc.e06-11-1039 PMID: 17409354

33. Marte L, Boronat S, Barrios R, Barcons-Simon A, Bolognesi B, Cabrera M, et al. Expression of Huntingtin and TDP-43 Derivatives in Fission Yeast Can Cause Both Beneficial and Toxic Effects. Int J Mol Sci. 2022 Apr 1; 23(7):3950. https://doi.org/10.3390/ijms23073950 PMID: 35409310

34. Salat-Canela C, Paulo E, Sa´nchez-Mir L, Carmona M, Ayte´ J, Oliva B, et al. Deciphering the role of the signal- and Sty1 kinase-dependent phosphorylation of the stress-responsive transcription factor Atf1 on gene activation. J Biol Chem. 2017 Aug 18; 292(33):13635–13644. https://doi.org/10.1074/jbc.M117.794339 PMID: 28652406

35. Lock A, Rutherford K, Harris MA, Hayles J, Oliver SG, Ba¨hler J, et al. PomBase 2018: user-driven reimplementation of the fission yeast database provides rapid and intuitive access to diverse, interconnected information. Nucleic Acids Res. 2019 Jan 8; 47(D1):D821–D827. https://doi.org/10.1093/nar/gky961 PMID: 30321395

36. Wood V, Gwilliam R, Rajandream MA, Lyne M, Lyne R, Stewart A, et al. The genome sequence of Schizosaccharomyces pombe. Nature. 2002 Feb 21; 415(6874):871–80. https://doi.org/10.1038/nature724 PMID: 11859360

37. Kim D, Paggi JM, Park C, Bennett C, Salzberg SL. Graph-based genome alignment and genotyping with HISAT2 and HISAT-genotype. Nat Biotechnol. 2019 Aug; 37(8):907–915. https://doi.org/10.1038/s41587-019-0201-4 PMID: 31375807

38. Li H, Handsaker B, Wysoker A, Fennell T, Ruan J, Homer N, et al. The Sequence Alignment/Map format and SAMtools. Bioinformatics. 2009 Aug 15; 25(16):2078–9. https://doi.org/10.1093/bioinformatics/btp352 PMID: 19505943

39. Bonfield JK, Marshall J, Danecek P, Li H, Ohan V, Whitwham A, et al. HTSlib: C library for reading/writing high-throughput sequencing data. Gigascience. 2021 Feb 16; 10(2):giab007. https://doi.org/10.1093/gigascience/giab007 PMID: 33594436

40. Ram´ırez F, Ryan DP, Gru¨ ning B, Bhardwaj V, Kilpert F, Richter AS, et al. deepTools2: a next generation web server for deep-sequencing data analysis. Nucleic Acids Res. 2016 Jul 8; 44(W1):W160–5. https://doi.org/10.1093/nar/gkw257 PMID: 27079975

41. Calvo IA, Gabrielli N, Iglesias-Baena I, Garc´ıa-Santamarina S, Hoe KL, Kim DU, et al. Genome-wide screen of genes required for caffeine tolerance in fission yeast. PLoS One. 2009 Aug 12; 4(8):e6619. https://doi.org/10.1371/journal.pone.0006619 PMID: 19672306

42. Degols G, Shiozaki K, Russell P. Activation and regulation of the Spc1 stress-activated protein kinase in Schizosaccharomyces pombe. Mol Cell Biol. 1996 Jun; 16(6):2870–7. https://doi.org/10.1128/MCB.16.6.2870 PMID: 8649397

43. Mutoh N, Kawabata M, Kitajima S. Effects of four oxidants, menadione, 1-chloro-2,4-dinitrobenzene, hydrogen peroxide and cumene hydroperoxide, on fission yeast Schizosaccharmoyces pombe. J Biochem. 2005 Dec; 138(6):797–804. https://doi.org/10.1093/jb/mvi179 PMID: 16428309

44. Prevorovsky´ M, Grousl T, Stanurova´ J, Rynes J, Nellen W, Půta F, et al. Cbf11 and Cbf12, the fission yeast CSL proteins, play opposing roles in cell adhesion and coordination of cell and nuclear division. Exp Cell Res. 2009 May 1; 315(8):1533–47. https://doi.org/10.1016/j.yexcr.2008.12.001 PMID: 19101542

45. Han TX, Xu XY, Zhang MJ, Peng X, Du LL. Global fitness profiling of fission yeast deletion strains by barcode sequencing. Genome Biol. 2010; 11(6):R60. https://doi.org/10.1186/gb-2010-11-6-r60 PMID: 20537132

46. Zuin A, Carmona M, Morales-Ivorra I, Gabrielli N, Vivancos AP, Ayte´ J, et al. Lifespan extension by calorie restriction relies on the Sty1 MAP kinase stress pathway. EMBO J. 2010 Mar 3; 29(5):981–91. https://doi.org/10.1038/emboj.2009.407 PMID: 20075862

47. Toone WM, Kuge S, Samuels M, Morgan BA, Toda T, Jones N. Regulation of the fission yeast transcription factor Pap1 by oxidative stress: requirement for the nuclear export factor Crm1 (Exportin) and the stress-activated MAP kinase Sty1/Spc1. Genes Dev. 1998 May 15; 12(10):1453–63. https://doi.org/10.1101/gad.12.10.1453 PMID: 9585505

48. Kudo N, Taoka H, Toda T, Yoshida M, Horinouchi S. A novel nuclear export signal sensitive to oxidative stress in the fission yeast transcription factor Pap1. J Biol Chem. 1999 May 21; 274(21):15151–8. https://doi.org/10.1074/jbc.274.21.15151 PMID: 10329722

49. Pancaldi V, Sarac¸ OS, Rallis C, McLean JR, Převorovsky´ M, Gould K, et al. Predicting the fission yeast protein interaction network. G3 (Bethesda). 2012 Apr; 2(4):453–67. https://doi.org/10.1534/g3.111.001560 PMID: 22540037

50. Saitoh S, Takahashi K, Nabeshima K, Yamashita Y, Nakaseko Y, Hirata A, et al. Aberrant mitosis in fission yeast mutants defective in fatty acid synthetase and acetyl CoA carboxylase. J Cell Biol. 1996 Aug; 134(4):949–61. https://doi.org/10.1083/jcb.134.4.949 PMID: 8769419

51. Matias AC, Pedroso N, Teodoro N, Marinho HS, Antunes F, Nogueira JM, et al. Down-regulation of fatty acid synthase increases the resistance of Saccharomyces cerevisiae cells to H2O2. Free Radic Biol Med. 2007 Nov 15; 43(10):1458–65. https://doi.org/10.1016/j.freeradbiomed.2007.08.003 PMID: 17936191

52. Sanso´ M, Vargas-Pe´rez I, Quintales L, Antequera F, Ayte´ J, Hidalgo E. Gcn5 facilitates Pol II progression, rather than recruitment to nucleosome-depleted stress promoters, in Schizosaccharomyces pombe. Nucleic Acids Res. 2011 Aug; 39(15):6369–79. https://doi.org/10.1093/nar/gkr255 PMID: 21515633

53. Johnsson A, Xue-Franze´n Y, Lundin M, Wright AP. Stress-specific role of fission yeast Gcn5 histone acetyltransferase in programming a subset of stress response genes. Eukaryot Cell. 2006 Aug; 5 (8):1337–46. https://doi.org/10.1128/EC.00101-06 PMID: 16896217

54. Nakamura T, Pluskal T, Nakaseko Y, Yanagida M. Impaired coenzyme A synthesis in fission yeast causes defective mitosis, quiescence-exit failure, histone hypoacetylation and fragile DNA. Open Biol. 2012 Sep; 2(9):120117. https://doi.org/10.1098/rsob.120117 PMID: 23091701

55. Pietrocola F, Galluzzi L, Bravo-San Pedro JM, Madeo F, Kroemer G. Acetyl coenzyme A: a central metabolite and second messenger. Cell Metab. 2015 Jun 2; 21(6):805–21. https://doi.org/10.1016/j.cmet.2015.05.014 PMID: 26039447

56. Sivanand S, Viney I, Wellen KE. Spatiotemporal Control of Acetyl-CoA Metabolism in Chromatin Regulation. Trends Biochem Sci. 2018 Jan; 43(1):61–74. https://doi.org/10.1016/j.tibs.2017.11.004 PMID: 29174173

57. Zhang M, Galdieri L, Vancura A. The yeast AMPK homolog SNF1 regulates acetyl coenzyme A homeostasis and histone acetylation. Mol Cell Biol. 2013 Dec; 33(23):4701–17. https://doi.org/10.1128/MCB.00198-13 PMID: 24081331

58. Ferna´ndez-Va´zquez J, Vargas-Pe´rez I, Sanso´ M, Buhne K, Carmona M, Paulo E, et al. Modification of tRNA(Lys) UUU by elongator is essential for efficient translation of stress mRNAs. PLoS Genet. 2013; 9 (7):e1003647. https://doi.org/10.1371/journal.pgen.1003647 PMID: 23874237

59. Bauer F, Matsuyama A, Candiracci J, Dieu M, Scheliga J, Wolf DA, et al. Translational control of cell division by Elongator. Cell Rep. 2012 May 31; 1(5):424–33. https://doi.org/10.1016/j.celrep.2012.04.001 PMID: 22768388

60. Villahermosa D, Fleck O. Elp3 and Dph3 of Schizosaccharomyces pombe mediate cellular stress responses through tRNALysUUU modifications. Sci Rep. 2017 Aug 3; 7(1):7225. https://doi.org/10.1038/s41598-017-07647-1 PMID: 28775286

61. Nugent RL, Johnsson A, Fleharty B, Gogol M, Xue-Franze´n Y, Seidel C, et al. Expression profiling of S. pombe acetyltransferase mutants identifies redundant pathways of gene regulation. BMC Genomics. 2010 Jan 22; 11:59. https://doi.org/10.1186/1471-2164-11-59 PMID: 20096118

62. Fan J, Krautkramer KA, Feldman JL, Denu JM. Metabolic regulation of histone post-translational modifications. ACS Chem Biol. 2015 Jan 16; 10(1):95–108. https://doi.org/10.1021/cb500846u PMID: 25562692

63. Święciło A. Cross-stress resistance in Saccharomyces cerevisiae yeast—new insight into an old phenomenon. Cell Stress Chaperones. 2016 Mar; 21(2):187–200. https://doi.org/10.1007/s12192-016-0667-7 PMID: 26825800

64. Lee J, Dawes IW, Roe JH. Adaptive response of Schizosaccharomyces pombe to hydrogen peroxide and menadione. Microbiology (Reading). 1995 Dec; 141 (Pt 12):3127–32. https://doi.org/10.1099/13500872-141-12-3127 PMID: 8574406

65. Crawford DR, Davies KJ. Adaptive response and oxidative stress. Environ Health Perspect. 1994 Dec; 102 Suppl 10(Suppl 10):25–8. https://doi.org/10.1289/ehp.94102s1025 PMID: 7705299

66. Wire´n M, Silverstein RA, Sinha I, Walfridsson J, Lee HM, Laurenson P, et al. Genomewide analysis of nucleosome density histone acetylation and HDAC function in fission yeast. EMBO J. 2005 Aug 17; 24 (16):2906–18. https://doi.org/10.1038/sj.emboj.7600758 PMID: 16079916

67. Du Y, Liu Z, Cao X, Chen X, Chen Z, Zhang X, et al. Nucleosome eviction along with H3K9ac deposition enhances Sox2 binding during human neuroectodermal commitment. Cell Death Differ. 2017 Jun; 24 (6):1121–1131. https://doi.org/10.1038/cdd.2017.62 PMID: 28475175

68. Gates LA, Shi J, Rohira AD, Feng Q, Zhu B, Bedford MT, et al. Acetylation on histone H3 lysine 9 mediates a switch from transcription initiation to elongation. J Biol Chem. 2017 Sep 1; 292(35):14456–14472. https://doi.org/10.1074/jbc.M117.802074 PMID: 28717009

69. Mitchell L, Huard S, Cotrut M, Pourhanifeh-Lemeri R, Steunou AL, Hamza A, et al. mChIP-KAT-MS, a method to map protein interactions and acetylation sites for lysine acetyltransferases. Proc Natl Acad Sci U S A. 2013 Apr 23; 110(17):E1641–50. https://doi.org/10.1073/pnas.1218515110 PMID: 23572591

70. Pillus L. MYSTs mark chromatin for chromosomal functions. Curr Opin Cell Biol. 2008 Jun; 20(3):326–33. https://doi.org/10.1016/j.ceb.2008.04.009 PMID: 18511253

71. Ferreira R, Eberharter A, Bonaldi T, Chioda M, Imhof A, Becker PB. Site-specific acetylation of ISWI by GCN5. BMC Mol Biol. 2007 Aug 30; 8:73. https://doi.org/10.1186/1471-2199-8-73 PMID: 17760996

72. Kim JH, Saraf A, Florens L, Washburn M, Workman JL. Gcn5 regulates the dissociation of SWI/SNF from chromatin by acetylation of Swi2/Snf2. Genes Dev. 2010 Dec 15; 24(24):2766–71. https://doi.org/10.1101/gad.1979710 PMID: 21159817

73. Park JM, Jo SH, Kim MY, Kim TH, Ahn YH. Role of transcription factor acetylation in the regulation of metabolic homeostasis. Protein Cell. 2015 Nov; 6(11):804–13. https://doi.org/10.1007/s13238-015-0204-y PMID: 26334401

74. Mitchell L, Lambert JP, Gerdes M, Al-Madhoun AS, Skerjanc IS, Figeys D, et al. Functional dissection of the NuA4 histone acetyltransferase reveals its role as a genetic hub and that Eaf1 is essential for complex integrity. Mol Cell Biol. 2008 Apr; 28(7):2244–56. https://doi.org/10.1128/MCB.01653-07 PMID: 18212056

75. Helmlinger D, Tora L. Sharing the SAGA. Trends Biochem Sci. 2017 Nov; 42(11):850–861. https://doi.org/10.1016/j.tibs.2017.09.001 PMID: 28964624

76. Helmlinger D, Marguerat S, Ville´n J, Swaney DL, Gygi SP, Ba¨hler J, et al. Tra1 has specific regulatory roles, rather than global functions, within the SAGA co-activator complex. EMBO J. 2011 Jun 3; 30(14):2843–52. https://doi.org/10.1038/emboj.2011.181 PMID: 21642955

77. McDonnell E, Crown SB, Fox DB, Kitir B, Ilkayeva OR, Olsen CA, Grimsrud PA, Hirschey MD. Lipids Reprogram Metabolism to Become a Major Carbon Source for Histone Acetylation. Cell Rep. 2016 Nov 1; 17(6):1463–1472. https://doi.org/10.1016/j.celrep.2016.10.012 PMID: 27806287

78. Mews P, Donahue G, Drake AM, Luczak V, Abel T, Berger SL. Acetyl-CoA synthetase regulates histone acetylation and hippocampal memory. Nature. 2017 Jun 15; 546(7658):381–386. https://doi.org/10.1038/nature22405 PMID: 28562591

79. Malecki M, Bitton DA, Rodr´ıguez-Lo´pez M, Rallis C, Calavia NG, Smith GC, et al. Functional and regulatory profiling of energy metabolism in fission yeast. Genome Biol. 2016 Nov 25; 17(1):240. https://doi.org/10.1186/s13059-016-1101-2 PMID: 27887640

80. Hedbacker K, Carlson M. SNF1/AMPK pathways in yeast. Front Biosci. 2008 Jan 1; 13:2408–20. https://doi.org/10.2741/2854 PMID: 17981722

81. Quijano C, Trujillo M, Castro L, Trostchansky A. Interplay between oxidant species and energy metabolism. Redox Biol. 2016 Aug; 8:28–42. https://doi.org/10.1016/j.redox.2015.11.010 PMID: 26741399

82. Horikawa M, Sakamoto K. Fatty-acid metabolism is involved in stress-resistance mechanisms of Caenorhabditis elegans. Biochem Biophys Res Commun. 2009 Dec 25; 390(4):1402–7. https://doi.org/10.1016/j.bbrc.2009.11.006 PMID: 19896458

83. Goh GYS, Winter JJ, Bhanshali F, Doering KRS, Lai R, Lee K, et al. NHR-49/HNF4 integrates regulation of fatty acid metabolism with a protective transcriptional response to oxidative stress and fasting. Aging Cell. 2018 Jun; 17(3):e12743. https://doi.org/10.1111/acel.12743 PMID: 29508513

84. Shimazu T, Hirschey MD, Newman J, He W, Shirakawa K, Le Moan N, et al. Suppression of oxidative stress by β-hydroxybutyrate, an endogenous histone deacetylase inhibitor. Science. 2013 Jan 11; 339(6116):211–4. https://doi.org/10.1126/science.1227166 PMID: 23223453

85. Lei I, Tian S, Gao W, Liu L, Guo Y, Tang P, et al. Acetyl-CoA production by specific metabolites promotes cardiac repair after myocardial infarction via histone acetylation. Elife. 2021 Dec 23; 10:e60311. https://doi.org/10.7554/eLife.60311 PMID: 34939931

86. Nelson ME, Lahiri S, Chow JD, Byrne FL, Hargett SR, Breen DS, et al. Inhibition of hepatic lipogenesis enhances liver tumorigenesis by increasing antioxidant defence and promoting cell survival. Nat Commun. 2017 Mar 14; 8:14689. https://doi.org/10.1038/ncomms14689 PMID: 28290443

87. Rysman E, Brusselmans K, Scheys K, Timmermans L, Derua R, Munck S, et al. De novo lipogenesis protects cancer cells from free radicals and chemotherapeutics by promoting membrane lipid saturation. Cancer Res. 2010 Oct 15; 70(20):8117–26. https://doi.org/10.1158/0008-5472.CAN-09-3871 PMID: 20876798

3.5 Interconnections between lipid metabolism, stress gene expression and chromatin modifications

Chromatin modifications are crucial in regulating all aspects of DNA biology including transcription and protection of structural chromatin such as centromeres and (sub)telomeres [180]. Histone acetylation and methylation were the first described histone modifications in the 1960s [98,181] and up to date histone acetylation (H3, H4) and H3K9 methylation remain to be the hallmarks of actively transcribed chromatin and constitutive heterochromatin, respectively. The acetylation of histone proteins is catalyzed by histone acetyltransferases that use acetyl-CoA as substrate [182]. Remarkably, acetyl-CoA is also the central molecule of the carbon metabolism, thus the nucleocytosolic pool, which is separate from the mitochondrial pool functioning in oxidative phosphorylation, covers the cellular needs for both histone acetylation and basic metabolism such as fatty acid synthesis. This interconnection between lipid metabolism and histone acetylation is manifested, for example, by bulk histone hyperacetylation and activation of gene expression when acetyl-CoA carboxylase is inhibited in the budding yeast [85]. However, the significance and the physiological consequences of such interconnections between the lipid metabolism and gene expression regulation are still only beginning to be understood. In addition to our published study showing that a decrease in fatty acid synthesis leads to increased expression of specific stress-response genes accompanied by promoter histone hyperacetylation [152] (**publication #3**), we describe here additional effects of deregulated lipid metabolism on chromatin biology. In this study we have used the following genetic models in order to study the effect of reduced FA synthesis on chromatin: the *cbf11Δ* cells lacking Cbf11 lipid metabolism transcription factor, which exhibit decreased lipid droplet content [150,183] (**publication #1**), and the *Pcut6MUT* strain which possesses a point mutation in the promoter of the *cut6* gene encoding ACC, which causes loss of Cbf11 binding and a 2-fold decrease in *cut6* transcript levels [184]. Strikingly, we have not identified any global change in histone acetylation upon FA synthesis inhibition in either *cbf11Δ* or *Pcut6MUT* (Figure 3.3A) which is in contrast with studies on the budding yeast [85,185]. The strain *ppc1-537* bearing a thermosensitive allele of the phosphopantothenate-cysteine ligase Ppc1, an enzyme involved in coenzyme A biosynthesis, was described to be defective in histone H3 and H4 acetylation when grown in the EMM medium [151], however, we have not detected any change in histone acetylation in the complex YES

medium (Figure 3.3A). In line with this observation, the *ppc1-537* strain is not thermosensitive when grown in the YES medium although lower cellular acetyl-CoA levels were confirmed as published previously [151,152] (**publication #3**) (data not shown).

Using ChIP-seq we have identified 702 and 95 genes with more than 1.5-fold increased H3K9 acetylation in *cbf11Δ* and *Pcut6MUT* cells, respectively, and 215 and 124 genes with more than 1.5-fold decreased H3K9 acetylation in *cbf11Δ* and *Pcut6MUT* cells, respectively (Figure 3.3B and C) [152] (**publication #3**). Moreover, there is a statistically significant overlap of affected genes in both strains with reduced FA synthesis (Figure 3.3B) pointing to the conclusion that the changes in H3K9 acetylation might be general for FA synthesis inhibition. In *cbf11Δ* the genes with increased H3K9 acetylation are enriched for GO terms [157] iron ion transport (p = 1.88e-05), transmembrane transport (p = 8.37e-05) and cellular response to oxidative stress (p = 0.00337). We have recently demonstrated the resistance of *cbf11Δ* cells to oxidative stress which further validates the observed increase in H3K9ac at stress genes [152] (**publication #3**). Interestingly, the genes with decreased H3K9 acetylation are enriched for GO term flocculation (p = 0.00188) and several flocculation genes are indeed downregulated (*pfl2, pfl9, pfl5* and *pfl7)* although *cbf11Δ* cells are known to be hyperflocculent [186,187]. In *Pcut6MUT* the genes with increased H3K9 acetylation are enriched for GO terms DNA integration (p = 0.00024) and UDP-D-galactose metabolic process (p = 0.00808) and the genes with decreased H3K9 acetylation are enriched for GO term transmembrane transport (p = 0.00200), amino acid transmembrane transport (p = 0.00461) and cell-cell adhesion (p = 0.00752). As expected since H3K9 acetylation is associated with active transcription [188], the observed changes in H3K9 acetylation also correlate with transcript levels in *cbf11Δ* cells (Figure 3.3C). In *Pcut6MUT* cells, transcription of many noncoding RNAs and transposons is induced, correlating with GO enrichment of H3K9ac for DNA integration and overall increase of H3K9ac occupancy at chromatin regions that are usually transcriptionally silent.

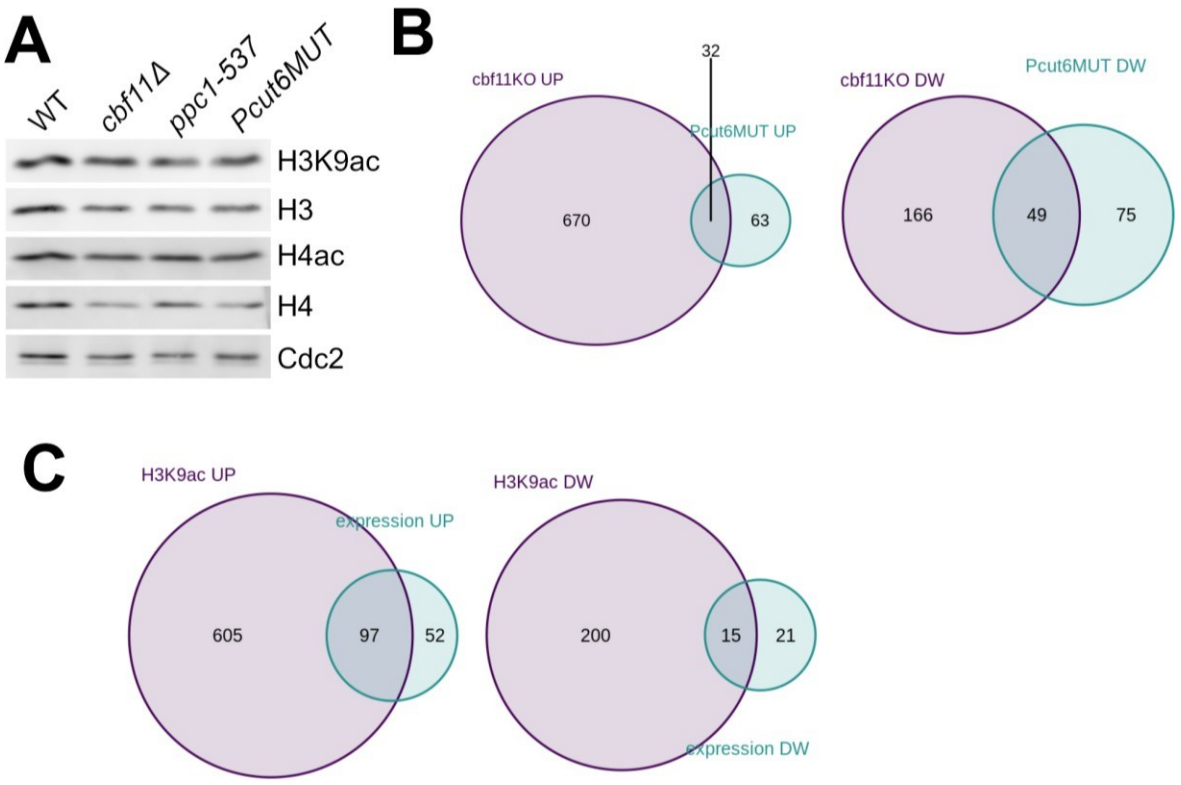

Fig 3.3 Genome-wide analysis of H3K9 acetylation in lipid mutants

(A) Western blot analysis of global H4 and H3K9 acetylation in WT and lipid metabolism mutants *cbf11Δ*, *ppc1-537* and *Pcut6MUT*. anti-Cdc2 antibody is used as a loading control. Two biological replicates were performed.

(B) Venn diagrams of genes with more than 1.5-fold increased (left) or decreased (right) H3K9 acetylation levels in *cbf11Δ* and *Pcut6MUT* cells compared to WT cells. Overlap significance was determined by the hypergeometric test. p = 4.77e-07 for genes with increased H3K9ac, p = 9.99e-37 for genes with decreased H3K9ac.

(C) Venn diagrams of genes with more than 1.5-fold increased H3K9 acetylation levels and genes with more than 2-fold higher expression levels (left), and genes with more than 1.5-fold decreased H3K9 acetylation levels and genes with more than 2-fold lower expression levels (right) in *cbf11Δ* cells. Expression data were from [150]. p = 3.19e-49 for genes with increased H3K9ac and expression, p = 3.53e-12 for genes with decreased H3K9ac and expression.

The evolutionary invention of telomeres solved "the end replication problem" in linear chromosomes, that is to protect linear DNA ends from replication associated erosion [189,190]. The region adjacent to telomeres has been named the subtelomere, although no universal definition based on structural or functional characteristics has been defined as it largely differs between species [191]. Investigation of chromosome ends is very complicated due to the repetitive nature

of telomeric and subtelomeric sequences, especially in organisms with large genomes. Therefore, *S. pombe* is used as an important model system for dissection of chromatin biology due to the relative ease of genetic manipulation and conservation of telomeric and subtelomeric chromatin structures and associated complexes [192]. In the fission yeast, the subtelomere is composed of two distinct domains: the subtelomere homologous domain (SH), which is adjacent to the telomeric repeats, and the subtelomere unique domain (ST), which is distal to the telomere. While the SH domain is rich in heterochromatin marks such as H3K9me2, HP1 (Swi6) and the shelterin complex and is thought to safeguard proper heterochromatin at the telomere, the ST domain is characterized by low levels of histone modifications (H3K9ac, H3K9me2, H3K4me3, H3K36me3) and facultative high chromosome condensation based on the cell cycle stage and external environment conditions (see schematic diagram in Figure 3.4A) [191,192]. We have discovered that the chromatin structure at the subtelomere is also regulated by lipid metabolism. In *cbf11Δ* and *Pcut6MUT* cells the H3K9me2 in the SH subtelomeric domain is diminished and, complementarily, the H3K9ac is slightly increased. Additionally, the increased H3K9ac in the lipid metabolism mutants spreads into the SH subtelomeric domain and these changes in chromatin modifications correlate with increased transcription from the subtelomeric regions in *cbf11Δ* and *Pcut6MUT* (Figures 3.4 and 3.5). Notably, the genome assembly available from Pombase [158,159] does not include complete subtelomeric assembly and due to the repetitive nature of the subtelomeres it is not possible to genuinely map standard short deep sequencing reads. Altered H3K9 modifications in *cbf11Δ* and *Pcut6MUT* cells do not appear to occur on all chromosomes to the same extent, for example H3K9me2 is reduced on both arms of chromosome I and II in *cbf11Δ* while only on the left arm of chrI and both arms of chrII in *Pcut6MUT* (Figures 3.4 and 3.5), which is likely caused by read mapping artifacts since the regions at the indicated boundary between SH and ST domains are 99% identical [193]. Analogous decrease in subtelomeric heterochromatin has been observed in TORC2 mutants [194] which further emphasizes the role of the subtelomeres in modulating transcription based on environmental factors.

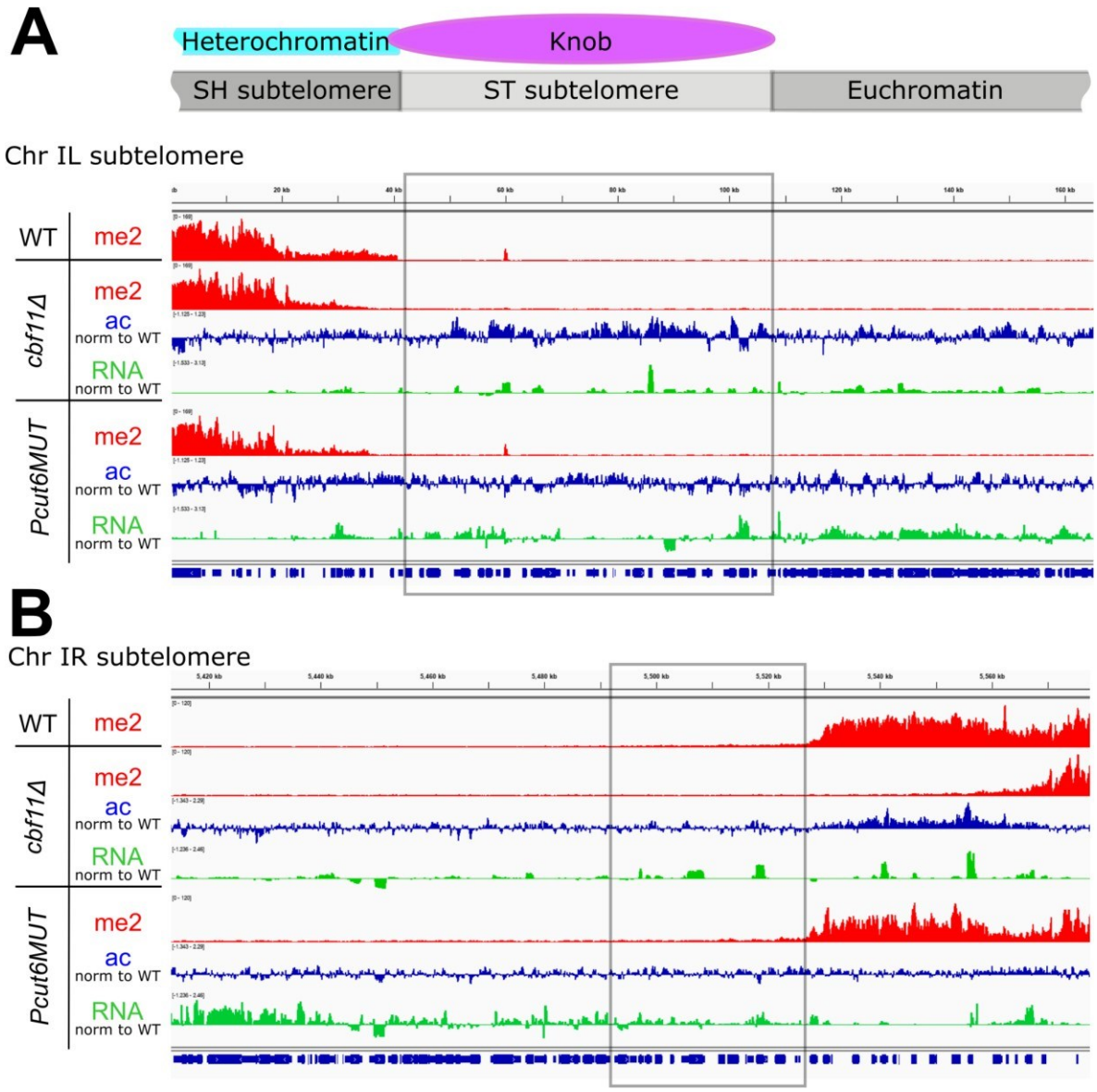

Fig 3.4 Subtelomeric heterochromatin is perturbed in lipid metabolism mutants - chromosome I. Profiles of H3K9me2, H3K9ac normalized to WT ChIP-seq signal, and gene expression RNA-seq normalized to WT in WT, *cbf11Δ* and *Pcut6MUT* cells in the left **(A)** and right **(B)** subtelomeric region of chromosome I were created in the IGV viewer [195]. Subtelomeric domains and corresponding chromatin structures are indicated above panel A. The gray box represents the approximate boundaries of the ST subtelomeric domain [193].

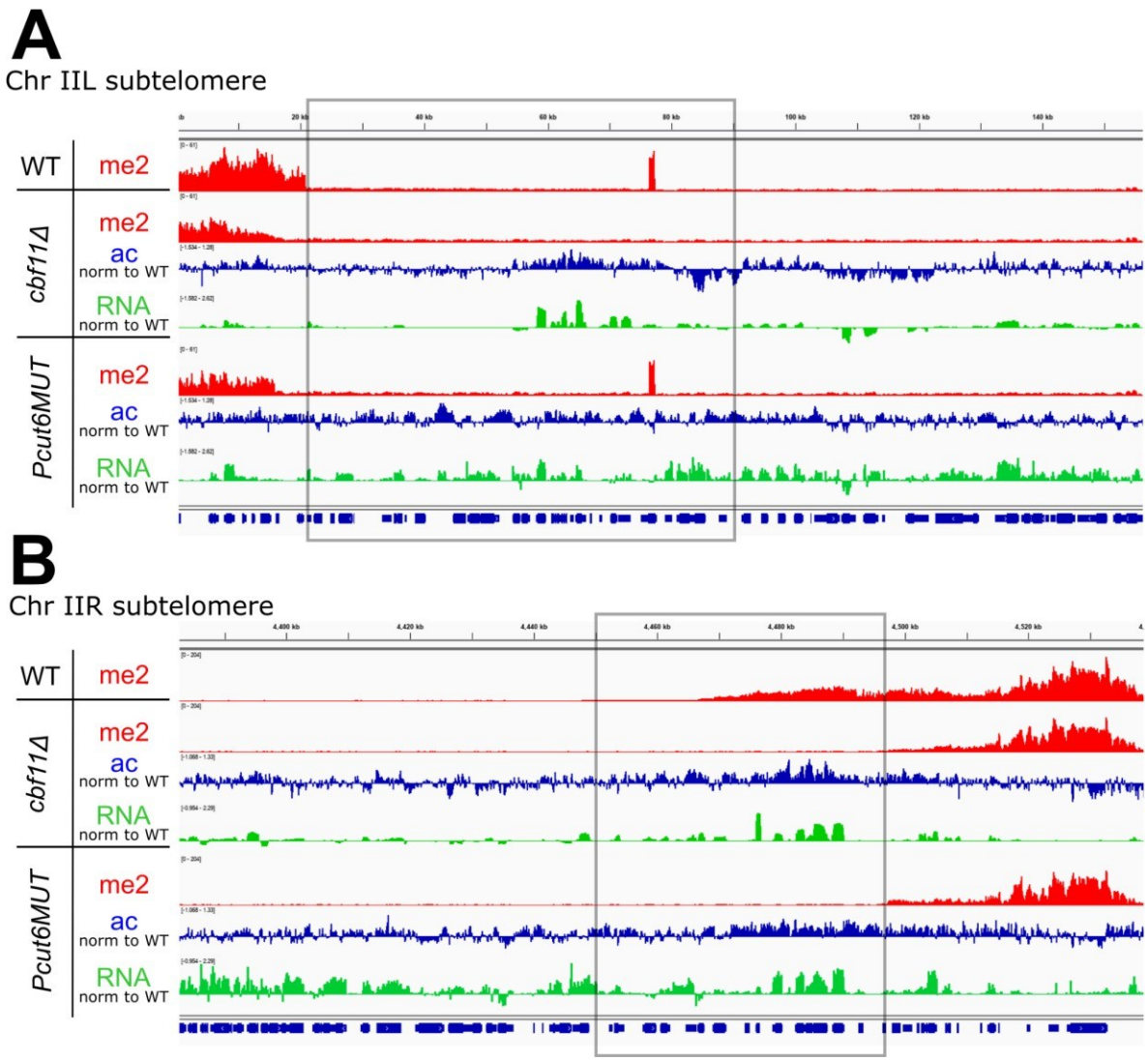

Fig 3.5 Subtelomeric heterochromatin is perturbed in lipid metabolism mutants - chromosome II. Profiles of H3K9me2, H3K9ac normalized to WT ChIP-seq signal, and gene expression RNA-seq normalized to WT in WT, *cbf11Δ* and *Pcut6MUT* cells in the left **(A)** and right **(B)** subtelomeric region of chromosome II were created in the IGV viewer [195]. The gray box represents the approximate boundaries of the ST subtelomeric domain as described in [193], however, the H3K9me2 occupancy on the right telomere of Chr II (B) suggests that the ST domain is located to the left of the indicated box, more distal from the telomere.

3.6 Altered cohesin dynamics and histone H3K9 modifications contribute to mitotic defects in the *cbf11Δ* lipid metabolism mutant

As a co-author of this manuscript I have performed the ChIP-seq experiments showing perturbed centromeric chromatin in cells lacking *cbf11* (Figure 4A and Supp. Figure 3BC).

Vishwanatha A, Princová J, Hohoš P, Zach R, Převorovský M. Altered cohesin dynamics and histone H3K9 modifications contribute to mitotic defects in the cbf11Δ lipid metabolism mutant. bioRxiv 2022.10.17.512562; doi: https://doi.org/10.1101/2022.10.17.512562 Review Commons in revision.

Although the text of this manuscript is not included in the presented thesis, the finding that lipid metabolism affects centromeric heterochromatin and the proposed hypothesis that increased H3K9me2 at the centromeres of *cbf11Δ* leads to accumulation of cohesin, a chromosome-associated multisubunit protein complex holding together sister chromatids after DNA replication until anaphase onset [196], are important in discussion of the overall impact of lipid metabolism on chromatin biology.

4. DISCUSSION

4.1 Regulation of lipid metabolism and mitotic fidelity by nitrogen-based nutrients

In *Schizosaccharomyces pombe*, the failure to segregate mitotic nuclei prior to cytokinesis can result in septum-mediated cleavage of the centrally positioned nucleus, the phenotype known as cell untimely torn or "cut" [197]. This mitotic defect typically results in gross nuclear damage and is in principle lethal. Mutants that show increased frequency of the "cut" phenotype can be divided into two major groups based on the function of the respective mutated gene. The first group includes genes directly linked to anaphase promotion and chromosome segregation, and the second group is composed of mutants linked to lipid metabolism [198]. *S. pombe* undergoes "closed" mitosis, which is not accompanied by nuclear envelope breakdown as in case of the open mitosis observed in mammals [199]. Large supply of membrane phospholipids is therefore required to satisfy the demand during rapid expansion of the nuclear envelope in the "closed" mitosis anaphase. As a result, decreased availability of membrane phospholipids leads to hampered nuclear elongation during anaphase associated with the collapse of the mitotic spindle [52,200]. The fission yeast lipid metabolism mutants *cbf11Δ* and *cut6-621* show the "cut" phenotype when grown in complex medium which contains ~0.06% nitrogen incorporated in a range of molecules such as amino acids, nucleobases and vitamins, and is considered to be relatively nitrogen-poor [147,187,201]. We have shown here that ammonium chloride (NH_4Cl) supplementation can alleviate the "cut" phenotype of *cbf11Δ* and *cut6-621* mutants [183] (**publication #1**). Moreover, addition of NH_4Cl modestly increased the lipid droplet content in WT cells, suggesting that the mechanism of NH_4Cl-mediated rescue of the "cut" phenotype is via increased availability of phospholipids for nuclear membrane elongation [183] (**publication #1**). Since NH_4Cl does not carry a carbon backbone it cannot be utilized in fatty acid synthesis and, therefore, likely affects lipid metabolism indirectly, possibly through nitrogen-sensitive signaling pathways. A likely player is the AMP-activated protein kinase (AMPK), an energy and stress sensor, which operates as a heterotrimeric complex consisting of catalytic α subunit and regulatory β and γ subunits [202]. In fission yeast, the catalytic AMPKα subunit Ssp2 is activated upon glucose or nitrogen starvation by Ssp1-dependent Thr189 phosphorylation [203]. Once activated, AMPK turns on catabolic

pathways and switches off ATP-consuming pathways by phosphorylating and regulating key enzymes in all branches of metabolism in order to maintain ATP homeostasis [204]. Importantly, AMPK inhibits acetyl-CoA carboxylase (ACC), the rate-limiting enzyme of fatty acid synthesis, in mammals and in the budding yeast [205]. The Ssp2-dependent inhibition of ACC seems to be conserved in *S. pombe* as suggested by the decreased levels of acetyl-CoA and increased levels of total fatty acids in the *ssp2Δ* mutant [206]. In line with the role of Ssp2 in the inhibition of fatty acid synthesis, the "cut" phenotype of the lipid metabolism mutant *cbf11Δ* is partially rescued by *ssp2* deletion (V. Zemlianski, unpublished results). Moreover, a recent study showed that nuclear envelope expansion is fueled by diacylglycerol (DAG) since DAG is depleted from the inner nuclear membrane during mitosis but phosphatidic acid (PA) does not accumulate, indicating that it is rerouted to membrane synthesis [207]. It is tempting to speculate that the DAG required for nuclear envelope expansion may be provided by TAG hydrolysis in nucleus-associated lipid droplets [19]. Taken together, we have shown that NH_4Cl affects mitotic fidelity and lipogenesis in *S. pombe*, however, it is not yet clear whether there is a causal relationship between increased fatty acid synthesis in nitrogen-rich environment and mitotic fidelity via providing sufficient supply of lipids for nuclear membrane expansion. Based on a recent finding demonstrating an important role of ACC-dependent tubulin palmitoylation in regulating mitotic spindle assembly, the potential involvement of fatty acids in additional aspects of mitosis, such as posttranslational modifications of crucial mitotic proteins should also be addressed [208].

4.2 Automated lipid droplet image analysis

Lipid droplets (LD) are evolutionarily conserved bodies composed mainly of triacylglycerols, steryl esters, an outer phospholipid monolayer and associated proteins [16]. LDs serve as centers for energy homeostasis but also function in lipotoxicity prevention and oxidative stress management, viral pathogenesis or protein quality control [16]. The physical properties of LDs such as number, volume and morphology can be used as a convenient proxy when assaying lipid metabolism under various growth conditions or when screening a panel of mutants. Due to variability in LD properties within a cell, techniques capable of analyzing the properties of individual LDs are of particular interest in studies of lipid metabolism.

Several approaches have been developed to study LD content and dynamics. Many employ LD staining with lipophilic dyes such as Nile Red or BODIPY 493/503. The latter shows more narrow excitation and emission spectra, and increased specificity towards neutral lipids (LDs) as opposed to phospholipids (membranes) [209]. Fluorimetric and flow-cytometry methods have been successfully used in various fungal species to discover genes and growth conditions that affect storage lipid content [210–212]. While these techniques are methods of choice for high-throughput applications when high numbers of mutants or environmental conditions need to be tested, they cannot measure the properties of individual LDs in cells. Coherent Raman scattering or digital holographic microscopy are label-free methods that yield LD-level data, but require specialized expensive equipment [213–215]. On the other hand, widefield fluorescence microscopy coupled with image analysis software tools allows for detailed description of individual LDs while using commonly available instruments. Several analysis workflows exist that feature various degrees of sophistication and automation in cell/LD detection from image data, and are usually optimized for specific cell types, such as metazoan cells [216–218] or budding yeasts [219,220]. Due to the limitations of the existing methods and the need to quantify LDs in *S. pombe*, we have developed an in-house tool with automated image analysis based on BODIPY 493/503 live cell staining and widefield fluorescence microscopy that we have used to quantitatively show that NH_4Cl supplementation leads to a modest increase in LD content [183] (**publication #1**). Later, we have improved this pilot image analysis tool and developed a workflow for 3-D LD content image analysis of three different yeast species. In addition to BODIPY 493/503 staining to visualize LDs we have included Cascade Blue dextran in the staining protocol to discriminate live cells from

dead ones and to determine cell boundaries. Before imaging, cells are immobilized on lectin-coated glass slides and subjected to z-stack imaging using a standard epifluorescence microscope. Images are then processed by an automated pipeline implemented in MATLAB, a widely used programming and computing platform. The pipeline performs image preprocessing, segmentation (cells vs. background, removal of dead cells), and LD identification based on 3-D reconstruction of the z-stack. LD volume and fluorescence intensity as well as number and intensity of LDs per cell voxel are then provided in a tabular format. We have demonstrated the functionality of the workflow in *Saccharomyces cerevisiae, Schizosaccharomyces pombe* and *Schizosaccharomyces japonicus*, a less characterized fission yeast emerging as a model organism for mitosis and yeast-hyphal transition [221], using growth conditions or mutants that affect cellular LD content [154] (**publication #2**). Although our automated image analysis tool has proven useful in analyzing LD content that would be otherwise laborious and potentially subjective to perform manually, the following limitations will need to be addressed to fully characterize single-cell LD content in yeast. First, the current image segmentation based on Cascade Blue dextran staining does not differentiate well between individual cells if they are physically touching. This issue can be partially suppressed by using less dense cell monolayers for imaging, but not solved completely because the fission yeast cells remain physically attached for a certain period after cytokinesis. Second, BODIPY 493/503 staining is quickly bleached when exposed to a high-intensity light source and, therefore, might easily lead to artifacts in the image analysis based on inconsistent handling of compared samples.

4.3 Sty1 MAPK in cell cycle and stress response

The cellular stress response is an adaptation mechanism that protects the cell from potential damage caused by changes in the intra- or extracellular environment. In the fission yeast, there are only three MAP kinases and one of them, the stress-activated protein kinase (SAPK) Sty1, is the master regulator of stress response [167,168]. Upon oxidative stress, Sty1 is phosphorylated by the upstream MAPK cascade, which leads to its relocalization from the cytoplasm to the nucleus, where it activates transcription mainly via the transcription factor Atf1 but also regulates other stress-relevant processes such as global translation inhibition or cell cycle arrest [167]. Previously, we have shown that Cbf11, the fission yeast transcription factor and regulator of lipid metabolism genes, is involved in the oxidative stress response [150]. Interestingly, while many Sty1-dependent genes are upregulated in cells lacking *cbf11* under normal conditions and their expression is further increased after H_2O_2 addition [150,152] (**publication #3**), exogenous oxidative stress imposition does not lead to Sty1 hyperphosphorylation as observed in WT cells (Figure 3.1B) [177]. However, even in *cbf11Δ* cells Sty1 relocalizes to the nucleus upon H_2O_2 treatment as expected based on the elevated stress-gene expression levels (Figure 3.1E). In order to explain this paradox we have tested whether the Sty1-deactivating phosphatases could be responsible for the low total phosphorylation levels of Sty1 in *cbf11Δ* cells. We have found that the gene expression levels of three phosphatases *ptc1*, *pyp1* and *pyp2* are indeed increased in *cbf11Δ* and that we can partially suppress the diminished Sty1 phosphorylation by inactivating Pyp1 or Pyp2 phosphatases (Figure 3.1A-C). Therefore, it seems plausible that increased activity of Pyp1 and Pyp2 phosphatases results in faster Sty1 phosphorylation turnover in *cbf11Δ*. Moreover, this increased activity of Sty1 phosphatases does not result in decreased Sty1-dependent stress-gene expression activation. Importantly, such oscillation of SAPK activity based on a negative feedback loop involving SAPK-inactivating phosphatase has been described in mammalian cells to be necessary for efficient induction of pro-inflammatory genes [222].

One of the crucial processes regulated during the stress response is cell cycle progression, which needs to be paused in order to remove damaged cellular parts and prevent propagation of the damage to further generations. Sty1 is orthologous to *S. cerevisiae* Hog1 and mammalian p38, all of which have the function to block cell cycle progression upon stress imposition. The ability of SAPKs to cause a cell cycle arrest appears to be crucial for cellular viability because both the

budding yeast Hog1 and the mammalian p38 have developed mechanisms to pause in any phase of the cell cycle in response to stress [223,224]. Less is known about the fission yeast SAPK. Upon hyperosmotic stress, activated Sty1 phosphorylates the Srk1 kinase at T463 of the regulatory domain, which leads to Srk1 activation and dissociation from Sty1 [169]. Activated Srk1 phosphorylates and thus inhibits Cdc25, the protein phosphatase promoting mitotic entry by activating the only fission yeast cyclin-dependent kinase Cdk1, leading to cell cycle arrest at G2 phase [225]. Because the mitotic entry depends on the balanced activities of the Cdc25 phosphatase and the Wee1 kinase both acting on Cdk1, a G2/M arrest might also be induced by Wee1 activation [226–228]. Hsl1-like protein kinase Cdr1 acts as a mitotic inducer by inhibiting Wee1 [229–232]. During osmotic stress Cdr1 is hyperphosphorylated in a Sty1-dependent manner, which leads to its inactivation and, as a result, an increase in Wee1 activity and delayed mitotic entry [170]. The same mechanism of Cdk1 inhibition via SAPK-Hsl1(Cdr1)-Swe1(Wee1) was observed also in *S. cerevisiae* [233,234]. We have showed that Sty1 activity is not only required for stress-gene expression, it appears to be also indispensable for maintaining viability in *cbf11Δ* cells [152] (**publication #3**). Is it because the *cbf11Δ* cells are experiencing endogenous stress and Sty1 is needed to induce proper stress response or is Sty1 activity required for other stress-unrelated processes in *cbf11Δ* cells? Our results do not support the former as loss of *cbf11* does not lead to ROS accumulation or hyperactivation of the stress-response pathways Sty1-Atf1 and Pap1 [152] (**publication #3**) and deletion of genes encoding major antioxidant enzymes such as catalase (*ctt1*) or sulfiredoxin (*srx1*) does not affect the viability of *cbf11Δ* cells [235]. On the other hand, inhibition of Sty1 kinase activity results in extreme cell elongation and nuclear fragmentation in *cbf11Δ* cells (Figure 3.2), thus suggesting a role in cell cycle regulation.

In addition to their role in stress response, p38 and Sty1 SAPKs have been implicated in cell cycle control under normal conditions. Several studies have shown that p38 is activated by mitogenic stimuli and leads to cell proliferation [236,237]. Moreover, loss of the Sty1 SAPK leads to pronounced cell elongation, thus pointing to the conclusion that Sty1 is a positive regulator of mitosis [174]. How can this paradox of SAPK activity leading to both cell cycle arrest and progression be explained? A likely candidate is the duration and intensity of SAPK activity. While cellular stress causes a strong and persistent SAPK activation leading to cell cycle arrest, mitogen-stimulated SAPK activity is associated with weaker and transient SAPK activity [238]. Under

normal non-stress conditions, p38 activity slightly increases during the G2/M phase and localizes to the centrosomes [239,240]. At the centrosomes, p38 was described to regulate timing of mitotic entry via modulation of Cdc25B activity [239]. Additionally, p38 can also promote timely spindle assembly [240]. Absence of p38 activity does not compromise mitotic fidelity but the duration of mitosis is increased due to longer metaphase spindles and a delay in satisfying the spindle assembly checkpoint [240]. This Sty1 activity may be essential to enable the already perturbed mitotic nuclear segregation in *cbf11Δ* cells, which display longer interval between spindle formation and anaphase onset compared to WT cells [241]. Nevertheless, Sty1 localization at the spindle pole bodies, the yeast equivalents of centrosomes, has not been described to date. Interestingly, synthetic growth defect was also observed upon deletion of Sty1-inactivating PP2C phosphatase Ptc1 in *cbf11Δ* mutant (Figure 3.1D), although deletion of Pyp1 or Pyp2 protein tyrosine phosphatases did not affect viability of *cbf11Δ* cells (data not shown). Therefore, Sty1 activity likely needs to be properly regulated to ensure *cbf11Δ* viability since both increase and decrease in Sty1 activity have detrimental effects. Alternatively, Ptc1 is also known to dephosphorylate Pmk1, the MAP kinase involved in the cell integrity pathway, and increased Pmk1 activity in *cbf11Δ ptc1Δ* may negatively affect mitotic progression [242]. Furthermore, p38/Sty1 can work as a cellular ruler, coordinating cell size and cell cycle progression [175,239,243]. Rum1 is the only CDK inhibitor in the fission yeast that ensures mitotic commitment (Start) only when the cells reach sufficient size [244–246]. Sty1 was suggested to function as a negative regulator of Rum1, thus positively regulating cell cycle progression [247]. Although this study demonstrated that Sty1 can phosphorylate Rum1 *in vitro* and overexpression of phosphomimicking Rum1 allele does not lead to massive DNA over-replication as caused by WT Rum1 allele overexpression, the physiological impact of Sty1-mediated Rum1 inhibition on cell cycle progression has not been elucidated [246,247]. Conceivably, based on the multiple roles of Sty1 in mitotic control, deregulation of Sty1 in *cbf11Δ* cells further aggravates mitotic defects, which lead to cell death. Taken together, the SAPK regulates a range of processes including cell cycle progression during stress, however, its activity is also important during normal non-stress conditions to regulate mitotic timing.

4.4 Lipid metabolism as a global and targeted regulator of the epigenetic states

Changes in intracellular metabolite levels that serve as substrates for histone "writers" have a profound effect on chromatin modifications and often result in altered gene expression [61]. Global alterations in the chromatin landscape are one of the hallmarks of differentiation [248] and interventions with α-KG or acetyl-CoA availability affect differentiation progression [72,83,249,250]. Generally, acetyl-CoA levels can be used as a proxy for assessing the cellular growth and global histone acetylation status. High acetyl-CoA levels induce cell growth and proliferation by promoting histone acetylation [251] while low levels of acetyl-CoA during starvation promote histone deacetylation and released acetate can be utilized for energy production and anabolism [83,252,253]. Intriguingly, detailed analyses of the chromatin modifications revealed that changes in acetyl-CoA availability lead not only to globally observable changes in total histone acetylation but also to locus-specific changes affecting particular gene expression programs or other nuclear functions such as DNA damage response [77]. In our recent study we have shown that decreased fatty acid synthesis in the fission yeast does not result in global histone hyperacetylation as described in the budding yeast (Figure 3.3A) [85,185] but rather causes a HAT-dependent increase in expression of specific stress-response genes, which leads to increased resistance to H_2O_2 [152] (**publication #3**). While the induction of the stress-gene expression in lipid metabolism mutant *cbf11Δ* still depends on components of the SAPK and Pap1 pathways, Sty1-Atf1 or Pap1 are not hyperactivated as when the cell is exposed to canonical stress conditions [152] (**publication #3**). Additionally, we have observed that diminished fatty acid synthesis leads to promoter histone hyperacetylation at stress genes and, since Atf1 transcription factor binds many target promoters even without stress imposition and phosphorylation by Sty1 [254], we proposed that such stress gene promoter hyperacetylation might lead to more accessible chromatin and interaction with the transcription machinery. Interestingly, a recent budding yeast study described that glucose starvation, and thus a decrease in acetyl-CoA availability, leads to global decrease in histone acetylation as well to reallocation of H3K9ac from growth-promoting genes to gluconeogenic and fat metabolism genes as a result of the combined activity of the Rpd3 HDAC and Gcn5 HAT, respectively [252].

The question of how the specificity of targeted changes in gene expression upon acetyl-CoA level perturbation is achieved remains unclear. One possibility is the *in situ* acetyl-CoA synthesis by enzymes such as acyl-CoA synthetase (ACSS2) or ATP-citrate lyase (ACLY) which produce substrate for histone acetylation directly at chromatin. Such mechanism has been observed in mouse neurons where ACSS2 is recruited to chromatin and leads to induction of specific genes important for hippocampal memory [142] or upon DNA-damage when ACLY is phosphorylated and associates with sites of DNA damage, thus facilitates histone acetylation and enables homologous recombination by recruiting BRCA1 [255]. Importantly, ACSS2- and ACLY-generated acetyl-CoA appears to be differentially used and associates with specific chromatin loci [142,255].

However, in case of perturbed fatty acid synthesis there is likely an excess of nucleocytoplasmic acetyl-CoA and the specificity of histone acetylation needs to be determined by a more downstream factor such as HAT. Curiously, HATs are promiscuous enzymes. In our study, we have identified two HATs, Gcn5 (SAGA complex) and Mst1 (NuA4 complex), as important for increased stress-gene expression in the *cbf11Δ* lipid metabolism mutant [152] (**publication #3**). Nevertheless, HATs mostly function as subunits of multiprotein co-activator complexes and other regulatory subunits may be responsible for providing the required specificity. For example, the SAGA subunit Tra1 promotes the interaction between specific transcription factors at some genomic loci but is dispensable at others [256,257]. Alternatively, spatial organization of chromosomes within nucleus or formation of nuclear condensates provide compelling explanations. Nuclear structures such as the nuclear envelope or nuclear pore complexes work as 3-D genome organizers and while the former is associated with gene silencing the latter acts as a scaffold for transcription complexes [258–260]. In recent years, liquid-liquid phase separation (LLPS) has become the leading-edge theory for spatiotemporal regulation of gene expression and other cellular processes [261]. The presence of intrinsically disordered regions (IDR), which are very abundant in eukaryotic proteomes including nuclear proteins, is a common feature of proteins capable of undergoing LLPS [262]. Although evidence for nuclear condensates formed by HATs is still very scarce [139,263], the presence of IDR in HAT modules as well as the documented role of LLPS in Pol II-mediated transcription encourage the possibility of LLPS-mediated specificity of histone acetylation [261].

In addition to inducing stress-response genes dispersed in the genome, mutations in the lipid metabolism regulators *cbf11Δ* and *Pcut6MUT* also lead to changes in subtelomeric and centromeric chromatin. Subtelomeres are approximately 100 kb long regions adjacent to telomeres with low transcriptional activity. They are formed by two domains: the subtelomere homologous domain (SH) adjacent to the telomere and the subtelomere unique domain (ST) adjacent to the euchromatic region [192]. While the SH domains of subtelomeres are heterochromatinized, formed by repetitive sequences and are highly similar on all arms of chromosomes I and II, the ST domains are poor in histone modifications and generally transcriptionally silent [193]. Together, both domains of the subtelomere function to protect the chromosome ends and prevent spreading of heterochromatin into the chromosome arms [264]. Interestingly, the levels of H3K9 methylation, a heterochromatin marker, are not uniformly distributed in the SH domains and contain a region proximal to the telomere with high H3K9me occupancy and a region proximal to ST domain with a lower plateau of H3K9me2 [265]. We have described that in the lipid metabolism mutants *cbf11Δ* and *Pcut6MUT* the H3K9me2 modification is suppressed in the subtelomeric region of low H3K9me2 while H3K9ac and transcription levels are increased (Figure 3.4). Similar behavior has been observed for TORC2, cohesin loader Mis4 and cohesin core component Rad21 mutants [194,266]. Whether the effects of TORC2, cohesin and lipid metabolism regulators Cbf11 and Cut6 at subtelomeric chromatin are related remains to be investigated. Moreover, the physiological impact of suppressing the low level of H3K9me2 at the telomere-distal part of the SH domain is not clear. This region is enriched for stress-responsive genes and is prone to sequence mutations which predispose the telomere-distal part of the SH domain to be important for genome evolution and adaptation to changing environmental conditions [267,268]. Thus it is plausible that changes in heterochromatinization of this region reflect the lipid metabolism status. Additionally, in *cbf11Δ* and *Pcut6MUT* mutants the increased transcript and H3K9ac levels extend into the adjacent ST domain, which is normally devoid of heterochromatin or euchromatin markers and highly condensed into “knobs” during the interphase [193]. Interestingly, the “knob” condensation is eliminated upon nitrogen starvation and leads to gene derepression in this region [193]. Therefore, metabolic signaling likely plays a role in transcription regulation of the subtelomeric region in both SH and ST domains. An intriguing property of the ST domain is the spatial clustering of chromosome I and II subtelomeres, which could mediate common regulation of subtelomeric

chromatin and gene expression by histone-modifying enzymes or metabolites [192,269]. Additionally, lipid metabolism enzymes such as Fas1, Lcf1 or Ole1, that are positively regulated by the Cbf11 transcription factor, have been shown to physically interact with the inner nuclear membrane protein Lem2 which is responsible for tethering heterochromatin to the nuclear envelope [150,270,271]. This mechanism of chromatin regulation facilitated by spatial proximity, in particular by nuclear envelope tethering, is utilized also in maintenance of centromeric heterochromatin [272]. Curiously, both the euchromatin mark H3K9ac and the heterochromatin mark H3K9me2 appear to be more abundant at the centromeric outer repeats of cells lacking *cbf11*, however, this discrepancy is likely caused by the repetitive nature of centromeric sequences (making it difficult to assay individual copies of the repeats separately) and, possibly, by cell-to-cell variation [241]. Heterochromatin at the centromere is crucial for sister centromere cohesion during mitosis [273]. We hypothesize that the increased H3K9me2 at the centromeres of *cbf11Δ* leads to the observed accumulation of cohesin and, potentially, to aggravation of mitotic defects in *cbf11Δ* cells [241]. In conclusion, lipid metabolism perturbation has a broad impact on chromatin regulation in the fission yeast. It is involved in targeted increase of stress gene expression resulting in increased oxidative stress resistance but also in global changes in the transcriptionally silenced regions of subtelomeres and centromeres.

5. CONCLUSIONS

This thesis has summarized my contributions to three published manuscripts and related unpublished results.

- We have developed a Matlab-based automated image analysis tool for quantification of lipid droplets in three yeast species. This tool allows unbiased measurements of individual lipid droplets within live cells in 3-D.
- Using our automated image analysis tool we have shown that supplementation with an easily metabolized nitrogen source such as NH_4Cl boosts total lipid content of fission yeast. Moreover, NH_4Cl supplementation also increases lipid droplet content and rescues mitotic defects in the lipid metabolism mutant *cbf11Δ*, thus suggesting a functional link between nitrogen signaling, lipid metabolism and mitotic fidelity.
- The functions of the SAPK Sty1 in stress response have been previously described in detail, however its function in cell cycle regulation is not well characterized. We have described that low levels of Sty1 phosphorylation in *cbf11Δ* are likely caused by high Pyp1- and Pyp2-dependent phosphorylation turnover and are sufficient to induce strong stress gene induction. Moreover, we have shown that Sty1 activity is vital for the viability of *cbf11Δ* cells, likely by ensuring cell cycle progression.
- We have demonstrated a novel interconnection between lipid metabolism and oxidative stress resistance. Upon inhibition of fatty acid synthesis, a subset of stress-responsive genes becomes derepressed, making cells more resistant to H_2O_2. Additionally, this process happens without triggering a classical stress response but is accompanied with increased histone acetylation at the derepressed stress genes and depends on the activity of the Gcn5 and Mst1 HATs.
- In addition to regulating stress-response genes, we have discovered that lipid metabolism perturbation also results in global changes in the transcriptionally silenced regions of subtelomeres and centromeres.

6. REFERENCES

1. Santos AL, Preta G. Lipids in the cell: organisation regulates function. Cell Mol Life Sci CMLS. 2018;75: 1909–1927. doi:10.1007/s00018-018-2765-4

2. Johnson AA, Stolzing A. The role of lipid metabolism in aging, lifespan regulation, and age-related disease. Aging Cell. 2019;18: e13048. doi:10.1111/acel.13048

3. Fernández LP, Gómez de Cedrón M, Ramírez de Molina A. Alterations of Lipid Metabolism in Cancer: Implications in Prognosis and Treatment. Front Oncol. 2020;10: 577420. doi:10.3389/fonc.2020.577420

4. Rysman E, Brusselmans K, Scheys K, Timmermans L, Derua R, Munck S, et al. De novo lipogenesis protects cancer cells from free radicals and chemotherapeutics by promoting membrane lipid saturation. Cancer Res. 2010;70: 8117–8126. doi:10.1158/0008-5472.CAN-09-3871

5. Nelson ME, Lahiri S, Chow JDY, Byrne FL, Hargett SR, Breen DS, et al. Inhibition of hepatic lipogenesis enhances liver tumorigenesis by increasing antioxidant defence and promoting cell survival. Nat Commun. 2017;8: 14689. doi:10.1038/ncomms14689

6. Lei I, Tian S, Gao W, Liu L, Guo Y, Tang P, et al. Acetyl-CoA production by specific metabolites promotes cardiac repair after myocardial infarction via histone acetylation. eLife. 2021;10: e60311. doi:10.7554/eLife.60311

7. Jeong D-W, Lee S, Chun Y-S. How cancer cells remodel lipid metabolism: strategies targeting transcription factors. Lipids Health Dis. 2021;20: 163. doi:10.1186/s12944-021-01593-8

8. Broadfield LA, Pane AA, Talebi A, Swinnen JV, Fendt S-M. Lipid metabolism in cancer: New perspectives and emerging mechanisms. Dev Cell. 2021;56: 1363–1393. doi:10.1016/j.devcel.2021.04.013

9. Snaebjornsson MT, Janaki-Raman S, Schulze A. Greasing the Wheels of the Cancer Machine: The Role of Lipid Metabolism in Cancer. Cell Metab. 2020;31: 62–76. doi:10.1016/j.cmet.2019.11.010

10. Arroyave-Ospina JC, Wu Z, Geng Y, Moshage H. Role of Oxidative Stress in the Pathogenesis of Non-Alcoholic Fatty Liver Disease: Implications for Prevention and Therapy. Antioxid Basel Switz. 2021;10: 174. doi:10.3390/antiox10020174

11. Mashek DG. Hepatic lipid droplets: A balancing act between energy storage and metabolic dysfunction in NAFLD. Mol Metab. 2021;50: 101115. doi:10.1016/j.molmet.2020.101115

12. Lopaschuk GD, Ussher JR, Folmes CDL, Jaswal JS, Stanley WC. Myocardial fatty acid metabolism in health and disease. Physiol Rev. 2010;90: 207–258. doi:10.1152/physrev.00015.2009

13. Abdurrachim D, Luiken JJFP, Nicolay K, Glatz JFC, Prompers JJ, Nabben M. Good and bad consequences of altered fatty acid metabolism in heart failure: evidence from mouse models. Cardiovasc Res. 2015;106: 194–205. doi:10.1093/cvr/cvv105

14. Dambrova M, Zuurbier CJ, Borutaite V, Liepinsh E, Makrecka-Kuka M. Energy substrate metabolism and mitochondrial oxidative stress in cardiac ischemia/reperfusion injury. Free Radic Biol Med. 2021;165: 24–37. doi:10.1016/j.freeradbiomed.2021.01.036

15. Sies H. Oxidative Stress: Concept and Some Practical Aspects. Antioxid Basel Switz. 2020;9: 852. doi:10.3390/antiox9090852

16. Olzmann JA, Carvalho P. Dynamics and functions of lipid droplets. Nat Rev Mol Cell Biol. 2019;20: 137–155. doi:10.1038/s41580-018-0085-z

17. Lundquist PK, Shivaiah K-K, Espinoza-Corral R. Lipid droplets throughout the evolutionary tree. Prog Lipid Res. 2020;78: 101029. doi:10.1016/j.plipres.2020.101029

18. Fujimoto T, Parton RG. Not just fat: the structure and function of the lipid droplet. Cold Spring Harb Perspect Biol. 2011;3: a004838. doi:10.1101/cshperspect.a004838

19. Meyers A, Del Rio ZP, Beaver RA, Morris RM, Weiskittel TM, Alshibli AK, et al. Lipid Droplets Form from Distinct Regions of the Cell in the Fission Yeast Schizosaccharomyces pombe. Traffic Cph Den. 2016;17: 657–669. doi:10.1111/tra.12394

20. Welte MA, Gould AP. Lipid droplet functions beyond energy storage. Biochim Biophys Acta Mol Cell Biol Lipids. 2017;1862: 1260–1272. doi:10.1016/j.bbalip.2017.07.006

21. Bersuker K, Peterson CWH, To M, Sahl SJ, Savikhin V, Grossman EA, et al. A Proximity Labeling Strategy Provides Insights into the Composition and Dynamics of Lipid Droplet Proteomes. Dev Cell. 2018;44: 97-112.e7. doi:10.1016/j.devcel.2017.11.020

22. Currie E, Guo X, Christiano R, Chitraju C, Kory N, Harrison K, et al. High confidence proteomic analysis of yeast LDs identifies additional droplet proteins and reveals connections to dolichol synthesis and sterol acetylation. J Lipid Res. 2014;55: 1465–1477. doi:10.1194/jlr.M050229

23. Nettebrock NT, Bohnert M. Born this way - Biogenesis of lipid droplets from specialized ER subdomains. Biochim Biophys Acta Mol Cell Biol Lipids. 2020;1865: 158448. doi:10.1016/j.bbalip.2019.04.008

24. Kwiatek JM, Han G-S, Carman GM. Phosphatidate-mediated regulation of lipid synthesis at the nuclear/endoplasmic reticulum membrane. Biochim Biophys Acta Mol Cell Biol Lipids. 2020;1865: 158434. doi:10.1016/j.bbalip.2019.03.006

25. Wang H, Airola MV, Reue K. How lipid droplets “TAG” along: Glycerolipid synthetic enzymes and lipid storage. Biochim Biophys Acta Mol Cell Biol Lipids. 2017;1862: 1131–1145. doi:10.1016/j.bbalip.2017.06.010

26. Thiam AR, Forêt L. The physics of lipid droplet nucleation, growth and budding. Biochim Biophys Acta. 2016;1861: 715–722. doi:10.1016/j.bbalip.2016.04.018

27. Schneiter R, Choudhary V. Seipin collaborates with the ER membrane to control the sites of lipid droplet formation. Curr Opin Cell Biol. 2022;75: 102070. doi:10.1016/j.ceb.2022.02.004

28. Wang H, Becuwe M, Housden BE, Chitraju C, Porras AJ, Graham MM, et al. Seipin is required for converting nascent to mature lipid droplets. eLife. 2016;5: e16582. doi:10.7554/eLife.16582

29. Henne WM, Reese ML, Goodman JM. The assembly of lipid droplets and their roles in challenged cells. EMBO J. 2018;37: e98947. doi:10.15252/embj.201898947

30. Zoni V, Nieto V, Endter LJ, Risselada HJ, Monticelli L, Vanni S. To Bud or Not to Bud: A Perspective on Molecular Simulations of Lipid Droplet Budding. Front Mol Biosci. 2019;6: 124. doi:10.3389/fmolb.2019.00124

31. de Vries J, Ischebeck T. Ties between Stress and Lipid Droplets Pre-date Seeds. Trends Plant Sci. 2020;25: 1203–1214. doi:10.1016/j.tplants.2020.07.017

32. Dubots E, Cottier S, Péli-Gulli M-P, Jaquenoud M, Bontron S, Schneiter R, et al. TORC1 regulates Pah1 phosphatidate phosphatase activity via the Nem1/Spo7 protein phosphatase complex. PloS One. 2014;9: e104194. doi:10.1371/journal.pone.0104194

33. Nguyen TB, Louie SM, Daniele JR, Tran Q, Dillin A, Zoncu R, et al. DGAT1-Dependent Lipid Droplet Biogenesis Protects Mitochondrial Function during Starvation-Induced Autophagy. Dev Cell. 2017;42: 9-21.e5. doi:10.1016/j.devcel.2017.06.003

34. Rambold AS, Cohen S, Lippincott-Schwartz J. Fatty acid trafficking in starved cells: regulation by lipid droplet lipolysis, autophagy, and mitochondrial fusion dynamics. Dev Cell. 2015;32: 678–692. doi:10.1016/j.devcel.2015.01.029

35. Valachovic M, Garaiova M, Holic R, Hapala I. Squalene is lipotoxic to yeast cells defective in lipid droplet biogenesis. Biochem Biophys Res Commun. 2016;469: 1123–1128. doi:10.1016/j.bbrc.2015.12.050

36. Bensaad K, Favaro E, Lewis CA, Peck B, Lord S, Collins JM, et al. Fatty acid uptake and lipid storage induced by HIF-1α contribute to cell growth and survival after hypoxia-reoxygenation. Cell Rep. 2014;9: 349–365. doi:10.1016/j.celrep.2014.08.056

37. Read A, Schröder M. The Unfolded Protein Response: An Overview. Biology. 2021;10: 384. doi:10.3390/biology10050384

38. Fei W, Wang H, Fu X, Bielby C, Yang H. Conditions of endoplasmic reticulum stress stimulate lipid droplet formation in Saccharomyces cerevisiae. Biochem J. 2009;424: 61–67. doi:10.1042/BJ20090785

39. Jarc E, Petan T. Lipid Droplets and the Management of Cellular Stress. Yale J Biol Med. 2019;92: 435–452.

40. Sadre R, Kuo P, Chen J, Yang Y, Banerjee A, Benning C, et al. Cytosolic lipid droplets as engineered organelles for production and accumulation of terpenoid biomaterials in leaves. Nat Commun. 2019;10: 853. doi:10.1038/s41467-019-08515-4

41. Bundó M, Shi X, Vernet M, Marcos JF, López-García B, Coca M. Rice Seeds as Biofactories of Rationally Designed and Cell-Penetrating Antifungal PAF Peptides. Front Plant Sci. 2019;10: 731. doi:10.3389/fpls.2019.00731

42. Popa C, Shi X, Ruiz T, Ferrer P, Coca M. Biotechnological Production of the Cell Penetrating Antifungal PAF102 Peptide in Pichia pastoris. Front Microbiol. 2019;10: 1472. doi:10.3389/fmicb.2019.01472

43. Son S-H, Park G, Lim J, Son CY, Oh SS, Lee JY. Chain flexibility of medicinal lipids determines their selective partitioning into lipid droplets. Nat Commun. 2022;13: 3612. doi:10.1038/s41467-022-31400-6

44. Hayles J, Nurse P. Introduction to Fission Yeast as a Model System. Cold Spring Harb Protoc. 2018;2018. doi:10.1101/pdb.top079749

45. Hedges SB. The origin and evolution of model organisms. Nat Rev Genet. 2002;3: 838–849. doi:10.1038/nrg929

46. Vyas A, Freitas AV, Ralston ZA, Tang Z. Fission Yeast Schizosaccharomyces pombe: A Unicellular “Micromammal” Model Organism. Curr Protoc. 2021;1: e151. doi:10.1002/cpz1.151

47. Meyers A, Chourey K, Weiskittel TM, Pfiffner S, Dunlap JR, Hettich RL, et al. The protein and neutral lipid composition of lipid droplets isolated from the fission yeast, Schizosaccharomyces pombe. J Microbiol Seoul Korea. 2017;55: 112–122. doi:10.1007/s12275-017-6205-1

48. Long AP, Manneschmidt AK, VerBrugge B, Dortch MR, Minkin SC, Prater KE, et al. Lipid droplet de novo formation and fission are linked to the cell cycle in fission yeast. Traffic Cph Den. 2012;13: 705–714. doi:10.1111/j.1600-0854.2012.01339.x

49. Cruz ALS, Carrossini N, Teixeira LK, Ribeiro-Pinto LF, Bozza PT, Viola JPB. Cell Cycle Progression Regulates Biogenesis and Cellular Localization of Lipid Droplets. Mol Cell Biol. 2019;39: e00374-18. doi:10.1128/MCB.00374-18

50. Karanasios E, Barbosa AD, Sembongi H, Mari M, Han G-S, Reggiori F, et al. Regulation of lipid droplet and membrane biogenesis by the acidic tail of the phosphatidate phosphatase Pah1p. Mol Biol Cell. 2013;24: 2124–2133. doi:10.1091/mbc.E13-01-0021

51. Choi H-S, Su W-M, Morgan JM, Han G-S, Xu Z, Karanasios E, et al. Phosphorylation of phosphatidate phosphatase regulates its membrane association and physiological functions in

Saccharomyces cerevisiae: identification of SER(602), THR(723), AND SER(744) as the sites phosphorylated by CDC28 (CDK1)-encoded cyclin-dependent kinase. J Biol Chem. 2011;286: 1486–1498. doi:10.1074/jbc.M110.155598

52. Makarova M, Gu Y, Chen J-S, Beckley JR, Gould KL, Oliferenko S. Temporal Regulation of Lipin Activity Diverged to Account for Differences in Mitotic Programs. Curr Biol CB. 2016;26: 237–243. doi:10.1016/j.cub.2015.11.061

53. Hapala I, Griac P, Holic R. Metabolism of Storage Lipids and the Role of Lipid Droplets in the Yeast Schizosaccharomyces pombe. Lipids. 2020;55: 513–535. doi:10.1002/lipd.12275

54. Lempp M, Farke N, Kuntz M, Freibert SA, Lill R, Link H. Systematic identification of metabolites controlling gene expression in E. coli. Nat Commun. 2019;10: 4463. doi:10.1038/s41467-019-12474-1

55. Jacob F, Monod J. Genetic regulatory mechanisms in the synthesis of proteins. J Mol Biol. 1961;3: 318–356. doi:10.1016/s0022-2836(61)80072-7

56. Ptashne M. How eukaryotic transcriptional activators work. Nature. 1988;335: 683–689. doi:10.1038/335683a0

57. Sukumaran A, Choi K, Dasgupta B. Insight on Transcriptional Regulation of the Energy Sensing AMPK and Biosynthetic mTOR Pathway Genes. Front Cell Dev Biol. 2020;8: 671. doi:10.3389/fcell.2020.00671

58. Jump DB. Fatty acid regulation of gene transcription. Crit Rev Clin Lab Sci. 2004;41: 41–78. doi:10.1080/10408360490278341

59. Zheng L, Roeder RG, Luo Y. S phase activation of the histone H2B promoter by OCA-S, a coactivator complex that contains GAPDH as a key component. Cell. 2003;114: 255–266. doi:10.1016/s0092-8674(03)00552-x

60. Li X, Egervari G, Wang Y, Berger SL, Lu Z. Regulation of chromatin and gene expression by metabolic enzymes and metabolites. Nat Rev Mol Cell Biol. 2018;19: 563–578. doi:10.1038/s41580-018-0029-7

61. Schvartzman JM, Thompson CB, Finley LWS. Metabolic regulation of chromatin modifications and gene expression. J Cell Biol. 2018;217: 2247–2259. doi:10.1083/jcb.201803061

62. Luger K, Mäder AW, Richmond RK, Sargent DF, Richmond TJ. Crystal structure of the nucleosome core particle at 2.8 A resolution. Nature. 1997;389: 251–260. doi:10.1038/38444

63. Huang H, Sabari BR, Garcia BA, Allis CD, Zhao Y. SnapShot: histone modifications. Cell. 2014;159: 458-458.e1. doi:10.1016/j.cell.2014.09.037

64. Strahl BD, Allis CD. The language of covalent histone modifications. Nature. 2000;403: 41–45. doi:10.1038/47412

65. Breiling A, Lyko F. Epigenetic regulatory functions of DNA modifications: 5-methylcytosine and beyond. Epigenetics Chromatin. 2015;8: 24. doi:10.1186/s13072-015-0016-6

66. Zhou K, Gaullier G, Luger K. Nucleosome structure and dynamics are coming of age. Nat Struct Mol Biol. 2019;26: 3–13. doi:10.1038/s41594-018-0166-x

67. Yu W, Wang Z, Zhang K, Chi Z, Xu T, Jiang D, et al. One-Carbon Metabolism Supports S-Adenosylmethionine and Histone Methylation to Drive Inflammatory Macrophages. Mol Cell. 2019;75: 1147-1160.e5. doi:10.1016/j.molcel.2019.06.039

68. Capuano F, Mülleder M, Kok R, Blom HJ, Ralser M. Cytosine DNA methylation is found in Drosophila melanogaster but absent in Saccharomyces cerevisiae, Schizosaccharomyces pombe, and other yeast species. Anal Chem. 2014;86: 3697–3702. doi:10.1021/ac500447w

69. Becker M, Müller S, Nellen W, Jurkowski TP, Jeltsch A, Ehrenhofer-Murray AE. Pmt1, a Dnmt2 homolog in Schizosaccharomyces pombe, mediates tRNA methylation in response to nutrient signaling. Nucleic Acids Res. 2012;40: 11648–11658. doi:10.1093/nar/gks956

70. Mentch SJ, Mehrmohamadi M, Huang L, Liu X, Gupta D, Mattocks D, et al. Histone Methylation Dynamics and Gene Regulation Occur through the Sensing of One-Carbon Metabolism. Cell Metab. 2015;22: 861–873. doi:10.1016/j.cmet.2015.08.024

71. Shi YG, Tsukada Y. The discovery of histone demethylases. Cold Spring Harb Perspect Biol. 2013;5: a017947. doi:10.1101/cshperspect.a017947

72. Carey BW, Finley LWS, Cross JR, Allis CD, Thompson CB. Intracellular α-ketoglutarate maintains the pluripotency of embryonic stem cells. Nature. 2015;518: 413–416. doi:10.1038/nature13981

73. Greer EL, Shi Y. Histone methylation: a dynamic mark in health, disease and inheritance. Nat Rev Genet. 2012;13: 343–357. doi:10.1038/nrg3173

74. Barnes CE, English DM, Cowley SM. Acetylation & Co: an expanding repertoire of histone acylations regulates chromatin and transcription. Essays Biochem. 2019;63: 97–107. doi:10.1042/EBC20180061

75. Lee KK, Workman JL. Histone acetyltransferase complexes: one size doesn't fit all. Nat Rev Mol Cell Biol. 2007;8: 284–295. doi:10.1038/nrm2145

76. Seto E, Yoshida M. Erasers of histone acetylation: the histone deacetylase enzymes. Cold Spring Harb Perspect Biol. 2014;6: a018713. doi:10.1101/cshperspect.a018713

77. Sivanand S, Viney I, Wellen KE. Spatiotemporal Control of Acetyl-CoA Metabolism in Chromatin Regulation. Trends Biochem Sci. 2018;43: 61–74. doi:10.1016/j.tibs.2017.11.004

78. Poirier Y, Antonenkov VD, Glumoff T, Hiltunen JK. Peroxisomal beta-oxidation--a metabolic pathway with multiple functions. Biochim Biophys Acta. 2006;1763: 1413–1426. doi:10.1016/j.bbamcr.2006.08.034

79. Zara V, Assalve G, Ferramosca A. Multiple roles played by the mitochondrial citrate carrier in cellular metabolism and physiology. Cell Mol Life Sci CMLS. 2022;79: 428. doi:10.1007/s00018-022-04466-0

80. Zaidi N, Swinnen JV, Smans K. ATP-citrate lyase: a key player in cancer metabolism. Cancer Res. 2012;72: 3709–3714. doi:10.1158/0008-5472.CAN-11-4112

81. Madiraju P, Pande SV, Prentki M, Madiraju SRM. Mitochondrial acetylcarnitine provides acetyl groups for nuclear histone acetylation. Epigenetics. 2009;4: 399–403. doi:10.4161/epi.4.6.9767

82. Li X, Yu W, Qian X, Xia Y, Zheng Y, Lee J-H, et al. Nucleus-Translocated ACSS2 Promotes Gene Transcription for Lysosomal Biogenesis and Autophagy. Mol Cell. 2017;66: 684-697.e9. doi:10.1016/j.molcel.2017.04.026

83. Wellen KE, Hatzivassiliou G, Sachdeva UM, Bui TV, Cross JR, Thompson CB. ATP-citrate lyase links cellular metabolism to histone acetylation. Science. 2009;324: 1076–1080. doi:10.1126/science.1164097

84. Sutendra G, Kinnaird A, Dromparis P, Paulin R, Stenson TH, Haromy A, et al. A nuclear pyruvate dehydrogenase complex is important for the generation of acetyl-CoA and histone acetylation. Cell. 2014;158: 84–97. doi:10.1016/j.cell.2014.04.046

85. Galdieri L, Vancura A. Acetyl-CoA carboxylase regulates global histone acetylation. J Biol Chem. 2012;287: 23865–23876. doi:10.1074/jbc.M112.380519

86. Trefely S, Lovell CD, Snyder NW, Wellen KE. Compartmentalised acyl-CoA metabolism and roles in chromatin regulation. Mol Metab. 2020;38: 100941. doi:10.1016/j.molmet.2020.01.005

87. Sabari BR, Zhang D, Allis CD, Zhao Y. Metabolic regulation of gene expression through histone acylations. Nat Rev Mol Cell Biol. 2017;18: 90–101. doi:10.1038/nrm.2016.140

88. Nitsch S, Zorro Shahidian L, Schneider R. Histone acylations and chromatin dynamics: concepts, challenges, and links to metabolism. EMBO Rep. 2021;22: e52774. doi:10.15252/embr.202152774

89. Wang Y, Guo YR, Liu K, Yin Z, Liu R, Xia Y, et al. KAT2A coupled with the α-KGDH complex acts as a histone H3 succinyltransferase. Nature. 2017;552: 273–277. doi:10.1038/nature25003

90. Li W, Long Q, Wu H, Zhou Y, Duan L, Yuan H, et al. Nuclear localization of mitochondrial TCA cycle enzymes modulates pluripotency via histone acetylation. Nat Commun. 2022;13: 7414. doi:10.1038/s41467-022-35199-0

91. Kebede AF, Nieborak A, Shahidian LZ, Le Gras S, Richter F, Gómez DA, et al. Histone propionylation is a mark of active chromatin. Nat Struct Mol Biol. 2017;24: 1048–1056. doi:10.1038/nsmb.3490

92. Tan M, Luo H, Lee S, Jin F, Yang JS, Montellier E, et al. Identification of 67 histone marks and histone lysine crotonylation as a new type of histone modification. Cell. 2011;146: 1016–1028. doi:10.1016/j.cell.2011.08.008

93. Wagner GR, Payne RM. Widespread and enzyme-independent Nε-acetylation and Nε-succinylation of proteins in the chemical conditions of the mitochondrial matrix. J Biol Chem. 2013;288: 29036–29045. doi:10.1074/jbc.M113.486753

94. Andrews FH, Shinsky SA, Shanle EK, Bridgers JB, Gest A, Tsun IK, et al. The Taf14 YEATS domain is a reader of histone crotonylation. Nat Chem Biol. 2016;12: 396–398. doi:10.1038/nchembio.2065

95. Xiong X, Panchenko T, Yang S, Zhao S, Yan P, Zhang W, et al. Selective recognition of histone crotonylation by double PHD fingers of MOZ and DPF2. Nat Chem Biol. 2016;12: 1111–1118. doi:10.1038/nchembio.2218

96. Li Y, Sabari BR, Panchenko T, Wen H, Zhao D, Guan H, et al. Molecular Coupling of Histone Crotonylation and Active Transcription by AF9 YEATS Domain. Mol Cell. 2016;62: 181–193. doi:10.1016/j.molcel.2016.03.028

97. Wang Y, Jin J, Chung MWH, Feng L, Sun H, Hao Q. Identification of the YEATS domain of GAS41 as a pH-dependent reader of histone succinylation. Proc Natl Acad Sci U S A. 2018;115: 2365–2370. doi:10.1073/pnas.1717664115

98. Allfrey VG, Faulkner R, Mirsky AE. Acetylation And Methylation of Histones and Their Possible Role in the Regulation of RNA Synthesis. Proc Natl Acad Sci U S A. 1964;51: 786–794. doi:10.1073/pnas.51.5.786

99. Zencir S, Dilg D, Shore D, Albert B. Pitfalls in using phenanthroline to study the causal relationship between promoter nucleosome acetylation and transcription. Nat Commun. 2022;13: 3726. doi:10.1038/s41467-022-30350-3

100. Martin BJE, Brind'Amour J, Kuzmin A, Jensen KN, Liu ZC, Lorincz M, et al. Transcription shapes genome-wide histone acetylation patterns. Nat Commun. 2021;12: 210. doi:10.1038/s41467-020-20543-z

101. Boija A, Mahat DB, Zare A, Holmqvist P-H, Philip P, Meyers DJ, et al. CBP Regulates Recruitment and Release of Promoter-Proximal RNA Polymerase II. Mol Cell. 2017;68: 491-503.e5. doi:10.1016/j.molcel.2017.09.031

102. Sansó M, Vargas-Pérez I, Quintales L, Antequera F, Ayté J, Hidalgo E. Gcn5 facilitates Pol II progression, rather than recruitment to nucleosome-depleted stress promoters, in Schizosaccharomyces pombe. Nucleic Acids Res. 2011;39: 6369–6379. doi:10.1093/nar/gkr255

103. Ginsburg DS, Govind CK, Hinnebusch AG. NuA4 lysine acetyltransferase Esa1 is targeted to coding regions and stimulates transcription elongation with Gcn5. Mol Cell Biol. 2009;29: 6473–6487. doi:10.1128/MCB.01033-09

104. Wakamori M, Okabe K, Ura K, Funatsu T, Takinoue M, Umehara T. Quantification of the effect of site-specific histone acetylation on chromatin transcription rate. Nucleic Acids Res. 2020;48: 12648–12659. doi:10.1093/nar/gkaa1050

105. Jiang G, Li C, Lu M, Lu K, Li H. Protein lysine crotonylation: past, present, perspective. Cell Death Dis. 2021;12: 703. doi:10.1038/s41419-021-03987-z

106. Liu J, Shangguan Y, Tang D, Dai Y. Histone succinylation and its function on the nucleosome. J Cell Mol Med. 2021;25: 7101–7109. doi:10.1111/jcmm.16676

107. Gowans GJ, Bridgers JB, Zhang J, Dronamraju R, Burnetti A, King DA, et al. Recognition of Histone Crotonylation by Taf14 Links Metabolic State to Gene Expression. Mol Cell. 2019;76: 909-921.e3. doi:10.1016/j.molcel.2019.09.029

108. Knight ZA, Shokat KM. Features of selective kinase inhibitors. Chem Biol. 2005;12: 621– 637. doi:10.1016/j.chembiol.2005.04.011

109. Fan J, Krautkramer KA, Feldman JL, Denu JM. Metabolic regulation of histone post-translational modifications. ACS Chem Biol. 2015;10: 95–108. doi:10.1021/cb500846u

110. Chen WW, Freinkman E, Wang T, Birsoy K, Sabatini DM. Absolute Quantification of Matrix Metabolites Reveals the Dynamics of Mitochondrial Metabolism. Cell. 2016;166: 1324-1337.e11. doi:10.1016/j.cell.2016.07.040

111. Wellen KE, Snyder NW. Should we consider subcellular compartmentalization of metabolites, and if so, how do we measure them? Curr Opin Clin Nutr Metab Care. 2019;22: 347–354. doi:10.1097/MCO.0000000000000580

112. Trefely S, Liu J, Huber K, Doan MT, Jiang H, Singh J, et al. Subcellular metabolic pathway kinetics are revealed by correcting for artifactual post harvest metabolism. Mol Metab. 2019;30: 61–71. doi:10.1016/j.molmet.2019.09.004

113. Decelle J, Veronesi G, Gallet B, Stryhanyuk H, Benettoni P, Schmidt M, et al. Subcellular Chemical Imaging: New Avenues in Cell Biology. Trends Cell Biol. 2020;30: 173–188. doi:10.1016/j.tcb.2019.12.007

114. Shen Y, Yue J, Xu W, Xu S. Recent progress of surface-enhanced Raman spectroscopy for subcellular compartment analysis. Theranostics. 2021;11: 4872–4893. doi:10.7150/thno.56409

115. Xue L, Schnacke P, Frei MS, Koch B, Hiblot J, Wombacher R, et al. Probing coenzyme A homeostasis with semisynthetic biosensors. Nat Chem Biol. 2022. doi:10.1038/s41589-022- 01172-7

116. Niemeyer J, Scheuring D, Oestreicher J, Morgan B, Schroda M. Real-time monitoring of subcellular H2O2 distribution in Chlamydomonas reinhardtii. Plant Cell. 2021;33: 2935–2949. doi:10.1093/plcell/koab176

117. Michaelis L, Menten ML, Johnson KA, Goody RS. The original Michaelis constant: translation of the 1913 Michaelis-Menten paper. Biochemistry. 2011;50: 8264–8269. doi:10.1021/bi201284u

118. Fierz B. Dynamic Chromatin Regulation from a Single Molecule Perspective. ACS Chem Biol. 2016;11: 609–620. doi:10.1021/acschembio.5b00832

119. Jiang Y, Li X, Morrow BR, Pothukuchy A, Gollihar J, Novak R, et al. Single-Molecule Mechanistic Study of Enzyme Hysteresis. ACS Cent Sci. 2019;5: 1691–1698. doi:10.1021/acscentsci.9b00718

120. Crickard JB, Lee J, Lee T-H, Reese JC. The elongation factor Spt4/5 regulates RNA polymerase II transcription through the nucleosome. Nucleic Acids Res. 2017;45: 6362–6374. doi:10.1093/nar/gkx220

121. Hansen L, Mariño-Ramírez L, Landsman D. Differences in local genomic context of bound and unbound motifs. Gene. 2012;506: 125–134. doi:10.1016/j.gene.2012.06.005

122. Slattery M, Zhou T, Yang L, Dantas Machado AC, Gordân R, Rohs R. Absence of a simple code: how transcription factors read the genome. Trends Biochem Sci. 2014;39: 381–399. doi:10.1016/j.tibs.2014.07.002

123. Zaret KS. Pioneer Transcription Factors Initiating Gene Network Changes. Annu Rev Genet. 2020;54: 367–385. doi:10.1146/annurev-genet-030220-015007

124. Hughes AL, Rando OJ. Mechanisms underlying nucleosome positioning in vivo. Annu Rev Biophys. 2014;43: 41–63. doi:10.1146/annurev-biophys-051013-023114

125. Zhu F, Farnung L, Kaasinen E, Sahu B, Yin Y, Wei B, et al. The interaction landscape between transcription factors and the nucleosome. Nature. 2018;562: 76–81. doi:10.1038/s41586-018-0549-5

126. Morgan MAJ, Shilatifard A. Reevaluating the roles of histone-modifying enzymes and their associated chromatin modifications in transcriptional regulation. Nat Genet. 2020;52: 1271–1281. doi:10.1038/s41588-020-00736-4

127. Stephens AD, Liu PZ, Banigan EJ, Almassalha LM, Backman V, Adam SA, et al. Chromatin histone modifications and rigidity affect nuclear morphology independent of lamins. Mol Biol Cell. 2018;29: 220–233. doi:10.1091/mbc.E17-06-0410

128. Lee DSW, Strom AR, Brangwynne CP. The mechanobiology of nuclear phase separation. APL Bioeng. 2022;6: 021503. doi:10.1063/5.0083286

129. Hyman AA, Weber CA, Jülicher F. Liquid-liquid phase separation in biology. Annu Rev Cell Dev Biol. 2014;30: 39–58. doi:10.1146/annurev-cellbio-100913-013325

130. Sabari BR, Dall'Agnese A, Young RA. Biomolecular Condensates in the Nucleus. Trends Biochem Sci. 2020;45: 961–977. doi:10.1016/j.tibs.2020.06.007

131. Fuxreiter M, Vendruscolo M. Generic nature of the condensed states of proteins. Nat Cell Biol. 2021;23: 587–594. doi:10.1038/s41556-021-00697-8

132. Schwarzacher HG, Wachtler F. The nucleolus. Anat Embryol (Berl). 1993;188: 515–536. doi:10.1007/BF00187008

133. Feric M, Vaidya N, Harmon TS, Mitrea DM, Zhu L, Richardson TM, et al. Coexisting Liquid Phases Underlie Nucleolar Subcompartments. Cell. 2016;165: 1686–1697. doi:10.1016/j.cell.2016.04.047

134. Zamudio AV, Dall'Agnese A, Henninger JE, Manteiga JC, Afeyan LK, Hannett NM, et al. Mediator Condensates Localize Signaling Factors to Key Cell Identity Genes. Mol Cell. 2019;76: 753-766.e6. doi:10.1016/j.molcel.2019.08.016

135. Brodsky S, Jana T, Mittelman K, Chapal M, Kumar DK, Carmi M, et al. Intrinsically Disordered Regions Direct Transcription Factor In Vivo Binding Specificity. Mol Cell. 2020;79: 459-471.e4. doi:10.1016/j.molcel.2020.05.032

136. Larson AG, Elnatan D, Keenen MM, Trnka MJ, Johnston JB, Burlingame AL, et al. Liquid droplet formation by HP1α suggests a role for phase separation in heterochromatin. Nature. 2017;547: 236–240. doi:10.1038/nature22822

137. Strom AR, Emelyanov AV, Mir M, Fyodorov DV, Darzacq X, Karpen GH. Phase separation drives heterochromatin domain formation. Nature. 2017;547: 241–245. doi:10.1038/nature22989

138. Wang L, Gao Y, Zheng X, Liu C, Dong S, Li R, et al. Histone Modifications Regulate Chromatin Compartmentalization by Contributing to a Phase Separation Mechanism. Mol Cell. 2019;76: 646-659.e6. doi:10.1016/j.molcel.2019.08.019

139. Gibson BA, Doolittle LK, Schneider MWG, Jensen LE, Gamarra N, Henry L, et al. Organization of Chromatin by Intrinsic and Regulated Phase Separation. Cell. 2019;179: 470-484.e21. doi:10.1016/j.cell.2019.08.037

140. Strom AR, Brangwynne CP. The liquid nucleome - phase transitions in the nucleus at a glance. J Cell Sci. 2019;132: jcs235093. doi:10.1242/jcs.235093

141. McDonnell E, Crown SB, Fox DB, Kitir B, Ilkayeva OR, Olsen CA, et al. Lipids Reprogram Metabolism to Become a Major Carbon Source for Histone Acetylation. Cell Rep. 2016;17: 1463–1472. doi:10.1016/j.celrep.2016.10.012

142. Mews P, Donahue G, Drake AM, Luczak V, Abel T, Berger SL. Acetyl-CoA synthetase regulates histone acetylation and hippocampal memory. Nature. 2017;546: 381–386. doi:10.1038/nature22405

143. Kekenes-Huskey PM, Scott CE, Atalay S. Quantifying the Influence of the Crowded Cytoplasm on Small Molecule Diffusion. J Phys Chem B. 2016;120: 8696–8706. doi:10.1021/acs.jpcb.6b03887

144. Katada S, Imhof A, Sassone-Corsi P. Connecting threads: epigenetics and metabolism. Cell. 2012;148: 24–28. doi:10.1016/j.cell.2012.01.001

145. Erdel F, Rippe K. Formation of Chromatin Subcompartments by Phase Separation. Biophys J. 2018;114: 2262–2270. doi:10.1016/j.bpj.2018.03.011

146. Garner RM, Molines AT, Theriot JA, Chang F. Vast heterogeneity in cytoplasmic diffusion rates revealed by nanorheology and Doppelgänger simulations. Biophys J. 2023; S0006- 3495(23)00089–9. doi:10.1016/j.bpj.2023.01.040

147. Petersen J, Russell P. Growth and the Environment of Schizosaccharomyces pombe. Cold Spring Harb Protoc. 2016;2016: pdb.top079764. doi:10.1101/pdb.top079764

148. Gregan J, Rabitsch PK, Rumpf C, Novatchkova M, Schleiffer A, Nasmyth K. High-throughput knockout screen in fission yeast. Nat Protoc. 2006;1: 2457–2464. doi:10.1038/nprot.2006.385

149. Di Y, Holmes EJ, Butt A, Dawson K, Mironov A, Kotiadis VN, et al. H_2O_2 stress-specific regulation of S. pombe MAPK Sty1 by mitochondrial protein phosphatase Ptc4. EMBO J. 2012;31: 563–575. doi:10.1038/emboj.2011.438

150. Převorovský M, Oravcová M, Tvarůžková J, Zach R, Folk P, Půta F, et al. Fission Yeast CSL Transcription Factors: Mapping Their Target Genes and Biological Roles. PloS One. 2015;10: e0137820. doi:10.1371/journal.pone.0137820

151. Nakamura T, Pluskal T, Nakaseko Y, Yanagida M. Impaired coenzyme A synthesis in fission yeast causes defective mitosis, quiescence-exit failure, histone hypoacetylation and fragile DNA. Open Biol. 2012;2: 120117. doi:10.1098/rsob.120117

152. Princová J, Salat-Canela C, Daněk P, Marešová A, de Cubas L, Bähler J, et al. Perturbed fatty-acid metabolism is linked to localized chromatin hyperacetylation, increased stress-response gene expression and resistance to oxidative stress. PLoS Genet. 2023;19: e1010582. doi:10.1371/journal.pgen.1010582

153. Zuin A, Carmona M, Morales-Ivorra I, Gabrielli N, Vivancos AP, Ayté J, et al. Lifespan extension by calorie restriction relies on the Sty1 MAP kinase stress pathway. EMBO J. 2010;29: 981–991. doi:10.1038/emboj.2009.407

154. Princová J, Schätz M, Ťupa O, Převorovský M. Analysis of Lipid Droplet Content in Fission and Budding Yeasts using Automated Image Processing. J Vis Exp JoVE. 2019. doi:10.3791/59889

155. Schroeder AB, Dobson ETA, Rueden CT, Tomancak P, Jug F, Eliceiri KW. The ImageJ ecosystem: Open-source software for image visualization, processing, and analysis. Protein Sci Publ Protein Soc. 2021;30: 234–249. doi:10.1002/pro.3993

156. Ramírez F, Ryan DP, Grüning B, Bhardwaj V, Kilpert F, Richter AS, et al. deepTools2: a next generation web server for deep-sequencing data analysis. Nucleic Acids Res. 2016;44: W160-165. doi:10.1093/nar/gkw257

157. Boyle EI, Weng S, Gollub J, Jin H, Botstein D, Cherry JM, et al. GO::TermFinder--open source software for accessing Gene Ontology information and finding significantly enriched Gene Ontology terms associated with a list of genes. Bioinforma Oxf Engl. 2004;20: 3710–3715. doi:10.1093/bioinformatics/bth456

158. Wood V, Gwilliam R, Rajandream M-A, Lyne M, Lyne R, Stewart A, et al. The genome sequence of Schizosaccharomyces pombe. Nature. 2002;415: 871–880. doi:10.1038/nature724

159. Harris MA, Rutherford KM, Hayles J, Lock A, Bähler J, Oliver SG, et al. Fission stories: using PomBase to understand Schizosaccharomyces pombe biology. Genetics. 2022;220: iyab222. doi:10.1093/genetics/iyab222

160. Bolger AM, Lohse M, Usadel B. Trimmomatic: a flexible trimmer for Illumina sequence data. Bioinforma Oxf Engl. 2014;30: 2114–2120. doi:10.1093/bioinformatics/btu170

161. Kim D, Paggi JM, Park C, Bennett C, Salzberg SL. Graph-based genome alignment and genotyping with HISAT2 and HISAT-genotype. Nat Biotechnol. 2019;37: 907–915. doi:10.1038/s41587-019-0201-4

162. Li H, Handsaker B, Wysoker A, Fennell T, Ruan J, Homer N, et al. The Sequence Alignment/Map format and SAMtools. Bioinforma Oxf Engl. 2009;25: 2078–2079. doi:10.1093/bioinformatics/btp352

163. Bonfield JK, Marshall J, Danecek P, Li H, Ohan V, Whitwham A, et al. HTSlib: C library for reading/writing high-throughput sequencing data. GigaScience. 2021;10: giab007. doi:10.1093/gigascience/giab007

164. Love MI, Huber W, Anders S. Moderated estimation of fold change and dispersion for RNA-seq data with DESeq2. Genome Biol. 2014;15: 550. doi:10.1186/s13059-014-0550-8

165. Gentleman RC, Carey VJ, Bates DM, Bolstad B, Dettling M, Dudoit S, et al. Bioconductor: open software development for computational biology and bioinformatics. Genome Biol. 2004;5: R80. doi:10.1186/gb-2004-5-10-r80

166. Huber W, Carey VJ, Gentleman R, Anders S, Carlson M, Carvalho BS, et al. Orchestrating high-throughput genomic analysis with Bioconductor. Nat Methods. 2015;12: 115–121. doi:10.1038/nmeth.3252

167. Papadakis MA, Workman CT. Oxidative stress response pathways: Fission yeast as archetype. Crit Rev Microbiol. 2015;41: 520–535. doi:10.3109/1040841X.2013.870968

168. Vivancos AP, Jara M, Zuin A, Sansó M, Hidalgo E. Oxidative stress in Schizosaccharomyces pombe: different H2O2 levels, different response pathways. Mol Genet Genomics MGG. 2006;276: 495–502. doi:10.1007/s00438-006-0175-z

169. López-Avilés S, Lambea E, Moldón A, Grande M, Fajardo A, Rodríguez-Gabriel MA, et al. Activation of Srk1 by the mitogen-activated protein kinase Sty1/Spc1 precedes its dissociation from the kinase and signals its degradation. Mol Biol Cell. 2008;19: 1670–1679. doi:10.1091/mbc.e07-07-0639

170. Opalko HE, Moseley JB. Dynamic regulation of Cdr1 kinase localization and phosphorylation during osmotic stress. J Biol Chem. 2017;292: 18457–18468. doi:10.1074/jbc.M117.793034

171. Madrid M, Gómez-Gil E, Cansado J. Negative control of cytokinesis by stress-activated MAPK signaling. Curr Genet. 2021;67: 715–721. doi:10.1007/s00294-021-01155-6

172. Salat-Canela C, Carmona M, Martín-García R, Pérez P, Ayté J, Hidalgo E. Stress-dependent inhibition of polarized cell growth through unbalancing the GEF/GAP regulation of Cdc42. Cell Rep. 2021;37: 109951. doi:10.1016/j.celrep.2021.109951

173. Nguyen AN, Shiozaki K. Heat-shock-induced activation of stress MAP kinase is regulated by threonine- and tyrosine-specific phosphatases. Genes Dev. 1999;13: 1653–1663. doi:10.1101/gad.13.13.1653

174. Shiozaki K, Russell P. Cell-cycle control linked to extracellular environment by MAP kinase pathway in fission yeast. Nature. 1995;378: 739–743. doi:10.1038/378739a0

175. Millar JB, Buck V, Wilkinson MG. Pyp1 and Pyp2 PTPases dephosphorylate an osmosensing MAP kinase controlling cell size at division in fission yeast. Genes Dev. 1995;9: 2117–2130. doi:10.1101/gad.9.17.2117

176. Shiozaki K, Russell P. Counteractive roles of protein phosphatase 2C (PP2C) and a MAP kinase kinase homolog in the osmoregulation of fission yeast. EMBO J. 1995;14: 492–502. doi:10.1002/j.1460-2075.1995.tb07025.x

177. Daněk P. The molecular mechanism of CSL protein participation in oxidative stress response in Schizosaccharomyces pombe. Diploma thesis, Charles University, Faculty of Science, Department of Cell Biology. 2015. Available: https://dspace.cuni.cz/handle/20.500.11956/3428

178. Gaits F, Degols G, Shiozaki K, Russell P. Phosphorylation and association with the transcription factor Atf1 regulate localization of Spc1/Sty1 stress-activated kinase in fission yeast. Genes Dev. 1998;12: 1464–1473. doi:10.1101/gad.12.10.1464

179. Wilkinson MG, Pino TS, Tournier S, Buck V, Martin H, Christiansen J, et al. Sin1: an evolutionarily conserved component of the eukaryotic SAPK pathway. EMBO J. 1999;18: 4210–4221. doi:10.1093/emboj/18.15.4210

180. Bannister AJ, Kouzarides T. Regulation of chromatin by histone modifications. Cell Res. 2011;21: 381–395. doi:10.1038/cr.2011.22

181. Murray K. The Occurence of Epsilon-N-methyl Lysine in Histones. Biochemistry. 1964;3: 10–15. doi:10.1021/bi00889a003

182. Berger SL. The complex language of chromatin regulation during transcription. Nature. 2007;447: 407–412. doi:10.1038/nature05915

183. Zach R, Tvaružková J, Schätz M, Tupa O, Grallert B, Prevorovský M. Mitotic defects in fission yeast lipid metabolism "cut" mutants are suppressed by ammonium chloride. FEMS Yeast Res. 2018;18: foy064. doi:10.1093/femsyr/foy064

184. Převorovský M, Oravcová M, Zach R, Jordáková A, Bähler J, Půta F, et al. CSL protein regulates transcription of genes required to prevent catastrophic mitosis in fission yeast. Cell Cycle Georget Tex. 2016;15: 3082–3093. doi:10.1080/15384101.2016.1235100

185. Zhang M, Galdieri L, Vancura A. The yeast AMPK homolog SNF1 regulates acetyl coenzyme A homeostasis and histone acetylation. Mol Cell Biol. 2013;33: 4701–4717. doi:10.1128/MCB.00198-13

186. Kwon E-JG, Laderoute A, Chatfield-Reed K, Vachon L, Karagiannis J, Chua G. Deciphering the transcriptional-regulatory network of flocculation in Schizosaccharomyces pombe. PLoS Genet. 2012;8: e1003104. doi:10.1371/journal.pgen.1003104

187. Prevorovský M, Grousl T, Stanurová J, Rynes J, Nellen W, Půta F, et al. Cbf11 and Cbf12, the fission yeast CSL proteins, play opposing roles in cell adhesion and coordination of cell and nuclear division. Exp Cell Res. 2009;315: 1533–1547. doi:10.1016/j.yexcr.2008.12.001

188. Wirén M, Silverstein RA, Sinha I, Walfridsson J, Lee H, Laurenson P, et al. Genome wide analysis of nucleosome density histone acetylation and HDAC function in fission yeast. EMBO J. 2005;24: 2906–2918. doi:10.1038/sj.emboj.7600758

189. Levy MZ, Allsopp RC, Futcher AB, Greider CW, Harley CB. Telomere end-replication problem and cell aging. J Mol Biol. 1992;225: 951–960. doi:10.1016/0022-2836(92)90096-3

190. Lingner J, Cooper JP, Cech TR. Telomerase and DNA end replication: no longer a lagging strand problem? Science. 1995;269: 1533–1534. doi:10.1126/science.7545310

191. Hocher A, Taddei A. Subtelomeres as Specialized Chromatin Domains. BioEssays News Rev Mol Cell Dev Biol. 2020;42: e1900205. doi:10.1002/bies.201900205

192. Yadav RK, Matsuda A, Lowe BR, Hiraoka Y, Partridge JF. Subtelomeric Chromatin in the Fission Yeast S. pombe. Microorganisms. 2021;9: 1977. doi:10.3390/microorganisms9091977

193. Matsuda A, Chikashige Y, Ding D-Q, Ohtsuki C, Mori C, Asakawa H, et al. Highly condensed chromatins are formed adjacent to subtelomeric and decondensed silent chromatin in fission yeast. Nat Commun. 2015;6: 7753. doi:10.1038/ncomms8753

194. Cohen A, Habib A, Laor D, Yadav S, Kupiec M, Weisman R. TOR complex 2 in fission yeast is required for chromatin-mediated gene silencing and assembly of heterochromatic domains at subtelomeres. J Biol Chem. 2018;293: 8138–8150. doi:10.1074/jbc.RA118.002270

195. Thorvaldsdóttir H, Robinson JT, Mesirov JP. Integrative Genomics Viewer (IGV): high-performance genomics data visualization and exploration. Brief Bioinform. 2013;14: 178–192. doi:10.1093/bib/bbs017

196. Onn I, Heidinger-Pauli JM, Guacci V, Unal E, Koshland DE. Sister chromatid cohesion: a simple concept with a complex reality. Annu Rev Cell Dev Biol. 2008;24: 105–129. doi:10.1146/annurev.cellbio.24.110707.175350

197. Yanagida M. Fission yeast cut mutations revisited: control of anaphase. Trends Cell Biol. 1998;8: 144–149. doi:10.1016/s0962-8924(98)01236-7

198. Zach R, Převorovský M. The phenomenon of lipid metabolism “cut” mutants. Yeast Chichester Engl. 2018;35: 631–637. doi:10.1002/yea.3358

199. Arnone JT, Walters AD, Cohen-Fix O. The dynamic nature of the nuclear envelope: lessons from closed mitosis. Nucl Austin Tex. 2013;4: 261–266. doi:10.4161/nucl.25341

200. Takemoto A, Kawashima SA, Li J-J, Jeffery L, Yamatsugu K, Elemento O, et al. Nuclear envelope expansion is crucial for proper chromosomal segregation during a closed mitosis. J Cell Sci. 2016;129: 1250–1259. doi:10.1242/jcs.181560

201. Saitoh S, Takahashi K, Nabeshima K, Yamashita Y, Nakaseko Y, Hirata A, et al. Aberrant mitosis in fission yeast mutants defective in fatty acid synthetase and acetyl CoA carboxylase. J Cell Biol. 1996;134: 949–961. doi:10.1083/jcb.134.4.949

202. Hardie DG, Ross FA, Hawley SA. AMPK: a nutrient and energy sensor that maintains energy homeostasis. Nat Rev Mol Cell Biol. 2012;13: 251–262. doi:10.1038/nrm3311

203. Valbuena N, Moreno S. AMPK phosphorylation by Ssp1 is required for proper sexual differentiation in fission yeast. J Cell Sci. 2012;125: 2655–2664. doi:10.1242/jcs.098533

204. Hardie DG. AMP-activated/SNF1 protein kinases: conserved guardians of cellular energy. Nat Rev Mol Cell Biol. 2007;8: 774–785. doi:10.1038/nrm2249

205. Woods A, Munday MR, Scott J, Yang X, Carlson M, Carling D. Yeast SNF1 is functionally related to mammalian AMP-activated protein kinase and regulates acetyl-CoA carboxylase in vivo. J Biol Chem. 1994;269: 19509–19515.

206. Chen Y, Hu X, Guo C, Yu Y, Lu H. Epe1 contributes to activation of AMPK by promoting phosphorylation of AMPK alpha subunit, Ssp2. Sci Rep. 2017;7: 3208. doi:10.1038/s41598- 017-03442-0

207. Foo S, Cazenave-Gassiot A, Wenk MR, Oliferenko S. Diacylglycerol at the inner nuclear membrane fuels nuclear envelope expansion in closed mitosis. J Cell Sci. 2023;136: jcs260568. doi:10.1242/jcs.260568

208. Fang C-T, Kuo H-H, Amartuvshin O, Hsu H-J, Liu S-L, Yao J-S, et al. Inhibition of acetyl- CoA carboxylase impaired tubulin palmitoylation and induced spindle abnormalities. Cell Death Discov. 2023;9: 4. doi:10.1038/s41420-023-01301-8

209. Karolin J, Johansson LB-A, Strandberg L, Ny T. Fluorescence and Absorption Spectroscopic Properties of Dipyrromethene boron Difluoride (BODIPY) Derivatives in Liquids, Lipid Membranes, and Proteins. J Am Chem Soc. 1994;116: 7801–7806. doi:10.1021/ja00096a042

210. Bozaquel-Morais BL, Madeira JB, Maya-Monteiro CM, Masuda CA, Montero-Lomeli M. A new fluorescence-based method identifies protein phosphatases regulating lipid droplet metabolism. PloS One. 2010;5: e13692. doi:10.1371/journal.pone.0013692

211. Sitepu IR, Ignatia L, Franz AK, Wong DM, Faulina SA, Tsui M, et al. An improved high- throughput Nile red fluorescence assay for estimating intracellular lipids in a variety of yeast species. J Microbiol Methods. 2012;91: 321–328. doi:10.1016/j.mimet.2012.09.001

212. Rostron KA, Lawrence CL. Nile Red Staining of Neutral Lipids in Yeast. Methods Mol Biol Clifton NJ. 2017;1560: 219–229. doi:10.1007/978-1-4939-6788-9_16

213. Gupta A, Dorlhiac GF, Streets AM. Quantitative imaging of lipid droplets in single cells. The Analyst. 2019;144: 753–765. doi:10.1039/c8an01525b

214. Wolinski H, Bredies K, Kohlwein SD. Quantitative imaging of lipid metabolism in yeast: from 4D analysis to high content screens of mutant libraries. Methods Cell Biol. 2012;108: 345–365. doi:10.1016/B978-0-12-386487-1.00016-X

215. Campos V, Rappaz B, Kuttler F, Turcatti G, Naveiras O. High-throughput, nonperturbing quantification of lipid droplets with digital holographic microscopy. J Lipid Res. 2018;59: 1301–1310. doi:10.1194/jlr.D085217

216. Dejgaard SY, Presley JF. New Method for Quantitation of Lipid Droplet Volume From Light Microscopic Images With an Application to Determination of PAT Protein Density on the Droplet Surface. J Histochem Cytochem Off J Histochem Soc. 2018;66: 447–465. doi:10.1369/0022155417753573

217. Deutsch MJ, Schriever SC, Roscher AA, Ensenauer R. Digital image analysis approach for lipid droplet size quantitation of Oil Red O-stained cultured cells. Anal Biochem. 2014;445: 87–89. doi:10.1016/j.ab.2013.10.001

218. Exner T, Beretta CA, Gao Q, Afting C, Romero-Brey I, Bartenschlager R, et al. Lipid droplet quantification based on iterative image processing. J Lipid Res. 2019;60: 1333–1344. doi:10.1194/jlr.D092841

219. Capus A, Monnerat M, Ribeiro LC, de Souza W, Martins JL, Sant'Anna C. Application of high-content image analysis for quantitatively estimating lipid accumulation in oleaginous yeasts with potential for use in biodiesel production. Bioresour Technol. 2016;203: 309–317. doi:10.1016/j.biortech.2015.12.067

220. Lv X, Liu J, Qin Y, Liu Y, Jin M, Dai J, et al. Identification of gene products that control lipid droplet size in yeast using a high-throughput quantitative image analysis. Biochim Biophys Acta Mol Cell Biol Lipids. 2019;1864: 113–127. doi:10.1016/j.bbalip.2018.11.001

221. Klar AJS. Schizosaccharomyces japonicus yeast poised to become a favorite experimental organism for eukaryotic research. G3 Bethesda Md. 2013;3: 1869–1873. doi:10.1534/g3.113.007187

222. Tomida T, Takekawa M, Saito H. Oscillation of p38 activity controls efficient pro-inflammatory gene expression. Nat Commun. 2015;6: 8350. doi:10.1038/ncomms9350

223. Duch A, de Nadal E, Posas F. The p38 and Hog1 SAPKs control cell cycle progression in response to environmental stresses. FEBS Lett. 2012;586: 2925–2931. doi:10.1016/j.febslet.2012.07.034

224. Tognetti S, Jiménez J, Viganò M, Duch A, Queralt E, de Nadal E, et al. Hog1 activation delays mitotic exit via phosphorylation of Net1. Proc Natl Acad Sci U S A. 2020;117: 8924–8933. doi:10.1073/pnas.1918308117

225. López-Avilés S, Grande M, González M, Helgesen A-L, Alemany V, Sanchez-Piris M, et al. Inactivation of the Cdc25 phosphatase by the stress-activated Srk1 kinase in fission yeast. Mol Cell. 2005;17: 49–59. doi:10.1016/j.molcel.2004.11.043

226. Gould KL, Nurse P. Tyrosine phosphorylation of the fission yeast cdc2+ protein kinase regulates entry into mitosis. Nature. 1989;342: 39–45. doi:10.1038/342039a0

227. Russell P, Nurse P. Negative regulation of mitosis by wee1+, a gene encoding a protein kinase homolog. Cell. 1987;49: 559–567. doi:10.1016/0092-8674(87)90458-2

228. Russell P, Nurse P. cdc25+ functions as an inducer in the mitotic control of fission yeast. Cell. 1986;45: 145–153. doi:10.1016/0092-8674(86)90546-5

229. Russell P, Nurse P. The mitotic inducer nim1+ functions in a regulatory network of protein kinase homologs controlling the initiation of mitosis. Cell. 1987;49: 569–576. doi:10.1016/0092-8674(87)90459-4

230. Coleman TR, Tang Z, Dunphy WG. Negative regulation of the wee1 protein kinase by direct action of the nim1/cdr1 mitotic inducer. Cell. 1993;72: 919–929. doi:10.1016/0092-8674(93)90580-j

231. Parker LL, Walter SA, Young PG, Piwnica-Worms H. Phosphorylation and inactivation of the mitotic inhibitor Wee1 by the nim1/cdr1 kinase. Nature. 1993;363: 736–738. doi:10.1038/363736a0

232. Wu L, Russell P. Nim1 kinase promotes mitosis by inactivating Wee1 tyrosine kinase. Nature. 1993;363: 738–741. doi:10.1038/363738a0

233. Clotet J, Escoté X, Adrover MA, Yaakov G, Garí E, Aldea M, et al. Phosphorylation of Hsl1 by Hog1 leads to a G2 arrest essential for cell survival at high osmolarity. EMBO J. 2006;25: 2338–2346. doi:10.1038/sj.emboj.7601095

234. Alexander MR, Tyers M, Perret M, Craig BM, Fang KS, Gustin MC. Regulation of cell cycle progression by Swe1p and Hog1p following hypertonic stress. Mol Biol Cell. 2001;12: 53–62. doi:10.1091/mbc.12.1.53

235. Tvarůžková J. The role of CSL proteins in oxidative stress response of Schizosaccharomyces pombe. Diploma thesis, Charles University, Faculty of Science, Department of Cell Biology. 2015. Available: https://dspace.cuni.cz/handle/20.500.11956/609

236. Maher P. p38 mitogen-activated protein kinase activation is required for fibroblast growth factor-2-stimulated cell proliferation but not differentiation. J Biol Chem. 1999;274: 17491– 17498. doi:10.1074/jbc.274.25.17491

237. Chen L, Mayer JA, Krisko TI, Speers CW, Wang T, Hilsenbeck SG, et al. Inhibition of the p38 kinase suppresses the proliferation of human ER-negative breast cancer cells. Cancer Res. 2009;69: 8853–8861. doi:10.1158/0008-5472.CAN-09-1636

238. Faust D, Schmitt C, Oesch F, Oesch-Bartlomowicz B, Schreck I, Weiss C, et al. Differential p38-dependent signalling in response to cellular stress and mitogenic stimulation in fibroblasts. Cell Commun Signal CCS. 2012;10: 6. doi:10.1186/1478-811X-10-6

239. Cha H, Wang X, Li H, Fornace AJ. A functional role for p38 MAPK in modulating mitotic transit in the absence of stress. J Biol Chem. 2007;282: 22984–22992. doi:10.1074/jbc.M700735200

240. Lee K, Kenny AE, Rieder CL. p38 Mitogen-activated Protein Kinase Activity Is Required during Mitosis for Timely Satisfaction of the Mitotic Checkpoint But Not for the Fidelity of Chromosome Segregation. Mol Biol Cell. 2010;21: 2150–2160. doi:10.1091/mbc.e10-02- 0125

241. Vishwanatha A, Princová J, Hohoš P, Zach R, Převorovský M. Altered cohesin dynamics and histone H3K9 modifications contribute to mitotic defects in the cbf11Δ lipid metabolism mutant. bioRxiv. 2022; 2022.10.17.512562. doi:10.1101/2022.10.17.512562

242. Takada H, Nishimura M, Asayama Y, Mannse Y, Ishiwata S, Kita A, et al. Atf1 Is a Target of the Mitogen-activated Protein Kinase Pmk1 and Regulates Cell Integrity in Fission Yeast. Mol Biol Cell. 2007;18: 4794–4802. doi:10.1091/mbc.e07-03-0282

243. Liu S, Ginzberg MB, Patel N, Hild M, Leung B, Li Z, et al. Size uniformity of animal cells is actively maintained by a p38 MAPK-dependent regulation of G1-length. eLife. 2018;7: e26947. doi:10.7554/eLife.26947

244. Correa-Bordes J, Nurse P. p25rum1 orders S phase and mitosis by acting as an inhibitor of the p34cdc2 mitotic kinase. Cell. 1995;83: 1001–1009. doi:10.1016/0092-8674(95)90215-5

245. Moreno S, Nurse P. Regulation of progression through the G1 phase of the cell cycle by the rum1+ gene. Nature. 1994;367: 236–242. doi:10.1038/367236a0

246. Moreno S, Labib K, Correa J, Nurse P. Regulation of the cell cycle timing of Start in fission yeast by the rum1+ gene. J Cell Sci Suppl. 1994;18: 63–68. doi:10.1242/jcs.1994.supplement_18.9

247. Matsuoka K, Kiyokawa N, Taguchi T, Matsui J, Suzuki T, Mimori K, et al. Rum1, an inhibitor of cyclin-dependent kinase in fission yeast, is negatively regulated by mitogen-activated protein kinase-mediated phosphorylation at Ser and Thr residues. Eur J Biochem. 2002;269: 3511–3521. doi:10.1046/j.1432-1033.2002.03033.x

248. Chen T, Dent SYR. Chromatin modifiers and remodellers: regulators of cellular differentiation. Nat Rev Genet. 2014;15: 93–106. doi:10.1038/nrg3607

249. Moussaieff A, Rouleau M, Kitsberg D, Cohen M, Levy G, Barasch D, et al. Glycolysis-mediated changes in acetyl-CoA and histone acetylation control the early differentiation of embryonic stem cells. Cell Metab. 2015;21: 392–402. doi:10.1016/j.cmet.2015.02.002

250. TeSlaa T, Chaikovsky AC, Lipchina I, Escobar SL, Hochedlinger K, Huang J, et al. α-Ketoglutarate Accelerates the Initial Differentiation of Primed Human Pluripotent Stem Cells. Cell Metab. 2016;24: 485–493. doi:10.1016/j.cmet.2016.07.002

251. Cai L, Sutter BM, Li B, Tu BP. Acetyl-CoA induces cell growth and proliferation by promoting the acetylation of histones at growth genes. Mol Cell. 2011;42: 426–437. doi:10.1016/j.molcel.2011.05.004

252. Hsieh W-C, Sutter BM, Ruess H, Barnes SD, Malladi VS, Tu BP. Glucose starvation induces a switch in the histone acetylome for activation of gluconeogenic and fat metabolism genes. Mol Cell. 2022;82: 60-74.e5. doi:10.1016/j.molcel.2021.12.015

253. Nirello VD, Rodrigues de Paula D, Araújo NVP, Varga-Weisz PD. Does chromatin function as a metabolite reservoir? Trends Biochem Sci. 2022;47: 732–735. doi:10.1016/j.tibs.2022.03.016

254. Eshaghi M, Lee JH, Zhu L, Poon SY, Li J, Cho K-H, et al. Genomic binding profiling of the fission yeast stress-activated MAPK Sty1 and the bZIP transcriptional activator Atf1 in response to H2O2. PloS One. 2010;5: e11620. doi:10.1371/journal.pone.0011620

255. Sivanand S, Rhoades S, Jiang Q, Lee JV, Benci J, Zhang J, et al. Nuclear Acetyl-CoA Production by ACLY Promotes Homologous Recombination. Mol Cell. 2017;67: 252-265.e6. doi:10.1016/j.molcel.2017.06.008

256. Helmlinger D, Marguerat S, Villén J, Swaney DL, Gygi SP, Bähler J, et al. Tra1 has specific regulatory roles, rather than global functions, within the SAGA co-activator complex. EMBO J. 2011;30: 2843–2852. doi:10.1038/emboj.2011.181

257. Bruzzone MJ, Grünberg S, Kubik S, Zentner GE, Shore D. Distinct patterns of histone acetyltransferase and Mediator deployment at yeast protein-coding genes. Genes Dev. 2018;32: 1252–1265. doi:10.1101/gad.312173.118

258. D'Angelo MA. Nuclear pore complexes as hubs for gene regulation. Nucl Austin Tex. 2018;9: 142–148. doi:10.1080/19491034.2017.1395542

259. Brueckner L, Zhao PA, van Schaik T, Leemans C, Sima J, Peric-Hupkes D, et al. Local rewiring of genome-nuclear lamina interactions by transcription. EMBO J. 2020;39: e103159. doi:10.15252/embj.2019103159

260. Gallardo P, Barrales RR, Daga RR, Salas-Pino S. Nuclear Mechanics in the Fission Yeast. Cells. 2019;8: 1285. doi:10.3390/cells8101285

261. Li W, Jiang H. Nuclear Protein Condensates and Their Properties in Regulation of Gene Expression. J Mol Biol. 2022;434: 167151. doi:10.1016/j.jmb.2021.167151

262. Uversky VN. Intrinsically disordered proteins in overcrowded milieu: Membrane-less organelles, phase separation, and intrinsic disorder. Curr Opin Struct Biol. 2017;44: 18–30. doi:10.1016/j.sbi.2016.10.015

263. Zhang Y, Brown K, Yu Y, Ibrahim Z, Zandian M, Xuan H, et al. Nuclear condensates of p300 formed though the structured catalytic core can act as a storage pool of p300 with reduced HAT activity. Nat Commun. 2021;12: 4618. doi:10.1038/s41467-021-24950-8

264. Tashiro S, Nishihara Y, Kugou K, Ohta K, Kanoh J. Subtelomeres constitute a safeguard for gene expression and chromosome homeostasis. Nucleic Acids Res. 2017;45: 10333–10349. doi:10.1093/nar/gkx780

265. Cam HP, Sugiyama T, Chen ES, Chen X, FitzGerald PC, Grewal SIS. Comprehensive analysis of heterochromatin- and RNAi-mediated epigenetic control of the fission yeast genome. Nat Genet. 2005;37: 809–819. doi:10.1038/ng1602

266. Dheur S, Saupe SJ, Genier S, Vazquez S, Javerzat J-P. Role for cohesin in the formation of a heterochromatic domain at fission yeast subtelomeres. Mol Cell Biol. 2011;31: 1088– 1097. doi:10.1128/MCB.01290-10

267. Mata J, Lyne R, Burns G, Bähler J. The transcriptional program of meiosis and sporulation in fission yeast. Nat Genet. 2002;32: 143–147. doi:10.1038/ng951

268. Oizumi Y, Kaji T, Tashiro S, Takeshita Y, Date Y, Kanoh J. Complete sequences of Schizosaccharomyces pombe subtelomeres reveal multiple patterns of genome variation. Nat Commun. 2021;12: 611. doi:10.1038/s41467-020-20595-1

269. Tashiro S, Handa T, Matsuda A, Ban T, Takigawa T, Miyasato K, et al. Shugoshin forms a specialized chromatin domain at subtelomeres that regulates transcription and replication timing. Nat Commun. 2016;7: 10393. doi:10.1038/ncomms10393

270. Hirano Y, Kinugasa Y, Kubota Y, Obuse C, Haraguchi T, Hiraoka Y. Inner nuclear membrane proteins Lem2 and Bqt4 interact with different lipid synthesis enzymes in fission yeast. J Biochem (Tokyo). 2023; mvad017. doi:10.1093/jb/mvad017

271. Barrales RR, Forn M, Georgescu PR, Sarkadi Z, Braun S. Control of heterochromatin localization and silencing by the nuclear membrane protein Lem2. Genes Dev. 2016;30: 133–148. doi:10.1101/gad.271288.115

272. Holla S, Dhakshnamoorthy J, Folco HD, Balachandran V, Xiao H, Sun L-L, et al. Positioning Heterochromatin at the Nuclear Periphery Suppresses Histone Turnover to Promote Epigenetic Inheritance. Cell. 2020;180: 150-164.e15. doi:10.1016/j.cell.2019.12.004

273. Bernard P, Maure JF, Partridge JF, Genier S, Javerzat JP, Allshire RC. Requirement of heterochromatin for cohesion at centromeres. Science. 2001;294: 2539–2542. doi:10.1126/science.1064027